

## HVDC CONVERTER TRANSFORMERS PROTECTION - DIFFERENTIAL FUNCTION ASSESSMENT

GLAUFE SANTOS DE OLIVEIRA

DISSERTAÇÃO DE MESTRADO EM ENGENHARIA ELÉTRICA

DEPARTAMENTO DE ENGENHARIA ELÉTRICA

FACULDADE DE TECNOLOGIA
UNIVERSIDADE DE BRASÍLIA

## Universidade de Brasília Faculdade de Tecnologia Departamento de Engenharia Elétrica

## HVDC Converter Transformers Protection - Differential Function Assessment

#### Glaufe Santos de Oliveira

DISSERTAÇÃO DE MESTRADO SUBMETIDA AO PROGRAMA DE PÓS-GRADUAÇÃO EM ENGENHARIA ELÉTRICA DA UNIVERSIDADE DE BRASÍLIA COMO PARTE DOS REQUISITOS NECESSÁRIOS PARA A OBTENÇÃO DO GRAU DE MESTRE.

APROVADA POR:	
Kleber Melo e Silva, D.Sc. (ENE/UnB) (Orientador)	
Antonio Felipe da Cunha de Aquino, D.Sc. (UFSC) (Examinador Externo)	
Rômulo Gonçalves Bainy, D.Sc. (University of Idaho) (Examinador Externo)	
Francis Arody Moreno Vasquez, D.Sc. (ENE/UnB) (Examinador Interno - Suplente)	
PUBLICAÇÃO: PPGEE.DM - 828/25	

Brasília/DF, 24 de março de 2025.

#### FICHA CATALOGRÁFICA

#### OLIVEIRA, GLAUFE

HVDC Converter Transformers Protection - Differential Function Assessment. [Brasília/DF] 2025.

xxiv, 182p., 210 x 297 mm (ENE/FT/UnB, Mestre, Dissertação de Mestrado, 2025).

Universidade de Brasília, Faculdade de Tecnologia, Departamento de Engenharia Elétrica.

Departamento de Engenharia Elétrica

1. HVDC

3. Transformadores Conversores

5. Proteção Diferencial de Sequência Negativa

7. Transitórios Eletromagnéticos

I. ENE/FT/UnB

2. ATP/ATPDraw

4. Proteção Diferencial de Fase

6. Complexo HVDC do Madeira

8. Sistemas de Potência

II. Título (série)

### REFERÊNCIA BIBLIOGRÁFICA

OLIVEIRA, GLAUFE (2025). HVDC Converter Transformers Protection - Differential Function Assessment. Dissertação de Mestrado, Publicação PPGEE.DM - 828/25, Departamento de Engenharia Elétrica, Universidade de Brasília, Brasília, DF, 182p.

#### CESSÃO DE DIREITOS

AUTOR: Glaufe Oliveira

TÍTULO: HVDC Converter Transformers Protection - Differential Function Assessment.

GRAU: Mestre ANO: 2025

É concedida à Universidade de Brasília permissão para reproduzir cópias desta Dissertação de Mestrado e para emprestar ou vender tais cópias somente para propósitos acadêmicos e científicos. O autor reserva outros direitos de publicação e nenhuma parte desta dissertação de mestrado pode ser reproduzida sem autorização por escrito do autor.

Glaufe Oliveira

Universidade de Brasília (UnB)

Campus Darcy Ribeiro

Faculdade de Tecnologia - FT

Departamento de Engenharia Elétrica(ENE)

Brasília - DF CEP 70919-970



### **ACKNOWLEDGEMENTS**

I wish to express my gratitude to God for the abundant grace in my life and His constant care, which strengthened me and allowed me to complete yet another stage.

To my wife, Júlia, for her patience when I was absent due to studies and work. I am deeply grateful for her prayers, unconditional support, affection, and care, with which she was always by my side, especially in the most challenging moments.

To my family, especially my parents Gladistone and Isabel, and my sister Glênia. I am thankful to them for all the support throughout my life, constant encouragement, wise advice, and prayers at all times.

To Professor Kleber, I thank him for his trust in me, his patience, his support, and his understanding of my work and study routine. I am also thankful to him for all the knowledge he shared during his guidance and his dedication in the classroom, allowing me to learn from an excellent teacher.

To my colleagues at ONS, who supported me, showed understanding, and were flexible, comprehending my sleepiness and tiredness during the shifts and helping me with shift changes whenever necessary.

To my boss, Gilson, for encouraging me to study and for his valuable understanding, allowing me to dedicate almost all my time to my dissertation in the final phase.

Finally, I express my sincere gratitude to my friends who, directly or indirectly, supported me throughout this journey. Each one of them has been essential in helping me reach this point.

### **ABSTRACT**

High Voltage Direct Current (HVDC) transmission offers financial and technical advantages for power transmission over long distances due to lower power loss during transmission, reduced need for reactive compensation, and the absence of stability problems caused by low voltages and high impedance in the AC transmission systems. With advances in power electronics since the 20<sup>th</sup> century, HVDC systems have grown, including in Brazil, which has invested in these systems due to its continental size and the distance between generation sources and the load. In this scenario, research related to the protection systems for these systems is essential, including converter transformers, which are necessary equipment for implementing and operating these systems. They are expensive and difficult to replace. Thus, the protection schemes need to function correctly and identify internal faults in the equipment. Therefore, this dissertation presents a detailed evaluation of the phase differential (ANSI code 87T), negative sequence differential (ANSI code 87Q), and Restrict Earth Fault (ANSI code REF or 87N) protection functions in HVDC converter transformers—with function 87T being the primary protection of the equipment. The analyses considered only converter transformers connected to converters operating as inverters. Simulations were performed on a model of the Madeira River LCC-HVDC Complex using the Alternative Transients Program (ATP/ATPDraw) software to perform these evaluations, simulating external faults to the transformers on the busbar to which they are connected and on an adjacent AC transmission line, and internal faults to the equipment, namely: phase-to-ground, phase-to-phase-to-ground, phase-to-phase, turn-toground, and turn-to-turn faults, all in the primary and secondary of the transformers of a pole. The energization of these transformers was also simulated. The protection functions were implemented in Python, and the performance of the functions was evaluated based on the simulation results. The results of the performance of these functions were discussed, with the evaluation of the best protection settings and describing the reasons for the performance failures found. Among the results, the following stand out: phase-to-ground and turn-to-ground faults in the secondary of the transformers that present performance failures due to improper blocking of functions or even lack of detection of internal faults.

Keywords: HVDC, ATP/ATPDraw, converter transformers, phase differential protection, negative sequence differential protection, Madeira River HVDC Complex, electromagnetic transients, power systems.

### **RESUMO**

Título: Proteção de Transformadores Conversores HVDC – Avaliação das Funções Diferenciais

A transmissão em corrente contínua em alta tensão (High Voltage Direct Current - HVDC) apresenta vantagens financeiras e técnicas para transmissão de potência em longas distâncias devido às menores perdas de potência na transmissão, a menor necessidade de compensação reativa e por não apresentar problemas de estabilidade causados por baixos valores de tensão e altas impedâncias em sistemas de transmissão CA. Com os avanços da eletrônica de potência a partir do século XX, o uso de sistemas HVDC tem crescido e isso inclui o Brasil, que tem investido nesses sistemas devido seu às suas dimensões continentais e à distância entre fontes de geração e a carga. Nesse cenário, pesquisas relacionadas aos sistemas de proteção desses sistemas são essenciais, o que inclui os transformadores conversores que são equipamentos fundamentais para implementação e funcionamento desses sistemas, tem um custo elevado e são de difícil substituição. Portanto, é necessário garantir o bom funcionamento de seus esquemas de proteção e a identificação tempestiva de falhas internas ao equipamento. Logo, essa dissertação apresenta uma avaliação detalhada das funções de proteção diferencial de fase (ANSI code 87T), diferencial de sequência negativa (ANSI code 87Q), e Restrict Earth Fault (ANSI code REF ou 87N) em transformadores conversores de sistemas HVDC—sendo a função 87T a principal proteção do equipamento. As análises consideraram apenas transformadores conversores conectados a conversores operando como inversores. Para realização dessas avaliações, foram realizadas simulações em um modelo do sistema LCC-HVDC do Complexo do Rio Madeira através do software Alternative Transients Program (ATP/ATPDraw), simulando faltas externas aos transformadores na barra em que eles estão conectados e em uma linha de transmissão CA adjacente, e faltas internas aos equipamentos, sendo elas: faltas fase-terra, fase-fase-terra, fase-fase, espira-terra e espira-espira, tanto no primário quanto no secundário dos transformadores de um polo. Foi simulada, também, a energização desses transformadores. As funções de proteção por sua vez, foram implementadas em Python e a partir dos resultados das simulações, a atuação das funções foram avaliadas. Os resultados da atuação dessas funções foram discutidos, avaliando-se os melhores ajustes de proteção e detalhando as razões dos problemas de desempenho encontrados. Destaque para faltas fase-terra e espira-terra no secundário dos transformadores que apresentam problemas de desempenho por bloqueios indevidos das funções ou nem mesmo detecção de faltas internas.

Palavras-chave: HVDC, ATP/ATPDraw, transformadores conversores, proteção diferencial de fase, proteção diferencial de sequência negativa, Complexo HVDC do Rio Madeira, transitórios eletromagnéticos, sistemas de potência.

# TABLE OF CONTENTS

Table o	of contents	i
List of	figures	iv
List of	tables	xvii
List of	symbols	xviii
Glossar	γ	xxii
Chapte	er 1 – Introduction	1
1.1	CONTEXTUALIZATION OF THE TOPIC	1
1.2	MOTIVATION	5
1.3	OBJECTIVES	6
1.4	CONTRIBUTIONS	6
1.5	PUBLICATIONS	7
1.6	TEXT ORGANIZATION	7
Chapte	er 2 – Fundamentals of HVDC Systems	9
2.1	HVDC CONVERTER STATIONS	9
	2.1.1 Six-pulse converters	11
	2.1.1.1 Commutation overlap in a thyristor converter	15
	2.1.1.2 Inverter operation	17
	2.1.1.3 Commutation Failure	19
	2.1.2 Twelve-pulse converters	20
2.2	CONVERTER TRANSFORMERS	23
2.3	DC AND AC FILTERS	24
2.4	SMOOTHING REACTOR	26
Chapte	er 3 – Fundamentals of Transformer Differential Protection	27
3.1	TYPES OF FAILURES IN CONVERTERS TRANSFORMERS	27

Table of Contents ii

3.2			ALS OF TRANSFORMER DIFFERENTIAL CURRENT PRO-	28
3.3			AT INFLUENCE THE OPERATION OF TRANSFORMER DIF-	31
	3.3.1	CT Satu	ration	31
	3.3.2	Inrush c	urrent	32
	3.3.3	Over-exc	citation	34
3.4			S AND CORRECTIONS TO PREVENT IMPROPER OPE- IFFERENTIAL PROTECTION	34
	3.4.1	Correction	on of current transformation ratios	34
	3.4.2	Zero-seq	uence current compensation	35
	3.4.3	Angular	phase shift correction	36
	3.4.4	Harmoni	ic restraint	37
	3.4.5	Harmoni	ic blocking	39
3.5	TRAN	NSFORMI	ER NEGATIVE-SEQUENCE DIFFERENTIAL FUNCTION (87Q)	40
3.6	REST	RICTED	EARTH FAULT PROTECTION (REF)	43
Chapte	er 4 – I	Literatur	e Review	46
4.1	SUMN	MARY OF	THE LITERATURE REVIEW	51
Chapte	er 5 – (	Computa	tional Implementations	53
5.1	HVDO	C SYSTE	M MODEL	53
	5.1.1	Madeira	River HVDC Complex	53
	5.1.2	HVDC S	System in ATP/ATPDraw	55
5.2	MODI		F DIFFERENTIAL PROTECTION FUNCTIONS	59
	5.2.1	Analog a	anti-aliasing filter	60
	5.2.2	Phasor I	Estimation	61
	5.2.3	Logic of	differential functions	63
		5.2.3.1	Adjustments and corrections to prevent improper operation of differential protection	63
		5.2.3.2	87T function	64
		5.2.3.3	87Q function	66
		5.2.3.4	REF function	68
5.3	BATC	CH SIMUI	LATIONS	68
Chapte	er 6 – I	Results P	Presentation and Analysis	70
6.1	PROT	ECTION	FUNCTION SETTINGS	71
6.2			AULTS TO CONVERTER TRANSFORMERS	72

Table of Contents iii

	6.2.1	500 kV Araraquara 2/Taubaté transmission line	72
	6.2.2	500 kV busbar at Substation Araraquara 2	73
6.3	ENEF	GIZATION OF CONVERTER TRANSFORMERS	76
6.4	INTE	RNAL FAULTS IN CONVERTER TRANSFORMERS	76
	6.4.1	Primary side	77
		6.4.1.1 Short circuit turn-to-ground	77
		6.4.1.2 Short circuit turn-to-turn	83
		6.4.1.3 Single-phase-to-ground short circuit	85
		6.4.1.4 Phase-to-phase short circuit	87
		6.4.1.5 Phase-to-phase-to-ground short circuit	88
	6.4.2	Secondary side	91
		6.4.2.1 Short circuit turn-to-ground	91
		6.4.2.2 Short circuit turn-to-turn	117
		6.4.2.3 Single-phase-to-ground short circuit	120
		6.4.2.4 Phase-to-phase short circuit	127
		6.4.2.5 Phase-to-phase-to-ground short circuit	131
6.5	SUMN	MARY OF THE RESULTS	136
	6.5.1	External Faults and Energization	136
	6.5.2	Internal Faults on Primary side	137
	6.5.3	Internal Faults on Secondary side	137
Chapte	er 7 –	Conclusions and Proposals for Future Work	142
Refere	nces		146

## LIST OF FIGURES

1.1	Various applications of an HVDC system	1
1.2	HVDC and HVAC transmission cost comparison	2
1.3	DC transmission lines in Brazil	4
2.1	Typical LCC-HVDC schematic (12-pulse monopole with metallic return)	9
2.2	Symbol for thyristor	10
2.3	Diode six-pulse AC/DC converter	11
2.4	Voltage and current AC plot	12
2.5	Voltage and current DC plot	13
2.6	Thyristor six-pulse AC/DC converter with a transformer	14
2.7	Voltage and current AC plot with transformer $(L_t = 0.1H)$ and ignition delay	
	$(\alpha = 30^{\circ})$	14
2.8	Voltage and current DC plot with transformer $(L_t = 0.1H)$ and ignition delay	
	$(\alpha = 30^{\circ})$	14
2.9	Converter equivalent circuit during commutation	16
2.10	Commutation from thy ristors T1 to T3 (phase A to B) in inversion mode. $\ \ .$	18
2.11	Inverter commutation failure simulation	19
2.12	DC current path during commutation failure	20
2.13	DC voltage of a twelve-pulse converter	22
2.14	AC current of a twelve-pulse converter	22
2.15	Part of a converter controller	23

List of Figures V

2.16	1100 kV HVDC converter transformer by Siemens	25
2.17	HVDC station with harmonic filters	26
3.1	Differential protection scheme to electromechanical relay with a (a) external fault and (b) internal fault	29
3.2	Differential protection scheme to electromechanical relay considering the restriction current	30
3.3	Operational plan to a differential protection	31
3.4	Typical magnetizing inrush current to transformers: (a) A-phase current to star-connected windings; (b) A-phase current to delta-connected windings	33
3.5	Phase shift groups	36
3.6	87T function fail operation due a transformer energization	38
3.7	87T function correct operation due harmonic restriction	38
3.8	87T function blocking by 2 <sup>nd</sup> harmonic	39
3.9	87T function blocking by 5 <sup>th</sup> harmonic	40
3.10	87T function operation to a turn-to-ground short circuit in 1% of the turns of a star terminal	41
3.11	87Q function operation to a turn-to-ground short circuit in 1% of the turns of a star terminal	42
3.12	87T function operation to a turn-to-turn short circuit in 5% of the turns of a delta terminal	42
3.13	87Q function operation to a turn-to-turn short circuit in 5% of the turns of a delta terminal	43
3.14	87T function operation to a turn-to-ground short circuit in 0.5% of the turns of a star terminal	44
3.15	87Q function operation to a turn-to-ground short circuit in 0.5% of the turns of a star terminal	45

List of Figures vi

3.16	REF function operation to a turn-to-ground short circuit in 0.5% of the turns of a star terminal	45
5.1	Schematic representation of HVDC Madeira River link operation modes: (a) Bipolar, (b) Monopolar Metallic Return, and (c) Monopolar Ground Return	55
5.2	CIGRE Benchmark model for HVDC LCC studies	56
5.3	Transformer configuration to turn-to-turn and turn-to-ground faults	57
5.4	Diagram of the evaluated power system: the Brazilian LCC-HVDC Madeira River link and the nearby AC system	58
5.5	IED structure implemented in Python	59
5.6	Graphical user interface developed in Python to manage and execute batch simulations in ATP, including configuration of fault types, locations, and protection functions	69
6.1	87Q function operation in (a) TFYY and (b) TFYD for a phase-to-phase-to-ground short circuit on the 500 kV busbar at Substation Araraquara 2	74
6.2	87Q function operation in (a) TFYY and (b) TFYD for a phase-to-phase short circuit on the 500 kV busbar at Substation Araraquara 2	74
6.3	500 kV busbar voltage of Substation Araraquara 2 for a phase-to-phase-to-ground short circuit on the busbar.	75
6.4	Bipole 1 current for a three-phase short circuit on the 500 kV busbar at Substation Araraquara 2	75
6.5	87Q function operation in (a) TFYY and (b) TFYD for a three-phase short circuit on the 500 kV busbar at Substation Araraquara 2	75
6.6	87Q function operation in (a) TFYY and (b) TFYD for the energization of the transformers	76
6.7	87T R.B.H. function operation in (a) TFYY and (b) TFYD for turn-to-ground short circuits on the primary side, with 100% power transmission in the bipoles.	78

List of Figures VII

6.8	eircuits on the primary side, with 100% power transmission in the bipoles	78
6.9	87T R.B.H. function operation in (a) TFYY and (b) TFYD for a turn-to-ground short circuit at 7% of the primary side, with 100% power transmission in the bipoles	78
6.10	87T function operation in (a) TFYY and (b) TFYD for a turn-to-ground short circuit at $7%$ of the primary side, with $100%$ power transmission in the bipoles	79
6.11	87T R.B.H. function operation in (a) TFYY and (b) TFYD for a turn-to-ground short circuit at 8% of the primary side, with 100% power transmission in the bipoles	80
6.12	87T function operation in (a) TFYY and (b) TFYD for a turn-to-ground short circuit at $8\%$ of the primary side, with $100\%$ power transmission in the bipoles.	80
6.13	87Q B.H. DLY function operation in (a) TFYY and (b) TFYD for turn-to-ground short circuits on the primary side, with 100% power transmission in the bipoles.	81
6.14	87Q B.H. DLY function operation in (a) TFYY and (b) TFYD for a turn-to-ground short circuit at 1% of the primary side, with 100% power transmission in the bipoles	81
6.15	87Q B.H. DLY function operation in (a) TFYY and (b) TFYD for a turn-to-ground short circuit at 2% of the primary side, with 100% power transmission in the bipoles	81
6.16	87T R.B.H. function operation with a SLP of 0.5 in (a) TFYY and (b) TFYD for turn-to-ground short circuits on the primary side, with 10% power transmission in the bipoles	82
6.17	87T R.B.H. function operation with a SLP of 0.3 in (a) TFYY and (b) TFYD for turn-to-ground short circuits on the primary side, with 10% power transmission in the bipoles	82
6.18	87Q B.H. DLY function operation in (a) TFYY and (b) TFYD for turn-to-ground short circuits on the primary side, with 10% power transmission in the bipoles.	82

List of Figures viii

6.19	REF B.H. function operation in (a) TFYY and (b) TFYD for turn-to-ground	
	short circuits on the primary side, with $100\%$ power transmission in the bipoles.	83
6.20	REF B.H. function operation in (a) TFYY and (b) TFYD for turn-to-ground short circuits on the primary side, with $10\%$ power transmission in the bipoles	83
6.21	87T R.B.H. function operation in (a) TFYY and (b) TFYD for turn-to-turn short circuits on the primary side, with 100% power transmission in the bipoles.	84
6.22	$87\mathrm{T}$ R.B.H. function operation in (a) TFYY and (b) TFYD for turn-to-turn short circuits on the primary side, with $10\%$ power transmission in the bipoles	84
6.23	87Q B.H. DLY function operation in (a) TFYY and (b) TFYD for turn-to-turn short circuits on the primary side, with 100% power transmission in the bipoles.	84
6.24	87T R.B.H. function operation in (a) TFYY and (b) TFYD for a single-phase-to-ground short circuit on the primary side, with 100% power transmission in the bipoles	85
6.25	87Q B.H. function operation in (a) TFYY and (b) TFYD for a single-phase-to-ground short circuit on the primary side, with 100% power transmission in the bipoles	QE
6.26	REF B.H. function operation in (a) TFYY and (b) TFYD for a single-phase-to-ground short circuit on the primary side, with 100% power transmission in the bipoles.	
6.27	87T R.B.H. function operation in (a) TFYY and (b) TFYD for a single-phase-to-ground short circuit on the primary side, with 10% power transmission in the	00
6.28	bipoles	86
	ground short circuit on the primary side, with 10% power transmission in the bipoles	86
6.29	REF B.H. function operation in (a) TFYY and (b) TFYD for a single-phase-to-ground short circuit on the primary side, with 10% power transmission in the bipoles	87
	~-r	J.

List of Figures ix

6.30	short circuit on the primary side, with 100% power transmission in the bipoles.	87
6.31	$87\mathrm{Q}$ B.H. function operation in (a) TFYY and (b) TFYD for a phase-to-phase short circuit on the primary side, with $100\%$ power transmission in the bipoles	88
6.32	87T R.B.H. function operation in (a) TFYY and (b) TFYD for a phase-to-phase short circuit on the primary side, with $10%$ power transmission in the bipoles.    .	88
6.33	$87\mathrm{Q}$ B.H. function operation in (a) TFYY and (b) TFYD for a phase-to-phase short circuit on the primary side, with $10\%$ power transmission in the bipoles	89
6.34	87T R.B.H. function operation in (a) TFYY and (b) TFYD for a phase-to-phase-to-ground short circuit on the primary side, with 100% power transmission in the bipoles	89
6.35	87Q B.H. DLY function operation in (a) TFYY and (b) TFYD for a phase-to-phase-to-ground short circuit on the primary side, with 100% power transmission in the bipoles	89
6.36	REF B.H. function operation in (a) TFYY and (b) TFYD for a phase-to-phase-to-ground short circuit on the primary side, with 100% power transmission in the bipoles	90
6.37	87T R.B.H. function operation in (a) TFYY and (b) TFYD for a phase-to-phase-to-ground short circuit on the primary side, with 10% power transmission in the bipoles	90
6.38	87Q B.H. function operation in (a) TFYY and (b) TFYD for a phase-to-phase-to-ground short circuit on the primary side, with 10% power transmission in the bipoles	90
6.39	REF B.H. function operation in (a) TFYY and (b) TFYD for a phase-to-phase-to-ground short circuit on the primary side, with 10% power transmission in the bipoles.	91
6.40	Diagram of the converter inverter evaluated to short circuits in the secondary of its converter transformers.	92

List of Figures X

6.41	87T function operation in TFYY <sub>1</sub> for turn-to-ground short circuits on the secondary side, with $100\%$ power transmission in the bipoles	93
6.42	87T R.B.H. function operation in TFYY $_1$ for turn-to-ground short circuits on the secondary side, with 100% power transmission in the bipoles	93
6.43	Blocking by $2^{nd}$ harmonic for turn-to-ground short circuits in the secondary of the converter transformer $TFYY_1$	94
6.44	87T R.H. function operation in TFYY <sub>1</sub> for turn-to-ground short circuits on the secondary side, with 100% power transmission in the bipoles	94
6.45	500 kV busbar voltage of the busbar at the substation Araraquara 2 for a turn-to-ground short circuit at 90% of the secondary of the converter transformer $TFYY_1$	95
6.46	Fault current loops in $Inv_1$ for a turn-to-ground short circuit at 90% of the secondary of the transformer $TFYY_1$	96
6.47	Currents on the secondary side of TFYY1 during a turn-to-ground short circuit at 90% of the secondary side, with 100% power transmission in the bipoles	97
6.48	Commutation failures of $Inv_1$ for a turn-to-ground short circuit at 90% of the secondary of the converter transformer $TFYY_1$	97
6.49	Pre-fault phase (a) and line (b) voltages for a turn-to-ground short circuit at $90\%$ of the secondary of the converter transformer TFYY <sub>1</sub>	98
6.50	Faulted-state phase (a) and line (b) voltages for a turn-to-ground short circuit at 90% of the secondary of the converter transformer $TFYY_1$	98
6.51	Currents on the primary side of TFYY <sub>1</sub> during a turn-to-ground short circuit at $90\%$ of the secondary side, with $100\%$ power transmission in the bipoles	99
6.52	87T function operation in TFYY <sub>1</sub> for a turn-to-ground short circuit at 90% of the secondary side, with 100% power transmission in the bipoles	99
6.53	87T R.B.H. function operation in TFYY <sub>1</sub> for a turn-to-ground short circuit at 90% of the secondary side, with 100% power transmission in the bipoles	99

List of Figures Xi

6.54	$2^{\rm nd}$ harmonic by fundamental for a turn-to-ground short circuit at 90% of the secondary of the converter transformer TFYY <sub>1</sub>	100
6.55	$5^{\rm th}$ harmonic by fundamental for a turn-to-ground short circuit at 90% of the secondary of the converter transformer TFYY <sub>1</sub>	100
6.56	87T function operation in TFYY <sub>1</sub> for a turn-to-ground short circuit at 55% of the secondary side, with 100% power transmission in the bipoles	101
6.57	Currents on the secondary side of TFYY1 during a turn-to-ground short circuit at 55% of the secondary side, with 100% power transmission in the bipoles	101
6.58	Fault current loops in $Inv_1$ to a short circuit turn-to-ground at 55% of the secondary of the transformer $TFYY_1$	102
6.59	Faulted-state phase (a) and line (b) voltages for a turn-to-ground short circuit at 55% of the secondary of the converter transformer TFYY <sub>1</sub>	103
6.60	Currents on the primary side of TFYY <sub>1</sub> during a turn-to-ground short circuit at $55\%$ of the secondary side, with $100\%$ power transmission in the bipoles	103
6.61	Currents phasor module on TFYY <sub>1</sub> during a turn-to-ground short circuit at $55\%$ of the secondary side, with $100\%$ power transmission in the bipoles	103
6.62	Currents on the secondary side of TFYY $_1$ during a turn-to-ground short circuit at 90% of the secondary side, with 10% power transmission in the bipoles	104
6.63	87T function operation in TFYY <sub>1</sub> for turn-to-ground short circuits on the secondary side, with $10\%$ power transmission in the bipoles	104
6.64	87T function operation in TFYD <sub>1</sub> for turn-to-ground short circuits on the secondary side, with 100% power transmission in the bipoles. $\dots$	105
6.65	87T function operation with a SLP of 0.1 in TFYD $_1$ for turn-to-ground short circuits on the secondary side, with 100% power transmission in the bipoles	106
6.66	Blocking by $2^{nd}$ harmonic for turn-to-ground short circuits in the secondary of the converter transformer $TFYD_1$	106
6.67	Blocking by $5^{th}$ harmonic for turn-to-ground short circuits in the secondary of the converter transformer $TFYD_1$	106

List of Figures Xii

6.68	Fault current loops in $Inv_2$ for a turn-to-ground short circuit at 90% of the secondary of the transformer $TFYD_1$	107
6.69	Currents on the secondary side of TFYD $_1$ during a turn-to-ground short circuit at 90% of the secondary side, with 100% power transmission in the bipoles	108
6.70	Commutation failures of $Inv_2$ for a turn-to-ground short circuit at 90% of the secondary of the converter transformer $TFYD_1$	108
6.71	Pre-fault phase (a) and line (b) voltages for a turn-to-ground short circuit at $90\%$ of the secondary of the converter transformer TFYD <sub>1</sub>	109
6.72	Faulted-state phase (a) and line (b) voltages for a turn-to-ground short circuit at $90\%$ of the secondary of the converter transformer TFYD <sub>1</sub>	109
6.73	Currents on the primary side of TFYD <sub>1</sub> during a turn-to-ground short circuit at $90\%$ of the secondary side, with $100\%$ power transmission in the bipoles	110
6.74	Currents phasor module on TFYD <sub>1</sub> during a turn-to-ground short circuit at $90\%$ of the secondary side, with $100\%$ power transmission in the bipoles	110
6.75	87T function operation in TFYY <sub>1</sub> for a turn-to-ground short circuit at 90% on the secondary side, with 100% power transmission in the bipoles	110
6.76	$2^{nd}$ harmonic by fundamental for a turn-to-ground short circuit at 90% of the secondary of the converter transformer TFYD <sub>1</sub>	111
6.77	$5^{\rm th}$ harmonic by fundamental for a turn-to-ground short circuit at 90% of the secondary of the converter transformer TFYD <sub>1</sub>	111
6.78	Currents on the secondary side of TFYD <sub>1</sub> during a turn-to-ground short circuit at 90% of the secondary side, with 10% power transmission in the bipoles	111
6.79	87T function operation in TFYD <sub>1</sub> for turn-to-ground short circuits on the secondary side, with $10\%$ power transmission in the bipoles	112
6.80	Currents on the secondary side of $TFYY_1$ during a turn-to-ground short circuit at 90% of the secondary side of $TFYD_1$	112
6.81	Currents on the secondary side of TFYD <sub>1</sub> during a turn-to-ground short circuit at 90% of the secondary side of TFYY <sub>1</sub>	113

List of Figures XIII

6.82	Currents on the secondary side of $\mathrm{TFYY}_2$ during a turn-to-ground short circuit	
	at 90% of the secondary side, with 100% power transmission in the bipoles	113
6.83	Currents on the secondary side of $\mathrm{TFYD}_2$ during a turn-to-ground short circuit	
	at 90% of the secondary side, with 100% power transmission in the bipoles	114
6.84	87Q function operation in (a) TFYY $_1$ and (b) TFYD $_1$ for turn-to-ground short	
	circuits on the secondary side, with 100% power transmission in the bipoles. $$	115
6.85	87Q DLY function operation in (a) TFYY <sub>1</sub> and (b) TFYD <sub>1</sub> for turn-to-ground	
	short circuits on the secondary side, with $100\%$ power transmission in the bipoles.	115
6.86	87Q function operation in TFYY <sub>1</sub> for a turn-to-ground short circuit at 55% the	
	secondary side, with $100\%$ power transmission in the bipoles	115
6.87	87Q function operation in TFYD <sub>1</sub> for a turn-to-ground short circuit at $10%$ the	
	secondary side, with 100% power transmission in the bipoles	116
6.88	87Q function operation in TFYD <sub>1</sub> for a turn-to-ground short circuit at $50%$ the	
	secondary side, with 100% power transmission in the bipoles	116
6.89	87Q DLY function operation in (a) TFYY $_1$ and (b) TFYD $_1$ for turn-to-ground	
	short circuits on the secondary side, with $10\%$ power transmission in the bipoles.	117
6.90	87Q DLY function operation in (a) TFYY $_1$ and (b) TFYD $_1$ for a turn-to-ground	
	short circuit at 68% the secondary side, with 10% power transmission in the	
	bipoles	117
6.91	Currents of (a) TFYY and (b) TFYD during a turn-to-turn short circuit at $90\%$	
	of the secondary side, with 100% power transmission in the bipoles	118
6.92	Currents of (a) TFYY and (b) TFYD during a turn-to-turn short circuit at $90\%$	
	of the primary side, with 100% power transmission in the bipoles	118
6.93	87T R.B.H. function operation in (a) TFYY and (b) TFYD for a turn-to-turn	
	short circuit on the secondary side, with $100\%$ power transmission in the bipoles.	119
6.94	87T R.B.H. function operation in (a) TFYY and (b) TFYD for a turn-to-turn	
	short circuit on the secondary side, with 10% power transmission in the bipoles.	119

List of Figures XiV

6.95	$87\mathrm{Q}$ B.H. DLY function operation in (a) TFYY and (b) TFYD for turn-to-turn short circuits on the secondary side, with $100\%$ power transmission in the bipoles.120
6.96	Currents on the secondary side of TFYY $_1$ during a single-phase-to-ground short circuit on the secondary side, with 100% power transmission in the bipoles 120
6.97	Faulted-state phase (a) and line (b) voltages for a single-phase-to-ground short circuit on the secondary side of $TFYY_1$
6.98	Currents on the primary side of TFYY $_1$ during a single-phase-to-ground short circuit on the secondary side, with 100% power transmission in the bipoles 121
6.99	87T function operation in TFYY $_1$ for a single-phase-to-ground short circuit on the secondary side, with 100% power transmission in the bipoles
6.100	$02^{\mathrm{nd}}$ harmonic by fundamental for a single-phase-to-ground short circuit on the secondary side of TFYY <sub>1</sub>
6.101	187T R.B.H. function operation in TFYY $_1$ for a single-phase-to-ground short circuit on the secondary side, with 100% power transmission in the bipoles 123
6.102	2 Currents on the secondary side of TFYY <sub>1</sub> during a single-phase-to-ground short circuit on the secondary side, with $10\%$ power transmission in the bipoles 123
6.103	387T function operation in TFYY <sub>1</sub> for a single-phase-to-ground short circuit on the secondary side, with $10\%$ power transmission in the bipoles
6.104	4Currents on the secondary side of TFYD <sub>1</sub> during a single-phase-to-ground short circuit on the secondary side, with $100\%$ power transmission in the bipoles $124$
6.105	5Currents on the primary side of TFYD <sub>1</sub> during a single-phase-to-ground short circuit on the secondary side, with 100% power transmission in the bipoles 124
6.106	587T function operation in TFYD <sub>1</sub> for a single-phase-to-ground short circuit on the secondary side, with $100\%$ power transmission in the bipoles
6.107	7 Currents on the secondary side of TFYD $_1$ during a single-phase-to-ground short circuit on the secondary side, with 10% power transmission in the bipoles 125
6.108	887T function operation in TFYD <sub>1</sub> for a single-phase-to-ground short circuit on the secondary side, with $10\%$ power transmission in the bipoles

List of Figures XV

6.109Faulted-state phase (a) and line (b) voltages for a single-phase-to-ground short	
circuit on the secondary of $TFYD_1$	.26
$6.110$ Commutation failures of $Inv_2$ for a single-phase-to-ground short circuit on the secondary of the converter transformer $TFYD_1$	26
6.111Currents on the secondary side of TFYY2 during a single-phase-to-ground short circuit on the secondary side, with $100%$ power transmission in the bipoles 1	26
6.112Currents on the secondary side of TFYD <sub>2</sub> during a single-phase-to-ground short circuit on the secondary side, with $100%$ power transmission in the bipoles 1	.27
6.11387Q DLY function operation in (a) TFYY <sub>1</sub> and (b) TFYD <sub>1</sub> for a single-phase-to-ground short circuit on the secondary side, with 100% power transmission in the bipoles	.27
6.11487Q DLY function operation in (a) TFYY <sub>1</sub> and (b) TFYD <sub>1</sub> for a single-phase-to-ground short circuit on the secondary side, with 10% power transmission in the bipoles	28
6.115 Fault current loops in $Inv_1$ for a phase-to-phase short circuit on the secondary of $TFYY_1$	29
6.116Currents on the secondary side of TFYY <sub>1</sub> during a phase-to-phase short circuit on the secondary side, with $100%$ power transmission in the bipoles	.30
$6.1172^{\rm nd}$ harmonic by fundamental for a phase-to-phase short circuit on the secondary side of TFYY <sub>1</sub>	.30
6.11887T R.B.H. function operation in TFYY <sub>1</sub> for a phase-to-phase short circuit on the secondary side, with 100% power transmission in the bipoles	.30
6.11987Q DLY function operation in TFYY <sub>1</sub> for a phase-to-phase short circuit on the secondary side, with $100%$ power transmission in the bipoles	.31
6.120Currents on the secondary side of TFYD <sub>1</sub> during a phase-to-phase short circuit on the secondary side, with $100%$ power transmission in the bipoles	.31
6.121Fault current loops in $Inv_1$ for a phase-to-phase short circuit on the secondary of $TFYD_1$	.32

List of Figures XVI

6.122Operational plan and operation logic of the 87T function and with harmonic and
blocking by harmonics for phase-to-phase short circuit in the secondary of the
converter transformer $TFYD_1$
6.12387Q DLY function operation in TFYD <sub>1</sub> for a phase-to-phase short circuit on the
secondary side, with $100\%$ power transmission in the bipoles
6.12487T R.B.H. function operation in (a) TFYY <sub>1</sub> and (b) TFYD <sub>1</sub> for a phase-to-
phase short circuit on the secondary side, with $10\%$ power transmission in the
bipoles
6.12587Q DLY function operation in (a) TFYY <sub>1</sub> and (b) TFYD <sub>1</sub> for a phase-to-phase
short circuit on the secondary side, with 10% power transmission in the bipoles. 13-
6.126Currents on the secondary side of (a) TFYY <sub>1</sub> and (b) TFYD <sub>1</sub> during a phase-
to-phase-to-ground short circuit on the secondary side, with $100\%$ power trans-
mission in the bipoles
$6.1272^{\mathrm{nd}}$ harmonic by fundamental for a phase-to-phase-to-ground short circuit on the
secondary of (a) TFYY <sub>1</sub> and (b) TFYD <sub>1</sub>
6.12887T R.B.H. function operation in (a) TFYY $_1$ and (b) TFYD $_1$ for a phase-to-
phase-to-ground short circuit on the secondary side, with $100\%$ power transmis-
sion in the bipoles
6.12987Q DLY function operation in (a) TFYY <sub>1</sub> and (b) TFYD <sub>1</sub> for a phase-to-phase-
to-ground short circuit on the secondary side, with $100\%$ power transmission in
the bipoles
6.13087T R.B.H. function operation in (a) TFYY <sub>1</sub> and (b) TFYD <sub>1</sub> for a phase-to-
phase-to-ground short circuit on the secondary side, with $10\%$ power transmis-
sion in the bipoles
6.13187Q DLY function operation in (a) TFYY <sub>1</sub> and (b) TFYD <sub>1</sub> for a phase-to-phase-
to-ground short circuit on the secondary side, with $10\%$ power transmission in
the bipoles

# LIST OF TABLES

3.1	Probability of occurrence of failures and faults in converter transformers 28
4.1	Summary of the main contributions of the reviewed literature
6.1	Protection function settings
6.2	Summary of external faults and energization scenarios
6.3	Summary of internal faults – Primary side with 100% transmission
6.4	Summary of internal faults – Primary side with 10% transmission
6.5	87T and 87Q function operation summary for turn-to-ground short circuit in the secondary of TFYY <sub>1</sub> for bipoles at 100% of power transmission 139
6.6	87T and 87Q function operation summary for turn-to-ground short circuit in the secondary of TFYY <sub>1</sub> for bipoles at 10% of power transmission
6.7	Summary of internal faults – Secondary side with 100% transmission 140
6.8	Summary of internal faults – Secondary side with 10% transmission

## LIST OF SYMBOLS

$a_0$	DC component of the signal applied in Fourier series	
$a_n$	Fourier coefficient	
$A_n$	Module of the $n^{rd}$ -order harmonic sinusoid in the Fourier series	
$b_n$	Fourier coefficient	
$C_{opt}$	Capacitive reactance in the ATP system	$[\Omega]$
$c_k$	Correction factor for the transformer CT connection	
$CTR_k$	Transformation ratio of the CT at each terminal	
f(t)	General periodic function in time domain of Fourier series	
h	Harmonic order to be estimated	
$h_{AC}$	Order of harmonics in AC side of an HVDC system	
$h_{DC}$	Order of harmonics in DC side of an HVDC system	
$h_x$	Fourier filter coefficient for one cycle	
$h_y$	Fourier filter coefficient for one cycle	
H(s)	3 <sup>rd</sup> -order filter transfer function	
H1	First amount of turns of phase A of the winding of each transformer	
H2	Amount of turns of phase A involved in turn-to-turn faults	
H3	Amount of turns of phase A involved in turn-to-ground faults	
$I_a$	Phase A current in the converter	[A]
$I_{adi}$	Adjusted current of element 87T when using harmonic restriction	[A]

List of Symbols XiX

$I_b$	Phase B current in the converter	[A]
$I_c$	Phase C current in the converter	[A]
$I_g$	Gate current of a Thyristor	[A]
$I_{h2}$	$2^{\mathrm{nd}}$ -order harmonic component of the operating current	[A]
$I_{h5}$	$5^{\rm nd}$ -order harmonic component of the operating current	[A]
$I_{op}$	Operation current of 87T function	[p.u.]
$I_{opr}$	Operation current of REF function	[p.u.]
$I_{opq}$	Operation current of 87Q function	[p.u.]
$I_{pickumin}$	Minimum pickup current for actuation of 87T function	[p.u.]
$I_{pickuminq}$	Minimum pickup current for actuation of 87Q function	[p.u.]
$I_{pickuminr}$	Minimum pickup current for actuation of REF function	[p.u.]
$I_{res}$	Restriction current of 87T function	[p.u.]
$I_{resq}$	Restriction current of 87Q function	[p.u.]
$I_{resr}$	Restriction current of REF function	[p.u.]
$k_2$	Proportionality constant used in harmonic restriction by $2^{\rm nd}$ harmonic	
$k_{2B}$	Proportionality constant used in harmonic blocking by $2^{\rm nd}$ harmonic	
$k_5$	Proportionality constant used in harmonic restriction by $5^{\rm nd}$ harmonic	
$k_{5B}$	Proportionality constant used in harmonic blocking by $5^{\rm nd}$ harmonic	
$k_r$	Stabilization factor of restriction current of 87T function	
$k_R$	Stabilization factor of REF function	
$L_t$	Converter transformer inductance	[H]
max()	Function that returns the maximum value of a set of values	
$M_{ heta}$	Transformer phase shift compensation matrix	
$M_{ heta,0}$	Transformer phase shift and zero-sequence compensation matrix	

List of Symbols XX

n	Order of harmonic sinusoids in Fourier series	
N	Number of samples per cycle contained in the sample window	
p	Number of pulses of an HVDC converter	
$S_{nom,MVA}$	Nominal power of the transformer	[MVA]
SLP	Slope of the restriction characteristic of 87T function	
$SLP_q$	Slope of the restriction characteristic of 87Q function	
t	Time	[s]
T	Signal period	
$TAP_k$	TAP for normalization of the transformer current in each terminal	
$V_a$	Phase A voltage	[V]
$V_{ab}$	Line voltage between phase A and B	[V]
$V_{ac}$	Line voltage between phase A and C	[V]
$V_b$	Phase B voltage	[V]
$V_{ba}$	Line voltage between phase B and A	[V]
$V_{bc}$	Line voltage between phase B and C	[V]
$V_c$	Phase C voltage	[V]
$V_{ca}$	Line voltage between phase C and A	[V]
$V_{cb}$	Line voltage between phase C and B	[V]
$V_{dc}(t)$	DC voltage of the six-pulse bridge in the time domain	[V]
$V_{dc,\alpha}$	DC average voltage of the six-pulse bridge for a firing angle greater than $0^\circ$	[V]
$V_{dc0}$	DC average voltage of the six-pulse bridge for an $0^\circ$ firing angle	[V]
$V_{dc0,\mu}$	DC average voltage of the six-pulse bridge during commutation overlap	[V]
$V_{nom,k,kV}$	Nominal voltage of the transformer at each terminal	[kV]
$V_p$	Amplitude of phase AC voltage	[V]
$x_k$	kth sample of the signal	

List of Symbols XXI

$X_{im}$	Imaginary part of the phasor	
$X_{opt}$	Inductive reactance in the ATP system	$[\Omega]$
$X_{re}$	Real part of the phasor	
$\alpha$	Firing angle	[degrees]
β	Ignition advance angle	[degrees]
δ	Extinction angle	[degrees]
$\Delta t$	Discrete period of one cycle	
$\theta$	Transformer angular phase shift	[degrees]
$\omega$	Angular frequency	[rad/s]
$\omega_0$	Angular frequency of signal applied in Fourier series	[rad/s]
$\phi_n$	Phase of the n <sup>rd</sup> -order harmonic sinusoid in the Fourier series	

### **GLOSSARY**

AC Alternating Current

ANAFAS Programa de Análise de Faltas Simultâneas

ANAREDE Programa de Análise de Redes Elétricas

ANSI American National Standards Institute

ATP Alternative Transients Program

BIPS Brazilian Interconnected Power System

BPA Bonneville Power Administration

CCC Capacitor Commutated Converter

CIGRE Conférence Internationale Des Grands Reseaux Electriques

CT Current Transformer

CTR Current Transformer Ratio

DC Direct Current

DC Bias DC or quasi-DC currents flowing through the neutral of transformers

EEUG European EMTP-ATP Users Group e.V.

EMTDC Electromagnetic Transients including DC

EMTP Electromagnetic Transients Program

FCDFT Full Cycle Discrete Fourier Transform Filter

FIIC Fault-Induced Inrush Current

GUI Graphical User Interface

HPP Hydro Power Plant

GLOSSARY XXIII

HVDC High Voltage Direct Current

IED Intelligent Electronic Device

IEEE Institute of Electrical and Electronics Engineers

LAPSE Laboratório de Proteção de Sistemas Elétricos

LCC Line-Commutated Converter

MM Mathematical Morphology

OLTC On-load Tap Changer

PSCAD Power System Computer Aided Design

REF Restrict Earth Fault Protection Function

RWEE Ratio of Wavelet Energy Entropy

SLP Slope

SUB Substation

TF13 Transformer  $n^{\circ}$  13

TFYD Converter Transformer Star-delta

TFYY Converter Transformer Star-star

UnB University of Brasilia

WCNPS Workshop on Communication Networks and Power Systems

WEE Wavelet Energy Entropy

ANSI code of Transformer Negative-Sequence Differential Protection Function

87Q B.H. Transformer Negative-Sequence Differential Protection Function with blocking by

harmonics

87Q DLY Transformer Negative-Sequence Differential Protection Function with delay

87T ANSI code of Transformer Differential Protection Function

87T B.H. Transformer Differential Protection Function with blocking by harmonics

GLOSSARY XXİV

87T R.B.H. Transformer Differential Protection Function with restrictions and blocking by harmonics

87T R.H. Transformer Differential Protection Function with restrictions by harmonics

## INTRODUCTION

#### 1.1 CONTEXTUALIZATION OF THE TOPIC

Power systems are primarily based on alternating current (AC) systems; however, advances in Power Electronics have introduced more solutions and equipment based on direct current (DC) systems, such as High Voltage Direct Current (HVDC) transmission systems, which, due to its various applications (briefly demonstrated in Figure 1.1) are increasingly gaining importance (KIM et al., 2009; WATSON; WATSON, 2020; STAN et al., 2022; PADIYAR, 2011).

Plant Complex
Wind Power ②

Wind Power ③

Plant ①

Plant ①

Plant ①

Sol Hz

Flant ①

Sol Hz

Flant ②

Flant ②

Flant ③

Fland Area

Figure 1.1: Various applications of an HVDC system.

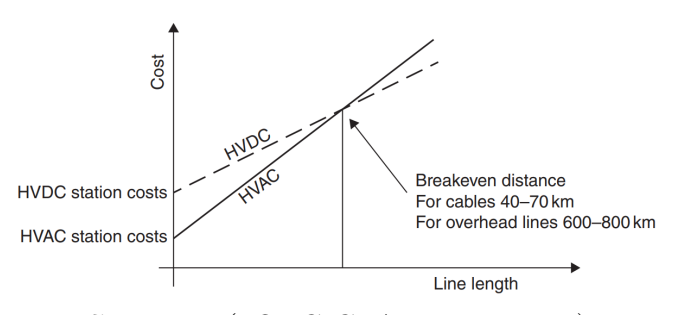
**Source:** (KIM *et al.*, 2009).

The inception of power systems was in DC, but AC systems soon proved to be more advantageous at the beginning due to the use of transformers and the possibility of transmitting electric power at different voltage levels, which resulted in lower losses in transmission systems by utilizing high voltages that are after stepped down and distributed for end-user consumption (HUGHES, 1993; JR, 2002). Electric power generation has also proven simpler in AC systems

due to the simplicity of synchronous generators and the greater ease of generating energy from various sources through these rotating machines (HUGHES, 1993; KIMBARK, 1971).

Nevertheless, even though AC systems are more adopted than DC systems, the advances in Power Electronics in the XX century made HVDC transmission systems an option for power transmissions over longer distances (KIM et al., 2009; PADIYAR, 2011; JOVCIC; AHMED, 2015). The initial capital investment of HVDC systems is higher than AC transmission lines because of the cost of the required apparatus, especially the AC-DC converters. However, as illustrated in Figure 1.2, as the distance increases, HVDC transmission lines require less investment when compared to AC systems in the order of 600-800 km and above, for overhead lines.

Figure 1.2: HVDC and HVAC transmission cost comparison.



Source: (JOVCIC; AHMED, 2015).

The reason for the result presented in Figure 1.2 is the intrinsic reactive energy of AC power systems. Because of the transmission line parameters of inductance and capacitance, and dependent on the power flow and the line length and height, this equipment can produce or consume reactive energy, which directly impacts the voltage of the system (KIMBARK, 1971). Therefore, for long lines, there is a need for reactors, capacitors, and synchronous or static compensators, i.e., the longer the line is, the higher the price to compensate for the effects of the line on the system (KIM et al., 2009; PADIYAR, 2011).

In DC lines, however, its parameters are almost purely resistive in a steady state, meaning a reactive compensation along the line is unnecessary. Besides, DC transmission lines need just two poles, while three-phase systems need three. So, to an equal voltage level, there are fewer costs with wires, towers, and isolation in DC transmission lines (PADIYAR, 2011).

Furthermore, HVDC systems have other advantages over AC transmission systems, such as:

- In AC systems, the maximum power transmitted in a line stably is inversely proportional to its reactance; therefore, the longer the line, the lower the maximum power that can be transmitted stably. This limitation does not occur in DC lines because systems interconnected by HVDC systems do not operate synchronously, so the angular difference between the systems does not define the power transmitted.
- DC lines have a lower environmental impact due to the smaller number of substations, smaller tower sizes, and lower audible noise, for example.
- The AC-DC and DC-AC conversion process of HVDC systems allows control of the transmitted power flow and the connection between systems asynchronously. These characteristics allow the connection between systems with different fundamental frequencies and control of the energy exchange between them.

In Brazil, investments have been made in HVDC systems due to the country's continental size and energy matrix, which primarily rely on hydroelectric power plants (EPE, 2021; ONS, 2024) that are often distant from major load centers. Furthermore, Brazil experiences significant economic and population development disparities, leading to substantial variations in power demand between the Amazon region (North) and other areas, especially the Southeast (ONS, 2024).

In this context, considering the vast hydroelectric potential of the Amazon region, four LCC-HVDC bipoles have been built to transmit energy from large power plants in the North directly to the Southeast. These bipoles were chosen because they offered the best cost-benefit ratio among the evaluated solutions, such as reinforcements in the AC system or a hybrid transmission system using both HVDC systems and AC transmission lines. These projects have expanded the Brazilian DC network, which already included two bipoles in operation since 1984. These existing bipoles transmit the energy produced at 50 Hz by the Itaipu binational plant to the Brazilian Interconnected Power System (BIPS) (Itaipu Binacional, 2024). Altogether, the six existing bipoles in Brazil can transmit up to 20,600 MW, underscoring the significance of these projects.

Furthermore, in line with the current trend of increasing renewable energy generation, the number of wind farms in the country has grown exponentially, primarily concentrated in the Northeast region. With this constant increase, the record of total wind generation in the Brazilian system has been broken several times in 2024, even serving up to 34% of the country's load in instantaneous energy power (ONS, 2023). Like the North region, the Northeast region can only accommodate part of the energy output they generate. Consequently, this surplus energy has also been transmitted through two of the existing bipoles besides the 500 kV AC interconnections, and the demand has grown to such an extent that a new bipole is planned to connect the country's Northeast and Midwest regions (EPE, 2022). All these bipoles are demonstrated in Figure 1.3.

2 × 4000 MW Belo Monte (Xingu) 2×2500 MW  $2 \times 3150 \text{ MW}$ Fraça Aranha  $2 \times 400 \text{ MW (BtB)}$ Madeira River (Porto Velho Collector) 2087 km  $1513~\mathrm{km}$ 2375 km2517 km600 kV DC line in operation  $800~\mathrm{kV}$  DC line in operation 800 kV DC line planned Araraquara 792 kmRio Terminal 820 km 2 × 3150 MV Itaipu (Foz do Iguaç

Figure 1.3: DC transmission lines in Brazil.

**Source:** Own authorship.

An essential part of HVDC systems is the converter transformers. They are part of the connection between DC and AC systems and, among their functions, they adjust the AC voltage level to the designed voltage level for the HVDC system, allow the increase of the number of pulses of the converter (reducing harmonics generated by AC-DC and DC-AC conversion), and play a critical role in converter control through their tap switching (JOVCIC; AHMED, 2015;

1.2 - MOTIVATION 5

ZHAO, 2018).

Additionally, converter transformers are costly to produce and transport due to their large size, resulting in extended replacement periods in equipment loss or relatively long maintenance periods in the event of breakdowns (ANDERSON et al., 2022; ZHAO, 2018). Therefore, protecting these devices is a fundamental part of the overall HVDC system protection strategy, making targeted studies of their specific protection requirements crucial.

#### 1.2 MOTIVATION

With the increasing importance of HVDC systems in Brazil and worldwide, studying converter transformer protection holds significant relevance. When a fault occurs within the transformer, even when it causes HVDC pole blocking, the fault location must be detected quickly, providing a reliable indication of an internal short circuit. This indication ensures that the transformer is not energized with a fault present, preventing the worsening of the failure and further damage to the equipment and enabling faster maintenance on the specific problem.

Despite the unique aspects of converter transformers, their fundamental operation is directly comparable to conventional transformers, and their protection generally utilizes traditional transformer protection functions such as transformer differential protections as the main ones (ANDERSON et al., 2022; BLACKBURN; DOMIN, 2007). However, since differential protection fundamentally compares the transformer terminals, the connection to the converter may or may not negatively impact the performance of these protections, and investigating this impact is crucial.

As a result, a few studies have been conducted explicitly addressing the differential protection of HVDC converter transformers. Moreover, none have assessed the transformer negative-sequence differential protection (ANSI code 87Q) or Restrict Earth Fault protection (ANSI code 87N or REF) functions nor examined turn-to-turn and turn-to-ground faults. Hence, in this work, a complete analysis of the current differential functions for transformers will be carried out, from transformer phase differential protection (ANSI code 87T) to the 87Q and REF functions. Also, faults in the phases and turns of the transformers will be evaluated.

1.3 - OBJECTIVES 6

#### 1.3 OBJECTIVES

The main objective of this dissertation is to evaluate the performance of the differential functions 87T, 87Q, and REF applied to HVDC converter transformers by a case study on the converter transformers connected to the inverter station of a bipole of the HVDC Madeira River link. Thereby, it was established the specific objectives:

- Conduct a literature review on the fundamentals of Direct Current (DC) Transmission and the typology of DC-AC Converters, as well as the fundamentals of phasor-based transformer differential protection and transformer negative-sequence differential protection function, applied to HVDC converter transformers;
- Adjust the Madeira Complex model on ATPDraw, modeled by (TAVARES, 2020) based on the CIGRE Benchmark System for HVDC studies, to simulations on converter transformers;
- Run simulations in the Alternative Transients Program (ATP) and finally evaluate the performance of 87T, 87Q, and REF protection in HVDC converter transformers connected to a converter operating in inverter mode, under different short circuit conditions.

#### 1.4 CONTRIBUTIONS

Present an evaluation of the performance of functions 87T, 87Q, and REF in HVDC converter transformers, verifying various scenarios of short circuits, interns, and externals to transformers. Therefore, it is expected that the challenges and benefits of this equipment protection are addressed, considering the particularities of the voltage and current signals in the CTs of these transformers, the harmonics in the network generated by the AC-DC conversion and inversion, and a reflection of possible solutions to the challenges noted.

Consequently, it is also expected to contribute to the evolution of the usability and reliability of HVDC systems in Brazil.

1.5 - PUBLICATIONS 7

#### 1.5 PUBLICATIONS

Part of the studies developed during the master's program conducted at the Electrical Systems Protection Laboratory (LAPSE-UnB) led to the publication of the following papers at an international conference:

- OLIVEIRA, G. S.; SILVA, C. C. de S.; RIBEIRO, N. S. S.; SILVA, K. M. "HVDC Converter Transformers Protection Part 2: Differential Function Assessment". 2023

  Workshop on Communication Networks and Power Systems (WCNPS), 2023, p. 1–7.
- SILVA, C. C. de S.; OLIVEIRA, G. S.; RIBEIRO, N. S. S.; SILVA, K. M. "HVDC Converter Transformers Protection Part 1: Signal Processing Aspects". 2023 Workshop on Communication Networks and Power Systems (WCNPS), 2023, p. 1–7.
- OLIVEIRA, G. S.; SILVA, K. M. "Assessment of Differential Protection Applied to LCC-HVDC Converter Transformers". *International Conference on Power Systems Transients (IPST)*, 2025, p. 1-8.

#### 1.6 TEXT ORGANIZATION

This work is organized as follows:

- Chapter 2 presents the basic operating principles of HVDC systems, including their converter stations, converter transformers, AC and DC filters, and smoothing reactors.
- Chapter 3 reviews the fundamentals of the transformer differential protection function and transformer negative-sequence differential protection function, citing the possible situations that may cause improper actuation of the protections and the solutions typically used.
- Chapter 4 provides a brief review of various scientific works that address the 87T function in HVDC converter transformers;
- Chapter 5 presents the ATP model used as well as the Madeira Complex, which is the HVDC base system to simulations, and the computational implementations in Python of

functions 87T, 87Q and REF.

- Chapter 6 presents the results found in computer simulations and addresses the analysis of the performance of differential protections in the modeled system.
- Chapter 7 presents the main conclusions of the work, emphasizing proposals for future research in the study area.

# FUNDAMENTALS OF HVDC SYSTEMS

This chapter presents the fundamentals of Line-Commutated Converter (LCC) HVDC systems, which are thyristor-based and whose technology matches the technology implemented in the Brazil bipoles.

Figure 2.1 shows a typical LCC-HVDC schematic interconnecting two AC systems and their main components, where the most relevant among them for this work and for a better understanding of LCC-HVDC systems will be discussed throughout this chapter.

**Smoothing Smoothing** Terminal 1 Terminal 2 reactor reactor AC system 1 Transformer CB AC system 2 3 phase  $V_{1g}$ ,  $f_1$ DC line  $I_{1dc}$  $I_{2dc}$ 3 phase  $V_{2q}$ ,  $f_2$ Thyristor **Thyristor**  $V_{2dcp}$ bridge  $V_{1dcp}$ bridge Transformer CB Thyristor **Thyristor** Transformer bridge bridge DC line Transformer Filters 3 Filters Electrodes Reactive power Reactive power compensation compensation Station 1 Communication Station 2 control control system

Figure 2.1: Typical LCC-HVDC schematic (12-pulse monopole with metallic return).

Source: (JOVCIC; AHMED, 2015).

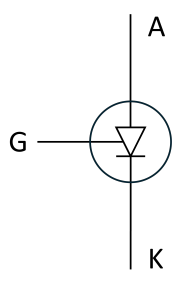
## 2.1 HVDC CONVERTER STATIONS

As mentioned before, the power electrical systems are AC-based. Hence, the applications of HVDC systems consist necessarily of two terminals: a rectifier station for AC/DC conversion

and an inverter station for DC/AC inversion, which permits transmission in DC between the stations.

In LCC-HVDC systems, the converter station is built by a set of thyristors connected and controlled to rectify or invert. This equipment has three terminal connections, as shown in Figure 2.2. They are A-anode, K-cathode, and G-gate.

Figure 2.2: Symbol for thyristor.



Source: Own authorship.

A thyristor can be understood as a controllable diode. When a current on the gate is applied  $(I_g > 0)$ , the device starts to work similarly to a diode. It conducts current from the anode to the cathode if a forward voltage across the device (voltage in A > voltage in K) exceeds its critical limit (KIM *et al.*, 2009). In this case, the device switches to the ON state.

After starting to conduct, the current on the gate can be removed, and the device will keep conducting while there is a forward voltage and the current remains above the holding level. To turn it off, the current through the device must drop below the holding current—a condition that typically occurs when the voltage across the device becomes zero or when it is reverse-biased (voltage in K> voltage in A). Once turned off, the thyristor behaves like an open circuit in both directions (OFF state) (KIM et al., 2009). Thus, it remains until the gate current is applied again, together with a forward voltage.

Considering the thyristor operation, the standard configuration and control used in LCC-HVDC converter stations will be presented below: a six-pulse converter (Graetz bridge) and a twelve-pulse converter.

#### 2.1.1 Six-pulse converters

To effectively understand AC/DC conversion and control in an HVDC converter, it is beneficial to begin with the simplest topology: a three-phase full-bridge diode converter (as shown in Figure 2.3). This converter operates similarly to a thyristor converter with a zero delay angle ( $\alpha$ ). Since the delay angle is used to control the thyristor pulses—essentially governing the converter—the diode converter is essentially a three-phase uncontrolled bridge (JOVCIC; AHMED, 2015).

 $V_{a} = V_{c}$   $V_{a} = V_{c}$   $D_{1}$   $D_{3}$   $D_{5}$   $V_{dc}$   $V_{dc}$   $D_{4}$   $D_{6}$   $D_{2}$ 

Figure 2.3: Diode six-pulse AC/DC converter.

Source: (JOVCIC; AHMED, 2015).

Assuming the AC system is symmetrical and balanced and the converter is connected to an infinite bus of zero source impedance (which eliminates any overlap in the conduction of the thyristors (KAMAKSHAIAH; V., 2011)), the phase voltages are phase-shifted by 120°, and its behavior is demonstrated in the voltage plot in Figure 2.4. Likewise, knowing that a diode will conduct just when its anode voltage is higher than its cathode, the currents  $I_a$ ,  $I_b$ , and  $I_c$  result can also be observed in Figure 2.4, at the current plot.

For a better understanding and example, and considering that Figure 2.4 represents the AC voltage and current of a converter operating as a rectifier, note that the current  $I_c$  is greater than zero at the beginning of the plot. This indicates that diode D5 behaves like a short circuit, and its anode voltage is practically equal to  $V_c$ . Therefore, the D1 anode voltage is higher than its cathode voltage, and it functions as an open circuit. Thereby, current  $I_a$  remains zero while

 $V_c$  is higher than  $V_a$ , and, after that, when  $V_a$  becomes higher than  $V_c$ , the situation reverses, D1 becomes a short circuit,  $I_a$  increases, and D5 becomes an open circuit.

In the meantime,  $V_b$  was in its negative half-cycle. Thus, the D6 cathode was more negative than its anode, making it also a short circuit and maintaining the electric potential difference  $V_{dc}$  and, consequently, the current  $I_{dc}$ , which can be observed in Figure 2.5. Consequently, the voltage  $V_{dc}$  and current  $I_{dc}$  never become negative, as expected for a DC circuit.

Furthermore, in this configuration, to a symmetrical and balanced three-phase system, there will always be two diodes conducting: one of D1, D3, or D5 and one of D4, D6, or D2, while the others work as an open circuit. Hence, the current  $I_{dc}$  will always be from D1, D3, or D5 to D4, D6, or D2. Thus, the sequence would be D1-D6, D1-D2, D3-D2, D3-D4, D5-D4, D5-D6 and starts over, changing the pair each  $60^{\circ}$  and each diode alone each  $120^{\circ}$ . Consequently, the voltage  $V_{dc}$  follows the voltage difference between phases:  $V_{ab}$ ,  $V_{ac}$ ,  $V_{bc}$ ,  $V_{ba}$ ,  $V_{ca}$  and  $V_{cb}$ .

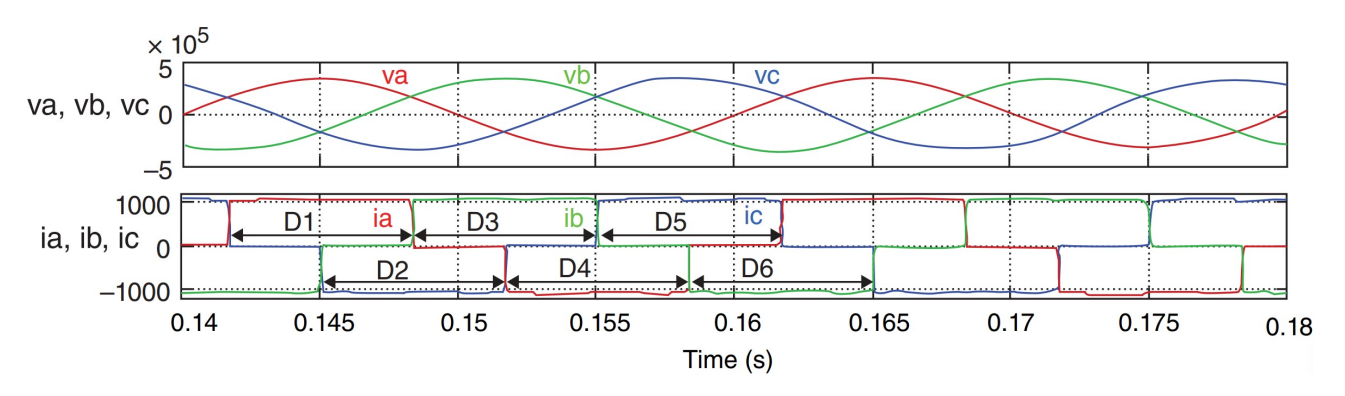


Figure 2.4: Voltage and current AC plot.

**Source:** Adapted from (JOVCIC; AHMED, 2015), with modifications.

Although the voltage  $V_{dc}$  is already a DC voltage, in Figure 2.5, it is clear that there is a ripple on this voltage and consequently on current  $I_{dc}$ . This ripple occurs because of the sinusoidal voltages. When D1 starts to conduct, i.e., D1-D6 conducting and  $V_{dc} = V_{ab}$ ,  $V_a$  is increasing more than  $V_b$  is decreasing, so in a specific moment,  $V_{dc}$  reaches the maximum and decreases with  $V_b$  increasing and  $V_a$  decreasing, repeating this cycle each 60°. Therefore, there are six cycles of this ripple in each cycle of the AC voltage. The diode bridge average DC voltage can be calculated by the integration of DC voltage  $V_{dc}(t) = \sqrt{3}V_p cos(\omega t)$  in ripple cycle  $(\omega t = \pi/3)$ , where  $V_p$  is the amplitude of phase AC voltage:

$$V_{dc0} = 2\frac{3}{2\pi} \int_{-\frac{\pi}{6}}^{+\frac{\pi}{6}} \sqrt{3} V_p \cos(\omega t) d(\omega t) = \frac{3\sqrt{3}}{\pi} V_p$$
 (2.1)

 $\times 10^{5}$ Vdc 5.54.5 1100 ldc ldc 1050 1000 <u></u> 0.145 0.15 0.155 0.16 0.165 0.17 0.175 0.18 Time (s)

Figure 2.5: Voltage and current DC plot.

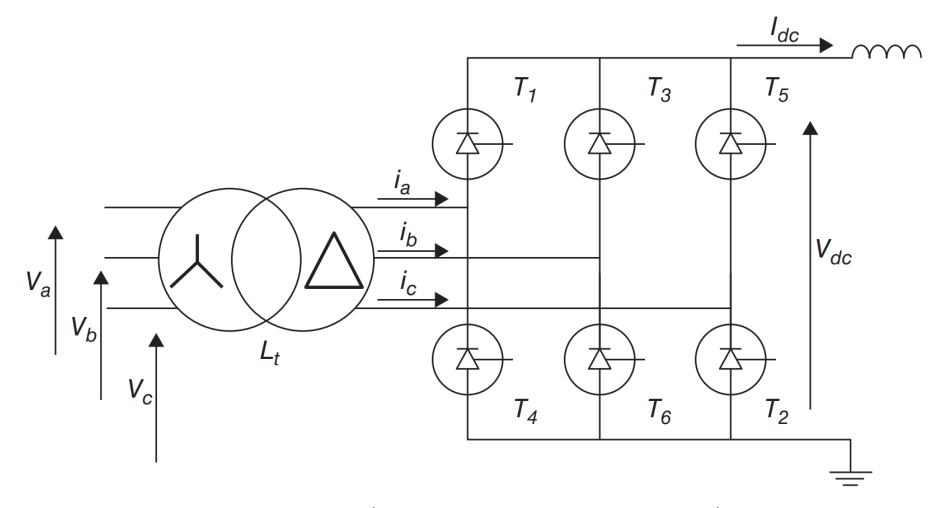
Source: Adapted from (JOVCIC; AHMED, 2015), with modifications.

Now, considering the converter topology in Figure 2.6, where instead of diodes, the bridge is configured with thyristors, the moment at which the thyristors start to conduct can be controlled through their gate current. Hence, the ON state can be delayed from the positive thyristor forward voltage instant, represented by the firing-delay angle  $\alpha$ .

Figures 2.7 and 2.8 compared with the current plot of Figure 2.4 and voltage plot of Figure 2.5 illustrate the impact of a delay from an  $\alpha = 30^{\circ}$  and the commutation overlap phenomenon (explained later) on thyristors current and  $V_{dc}$  voltage.

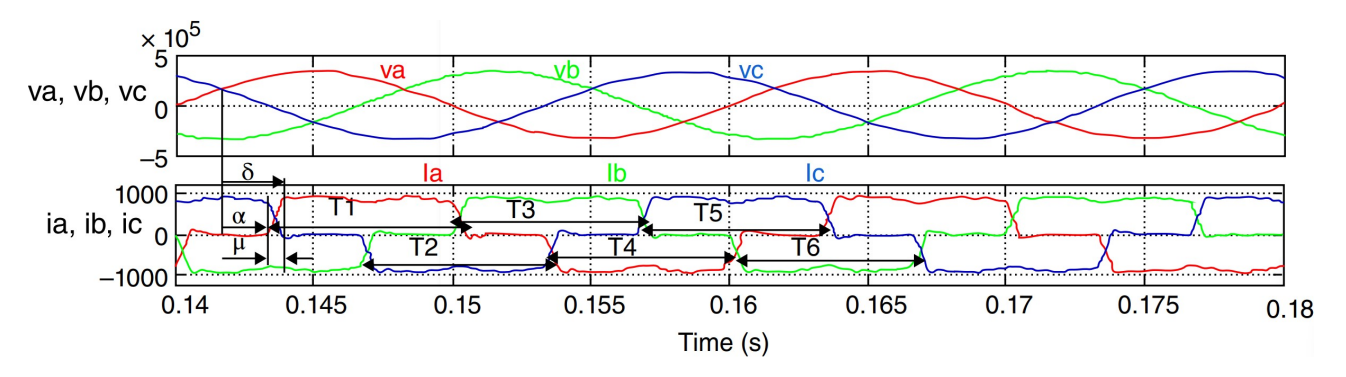
Observing the  $V_{dc}$  plot on Figure 2.8, it becomes clear that a higher  $\alpha$  value decreases the bridge DC voltage average. For instance, delaying the ON state of T1 as demonstrated in Figure 2.7,  $V_{dc} = V_{cb}$  for a longer time, while in this time,  $V_c$  is decreasing and  $V_b$  is increasing, reducing  $V_{dc}$  and, hence,  $V_{dc}$  average (Figure 2.8).

Figure 2.6: Thyristor six-pulse AC/DC converter with a transformer.



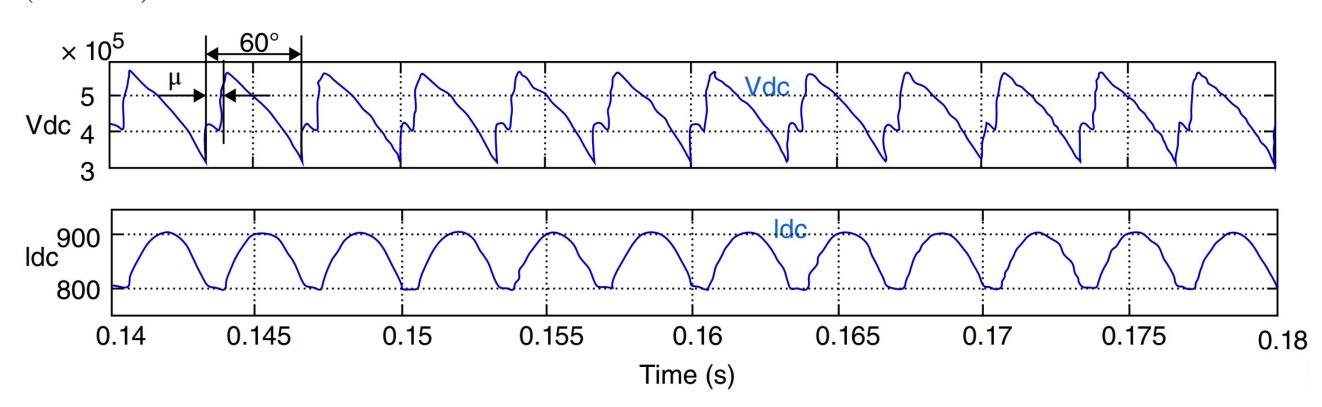
Source: (JOVCIC; AHMED, 2015).

Figure 2.7: Voltage and current AC plot with transformer  $(L_t = 0.1H)$  and ignition delay  $(\alpha = 30^{\circ})$ .



Source: Adapted from (JOVCIC; AHMED, 2015), with modifications.

Figure 2.8: Voltage and current DC plot with transformer  $(L_t = 0.1H)$  and ignition delay  $(\alpha = 30^{\circ})$ .



Source: Adapted from (JOVCIC; AHMED, 2015), with modifications.

Therefore, neglecting again the commutation overlap for a while, the average DC voltage of the thyristor converter can be obtained by adding the delay angle to the integration:

$$V_{dc0,\alpha} = 2\frac{3}{2\pi} \int_{-\frac{\pi}{6} + \alpha}^{+\frac{\pi}{6} + \alpha} \sqrt{3} V_p \cos(\omega t) d(\omega t) = \frac{3\sqrt{3}}{\pi} V_p \cos\alpha$$
 (2.2)

In other words:

$$V_{dc0,\alpha} = V_{dc0}\cos\alpha\tag{2.3}$$

Equation 2.3 then demonstrates that the output voltage of the thyristor converter can be controlled by  $\alpha$ .

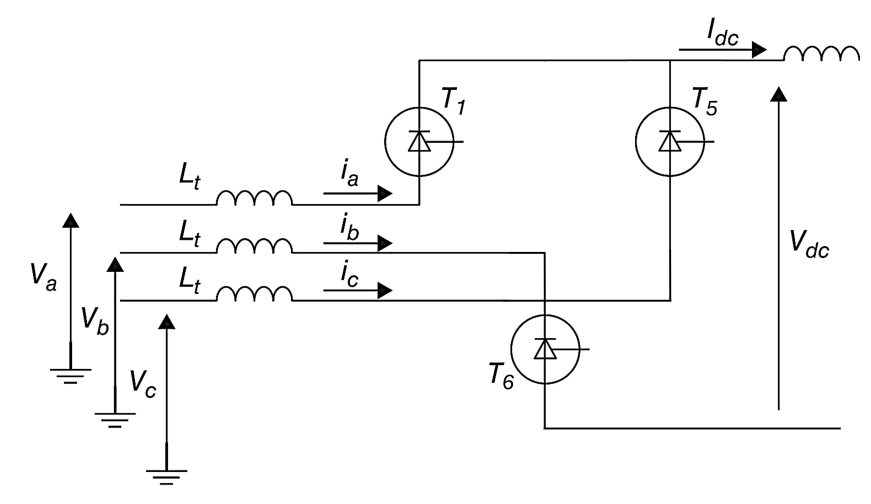
## 2.1.1.1 Commutation overlap in a thyristor converter

The commutation overlap occurs due to the reactance of the AC system connected to the converter, mainly the converter transformer inductance (JOVCIC; AHMED, 2015; KIM et al., 2009). This inductance opposes the current variation at thyristors and impedes the instantaneous commutation between thyristor pairs. To illustrate, with a transformer inductance  $(L_t)$  of 0.1H, the commutation of T1 to ON state takes the time shown in Figure 2.7, represented by angle  $\mu$ , after a pulse on its gate (JOVCIC; AHMED, 2015). In the same way, T5 takes an equal time to commutate to the OFF state. For this reason, three thyristors conduct simultaneously during commutation overlap, as exemplified in Figure 2.9. Thus, the sequence of thyristor conducting become T5-T1-T6, T1-T6, T6-T1-T2, T1-T2, T1-T3-T2, T3-T2, T2-T3-T4, T3-T4, T3-T4, T3-T4, T5-T4, T4-T5-T6, T5-T6 (KIMBARK, 1971).

The consequence of three thyristors simultaneously conducting is that the  $V_{dc}$  voltage is no longer the difference between the voltage of two phases. At this time, there is an elevation and a reduction of  $V_{dc}$ , as well observed in Figure 2.8, where the conclusion of DC voltage elevation happens just after the overlap commutation.

To calculate  $V_{dc}$  during commutation overlap, observing the Figure 2.9 is helpful. From there, it can be assumed:

Figure 2.9: Converter equivalent circuit during commutation.



Source: Adapted from (JOVCIC; AHMED, 2015), with modifications.

$$V_a = L_t \frac{\mathrm{d}I_a}{\mathrm{d}t} + V_{dc,\mu} \tag{2.4}$$

$$V_c = L_t \frac{\mathrm{d}I_c}{\mathrm{d}t} + V_{dc,\mu} \tag{2.5}$$

Then, assuming balanced  $L_t$  inductances,  $I_a$  is equal to  $-I_c$ , as well as demonstrated in Figure 2.7. Therefore (FERNANDES, 2020):

$$\frac{\mathrm{d}I_a}{\mathrm{d}t} + \frac{\mathrm{d}I_c}{\mathrm{d}t} = 0\tag{2.6}$$

$$\frac{V_a - V_{dc,\mu}}{L_t} + \frac{V_c - V_{dc,\mu}}{L_t} = 0 {(2.7)}$$

Thus,  $V_{dc,\mu}$  is obtained:

$$V_{dc} = \frac{V_a + V_c}{2} \tag{2.8}$$

Finally, as shown in Figure 2.8, the overlap commutation causes a reduction of average DC voltage by the average of  $V_{dc}$  during commutation  $(V_{dc0,\mu})$ . This voltage drop can be calculated considering the surface is below the curve (JOVCIC; AHMED, 2015):

$$V_{dc0,\mu} = \frac{1}{2\pi/3} \int_{\alpha}^{\delta} \left[ V_a - \frac{V_a + V_c}{2} \right] d(\omega t)$$
 (2.9)

$$V_{dc0,\mu} = \frac{V_{dc0}}{2} (\cos \alpha - \cos \delta) \tag{2.10}$$

Whereupon  $\delta = \alpha + \mu$ , and, accordingly:

$$V_{dc} = V_{dc0} \cos \alpha - V_{dc0,\mu} \tag{2.11}$$

$$V_{dc} = V_{dc0} \frac{\cos \alpha - \cos \delta}{2} \tag{2.12}$$

#### 2.1.1.2 Inverter operation

Based on Equation (2.3) and all previous considerations, the DC voltage becomes negative as the  $\alpha$  increases over 90°, and the converter operates as an inverter. Then, like the HVDC configuration shown in Figure 2.1, while a terminal operates with a firing angle below 90° (rectifier station), the other terminal necessarily operates as an inverter (90° <  $\alpha$  < 180°). Thus, working as inverters, the thyristors 1, 3, and 5 will conduct when their cathode voltages are the most negative. In contrast, thyristors 4, 6, and 2 will conduct when their anode voltages are the highest positive relative to other thyristors in the same group.

Moreover, the commutation delay caused by reactance requires considering an extinction angle ( $\delta$ ) on the  $\alpha$  calculation to guarantee enough margin for thyristors to conclude their commutation. Consequently, a total inverter operation ( $\alpha = 180^{\circ}$ ) can not be reached, being necessary to calculate the superior limit that ensures the commutation conclusion and avoids a commutation failure on inverter operation (ARRILLAGA, 2008; KIM *et al.*, 2009; PADIYAR, 2011; JOVCIC; AHMED, 2015). Then, it is helpful to use the following angle definitions for inversion mode (JOVCIC; AHMED, 2015):

- Ignition advance angle  $\beta = 180^{\circ} \alpha$ . Thereby  $\cos(\beta) = -\cos(\alpha)$ .
- Extinction advance angle  $\gamma = 180^{\circ} \delta$ ,  $\cos \gamma = -\cos \delta$ . So:  $\mu = \delta \alpha = \beta \gamma$ .

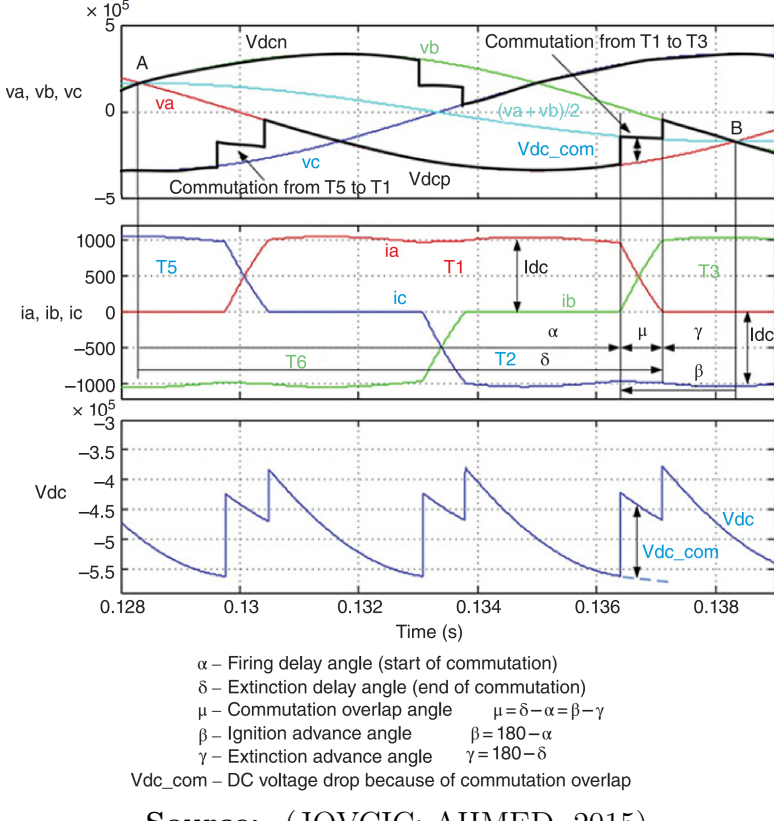


Figure 2.10: Commutation from thyristors T1 to T3 (phase A to B) in inversion mode.

Source: (JOVCIC; AHMED, 2015)

Figure 2.10 demonstrates how inverter operations perform and the extinction angle importance. In the case of a  $\beta = 0^{\circ}$ , the thyristor T1 would still conduct right after point B when  $V_a$  is already higher than  $V_b$ . So, even with a pulse on the T3 gate, T3 would not conduct because its cathode would equal  $V_a$ , keeping T1 forward-biased and T3 backward-biased, performing as an open circuit. In this way, there would not be a commutation.

Finally, writing Equation 2.11 and 2.12 with the inverter angles:

$$V_{dc} = -V_{dc0}\cos\beta - V_{dc0.u} \tag{2.13}$$

$$V_{dc} = -V_{dc0} \frac{\cos \beta - \cos \gamma}{2} \tag{2.14}$$

#### 2.1.1.3 Commutation Failure

As mentioned, the extinction angle is critical to avoid commutation failures in inverter operation. In cases where a commutation overlap lasts longer than expected, or the extinction angle is insufficient, the commutation between two thyristors does not complete before the thyristor being turned off is blocked by reverse voltage. So, the thyristor continues to conduct during the next cycle. Thus, shortly after the failure, after the following 60°, the opposite thyristor of the same phase in this converter is triggered, creating a short circuit between the DC terminals of the inverter (PADIYAR, 2011; JOVCIC; AHMED, 2015).

Figure 2.11 illustrates a commutation failure caused by reduced AC voltage in the system, which leads to an increase in DC current, consequently prolonging the commutation overlap between thyristors T1 and T3. As this overlap duration increases, a point is reached where voltage  $V_a$  exceeds  $V_b$  while both thyristors are still conducting, causing T3 to be blocked again. At the same time, T1 continues to conduct, resulting in a commutation failure. Then, immediately after T3 blocking, T4—connected to the same phase as T1—is triggered, causing a DC short circuit, as depicted in Figure 2.12.

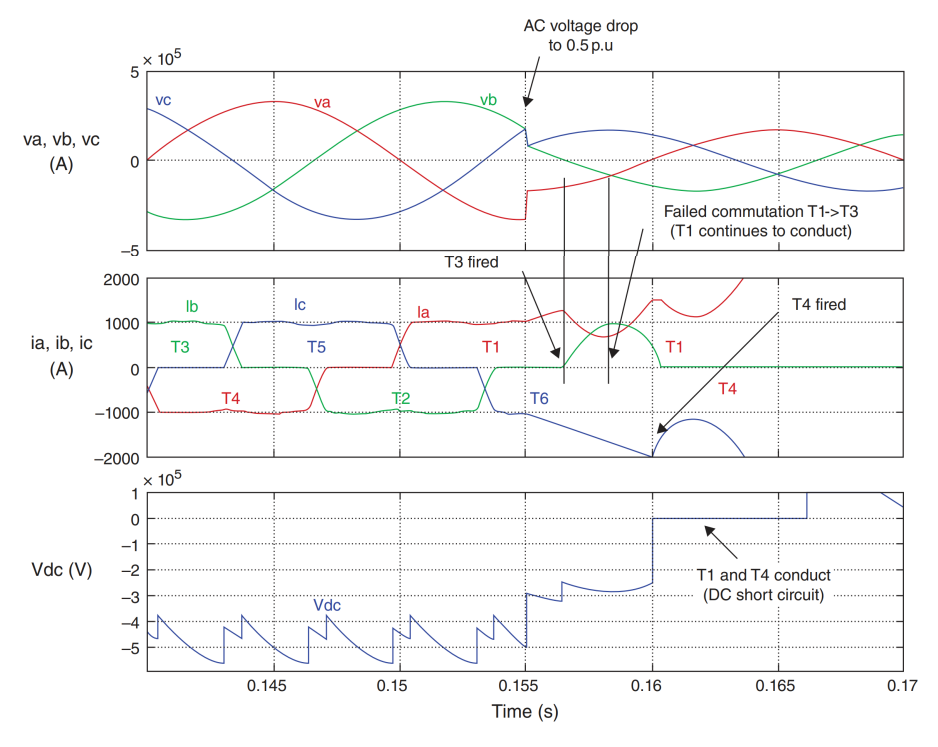


Figure 2.11: Inverter commutation failure simulation.

Source: (JOVCIC; AHMED, 2015)

 $V_{a} = 0$   $V_{a} = 0$   $V_{b} = V_{c}$   $V_{dc} = 0$   $V_{dc} = 0$   $V_{dc} = 0$ 

Figure 2.12: DC current path during commutation failure.

Source: (JOVCIC; AHMED, 2015)

Commutation failures themselves are not critical phenomena for HVDC systems. The converters tend to recover within a few cycles if the cause of the failure is solved (JOVCIC; AHMED, 2015). The primary consequences of commutation failures are the reduction of  $V_{dc}$  to zero and an increase in the HVDC system current, alongside interruption of the AC current and, thus, power flow to the AC system (PADIYAR, 2011). Nevertheless, the increase in DC current is limited by the smoothing reactor in the HVDC system, and the AC system experiences no voltage reduction, nor does it see the fault. For weaker AC systems, however, the interruption of power flow may cause a disturbance due to the decrease in active power (JOVCIC; AHMED, 2015).

The recovery of the HVDC system after a commutation failure depends primarily on the control system response and the AC system voltage. Generally, if there is an increase in angle  $\beta$  after detecting a commutation failure, there is a high likelihood of subsequent commutation failures not occurring (PADIYAR, 2011).

## 2.1.2 Twelve-pulse converters

Although the controlled six-pulse converters are functional in converting AC voltage to DC, there remains a ripple in voltage and current, as shown in Figure 2.8, that can be reduced to improve the HVDC system and reduce the negative impact on the AC system. The commuta-

tion between thyristors causes a non-sinusoidal AC current format (Figure 2.7). Consequently, HVDC converters generate characteristic harmonics intrinsic to their functioning, voltage harmonics on the DC side, and current harmonics on the AC side (ARRILLAGA, 2008).

Noncharacteristic harmonics are also generated. It results from a non-ideal system, including, for example, an unbalanced AC system, converter transformer asymmetry, and converter asymmetry (JOVCIC; AHMED, 2015).

The characteristic harmonics generated by HVDC converters are based on the number of pulses of the converter configuration (ARRILLAGA, 2008; PADIYAR, 2011). For a converter, the order of harmonics presented are (PADIYAR, 2011):

• On DC side:

$$h_{DC} = np (2.15)$$

• On AC side:

$$h_{AC} = np \pm 1 \tag{2.16}$$

where n is an integer and p is the number of pulses.

Thus, the six-pulse converter lowest AC current harmonics are 5<sup>th</sup> and 7<sup>th</sup>, which causes a wider range of harmonics and, consequently, the need for more filters to soften the impact on the AC system.

The better way to reduce the issue is by increasing the number of pulses. The more common approach is using a twelve-pulse converter, where the lowest AC current harmonics become 11<sup>th</sup> and 13<sup>th</sup>, while the lowest DC voltage harmonic becomes 12<sup>th</sup>. This strategy reduces the amount of harmonics and, consequently, the number of filters.

The twelve-pulse converter is built by two six-pulse converters connected in series, as observed in 2.1; after that, the converter DC voltage is the sum of the two six-pulse converter DC voltage. Moreover, to perform this configuration, it is necessary to use specific configurations of the converter transformers to maintain a 30° phase shift between the voltage of two converters. For instance, in 2.1, there is a standard twelve-pulse configuration with a star-star (Y : Y) converter transformer parallel with a star-delta  $(Y : \Delta)$  converter transformer. The reason for

that is demonstrated in Figure 2.13, where the resulting DC voltage turns to a cycle each 30° (i.e., twelve pulses). This modification reduces the ripple and the harmonics.

Voltage (V)

V12,DC

30°

VY,DC

VA,DC

60°

60°

Figure 2.13: DC voltage of a twelve-pulse converter.

Source: Own authorship.

Time (s)

The harmonic reduction cause on the AC side is shown in Figure 2.14. Based on Kirchhoff's current law, the current in the AC side is the sum of the currents of the two transformers. Therefore, with the 30° phase shift, the current becomes closer to a sinusoidal signal.

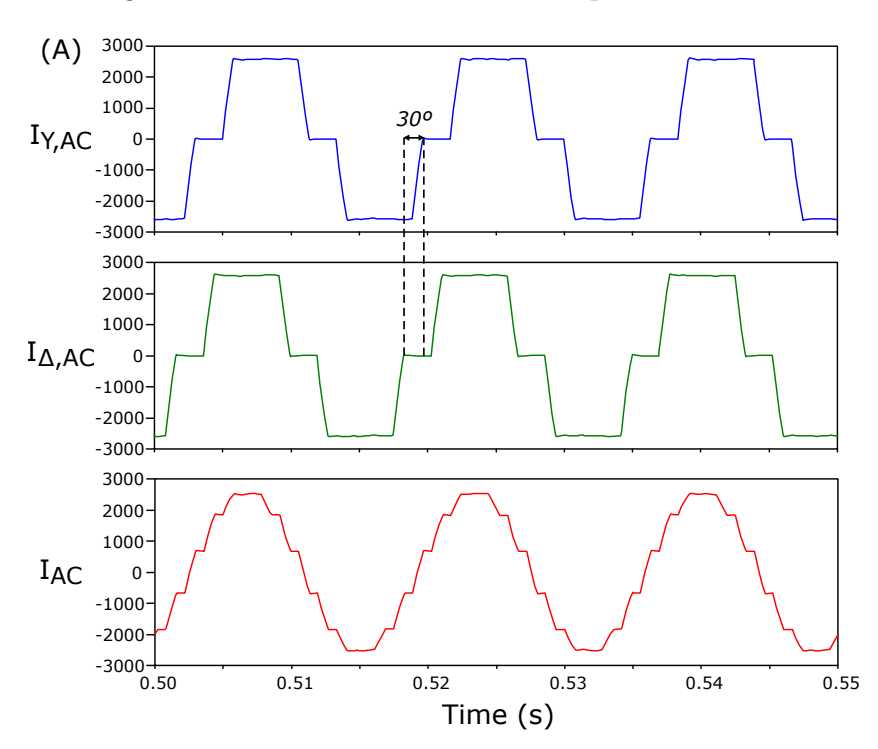


Figure 2.14: AC current of a twelve-pulse converter.

Source: Own authorship.

#### 2.2 CONVERTER TRANSFORMERS

The converter transformers are essential equipment for HVDC systems. Their primary function is to adapt the AC voltage to the level required by the converters. For this reason, besides the nominal voltage transformation, the converter controller uses the transformer tap changer in cooperation with  $\alpha$  to maintain the desired DC voltage with a safe  $\alpha$  and  $\beta$  margin and limit the impact of steady-state AC voltage variations on the converter (ZHAO, 2018). Part of a simplified controller schematic of an HVDC converter operating as a rectifier is demonstrated in Figure 2.15, where it is possible to observe the relation between the control by angle and the tap changer to help maintain a nominal operating angle.

Typically,  $\alpha$  ranges from 15° to 20° to have a sufficient margin to compensate disturbances to the AC voltage, and low enough to reduce reactive power and harmonics. Simultaneously, in inverter operation,  $\gamma$  is restrained to 17-18° to avoid commutation failures (ARRILLAGA, 2008; KIM *et al.*, 2009; PADIYAR, 2011; JOVCIC; AHMED, 2015).

 $\alpha = 18 deg$ Switch  $\delta_2$   $\delta_3$   $\delta_4$ firings  $\delta_3$   $\delta_4$ interval  $\delta_5$   $\delta_6$ Tap changer controller

Up step logic and down step logic  $\alpha = 18 deg$ Tap changer command

Figure 2.15: Part of a converter controller.

Source: Adapted from (JOVCIC; AHMED, 2015), with modifications.

Furthermore, the converter transformers also contribute to other functions (ZHAO, 2018):

- Galvanic isolation between AC and DC systems;
- Limiting the fault currents flowing back to the AC systems when a short circuit occurs on the valve arms or the DC busbar;

• Providing the necessary phase shift between two six-pulse converters to employ a twelvepulse converter.

Converter transformers are similar to conventional transformers; however, due to their interconnection with AC systems and converters, they have some differences in their construction materials to handle the superimposed requirements of both sides (ZHAO, 2018). In addition to the insulation and performance requirements of conventional power transformers, the HVDC converter transformer should handle DC voltage and current stresses and a substantially more significant amount of harmonics due to the converters, which causes additional losses and stresses in the windings (ZHAO, 2018).

The design requirements of converter transformers result in equipment that is physically very large (Figure 2.16) and expensive to manufacture and transport. Consequently, in the event of equipment loss or failure, replacement and repair processes are associated with extended lead times and prolonged maintenance periods (ANDERSON et al., 2022; ZHAO, 2018). Furthermore, an essential aspect of the design and construction of converter transformers is their inherent inductance, which is the primary contributor to commutation overlap (JOVCIC; AHMED, 2015; KIM et al., 2009). This characteristic can significantly influence both the occurrence and prevention of commutation failures in LCC-HVDC systems.

#### 2.3 DC AND AC FILTERS

Subsection 2.1.2 explains briefly about the impact of the harmonics generated by HVDC systems. These impacts decrease the energy quality of AC grids around HVDC systems and the DC voltage of HVDC systems themselves. For this reason, installing filters on the AC and DC sides is necessary to mitigate some of these impacts.

The primary source of these harmonics in a regular operation is the rectification and inversion process of converters, which are based on thyristors commutation and generate harmonics on the AC and DC sides. After that, another great source of harmonics is the inrush current caused by converter transformers during energization.

As also seen in Subsection 2.1.2, the harmonics generated by HVDC converters depend on the number of converter pulses, so the order of harmonics generated is defined by Equations



Figure 2.16: 1100 kV HVDC converter transformer by Siemens.

Source: (T&D India, 2017)

2.15 and 2.16. I.e., np at the DC side and  $np \pm 1$  at the AC side, where n is an integer, and p is the number of pulses. Consequently, it is clear that increasing the number of pulses of a converter is a method to mitigate harmonics; however, increasing the number of pulses requires more expensive transformers. Then, for the 12-pulse converters, filters at both the AC and DC sides are more economically viable for reducing the quantity of harmonics.

While DC filters are exclusively used to reduce harmonics, AC filters also provide a reactive power supply, compensating part of the reactive absorbed by converters due to the phase shift between voltage and current because of  $\alpha$  and  $\beta$  and commutation overlap. This reactive compensation is significant because the demand for reactive power can reach 60% of DC link active power (ARRILLAGA, 2008).

Usually, AC filters are tuned filters for the two or four lowest AC harmonics, like 11<sup>th</sup> and 13<sup>th</sup> to 12-pulse converters, and damped (high-pass) filters for higher order harmonics (JOVCIC; AHMED, 2015). At the same time, DC filters are commonly 12<sup>th</sup>-order to 12-pulse converters in HVDC systems with overhead lines, as the DC cables have a high capacitance that naturally reduces harmonics. Figure 2.17 shows an example of filter arrangement for a 12-pulse HVDC terminal.

AC system three-phase V<sub>s</sub>, f<sub>s</sub> wither three-phase V<sub>s</sub>, f<sub>s</sub> the three-phase V<sub>s</sub> the three-phase V<sub>s</sub> the three-phase V<sub>s</sub> the three-phase V<sub>s</sub> that three-phase V<sub>s</sub> the three-phase V<sub>s</sub> the three-phase V<sub>s</sub> that three-phase V<sub>s</sub> 
Figure 2.17: HVDC station with harmonic filters.

# Source: (JOVCIC; AHMED, 2015)

#### 2.4 SMOOTHING REACTOR

The smoothing reactor is a crucial component in the operation of HVDC systems. It is connected in series with the system line or the intermediate circuit for Back-to-Back systems. Its primary functions are as follows (PADIYAR, 2011; KIM et al., 2009):

- Reducing sudden increases in DC current during AC system voltage dips or DC system faults due to its inductive characteristic, which inherently opposes changes in current.
- Minimizing occurrences of commutation failure in the inverter by limiting current surges caused by disturbances beyond the system's control.
- Smoothing the ripple in the direct current to prevent the current from becoming discontinuous at light loads and decreasing DC harmonic voltages and currents.
- Limiting the current in the thyristors during converter bypass pair operation due to the discharge of the shunt capacitance of the DC line.

# FUNDAMENTALS OF TRANSFORMER DIFFERENTIAL PROTECTION

# 3.1 TYPES OF FAILURES IN CONVERTERS TRANSFORMERS

To correctly define the protections for any equipment, it is necessary to understand the types of faults to which the equipment is subject. Thus, it is viable to classify the possible faults for power transformers as follows (ZHAO, 2018; GRID, 2011):

- Winding failures due to internal short circuits, e.g., turn-to-turn and sing-phase-to-ground faults.
- Core faults due to failures in core insulation or short-circuited laminations.
- Terminal failures due to excessive fault currents or short circuits caused by inadequate connections.
- On-load tap changer (OLTC) faults.
- Transformer tank or other accessories faults.
- Failures due to abnormal operating conditions such as over-flux, overload, and overvoltage.
- Delayed clearance of external faults and impact on transformer temperature.

Statistically, the probability of occurrence of these faults in converters transformers was collected by CIGRE Joint Working Group A2/B4.28 (CIGRÉ, 2010 apud ZHAO, 2018) based on surveys over the period 2003 to 2008, and the results are summarized in Table 3.1 (IEEE, 2008):

Type of Failure	100 %	Type of Fault
Connection	34%	Phase-to-phase, Phase-to-ground, Phase-to-phase-to-ground
DC-side Winding	22%	Turn-to-ground, Turn-to-turn
OLTC	20%	Turn-to-ground, Turn-to-turn
Bushing	9%	Phase-to-phase, Phase-to-ground, Phase-to-phase-to-ground
Core	9%	Core fault, Turn-to-turn
AC-side Winding	6%	Turn-to-ground, Turn-to-turn
Shields	0%	-

Table 3.1: Probability of occurrence of failures and faults in converter transformers.

**Source:** Own authorship.

Thus, given that differential functions constitute the main protection against internal transformer faults, their accurate parameterization is of critical importance.

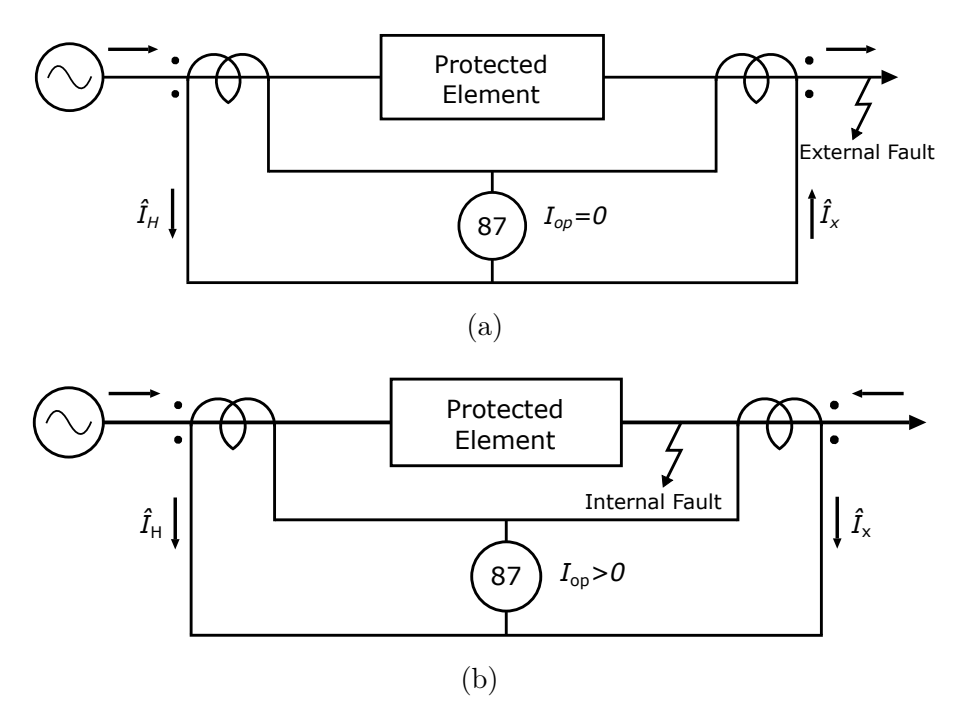
# 3.2 FUNDAMENTALS OF TRANSFORMER DIFFERENTIAL CURRENT PROTEC-TION (87T)

Differential current protection is widely used for transformer protection (ANSI code 87T) because it is reliable and features relatively simple logic that covers the vast majority of faults that occur in these devices. The function is based on Kirchhoff's Current Law, which assumes that under normal operating conditions—and by analyzing the transformer as a node—the sum of the currents at the transformer terminals should be zero after compensating for the turns ratio and considering the voltage difference between the terminals. If this condition is not satisfied, it indicates a current imbalance at this node, which likely corresponds to an internal fault current within the transformer.

Studying a simple implementation of this protection for electromechanical relays is helpful to illustrate its logic, starting with Figures 3.1a and 3.1b. These figures clearly demonstrate how the protection operation is based on the measurement (electromechanical relays) of the operating current  $(I_{op})$ , which, considering an ideal transformer, is always zero for external faults (Figure 3.1a) and greater than zero for internal faults (Figure 3.1b).

For micro-processed numerical relays, however, the logic remains the same, but the operating current can be calculated by Equation 3.1 (GUZMAN *et al.*, 2005):

Figure 3.1: Differential protection scheme to electromechanical relay with a (a) external fault and (b) internal fault.



Source: Own authorship.

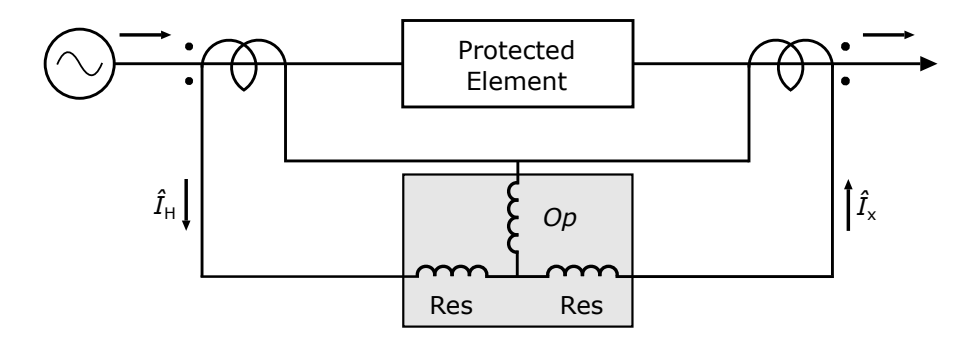
$$I_{op} = |\hat{I}_1 + \hat{I}_2| \tag{3.1}$$

where  $\hat{I}_1$  is the current in the secondary of the primary side CT and  $\hat{I}_2$  is the current in the secondary of the secondary side CT.

Nevertheless, for real-world applications, various errors and peculiarities of transformers result in operating currents different from zero under regular system and equipment conditions (these errors and peculiarities will be discussed in detail throughout this work). The concept of Percent Differential Protection is then used to avoid incorrect operations, which can also be illustrated by a simple implementation of the protection for electromechanical relays, as shown in Figure 3.2.

In this configuration, the operating coil induces the closing of a relay actuation switch, while the restraining coils (proportionally smaller) induce the opening of this switch. In this way, for external faults, the small values of the operating current are insufficient to trigger the protection. In contrast, the operating current tends to increase for internal faults and cause protection to trip.

Figure 3.2: Differential protection scheme to electromechanical relay considering the restriction current.



Source: Own authorship.

Thus, considering micro-processed numerical relays, the restraining current can be calculated using Equations 3.2, 3.3, and 3.4 (GUZMAN *et al.*, 2005):

$$I_{res} = k_r \cdot (|\hat{I}_1| + |\hat{I}_2|) \tag{3.2}$$

$$I_{res} = k_r \cdot |\hat{I}_1 - \hat{I}_2| \tag{3.3}$$

$$I_{res} = max(|\hat{I}_1|,|\hat{I}_2|)$$
 (3.4)

where  $\hat{I}_1$  is the current in the secondary of the primary side CT,  $\hat{I}_2$  is the current in the secondary of the secondary side CT, and  $k_r$  is a stabilization factor that can generally be defined as 0.5 or 1.0 (FERRER *et al.*, 2010). Equation 3.2 is the one that will be used in this work.

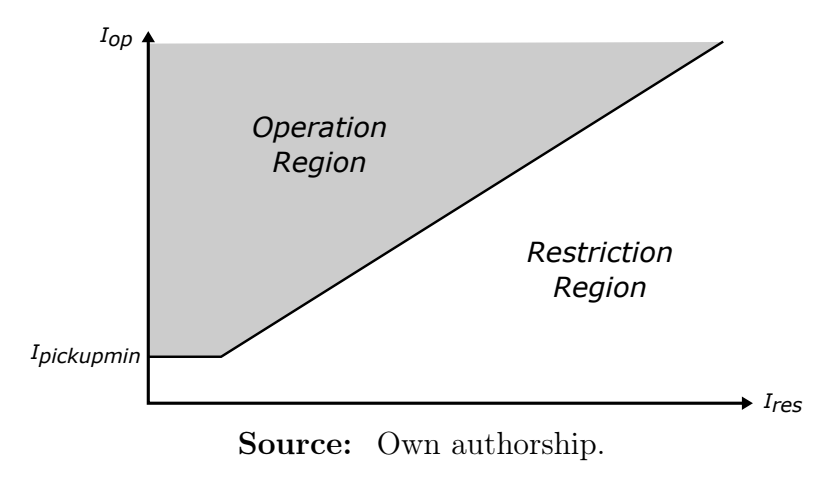
Additionally, for configuring the protection, the Slope (SLP) is also considered, which is a sensitivity factor of the protection that defines the percentage of the restraining current that the operating current must exceed to trigger the actuation, thus also defining the Slope of the operating curve (Figure 3.3), and the  $I_{pickupmin}$ , which is the minimum operating current for which the relay starts to be sensitized, avoiding measurement errors of the CTs and transformation ratios.

Therefore, the protection decision occurs when Equations 3.5 and 3.6 are satisfied, and this condition can be visualized in a current graph,  $I_{op}$  vs.  $I_{res}$ , as shown in Figure 3.3:

$$I_{op} > SLP \cdot I_{res} \tag{3.5}$$

$$I_{op} > I_{pickupmin}$$
 (3.6)

Figure 3.3: Operational plan to a differential protection.



# 3.3 FACTORS THAT INFLUENCE THE OPERATION OF TRANSFORMER DIFFE-RENTIAL PROTECTION

As mentioned above, particularities and errors related to transformers can negatively impact differential protection, primarily through incorrect protection operation. Two of these factors have already been mentioned and addressed: measurement errors of the CTs and transformation ratio errors, which are mitigated by adjusting the  $I_{pickupmin}$ . However, other factors are not easily resolved and require a more in-depth examination.

#### 3.3.1 CT Saturation

Current transformers, as well as any transformer, have non-linear characteristics due to their ferromagnetic core. Consequently, they work based on a hysteresis curve. From such current values in the transformer's primary side, there is a CT saturation, and the current in the secondary has an incorrect proportion relative to the current in the primary. Typically, CTs are designed to work around the knee point of their hysteresis curve, even during fault conditions, far from their saturation point. However, due to unforeseen faults very close to CTs, systems that have a short circuit power increase without a CT update, or poorly designed CTs, incorrect operations of the differential functions may occur.

These incorrect operations are (BLACKBURN; DOMIN, 2007):

- Protection operation to external faults due to the distorted secondary current waveforms caused by saturation.
- Protection operation delay to internal faults due to the harmonics resulting from saturation (Subsections 3.4.4 and 3.4.5).

# 3.3.2 Inrush current

The phenomenon of magnetizing inrush current is transient. It occurs in a transformer whenever the polarity and magnitude of the residual flux do not match the polarity and magnitude of the ideal instantaneous value of the steady-state flux at the moment of energization (CIGRÉ, 2011a). The magnetic flux is directly proportional to the applied voltage; then, the steady-state flux depends on the steady-state voltage. Hence, when the flux caused by the system's voltage is not equal to residual flux, there is this phenomenon with a high magnetizing current that equalizes the flux in the transformer core with the steady-state flux. Consequently, the inrush current may be despised when the connection occurs when the steady-state flux is equal or very close to residual flux.

Additionally, inrush currents can reach magnitudes of 8 to 30 times the transformer nominal current, are rich in DC components, both even and odd harmonics, and have a very slow decay time constant, varying from about 10 cycles to as long as 1 min in highly inductive circuits (BLACKBURN; DOMIN, 2007). The presence of these currents can lead to incorrect operations of the differential protection functions, as they do not flow symmetrically through both sides of the transformer. Such currents may arise in three distinct scenarios (BLACKBURN; DOMIN, 2007; ANDERSON et al., 2022):

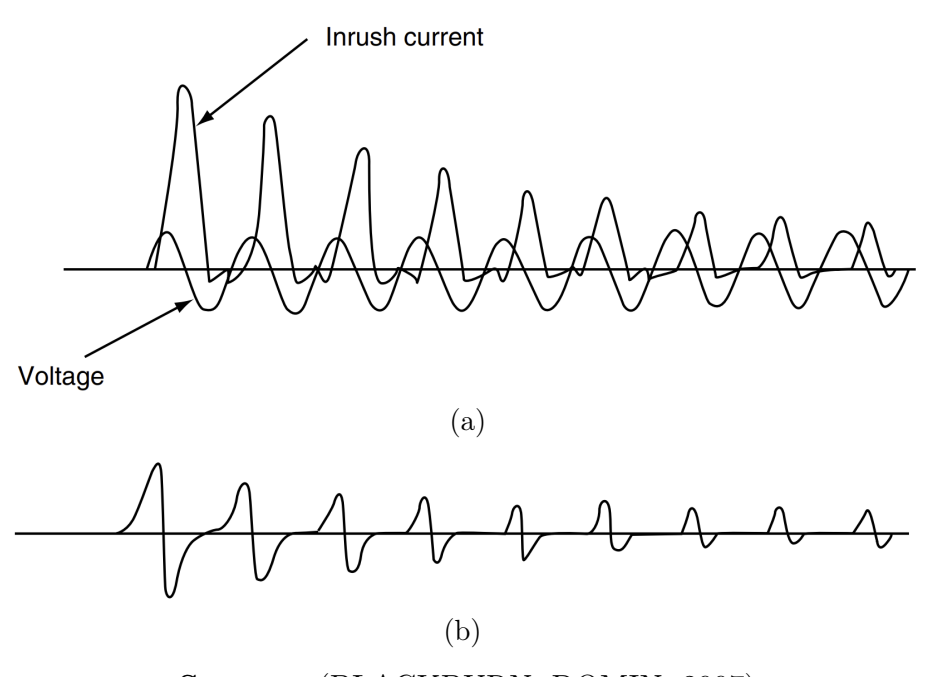
• During the energization of the transformer.

- Clearing a fault near the transformer: the voltage dip during the fault and its subsequent recovery upon fault clearance can produce a remagnetization transient, although the resulting inrush is typically smaller since the transformer is already energized.
- During the energization of a parallel transformer, due to the voltage fall caused by the irregular inrush current of the energized transformer.

The reason for the last two situations is similar to the first: the flux difference caused by voltage variation.

Therefore, for correct operation of the differential protection, it is necessary to identify these currents so they are not mistaken for internal faults. The phenomenon's characteristics are used to identify it, considering the high level of harmonics, with a strong presence of the  $2^{\text{nd}}$  harmonic (GUZMAN *et al.*, 2005), making it possible to increase  $I_{res}$  or block the protection. Typically, the  $2^{\text{nd}}$  harmonic component of inrush currents reaches 15% or more of the fundamental current, and this value can currently be reduced with improvements in transformer design and core (BLACKBURN; DOMIN, 2007).

Figure 3.4: Typical magnetizing inrush current to transformers: (a) A-phase current to star-connected windings; (b) A-phase current to delta-connected windings.



Source: (BLACKBURN; DOMIN, 2007)

#### 3.3.3 Over-excitation

Another relevant point that can affect the protection occurs because the magnetizing flux of a transformer core is directly proportional to the applied voltage and inversely proportional to the system frequency (GUZMAN *et al.*, 2005). Thus, when subjected to overvoltage or under frequency (or both conditions simultaneously), the transformer core can become saturated, producing odd harmonics in the exciting current (mainly the 3<sup>rd</sup> and 5<sup>th</sup> harmonics), which can incorrectly sensitize the differential protection (BLACKBURN; DOMIN, 2007).

Over-excitation is identified using the  $5^{th}$  harmonic to avoid this problem, increasing  $I_{res}$  or blocking the protection, in the same way as with inrush current, which will be explained further.

Although the 3<sup>rd</sup> harmonic is also helpful in identifying over-excitation, it is not viable for delta-connected windings, so typically only the 5<sup>th</sup> harmonic is used (BLACKBURN; DOMIN, 2007).

# 3.4 ADJUSTMENTS AND CORRECTIONS TO PREVENT IMPROPER OPERA-TION OF DIFFERENTIAL PROTECTION

#### 3.4.1 Correction of current transformation ratios

In the case of transformers, due to the voltage difference between the terminals, it is typical for the current transformer ratios (CTR) to be different. Therefore, with different CTRs, the secondary current of the CTs for the same primary current or for primary currents that should be equivalent (considering the voltage difference at the transformer terminals) will be different. Thus, to implement the mentioned equations, it is necessary to normalize the currents at the terminals to be comparable. To achieve this, Equation 3.7 is used to normalize the currents at each terminal (FERRER et al., 2010).

$$\hat{I}_{2,k,pu} = \frac{\hat{I}_{2,k}}{TAP_k} \tag{3.7}$$

$$TAP_k = \frac{1000 \cdot S_{nom,MVA} \cdot c_k}{\sqrt{3} \cdot V_{nom,k,kV} \cdot CTR_k}$$
(3.8)

where:

- $\hat{I}_{2,k}$ : Current in the secondary of the CT at a terminal;
- $S_{nom,MVA}$ : Nominal power of the transformer;
- $c_k$ : Correction factor for the CT connection (equal to 1 for star-connected CTs and  $\sqrt{3}$  for delta-connected CTs);
- $V_{nom,k,kV}$ : Nominal voltage of the transformer at each terminal;
- $CTR_k$ : Transformation ratio of the CT at each terminal.

#### 3.4.2 Zero-sequence current compensation

For internal single-phase-to-ground faults, zero-sequence currents flow in the system connected to the side of the transformer where the fault is. However, suppose the other winding of the same transformer is connected in delta. In that case, the zero-sequence is not transferred to the system connected to this winding and circulates within the delta connection, which can generate an incorrect trip (TAVARES, 2014; PERES, 2020).

Hence, to avoid such operations, zero-sequence currents are disregarded from the currents measured in the star windings or delta windings that have grounding transformers in the protection zone, using the matrix Equation 3.9, where the currents  $\hat{I}_a$ ,  $\hat{I}_b$ , and  $\hat{I}_c$  are the secondary currents of the CT and the currents  $\hat{I}_{a,C}$ ,  $\hat{I}_{b,C}$ , and  $\hat{I}_{c,C}$  are the corrected currents (ZIEGLER, 2012).

$$\begin{bmatrix}
\hat{I}_{a,C} \\
\hat{I}_{b,C} \\
\hat{I}_{c,C}
\end{bmatrix} = \frac{1}{3} \begin{bmatrix}
2 & -1 & -1 \\
-1 & 2 & -1 \\
-1 & -1 & 2
\end{bmatrix} \cdot \begin{bmatrix}
\hat{I}_{a} \\
\hat{I}_{b} \\
\hat{I}_{c}
\end{bmatrix}$$
(3.9)

# 3.4.3 Angular phase shift correction

Besides zero-sequence compensation, another critical point and source of errors is the angular displacement of the currents between these windings. Different connections between both sides of the transformer cause this displacement. It can also cause incorrect operations of the 87T protection, making it necessary to compensate one current for the other (IEEE, 2008). Usually, the phase shifts are multiples of 30°, and transformers are classified by phase shift groups that indicate their phase shift. Figure 3.5 demonstrates these groups, where 'y' means a star connection, 'd' a delta connection, and 'z' is a zig-zag connection. The letter size indicates the connection side (capital letter to the high side), and the number indicates the phase shift when multiplied by 30° (IEC, 2011).

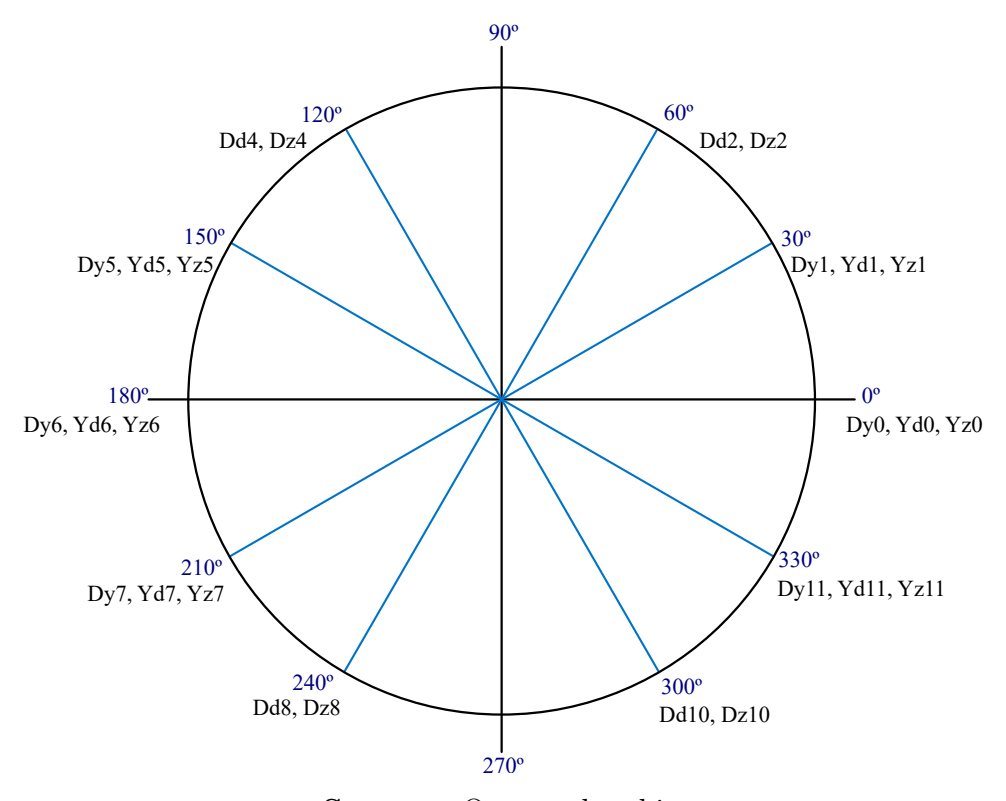


Figure 3.5: Phase shift groups.

**Source:** Own authorship.

Thus, using micro-processed numerical relays, this correction can also be performed through a matrix equation, multiplying the phase currents of one terminal (the low-voltage terminal in this work) by the matrix in equation 3.10, where  $\theta$  is the transformer angular phase shift (GAJIC, 2008):

$$M_{\theta} = \frac{1}{3} \begin{bmatrix} 1 + 2\cos\theta & 1 + 2\cos(\theta + 120^{\circ}) & 1 + 2\cos(\theta - 120^{\circ}) \\ 1 + 2\cos(\theta - 120^{\circ}) & 1 + 2\cos\theta & 1 + 2\cos(\theta + 120^{\circ}) \\ 1 + 2\cos(\theta + 120^{\circ}) & 1 + 2\cos(\theta - 120^{\circ}) & 1 + 2\cos\theta \end{bmatrix}$$
(3.10)

Equations 3.9 and 3.10 can also be combined when convenient and summarized in Equation 3.11:

$$M_{\theta,0} = \frac{2}{3} \begin{bmatrix} \cos \theta & \cos (\theta + 120^{\circ}) & \cos (\theta - 120^{\circ}) \\ \cos (\theta - 120^{\circ}) & \cos \theta & \cos (\theta + 120^{\circ}) \\ \cos (\theta + 120^{\circ}) & \cos (\theta - 120^{\circ}) & \cos \theta \end{bmatrix}$$
(3.11)

## 3.4.4 Harmonic restraint

As seen earlier in Subsections 3.3.2 and 3.3.3, the phenomena of inrush current and over-excitation can cause incorrect trips in the 87T protection. However, these phenomena can be identified by the strong presence of the  $2^{\text{nd}}$  (inrush) and  $5^{\text{th}}$  (over-excitation) harmonics (FERRER *et al.*, 2010).

As also mentioned, one way to solve these problems is to increase the restraining current when these harmonics are present (IEEE, 2008). For this, the 2<sup>nd</sup> and 5<sup>th</sup> harmonic components of the operating current ( $I_{h2}$  and  $I_{h5}$  respectively) are obtained, and a percentage of each is added to the restraining current. Therefore, the protection operation obeys Equation 3.12:

$$I_{op} > SLP \cdot I_{res} + \frac{I_{h2}}{k_2} + \frac{I_{h5}}{k_5}$$
 (3.12)

where  $k_2$  and  $k_5$  are proportionality constants that relate the fundamental current to the harmonic order currents.

Therefore, the equation 3.12 can also be described as equation 3.13:

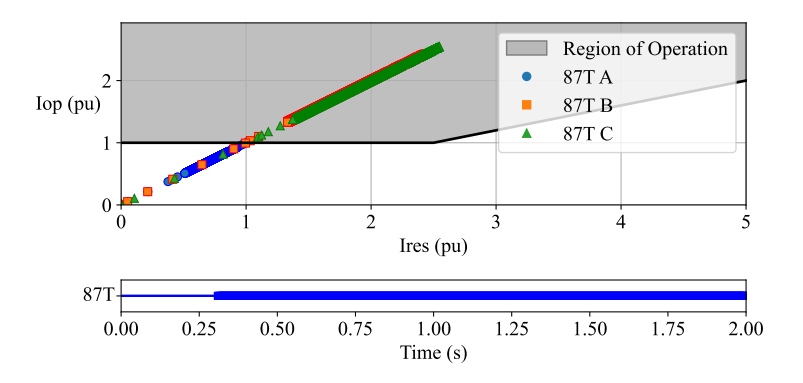
$$I_{op} > SLP \cdot I_{adi} \tag{3.13}$$

where  $I_{adj}$  is called adjusted current and is calculated by equation 3.14.

$$I_{adj} = I_{res} + \frac{1}{SLP} \cdot \left(\frac{I_{h2}}{k_2} + \frac{I_{h5}}{k_5}\right)$$
 (3.14)

To illustrate, Figure 3.6 shows the result of the 87T function for the energization of the same transformer used earlier in 3.4.3. In this case, no fault occurrence was observed, only energization, but harmonic restraint was not used.

Figure 3.6: 87T function fail operation due a transformer energization.

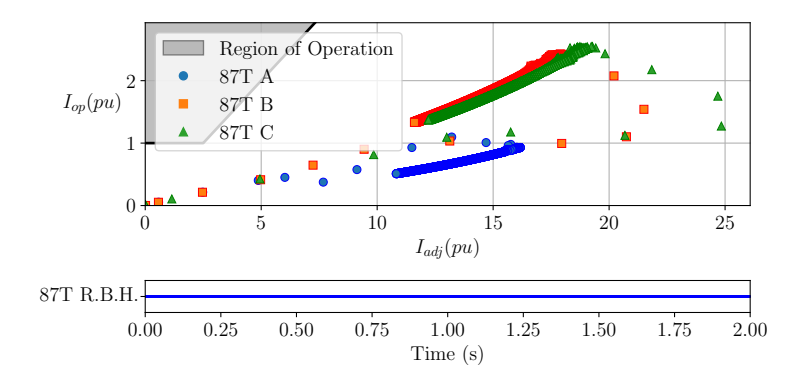


**Source:** Own authorship.

Consequently, due to the non-use of harmonic restraint, it is observed that there would be an incorrect operation after a regular switching of the transformer. The application of harmonic restraint is strictly necessary.

The need for harmonic restraint becomes evident when observing Figure 3.7, which presents the same protection for the same transformer in the same energization but with harmonic restraints applied.

Figure 3.7: 87T function correct operation due harmonic restriction.



Source: Own authorship.

Therefore, the protection becomes more reliable and operates correctly with the restraint.

# 3.4.5 Harmonic blocking

The harmonic blocking logic has the same objective as the restraining logic; however, instead of raising the restraining current, it blocks the protection when its conditions are met.

In this logic, the operating current is directly compared to its harmonics, and when the amount of harmonics exceeds the maximum stipulated percentage, the blocking is performed (FERRER et al., 2010).

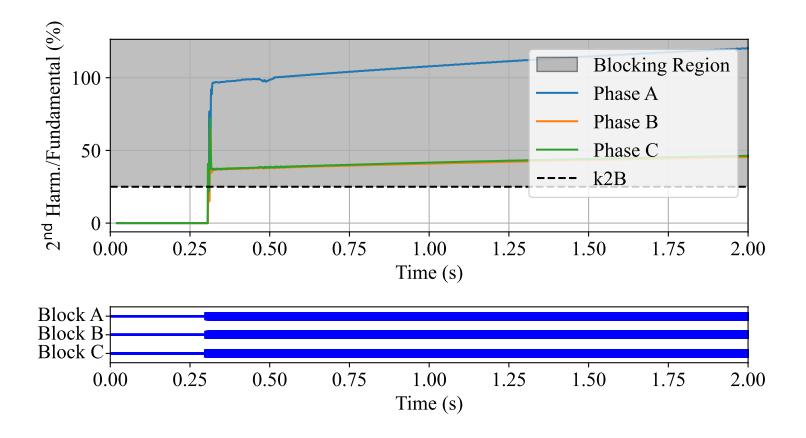
Consequently, blocking occurs when one of the following Equations (3.15 or 3.16) is satisfied (IEEE, 2008; GUZMÁN *et al.*, 2009):

$$k_{2B} < \frac{I_{h2}}{I_{op}}$$
 (3.15)

$$k_{5B} < \frac{I_{h5}}{I_{op}}$$
 (3.16)

Figures 3.8 and 3.8 exhibit the harmonic blocking logic for the same energization of the same transformer used to illustrate the restraining. In this case, a value of 25% was used for  $k_{2B}$  and  $k_{5B}$ , and the graphs correspond to the percentage of harmonics relative to the fundamental over time.

Figure 3.8: 87T function blocking by 2<sup>nd</sup> harmonic.



**Source:** Own authorship.

Thus, it is observed that for the 2<sup>nd</sup> harmonic (Figure 3.8), the blocking would be activated, given that the percentage of the 2<sup>nd</sup> harmonic considerably exceeds the stipulated 25%, which corroborates what was explained about the characterization of an inrush current.

5<sup>th</sup> Harm./Fundamental (%) Blocking Region Phase A 40 Phase B Phase C 20 0.25 0.75 1.75 0.50 1.00 1.25 1.50 0.00 2.00 Time (s) 1.25 0.00 0.25 0.50 0.75 1.00 1.50 1.75 2.00 Time (s)

Figure 3.9: 87T function blocking by 5<sup>th</sup> harmonic.

Source: Own authorship.

In Figure 3.9, related to the 5<sup>th</sup> harmonic, it is verified that the blocking operates for a very short time, corroborating the statement that the 5<sup>th</sup> harmonic is used for cases of over-excitation.

It is worth noting that these methods bring more reliability to the protection but may delay its operation in internal faults that cause core saturation or faults that occur during the transformer energization (IEEE, 2008).

# 3.5 TRANSFORMER NEGATIVE-SEQUENCE DIFFERENTIAL FUNCTION (87Q)

Despite all the corrections discussed previously, the 87T function still faces some other challenges in its operation. Depending on specific load and maneuvering conditions, the 87T function may not detect some turn-to-turn or turn-to-ground faults. These conditions are especially true during high loading on the transformer and/or a small percentage of short-circuited turns or when a turn-to-ground short circuit is very close to the neutral, causing minimal phase current impact (KASZTENNY et al., 2015).

In these cases, the concept of the transformer negative-sequence differential function is used. This function follows the same logic as the 87T function. However, it uses the negative sequence components of the phase currents, taking advantage of the fact that, even if the fault does not sufficiently impact the currents at the transformer terminals, they are still asymmetrical and cause negative sequence currents in the system (FERRER et al., 2010; KASZTENNY et al., 2015).

Consequently, the function operates based on Equations 3.17, 3.18, 3.19, and 3.20 (FERRER et al., 2010):

$$I_{opq} = |\hat{I}_{1q} + \hat{I}_{2q}| \tag{3.17}$$

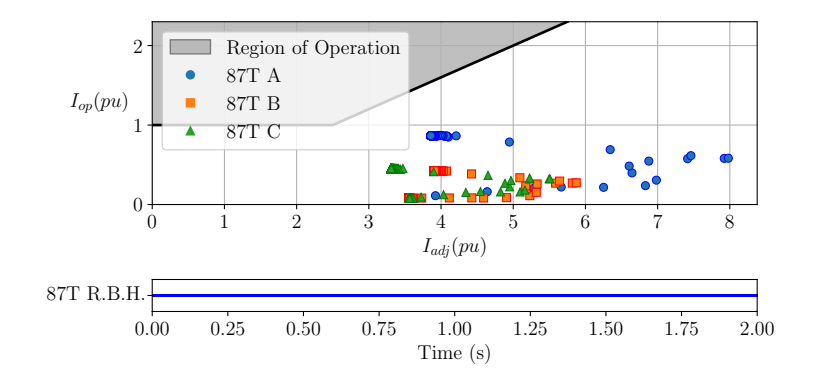
$$I_{resq} = \max(|\hat{I}_{1q}|, |\hat{I}_{2q}|) \tag{3.18}$$

$$I_{opq} > SLP_q \cdot I_{resq} \tag{3.19}$$

$$I_{opq} > I_{pickupminq} \tag{3.20}$$

For the same transformer with the same settings and system as used in previous section 3.4, in the occurrence of a turn-to-ground fault in 1% of a star winding (considering the start of the turn from the connection with the neutral), that is, a fault very close to the neutral, the result of the 87T function is verified in Figure 3.10: the protection does not operate.

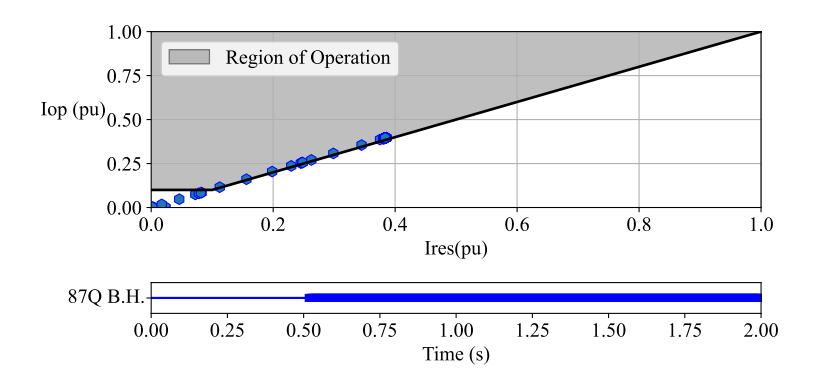
Figure 3.10: 87T function operation to a turn-to-ground short circuit in 1% of the turns of a star terminal.



**Source:** Own authorship.

Conversely, in Figure 3.11 shows that, for the 87Q function, considering all equal, the protection operates normally, as expected.

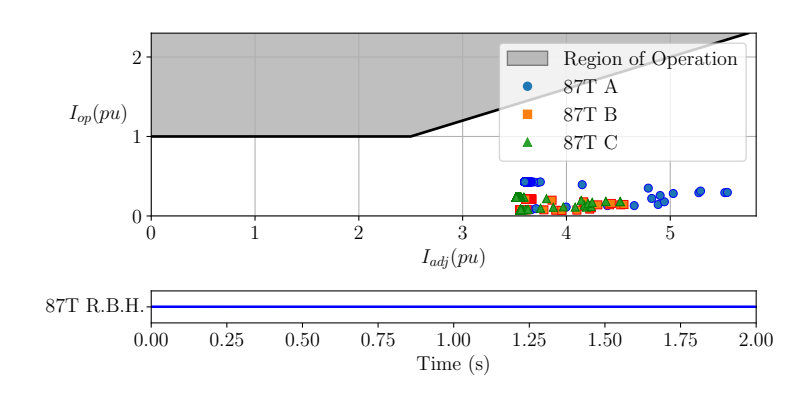
Figure 3.11: 87Q function operation to a turn-to-ground short circuit in 1% of the turns of a star terminal.



**Source:** Own authorship.

Another challenge to be addressed for the 87T function, which is assisted by the 87Q function, is related to turn-to-turn faults involving a small percentage of turns. Thus, considering all the system equal again, but with a turn-to-turn short taking 5% of a delta winding, the 87T function is not sensitized again (Figure 3.12), but the 87Q operates normally (Figure 3.13).

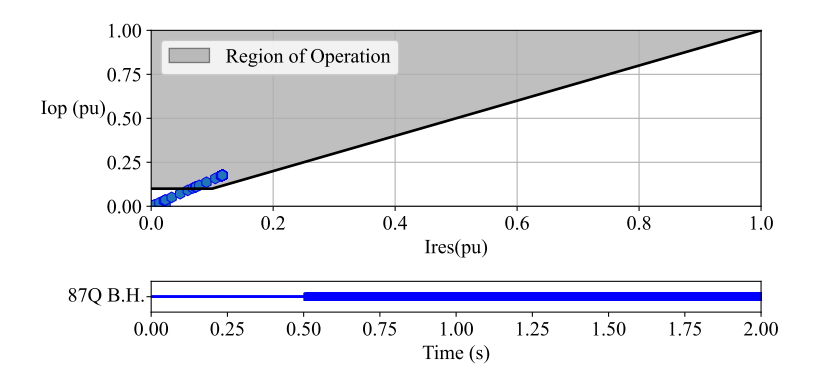
Figure 3.12: 87T function operation to a turn-to-turn short circuit in 5% of the turns of a delta terminal.



**Source:** Own authorship.

Furthermore, the 87Q function should also not operate for inrush or over-excitation currents of the transformer, utilizing the harmonic blocking logic for this purpose. However, since the 87Q element is very sensitive to detecting unbalanced faults, it may act incorrectly for unbalanced external faults, especially when the CT is saturated (GUZMÁN et al., 2009 apud

Figure 3.13: 87Q function operation to a turn-to-turn short circuit in 5% of the turns of a delta terminal.



**Source:** Own authorship.

PERES, 2020). Therefore, a two-cycle delay is typically used for its actuation (FERRER et al., 2010).

# 3.6 RESTRICTED EARTH FAULT PROTECTION (REF)

Another alternative approach for correct identification and operation in turn-to-ground faults very close to neutral cases in grounded star-connected transformers is the restricted earth fault protection function. The phase currents are small in these cases, while the neutral current is high (FERRER et al., 2010).

In its differential form, the REF element can be implemented by comparing the neutral current  $(\hat{I}_N)$  of a star-grounded winding and the zero-sequence current calculated from the currents at the transformer terminals  $(\hat{I}_0)$ .

Therefore, the operating currents  $(I_{opr})$  and restraining currents  $(I_{resr})$  can be calculated according to Equations 3.21 and 3.18 (TAJ et al., 2011):

$$I_{opr} = |\hat{I}_N| \tag{3.21}$$

$$I_{resr} = k_R \cdot (|\hat{I}_N - 3\hat{I}_0| - |\hat{I}_N + 3\hat{I}_0|)$$
(3.22)

where  $(k_R)$  is a stabilization factor.

Thus, the function operates under the following conditions (Equations 3.23 and 3.24):

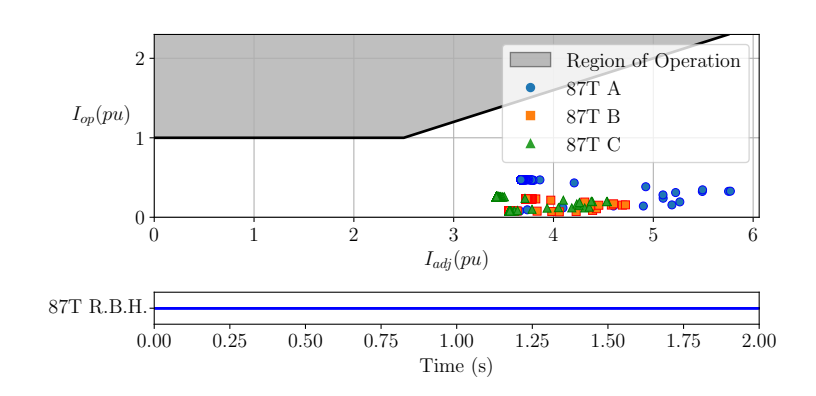
$$I_{opr} > I_{resr} \tag{3.23}$$

$$I_{opr} > I_{pickupminr}$$
 (3.24)

Considering a turn-to-ground fault in 0.5% of the turn from the connection with the neutral, it is again verified that the 87T does not operate (Figure 3.14) and that this time, the 87Q operates with a minimal margin (Figure 3.15), with a risk of not operating. Thus, one possibility would be to make both protections more sensitive, running the risk of unintended operations but ensuring fault operation.

However, analyzing Figure 3.16, which represents the REF function, it is found that it operates without any problems, with even a considerable margin between the operating current and the restraining current. This operation allows for maintaining less sensitive settings for the 87T and 87Q functions without compromising the transformer safety.

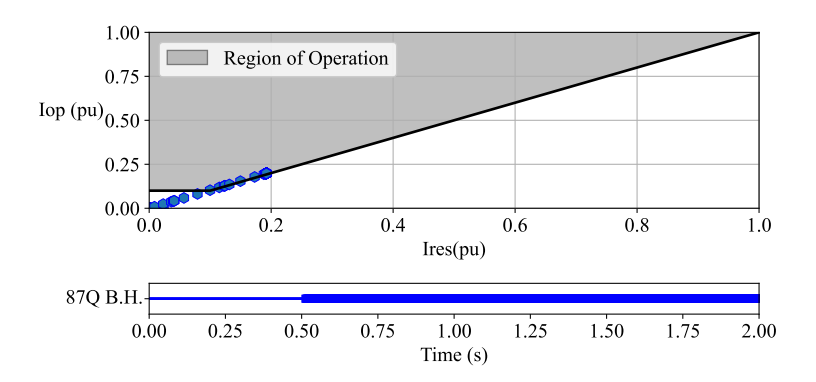
Figure 3.14: 87T function operation to a turn-to-ground short circuit in 0.5% of the turns of a star terminal.



**Source:** Own authorship.

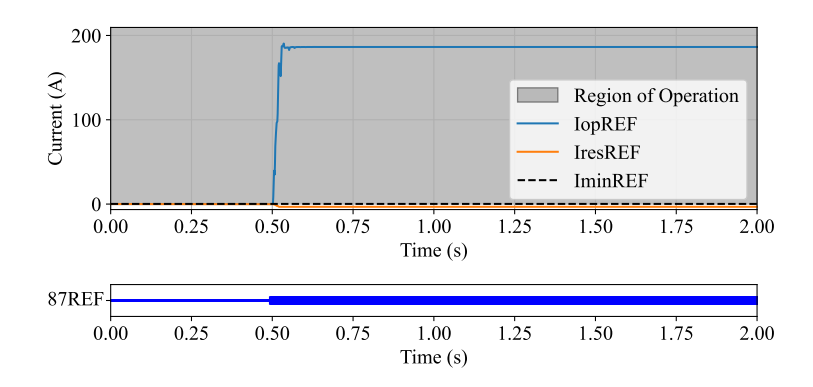
It is worth noting that for turn-to-ground faults in delta windings, the REF will not operate since there is no connection between the winding and the neutral. In these cases, for extreme conditions where the 87T is not sensitized (interval close to half of the winding), the transformer should be protected by the 87Q.

Figure 3.15: 87Q function operation to a turn-to-ground short circuit in 0.5% of the turns of a star terminal.



Source: Own authorship.

Figure 3.16: REF function operation to a turn-to-ground short circuit in 0.5% of the turns of a star terminal.



Source: Own authorship.

# LITERATURE REVIEW

This chapter presents a literature review on the performance of differential protection functions applied to HVDC converter transformers, aiming to contextualize the topic and support the research and findings of this work. Each referenced study is briefly described, highlighting its main ideas and contributions. Finally, Table 4.1 provides a summary of the literature reviewed throughout the chapter.

In 2011, CIGRE published a report from the JWG B5/B4.25 working group on the impacts of HVDC stations on AC system protection (CIGRÉ, 2011b). This report identified and addressed problems with the differential protection of adjacent transformers and converter transformers due to DC or quasi-DC currents flowing through the neutral of these transformers (DC Bias) (ZHAO, 2018).

For adjacent transformers, it was found that the differential protection could not operate due to the presence of a 2<sup>nd</sup> harmonic when in mono-pole ground operation mode in the links. Therefore, the Excitation Impedance Scheme protection function was recommended for these transformers. This function calculates the transformer excitation impedance using fault components of its terminal voltages and currents, allowing internal faults to be distinguished from external ones based on the impedance's magnitude and phase angle. If either criterion (low magnitude or phase between -180° and 0°) is met, the relay trips.

For converter transformers, function 87T was recommended together with function 87N, while function 87Q was not mentioned. However, DC saturation protection was recommended to deal with DC magnetic bias. Given that DC bias can result in core saturation and, consequently, zero-sequence third harmonic currents in the transformer's primary windings.

Lin et al. (2014), motivated by a real case that occurred in the Tianguang HVDC link, where a malfunction occurred in the  $2^{nd}$  harmonic restraint of the differential protection of the converter transformer, evaluated the use of the  $2^{nd}$  harmonic to identify energization in the

converter transformers. To this end, simulations based on RTDS were performed using a model of the 800 kV Chusui HVDC link and simulations of the response of the 87T function with  $2^{nd}$  harmonic blocking.

The following events were verified: energization of the transformers at no load, single-phase-to-ground fault in the secondary, phase-to-phase-to-ground fault in the secondary, and three-phase-to-ground fault in the secondary. Thus, improper actuation for energizing the transformers was verified due to failure in the 2<sup>nd</sup> harmonic blocking and non-actuation for the faults evaluated due to the presence of the 2<sup>nd</sup> harmonic.

Therefore, Lin et al. (2014) observed a time difference between the sudden voltage variation and the appearance of an operating current from the 87T function during transformer energization. Based on this phenomenon, they proposed an energization identification method that uses this time difference, achieving correct 87T operation for both energization and internal faults, as verified through simulations.

Zhao (2018) evaluated the behavior of phase differential protection with harmonic blocking for internal faults in converter transformers. For this purpose, the CIGRE HVDC benchmark test system in PSCAD/EMTDC was used to simulate the faults, and the differential protection was modeled to respond to the simulation results. As a result, Zhao (2018) identified the occurrence of undue blocking of the differential protection in the occurrence of asymmetric internal ground faults on the DC side of the converter transformers. According to the analyses performed, the blocking occurred due to a significant value of the DC component in the fault currents that flowed through the fault point and caused a half-cycle saturation in the converter transformers, which led to an increase in the 2<sup>nd</sup> harmonic component in the transformer currents. Thus, the differential protection was blocked due to the 2<sup>nd</sup> harmonic component exceeding the blocking limit, so Zhao (2018) assessed the need to use a new method to identify the energization of converter transformers other than by the 2<sup>nd</sup> harmonic component.

Danhui *et al.* (2018) evaluated the impact of commutation failures in the inverters of an HVDC link on the 87T function of converter transformers. The work used the CIGRE HVDC benchmark model in the PSCAD/EMTC software to perform simulations. It verified the presence of 2<sup>nd</sup> harmonic currents above the blocking percentage for single-phase-to-ground faults, delaying the actuation of the protection.

Therefore, Danhui *et al.* (2018) related this phenomenon to the presence of commutation failures, and, to confirm the impact of the commutation failure on the improper blocking of the function and to try to solve the problem, a countermeasure was proposed to perform the blocking so that, with the countermeasure, the blocking of the function only occurs if the inverter's commutation failure protection does not act within 0.03 seconds. If it acts, even with the presence of 2<sup>nd</sup> harmonic, there is no blocking of the function. Thus, simulating the faults using the countermeasure, the function was not blocked.

Zheng et al. (2018) was based on the statement in (XIAO et al., 2006) that the unidirectional characteristics of thyristors result in a 2<sup>nd</sup> harmonic current in converter transformers after faults in their secondary to investigate this phenomenon and its impacts. To this end, Zheng et al. (2018) analyzed the operation of an HVDC converter rectifier during a fault in the converter transformer valve side and verified the occurrence of a phenomenon called fault-induced inrush current (FIIC). During the fault, there is an increase in the DC current in the transformer, causing an aperiodic offset in its voltage, which contributes to a half-cycle saturation in its core and results in a high 2<sup>nd</sup> harmonic current, which can cause undue blocking of the differential protection.

By then evaluating the level of 2<sup>nd</sup> harmonics and its impact on differential protection through simulations in PSCAD/EMTC, Zheng *et al.* (2018) found a high level of 2<sup>nd</sup> harmonics above 15% (reference value for blocking protection) for ground faults external to the transformer, but on the valve side, also a high level of 2<sup>nd</sup> harmonics above 15% for ground faults internal to the transformer also on the valve side, however, with rapid decay, and finally, in the same way, a high level of 2<sup>nd</sup> harmonics above 15% for ground faults that are initially external and become internal on the valve side (transferred faults), however, with a longer duration above 15% concerning the other faults evaluated.

Therefore, it was observed a blocking of the differential protection for external faults, which was beneficial to the functioning of the function, a delay in the activation of the protection for internal faults, and a more significant negative impact for transferred ground faults, where for these faults, it has had a failure in the activation of the protection after 0.08 seconds of fault.

Zhao & Crossley (2019) investigates the causes of erroneous blocking of the differential function in converter transformers using the CIGRE HVDC benchmark test system in PS-

CAD/EMTDC. As the root cause, the evaluations confirm the half-cycle saturation caused by DC components in the fault currents for single-phase-to-ground and phase-to-phase-to-ground short-circuits in the valve side of converter transformers. This saturation increases second harmonic components and can lead to erroneous blocking of differential protection during genuine internal faults.

To address this, Zhao & Crossley (2019) propose a method based on mathematical morphology (MM) that incorporates a waveform symmetry criterion and an improved morphological gradient criterion. This approach discriminates between inrush and internal fault conditions more effectively than traditional harmonic blocking.

Simulation results validate that the proposed method accurately distinguishes between inrush and internal faults, even in complex scenarios such as inrush with current transformer (CT) saturation and sympathetic inrush, ensuring reliable and prompt differential protection operation without unnecessary blocking.

Zheng et al. (2021a) performs a more in-depth analysis of fault-induced inrush currents in converter transformers on the rectifier side of HVDC systems using an HVDC model in PSCAD/EMTC. In addition to what was analyzed in (ZHENG et al., 2018), in this work, the differences in generation and characteristics of the FIIC between star-star and star-delta transformers were evaluated, as well as the control and protection system of the HVDC link was considered in the simulations and analyses to verify its impact on the FIIC and vice versa, and a countermeasure for the effects of the FIIC on the differential protection of converter transformers was proposed.

Thus, Zheng et al. (2021a) confirmed that single-phase-to-ground faults on the valve side of converter transformers can cause undue blocking in their differential protections due to the presence of a 2<sup>nd</sup> harmonic current that occurs due to FIICs. He found that for star-star converter transformers, FIICs happen in the three phases of the transformer, while for star-delta transformers, FIIC occurs only in the phase in fault and in one more phase. Furthermore, finally, he proposed that the undue blocking of differential protections can be solved by accelerating the emission of the rectifier force retard to equal or less than 7 ms so that the interruption of the current prevents the generation of FIIC in the faulted transformer or reduces it.

Zheng et al. (2021b) also analyzed the generation and characteristics of FIICs and their

impact on the differential protection of converter transformers due to single-phase-to-ground faults on the valve side of these transformers, but this time, on the transformers on the inverter side of an HVDC link. Moreover, an HVDC model in PSCAD/EMTC was also used for simulations.

As a result, Zheng et al. (2021b) noticed that the fault current on the valve side of the transformer after the fault depends mainly on the conduction states of the common anode thyristors and in which transformer of the bipole/pole the fault occurred. He also concluded that the commutation failure on the inverter side could accelerate the generation of an FIIC and, consequently, the saturation of the transformer according to the faulted thyristor, and, finally, reached conclusions very similar to (ZHENG et al., 2018) regarding the blocking of differential protection for converter transformers on the rectifier side. That is, blocking of protection for external faults on the valve side, possible delay for internal faults on the valve side, and blocking for transferred faults on the valve side.

Zheng et al. (2021c) performs the same analyses and reaches the same conclusions regarding the characteristics and origin of FIICs as (ZHENG et al., 2018), (ZHENG et al., 2021a), and (ZHENG et al., 2021b). However, he assesses that accelerating the emission of force retard proposed by Zheng et al. (2021a) does not solve all the possibilities of improper blocking of the differential protection of HVDC link converter transformers caused by FIICs. Therefore, Zheng et al. (2021c) proposes a new method to avoid improper blocking.

This method consists of, when the operating current of the transformer differential protection is within the tripping zone (without harmonic restriction), and the 2<sup>nd</sup> harmonic component is above the blocking limit, then confirming whether the fault is internal to the converter as a whole (transformer plus converter) by the converter differential protection and whether the zero sequence current of the transformer on the valve side is above a limit value.

The method is based on the proposition that FIICs are caused by a DC current that passes through the transformer phases and flows through the ground fault connection on the valve side. Therefore, if the sum of the zero sequence currents of the secondary phases of the converter transformer is higher than an acceptable error value (indicated as 0.12 pu in the work), Zheng et al. (2021c) then proposes that the differential protection should be activated by disconnecting the transformer and demonstrates its effectiveness through a simulation in PSCAD/EMTDC.

Deng et al. (2019) did not evaluate operational errors of differential functions in converter transformers resulting directly from short circuits, such as 2<sup>nd</sup> harmonic blocking caused by FIICs. However, understanding the problem of failures due to CT saturation and possible undue blocking by 2<sup>nd</sup> harmonic during the energization of faulty transformers or in the occurrence of DC BIAS, he introduces an advanced protection scheme for converter transformers, using a hybrid AC/DC transmission system modeled in PSCAD/EMTDC to evaluate performance.

Therefore, Deng et al. (2019) proposed a method based on the "Ratio of Wavelet Energy Entropy" (RWEE), which utilizes the distinctive energy entropy (WEE) patterns in fault components of primary and secondary current signals. When an internal fault occurs, the primary current's WEE is significantly higher than the secondary side, yielding a high RWEE. However, WEE values on both sides are similar for external faults or disturbances, resulting in an RWEE close to one.

The RWEE criterion simulations demonstrate robust performance, accurately detecting internal faults without being impacted by CT saturation, inrush currents, or noise, which may enhance the reliability of differential protection by ensuring precise fault detection under various conditions, providing a significant improvement over traditional methods.

# 4.1 SUMMARY OF THE LITERATURE REVIEW

Table 4.1: Summary of the main contributions of the reviewed literature.

Reference	Main Contribution	
(CIGRÉ, 2011b)	Highlighted challenges in differential protection of adjacent and converter transformers due to DC bias from monopole ground operation. Recommended Excitation Impedance Scheme for adjacent transformers and the use of 87T with 87N for converter transformers.	
(LIN et al., 2014)	Investigated the malfunction of 2 <sup>nd</sup> harmonic blocking in 87T during energization. Proposed a method based on the time difference between voltage change and operating current to distinguish between energization and internal faults, improving relay decision-making.	

(Continued on next page)

Reference	Main Contribution	
(ZHAO, 2018)	Simulated internal faults on the DC side of converter transformers and found that 2 <sup>nd</sup> harmonic blocking could incorrectly prevent 87T operation. Identified DC-induced half-cycle saturation as the root cause and suggested developing alternative energization detection strategies.	
(DANHUI et al., 2018)	Observed delayed protection due to undue blocking by 2 <sup>nd</sup> harmonic current and linked commutation failures to the phenomenon; they proposed blocking conditioned by commutation failures on inverter protection operation.	
(ZHENG et al., 2018)	Studied fault-induced inrush current (FIIC) and its contribution to 2 <sup>nd</sup> harmonic distortion in valve-side faults. Showed how FIIC leads to incorrect blocking or delayed activation of 87T, especially during internal and transferred faults, emphasizing the need for improved protection methods.	
(ZHAO; CROSSLEY, 2019)	Analyzed single-phase and two-phase faults causing half-cycle saturation and excess 2 <sup>nd</sup> harmonic. Proposed a new method using mathematical morphology with waveform symmetry and morphological gradients to distinguish inrush from internal faults, avoiding misoperation.	
(ZHENG et al., 2021a)	Extended previous FIIC studies to compare star-star and star- delta transformer connections. Verified that FIIC characteris- tics vary by connection type and proposed reducing rectifier force retard delay to 7 ms as a mitigation strategy for preven- ting blocking of differential protection.	
(ZHENG et al., 2021b)	Focused on inverter-side converter transformers, finding that FIIC generation depends on thyristor conduction and commutation failure. Observed blocking during external and transferred faults and delayed response for internal faults, reaffirming prior rectifier-side findings.	
(ZHENG et al., 2021c)	Proposed a hybrid detection method for internal faults using converter-level differential protection and monitoring zero-sequence current. This strategy helps avoid blocking due to FIIC by verifying ground current presence and converter fault localization before tripping.	
(DENG et al., 2019)	Introduced a novel fault detection method based on Ratio of Wavelet Energy Entropy (RWEE) to identify internal faults. Demonstrated high resilience against CT saturation, inrush, and noise, offering improved reliability over traditional harmonic-based schemes.	

Source: Own authorship based on literature review.

# COMPUTATIONAL IMPLEMENTATIONS

This chapter describes the computational implementation for the simulations performed in this work. These simulations were performed in three distinct stages:

The first stage was to adjust the system to be analyzed in software for simulating electromagnetic transients. The adjustments were made so that it represented a real HVDC system in the Brazilian electrical system, and its simulation results were consistent with reality.

The second stage was to perform simulations of several fault scenarios in the system and obtain the signals of the electromagnetic transients that occurred in response to the faults.

The third and final stage was to model the differential functions of the transformers in Python and simulate the response of these functions to the signals obtained.

The following sections detail these steps.

### 5.1 HVDC SYSTEM MODEL

### 5.1.1 Madeira River HVDC Complex

The simulation system was based on and seeks to simulate the HVDC link called the Madeira River HVDC Complex. This complex was built to transport the generation of two hydroelectric plants that are among the five largest plants in Brazil in terms of total installed generation capacity: Jirau HPP and Santo Antônio HPP, which together can generate up to 7,318 MW – 3,750 MW at Jirau HPP and 3,568 MW at Santo Antônio HPP.

As explained previously, due to the continental size of Brazil and the difference between regions, these plants were built in the state of Rondônia, in the middle of the Brazilian Amazon, where sufficient hydraulic potential was found. However, the state's AC system cannot handle or consume this amount of generation, so the Madeira River HVDC Links were built to transmit

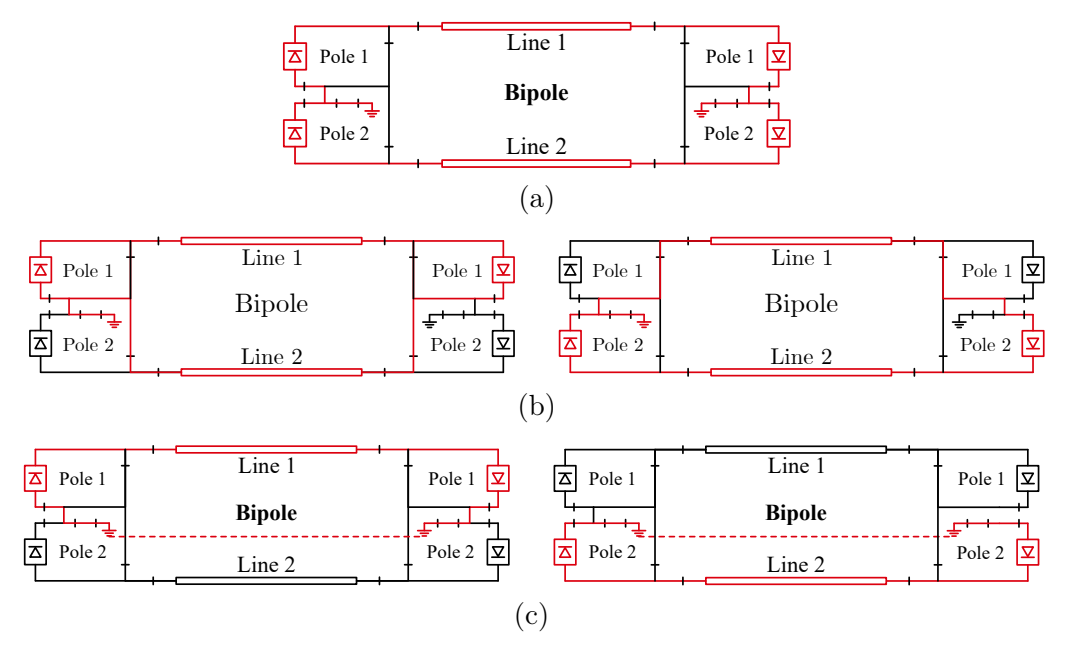
most of this generation directly to the country's load center, the Southeast region. At the same time, a small part is connected to the AC system of the state of Rondônia. Thus, the Jirau and Santo Antônio HPPs operate asynchronously with the rest of the BIPS, with only six generating units from the Santo Antônio HPP connected directly to the BIPS via the Rondônia AC grid.

The system is, therefore, composed of two LCC-HVDC technology bipoles, with a nominal power of 3,150 MW each and a nominal voltage of  $\pm 600$  kV. They interconnect the Coletora Porto Velho 500 kV substation (asynchronous with the rest of the BIPS) and the Araraquara 2 500 kV substation (synchronous with the rest of the BIPS) via 2,375 km of DC lines. The two bipoles offer considerable operational flexibility, with each capable of operating in the following modes:

- Bipolar: Two 12-pulse converters operating at each terminal (two poles), with one functioning as the positive pole and the other as the negative pole (Figure 5.1a).
- Monopolar Metallic Return: A 12-pulse converter operating at each terminal (one pole), with the return current passing through the DC line of the other pole, which remains blocked (Figure 5.1b).
- Monopolar Ground Return: A 12-pulse converter operating at each terminal (one pole), where the return current flows through the ground electrode reference at each terminal (Figure 5.1c).

The complex is connected to the Acre-Rondônia 230 kV system in two ways: two Back-to-Back converter blocks with a power of 400 MW each at  $\pm$  37.8 kV and Capacitor Commutated Converter (CCC) topology and the Transformer n° 13 (TF13) of 525/230 kV and 465 MVA. The Back-to-Back allows the transfer of part of the plants' generation to the Acre-Rondônia system asynchronously in addition to the six units of the Santo Antônio HPP. At the same time, the TF13 is used for specific maneuvers in HVDC links.

Figure 5.1: Schematic representation of HVDC Madeira River link operation modes: (a) Bipolar, (b) Monopolar Metallic Return, and (c) Monopolar Ground Return.



**Source:** Own authorship.

# 5.1.2 HVDC System in ATP/ATPDraw

To simulate the Madeira River HVDC Complex at the ATP, a modified system was used based on the Benchmark model for HVDC LCC studies by CIGRE (5.2) created by (TAVA-RES, 2020). Some changes were made to this system to make the system configuration and, consequently, the simulations more realistic. Among these changes, disconnecting switches were added between the poles to simulate pole blocking. Since the analyses focused on the converter transformers, circuit breakers were added to their terminals. Additionally, according to the field configuration and to enable differential protection, current transformers were inserted into the transformer terminals, taking into account their saturation characteristics and measurement errors (EMTP..., 2004). As the main change, the converter transformers in the inverter of the first pole were replaced by converter transformers using the saturable transformer model, including their saturation characteristics (Leuven EMTP Center, 1987) and actual parameters, and modeled in such a way as to enable simulations of turn-to-turn and turn-to-ground faults. This modeling choice was made considering that the constructive differences between converter transformers for HVDC systems and conventional transformers are specifically in their physical

capacity to withstand AC and DC stresses (ZHAO, 2018), and the model provided for use in the ATP was sufficient for the analyses studied.

Figure 5.3 shows the circuit modeled on the turns of these transformers in order to simulate such internal faults. According to Figure 5.3, the turns of a phase on each side of the transformer are divided into H1, H2, and H3, where H2 and H3 are ATP variables that can have their values changed according to the simulation. At the same time, H1 is always H1 = 1.0 - H2 - H3.

Furthermore, two switches are connected in the phases divided by the variables. One of them connects H1 and H3, having the percentage of turns equal to H2 between the connection nodes, whereas the other switch connects a percentage of turns equal to H3 to ground.

Therefore, to simulate a turn-to-turn fault, it is necessary to keep the ground switch open and close the switch connecting H1 and H2 in the simulation, while the percentage of turns involved in the turn-to-turn fault is defined by H2. Similarly, to simulate a turn-to-ground fault, keep the turn-to-turn switch open and close the ground switch, defining the percentage of turns of the fault by H3.

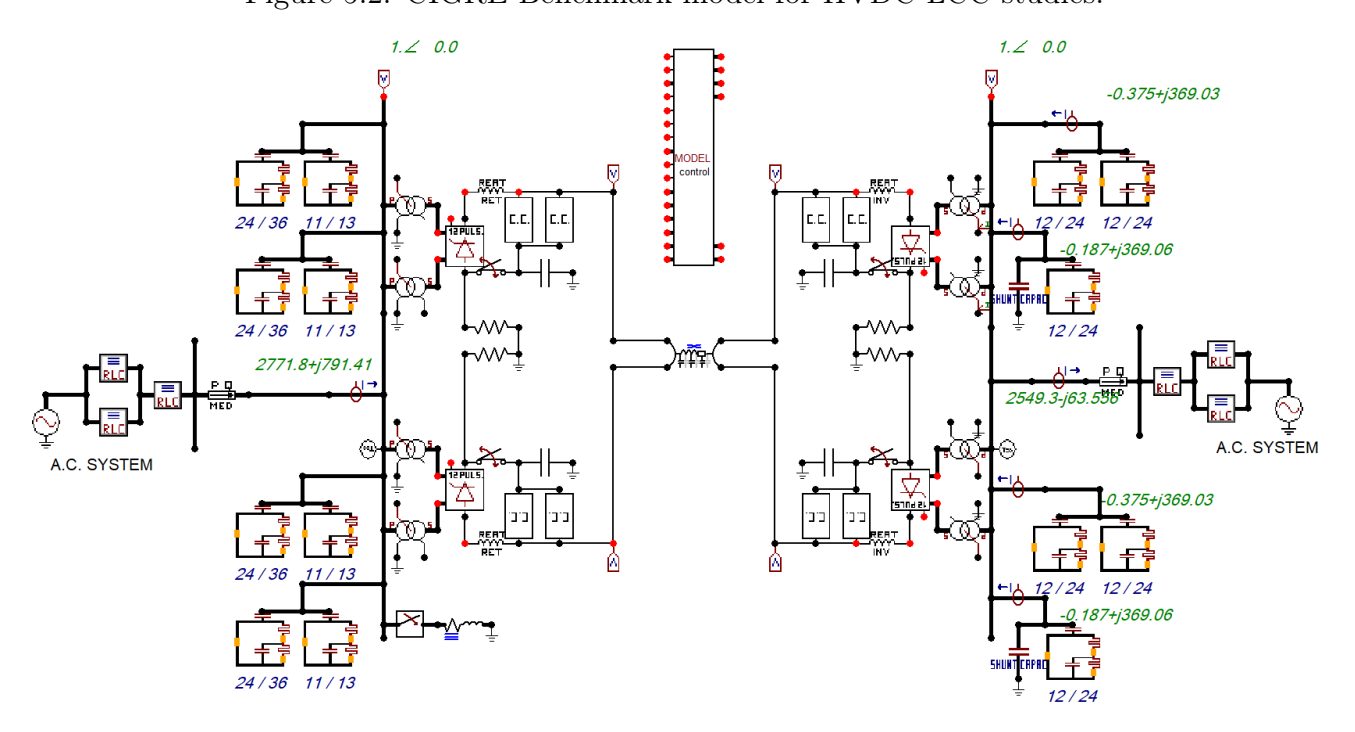
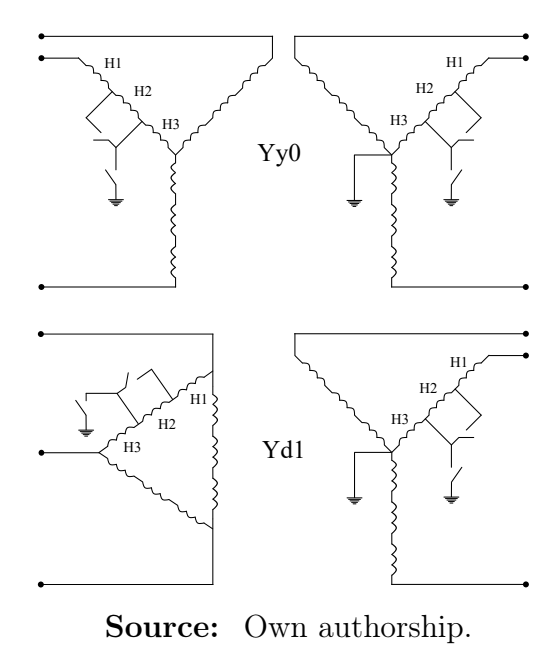


Figure 5.2: CIGRE Benchmark model for HVDC LCC studies.

**Source:** Own authorship.

Figure 5.3: Transformer configuration to turn-to-turn and turn-to-ground faults.



Ultimately, the transformers were adjusted so that these simulations could be performed on both sides of the transformers of a specific pole, both in star-star and star-delta configurations.

The other changes in the CIGRE Benchmark model that enabled a coherent simulation of the Madeira River HVDC Complex were made by (TAVARES, 2020). Namely:

- An additional bipole was added in parallel to represent Bipole 2, which was considered operational in the simulations and assumed to transmit the same power as Bipole 1.
- The Coletora Porto Velho substation was added to the AC grid considering the generation of the Jirau and Santo Antônio HPPs and disregarding the Back-to-Back. In addition, to simulate the operation of the DC links connected to the BIPS, part of the 500 kV Southeast area and part of the 230 kV Acre-Rondônia area connected by Transformer n° 13 were also added.

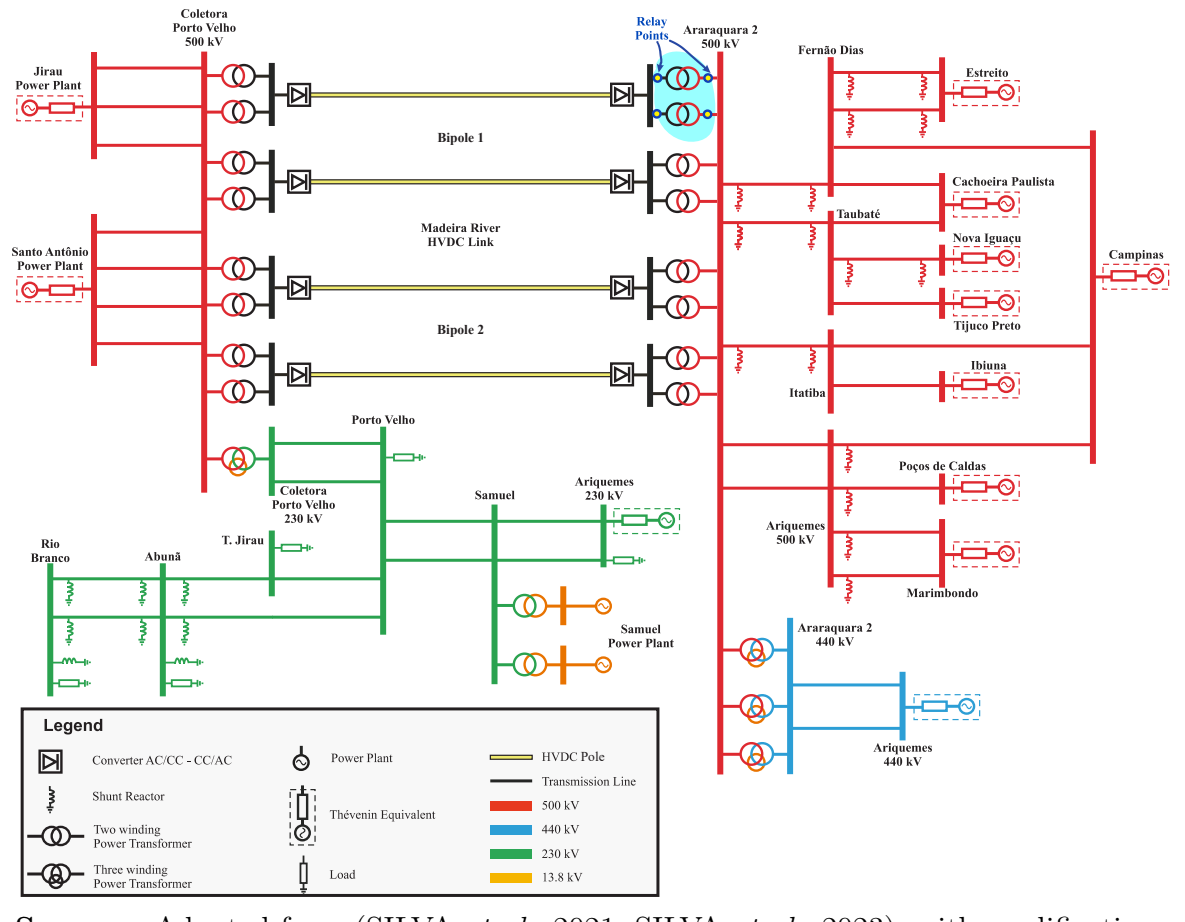
This more simplified configuration was used due to the absence of an initial model representing the Back-to-Back converters. However, the configuration faithfully represents a possible operation of the bipoles, mainly for the inverter terminal. The diagram in Figure 5.4 demonstrates the system in a simplified form.

• The parameters in the ATP used in reactors, transformers, and transmission lines were

converted to Inductance (mH) and Capacitance  $(\mu H)$ , considering that the CIGRE Benchmark model has values for inductive reactance  $(X_{opt})$  and capacitive reactance  $(C_{opt})$  equal to zero.

- The settings of the initiating sources at the inverter and rectifier terminals were modified to a better operating point for starting the transmission of active power in the links, which is equivalent to unlocking them. These modifications were done because the ATP calculates the power flow based on the values declared for each initiating source.
- The transmission lines were modeled using the distributed parameter model (LineZT\_3) and constants at the frequency of ideally transposed three-phase transmission lines.
- The equivalent added AC network was modeled with actual data obtained from transmission companies and validated by ANAREDE and ANAFAS.

Figure 5.4: Diagram of the evaluated power system: the Brazilian LCC-HVDC Madeira River link and the nearby AC system.



Source: Adapted from (SILVA et al., 2021; SILVA et al., 2023), with modifications.

In other aspects, there were no changes in the CIGRE Benchmark model. AC filters are used to eliminate harmonics of orders 11<sup>th</sup>, 13<sup>th</sup>, 24<sup>th</sup>, and 36<sup>th</sup> on the rectifier side and orders 12<sup>th</sup> and 24<sup>th</sup> on the inverter side. In contrast, on the DC side, filters are used to eliminate harmonics of orders 12<sup>th</sup> and 24<sup>th</sup>. This configuration follows the needs of 12-pulse converters, as explained in section 2.3. The model also has smoothing reactors in series with the DC line (section 2.4), and the DC line parameters are calculated using the Bergeron model for a frequency of 0.001 Hz. With this model, the line resistance is better adjusted to the behavior on the DC side (SARCINELLI et al., 2014 apud TAVARES, 2020).

Finally, as the ATP does not have interpolation, all simulations were performed with a timestep of 2.5  $\mu s$  so that the result would be as close as possible to the results of the original CIGRE HVDC model, initially built in PSCAD/EMTDC (??).

### 5.2 MODELING OF DIFFERENTIAL PROTECTION FUNCTIONS

The differential functions were modeled in Python 3.11 to simulate all aspects of an Intelligent Electronic Device (IED) installed in the field. Then, codes were implemented to acquire current data from the CTs of the converter transformers simulated in the ATP. Then, codes were implemented to process these data using analog anti-aliasing filtering, a sample/holder circuit, an Analog/Digital converter, phasor estimation, and the logic of the differential functions. Figure 5.5 shows a diagram representing the process, and each step will be discussed.

HVDC System Model

Current Transformers

Analog Antialiasing Filtering

Analog Holder

Sample/Holder

Analogic/Digital Converter

Phasor Estimation

Differential Function Logic

Figure 5.5: IED structure implemented in Python

**Source:** Own authorship.

# 5.2.1 Analog anti-aliasing filter

The modeled differential functions use the fundamental, 2<sup>nd</sup>-order, and 5<sup>th</sup>-order components of the transformer currents in their calculations, as explained in subsections 3.4.4 and 3.4.5. To restrict the current signals to these frequencies and avoid aliasing during sampling in the A/D conversion, the analog anti-aliasing filter is used before the sampling process. The filter used in this work is a 3<sup>rd</sup>-order low-pass Butterworth with a cutoff frequency of 480 Hz, which enabled the filtered signals to be resampled at a rate of 16 samples per 60 Hz cycle to be then estimated and used by the protection functions, simulating a real IED.

The transfer function of the filter used is

$$H(s) = \frac{9.0958 \times 10^6}{s^2 + 4.2652 \times 10^6 + 9.0958 \times 10^6}$$
 (5.1)

The filter was modeled using the functions butter and lsim of SciPy library in Python, as shown in the Code 5.1, and detailed below:

```
1 import numpy as np
2 from scipy.signal import butter, lsim
5 # Arguments:
                Signal coming from ATP
      - sig:
        - dt:
                 Calculation step used in the ATP
7 #
 #
                 simulation
                Cutoff frequency of the anti-aliasing #
        - fc:
 #
                 filter
        - order: Order of the anti-aliasing filter
11
14 # "Continuous" time
t = np.arange(len(sig)) * dt
17 # Analog anti-aliasing filter calculation
18 fcn = butter(order, 2 * np.pi * fc, btype='low', analog=True)
20 # Filtered signal
21 tout, sigf, xout = lsim((fcn[0], fcn[1]), sig, t)
```

Code 5.1: Part of the analog anti-aliasing filter model implemented in Python.

- butter: returns the transfer function (numerator and denominator) for a 3<sup>rd</sup>-order Butterworth filter with a cutoff frequency of 480 Hz.
- lsim: applies the Butterworth filter of the butter function to the current signal and returns

the filtered signal.

### 5.2.2 Phasor Estimation

Differential functions are based on the phasor values of transformer currents and not on their instantaneous values. Thus, as previously reported, part of calculating functions in an IED is the phasor estimation of AC signals. In the case of transformers' differential functions, the fundamental component and the  $2^{nd}$ -order and  $5^{th}$ -order components are estimated. The algorithm used to estimate phasors in this work was the Modified Cosine Filter (HART *et al.*, 2000).

The Modified Cosine Filter was developed by Hart *et al.* (2000) to improve the Digital Cosine Filter developed by Schweitzer & Hou (1993).

The Cosine Filter was created based on the observation that the imaginary filter of the Full Cycle Discrete Fourier Transform (FCDFT) is more affected by the DC component than the real filter. The conclusion was that if the imaginary component of the algorithm could be calculated from the real component, the impact of a DC current would be attenuated in the estimated phasor. Therefore, to construct the filter, the real component of the phasor is first calculated using Fourier filters, and then, based on the orthogonality principle of a complex value, the imaginary component is derived from the real component. In other words, the imaginary value is obtained by shifting the real component by 90°.

This strategy proved to be effective in filtering the exponentially decaying DC component. However, it introduces a quarter-cycle delay in the phasor estimation due to the calculation of the imaginary component.

Subsequently, the Modified Cosine Filter was developed. Its objective was to retain the improvement in DC component filtering while reducing the estimation time. To achieve this, the calculation of the real part remained unchanged, and the imaginary part was still derived from the real part but with only one additional sample instead of a quarter-cycle delay. This alteration made the estimation faster while still providing effective filtering of the DC component. The real and imaginary parts of the Modified Cosine filter are defined by Equations 5.2 and 5.3, respectively.

$$X_{re}(k) = \frac{2}{N} \sum_{n=1}^{N} x(k - N + n) \cos \frac{2\pi hn}{N}$$
 (5.2)

$$X_{im}(k) = \frac{X_{re}(k-1)\cos\frac{2\pi}{N} - X_{re}(k)}{\sin\frac{2\pi}{N}}$$
 (5.3)

The term x(k - N + n) is the n-th sample of the k-th data of the windowed signal X and the h is the harmonic to be estimated (1 = fundamental signal).

Part of the code related to implementing the phasor estimation model equations in Python is presented in Code 5.2.

```
1 import numpy as np
def COSMOD(x, h, N, NumPoints):
      #-----#
6
      # Arguments:
        - x:
                       Filtered and converted digital
     #
                       signal
                      Order of harmonic component
     # - h:
     # - N:
                      Sampling rate (number of samples
11
                       per 60 Hz cycle)
      \mbox{\tt\#} - \mbox{\tt NumPoints:} Size of the filtered and converted \mbox{\tt\#}
                       digital signal.
14
      # Calculate the angular step (theta)
      theta = h * 2 * np.pi / N
18
      # Initialize arrays for phasor estimates
19
      X = np.zeros(NumPoints, dtype=complex) # Final phasor estimate
20
      Xre = np.zeros(NumPoints) # Real part of the phasor
      Xim = np.zeros(NumPoints) # Imaginary part of the phasor
      # Iterate through the samples, starting from the N-th sample
24
      for k in range(N, NumPoints):
25
26
          # Calculate real part of the phasor (Equation 1)
          Xre[k] = 0
          for n in range(0, N):
              Xre[k] += (2 / N) * np.cos(n * theta) * x[k - N + n]
30
31
          # Calculate imaginary part of the phasor (Equation 2)
          Xim[k] = (Xre[k - 1] - (Xre[k] * np.cos(theta))) / np.sin(theta)
33
34
          # Rotation angle
          # Apply phase rotation to compensate for sampling
             (only after initial N samples)
37
          if k > N:
38
              X[k] = rotaPhasor(complex(Xre[k], Xim[k]), k * theta)
39
      return X
41
42
```

```
# Function to rotate a phasor by a given angle

def rotaPhasor(Y, angRot):
    # Calculate the real part of the rotated phasor
    re_rot = np.real(Y) * np.cos(angRot) + np.imag(Y) * np.sin(angRot)

# Calculate the imaginary part of the rotated phasor
    im_rot = - np.real(Y) * np.sin(angRot) + np.imag(Y) * np.cos(angRot)

# Return the rotated phasor as a complex number
    return complex(re_rot, im_rot)
```

Code 5.2: Part of the phasor estimation model implemented in Python.

# 5.2.3 Logic of differential functions

From the estimated phasors, the next step is the logic of the differential functions, with a first stage of adjustments of the terminal currents, according to Section 3.4, and then the calculations of each logic itself.

# 5.2.3.1 Adjustments and corrections to prevent improper operation of differential protection

The first adjustment is the correction of the current transformer ratios. The adjustment was made by implementing the Equations 3.8 and 3.7 in Python.

After that, the zero sequence compensation was applied to the high voltage terminals of converter transformers connected in a grounded star per Equation 3.9.

Lastly, the phase shift correction applies only to star-delta converter transformers as an application of Equation 3.11 to the current on the delta connection side (low voltage terminal). For the star-star transformer, to standardize the code, the value 1 was used as the correction factor, i.e., no change.

Such adjustments were implemented in Python to fundamental, 2<sup>nd</sup>-order, and 5<sup>th</sup>-order components. Code 5.3 shows the implementation for the fundamental component.

```
# - CX:
               Correction factor for CT connection at
  #
               low voltage terminal
                                                                         #
9
10 #
                                                                         #
     - VHn:
               Nominal voltage of the transformer at
11 #
                                                                         #
               high voltage terminal
    - VXn:
12 #
              Nominal voltage of the transformer at
               low voltage terminal
                                                                         #
13 #
14 #
     - RTCH:
               Transformation ratio of the CT at
                                                                         #
15 #
               high voltage terminal
16 #
     - RTCX:
               Transformation ratio of the CT at low voltage terminal
17 #
               low voltage terminal
18 #
    - NumPoints: Size of the current estimated
                                                                         #
19 # - IaH_FCOS: Phase a current estimated by Modified Cosine filter
20 # - IbH_FCOS: Phase b current estimated by Modified Cosine filter
21 # - IcH_FCOS: Phase c current estimated by Modified Cosine filter
    - MH:
                 Zero sequence compensation factor
22 #
23 #
     - MX:
                 Angular phase-shift correction factor
24
25
26 # Calculation of TAPs for each Transformer
_{27} TAPH = (1000 * Sn * CH) / (np.sqrt(3) * VHn * RTCH)
28 TAPX = (1000 * Sn * CX) / (np.sqrt(3) * VXn * RTCX)
  \# TAPN = (1000 * Sn * CH) / (np.sqrt(3) * VHn * EQP.RTCN)
31 IaHW = np.zeros(dados.NumPontos, dtype=complex)
32 IbHW = np.zeros(dados.NumPontos, dtype=complex)
33 IcHW = np.zeros(dados.NumPontos, dtype=complex)
34 IaXW = np.zeros(dados.NumPontos, dtype=complex)
35 IbXW = np.zeros(dados.NumPontos, dtype=complex)
36 IcXW = np.zeros(dados.NumPontos, dtype=complex)
37
  for k in range(0, NumPoints):
      # Adjustment of HV and LV currents - Fundamental Component
40
      IabcH = np.array([[IaH_FCOS[k]], [IbH_FCOS[k]], [IcH_FCOS[k]]])
41
      IabcHW = (1 / TAPH) * (MH @ IabcH) if type(MH) != int else \
               (1 / TAPH) * (MH * IabcH)
43
      IaHW[k] = IabcHW[0]
44
      IbHW[k] = IabcHW[1]
46
      IcHW[k] = IabcHW[2]
47
      IabcX = np.array([[IaX_FCOS[k]], [IbX_FCOS[k]], [IcX_FCOS[k]]])
48
      IabcXW = (1 / TAPX) * (MX @ IabcX) if type(MX) != int else \
49
                (1 / TAPX) * (MX * IabcX)
      IaXW[k] = IabcXW[0]
51
      IbXW[k] = IabcXW[1]
      IcXW[k] = IabcXW[2]
```

Code 5.3: Part of the Python implementation of the fundamental current adjustments.

# 5.2.3.2 87T function

With the corrected currents, the operation currents are calculated by Equation 3.1, and the restrain currents are calculated by Equation 3.2. Then, the operation of the 87T function without harmonic restriction is calculated based on Equations 3.5 and 3.6. At the same time, the operation of the 87T function with harmonic restriction is based on Equations 3.12 and 3.6. Lastly, the operation of 87T with restrain and blocking by harmonics obeys Equations 3.15 and 3.16. All these implementations are detailed in Code 5.4.

```
1 import numpy as np
87T FUNCTION
IopA = np.zeros(dados.NumPontos, dtype=float)
8 IopB = np.zeros(dados.NumPontos, dtype=float)
9 IopC = np.zeros(dados.NumPontos, dtype=float)
10 IopA_2h = np.zeros(dados.NumPontos, dtype=float)
11 IopB_2h = np.zeros(dados.NumPontos, dtype=float)
12 IopC_2h = np.zeros(dados.NumPontos, dtype=float)
13 IopA_5h = np.zeros(dados.NumPontos, dtype=float)
14 IopB_5h = np.zeros(dados.NumPontos, dtype=float)
15 IopC_5h = np.zeros(dados.NumPontos, dtype=float)
16 IresA = np.zeros(dados.NumPontos, dtype=float)
17 IresB = np.zeros(dados.NumPontos, dtype=float)
18 IresC = np.zeros(dados.NumPontos, dtype=float)
19 IresA_harm = np.zeros(dados.NumPontos, dtype=float)
20 IresB_harm = np.zeros(dados.NumPontos, dtype=float)
21 IresC_harm = np.zeros(dados.NumPontos, dtype=float)
22 BloqA_2h = np.zeros(dados.NumPontos, dtype=float)
23 BloqB_2h = np.zeros(dados.NumPontos, dtype=float)
24 BloqC_2h = np.zeros(dados.NumPontos, dtype=float)
25 BloqA_5h = np.zeros(dados.NumPontos, dtype=float)
26 BloqB_5h = np.zeros(dados.NumPontos, dtype=float)
27 BloqC_5h = np.zeros(dados.NumPontos, dtype=float)
28 TRIP87T = np.zeros(Dados.NumPontos)
29 TRIP87T_resharm = np.zeros(Dados.NumPontos)
30 TRIP87T_bloqharm = np.zeros(Dados.NumPontos)
31
  TRIP87T_resbloqharm = np.zeros(Dados.NumPontos)
32
  for k in range(0, NumPoints):
33
34
      # Calculation of operating currents
35
      IopA[k] = np.abs(IaHW[k] + IaXW[k])
36
      IopB[k] = np.abs(IbHW[k] + IbXW[k])
      IopC[k] = np.abs(IcHW[k] + IcXW[k])
      # Calculation of operating currents - 2nd Harmonic
40
      IopA_2h[k] = np.abs(IaHW_2h[k] + IaXW_2h[k])
41
42
      IopB_2h[k] = np.abs(IbHW_2h[k] + IbXW_2h[k])
      IopC_2h[k] = np.abs(IcHW_2h[k] + IcXW_2h[k])
43
      # Calculation of operating currents - 5th Harmonic
      IopA_5h[k] = np.abs(IaHW_5h[k] + IaXW_5h[k])
46
      lopB_5h[k] = np.abs(lbHW_5h[k] + lbXW_5h[k])
47
      IopC_5h[k] = np.abs(IcHW_5h[k] + IcXW_5h[k])
48
      # Calculation of restraint currents
50
      IresA[k] = (np.abs(IaHW[k]) + np.abs(IaXW[k]))
```

```
IresB[k] = (np.abs(IbHW[k]) + np.abs(IbXW[k]))
52
      IresC[k] = (np.abs(IcHW[k]) + np.abs(IcXW[k]))
53
54
      # Calculation of adjusted currents by harmonics
      IadjA[k] = IresA[k] + (1 / SLP) * ((100 / k2) * IopA_2h[k] + 
56
                           (100 / k5) * IopA_5h[k])
      IadjB[k] = IresB[k] + (1 / SLP) * ((100 / k2) * IopB_2h[k] + 
                           (100 / k5) * IopB_5h[k])
      IadjC[k] = IresC[k] + (1 / SLP) * ((100 / k2) * IopC_2h[k] + 
60
                           (100 / k5) * IopC_5h[k])
61
      # Calculation of Harmonic Blocking variables
63
      BloqA_2h[k] = ((IopA_2h[k] / IopA[k]) * 100) if IopA[k] != 0 else 0
64
      BloqB_2h[k] = ((IopB_2h[k] / IopB[k]) * 100) if IopB[k] != 0 else 0
      BloqC_2h[k] = ((IopC_2h[k] / IopC[k]) * 100) if IopC[k] != 0 else 0
      BloqA_5h[k] = ((IopA_5h[k] / IopA[k]) * 100) if IopA[k]
                                                                 != 0 else 0
67
      BloqB_5h[k] = ((IopB_5h[k] / IopB[k]) * 100) if IopB[k] != 0 else 0
68
      BloqC_5h[k] = ((IopC_5h[k] / IopC[k]) * 100) if IopC[k] != 0 else 0
69
70
71
      ##### Actuation of function 87T #####
72
73
      # Actuation WITHOUT harmonic restriction
      if (IopA[k] > SLP * IresA[k] and IopA[k] > Imin) or \
75
               (IopB[k] > SLP * IresB[k] and IopB[k] > Imin) or 
               (IopC[k] > SLP * IresC[k] and IopC[k] > Imin):
77
          TRIP87T[k] = 1
78
79
      # Actuation WITH only harmonic restriction
80
      if (IopA[k] > (SLP * IadjA[k]) and IopA[k] > Imin) or \
               (IopB[k] > (SLP * IadjB[k]) and IopB[k] > Imin) or \setminus
               (IopC[k] > (SLP * IadjC[k]) and IopC[k] > Imin):
83
          TRIP87T_resharm[k] = 1
84
85
      # Actuation WITH only blocking by harmonics
      if TRIP87T[k] and ((BloqA_2h[k] < k2B) and (BloqB_2h[k] < k2B) and
87
                          (BloqC_2h[k] < k2B) and (BloqA_5h[k] < k5B) and
                          (BloqB_5h[k] < k5B) and (BloqB_5h[k] < k5B)):
          TRIP87T_bloqharm[k] = 1
90
91
      # Actuation WITH restriction and blocking by harmonics
92
      if TRIP87T_resharm[k] and \
93
                       ((BloqA_2h[k] < k2B) and (BloqB_2h[k] < k2B) and
94
                        (BloqC_2h[k] < k2B) and (BloqA_5h[k] < k5B) and
95
                        (BloqB_5h[k] < k5B) and (BloqB_5h[k] < k5B)):
96
          TRIP87T_resbloqharm[k] = 1
```

Code 5.4: Part of the Python implementation of the 87T function.

### 5.2.3.3 87Q function

As for function 87T, with the corrected currents, function 87Q is calculated by implementing the Equations 3.17, 3.18, 3.19, and 3.20. Harmonic blocking uses the same equations and

calculations demonstrated in the 87T function. The Code 5.5 shows the implementation of the function.

```
import numpy as np
4 ######
               87Q FUNCTION
7 IHQ = np.arange(0, Dados.NumPontos, dtype=complex)
8 IXQ = np.arange(0, Dados.NumPontos, dtype=complex)
9 IopQ = np.arange(0, Dados.NumPontos, dtype=float)
10 IresQ = np.arange(0, Dados.NumPontos, dtype=float)
TRIP87Q = np.zeros(Dados.NumPontos)
12 TRIP87Q_bloqharm = np.zeros(Dados.NumPontos)
_{13} T = 1/60
14 \text{ ti} = 0
 for k in range(0, NumPoints):
16
      # Calculation of negative sequence currents
18
      a = complex(np.cos(2 * np.pi / 3), np.sin(2 * np.pi / 3))
19
      IHQ[k] = (1 / 3) * (IaHW[k] + ((a ** 2) * IbHW[k]) + (a * IcHW[k]))
20
      IXQ[k] = (1 / 3) * (IaXW[k] + ((a ** 2) * IbXW[k]) + (a * IcXW[k]))
21
23
      # Calculation of operating currents
      IopQ[k] = np.abs(IHQ[k] + IXQ[k])
24
      # Calculation of restraint currents
26
      IresQ[k] = np.max([np.abs(IHQ[k]), np.abs(IXQ[k])])
27
28
      ##### Actuation of function 87Q ######
29
      # Actuation WITHOUT delay and WITHOUT blocking by harmonics
30
      if IopQ[k] > SLPQ * IresQ[k] and IopQ[k] > IminQ:
31
          TRIP87Q[k] = 1
      # Actuation WITHOUT delay and WITH blocking by harmonics
34
      if TRIP87Q[k] == 1 and ((BloqA_2h[k] < k2B) and (BloqB_2h[k] < k2B)
35
                         and (BloqC_2h[k] < k2B) and (BloqA_5h[k] < k5B)
                         and (BloqB_5h[k] < k5B) and (BloqB_5h[k] < k5B)):
          TRIP87Q_bloqharm[k] = 1
38
39
      # Actuation WITH a delay of two cycles and WITHOUT blocking by harmonics
40
      if TRIP87Q[k] == 1 and TRIP87Q[k - 1] == 0:
          ti = t[k]
42
43
      if (t[k] - ti) > (T * 2) and TRIP87Q[k] == 1:
          TRIP87Qdly[k] = 1
45
46
      # Actuation WITH a delay of two cycles and WITH blocking by harmonics
      if TRIP87Qdly[k] == 1 and ((BloqA_2h[k] < k2B) and (BloqB_2h[k] < k2B)
                            and (BloqC_2h[k] < k2B) and (BloqA_5h[k] < k5B)
49
                            and (BloqB_5h[k] < k5B) and (BloqB_5h[k] < k5B)):
50
          TRIP87Qdly_bloqharm[k] = 1
```

Code 5.5: Part of the Python implementation of the 87Q function.

### 5.2.3.4 REF function

Considering their ground connections, the REF function applies only to the high-voltage side of the converter transformers. Therefore, the function is calculated using only the currents of the high-voltage terminal and from the implementation of equations 3.21, 3.22, 3.23, and 3.24. Code 5.6 demonstrates the implementation of the function.

```
import numpy as np
REF FUNCTION
6 Iz_REF = np.zeros(dados.NumPontos, dtype=complex)
 In_REF = np.zeros(dados.NumPontos, dtype=complex)
8 IopREF = np.zeros(dados.NumPontos, dtype=float)
9 IresREF = np.zeros(dados.NumPontos, dtype=float)
10
for k in range(0, NumPoints):
12
     # Zero sequence current and neutral current
     Iz_REF[k] = IaH_FCOS[k] + IbH_FCOS[k] + IcH_FCOS[k]
     In_REF[k] = IN_FCOS[k]
14
     # Calculation of operating and restriction currents
16
     IopREF[k] = np.abs(In_REF[k])
17
     IresREF[k] = kr * ((np.abs(In_REF[k] - Iz_REF[k])) - (np.abs(In_REF[k] +
     Iz_REF[k])))
19
     ##### Actuation of function REF #####
20
     # Actuation WITHOUT blocking by harmonics
22
     if IopREF[k] > IresREF[k] and IopREF[k] > IminREF:
         TRIPREF[k] = 1
23
24
     # Actuation WITH blocking by harmonics
     if TRIPREF[k] == 1 and ((BloqA_2h[k] < k2B) and (BloqB_2h[k] < k2B)
26
                       and (BloqC_2h[k] < k2B) and (BloqA_5h[k] < k5B)
27
                       and (BloqB_5h[k] < k5B) and (BloqB_5h[k] < k5B)):
28
         TRIPREF_bloqharm[k] = 1
```

Code 5.6: Part of the Python implementation of the REF function.

### 5.3 BATCH SIMULATIONS

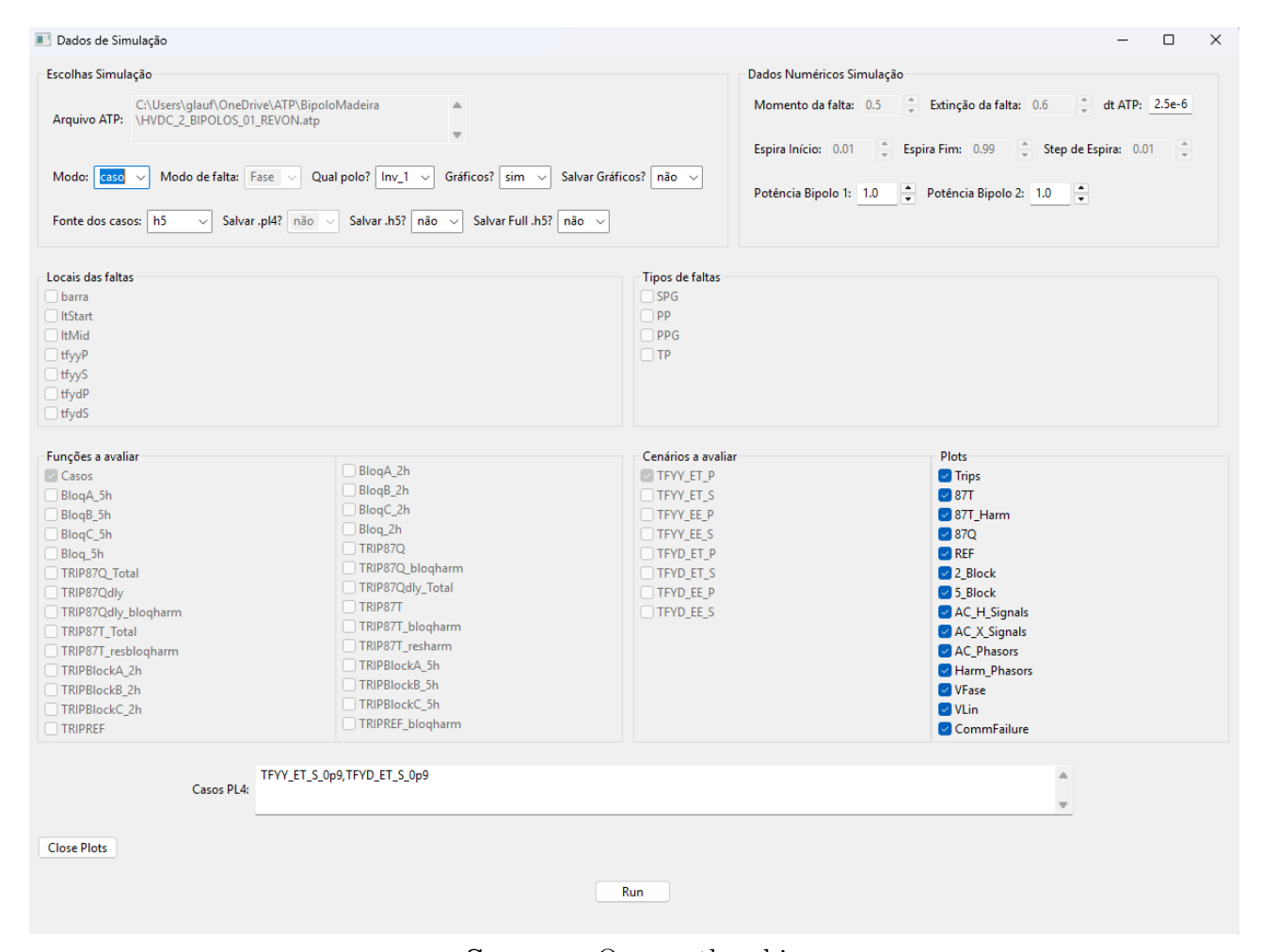
As seen in Chapter 3, the location of the internal fault in the transformer impacts whether or not its differential protections operate. Therefore, the evaluation of these protections must be carried out in-depth, checking several possible scenarios.

With this in mind, batch simulations were performed using a Python routine that edits the at the analyzed system to include simulation parameters for a specific event,

runs the simulation in ATP, and then executes the simulation of the differential functions. In this manner, the Python routine automatically executed the flow depicted in Figure 5.5 for several configured scenarios and saved the results for analysis.

The development of this routine was initially based on the open-source Python library pyATP, available on GitHub (PDB5627, 2016). The library was then adapted to meet the specific requirements of this work. Additionally, a graphical user interface (GUI) was created to facilitate the configuration and execution of the simulations. This GUI is shown in Figure 5.6.

Figure 5.6: Graphical user interface developed in Python to manage and execute batch simulations in ATP, including configuration of fault types, locations, and protection functions.



Source: Own authorship.

# RESULTS PRESENTATION AND ANALYSIS

In this work, the performance of the 87T, 87Q, and REF protection functions is evaluated exclusively for the converter transformers connected to the inverter station of Bipole 1 at the Araraquara 2 substation, with a primary focus on the converter transformers of Pole 1.

The converter transformers of Pole 1 will be referred to as TFYD and TFYY, and their terminals will be considered as the primary side, connected to the AC network, and the secondary side, connected to the converters. Additionally, the configuration of TFYD is grounded star on the primary side and delta on the secondary side. In contrast, TFYY is grounded star on the primary side and ungrounded star on the secondary side.

The performance of function 87T was evaluated under two scenarios: without restrictions by harmonics and with harmonic restrictions and blocking (87T R.B.H.). Similarly, function 87Q was assessed with harmonic blocking (87Q B.H.), without harmonic blocking, with delay (87Q DLY), and without delay.

In addition to these assessments, the REF function was evaluated with (REF B.H.) and without harmonic blocking. However, unlike the previous functions, the REF evaluation was exclusively on the primary side of the transformers and only for faults with ground connections. This approach was because of the concept of the function and because the secondary of the TFYY transformer is ungrounded, and the secondary of the TFYD transformer is connected in delta.

Several faults were evaluated considering two different transmission values in the bipoles: 10% (minimum value) and 100%. In all cases, the two bipoles had the same power and operated in a balanced manner. These different transmission values were considered to evaluate the performance of the differential elements more comprehensively, considering that the high power flow in the transformers impacts the performance of the 87T function.

External and internal faults were evaluated to verify the selectivity and reliability of diffe-

rential functions. The internal fault scenarios were chosen according to the fault probabilities presented in Section 3.1. The events evaluated were:

- Turn-to-turn faults taking from 1 to 100% of the turns in both the primary and secondary of the converter transformers.
- Turn-to-ground faults taking from 1 to 100% of the turns in both the primary and secondary of the converter transformers.
- Single-phase-to-ground, phase fault at converter transformers' primary and secondary terminals.
- Single-phase-to-ground, phase-to-phase, phase-to-phase-to-ground, and three-phase faults at the beginning and middle of an AC transmission line connected to the Araraquara 2 Substation.
- Energization of the converter transformers.

Turn-to-ground, turn-to-turn, and single-phase-to-ground short circuits were all simulated on phase A of the equipment, while phase-to-phase and phase-to-phase-to-ground short circuits were simulated on phases A and B.

# 6.1 PROTECTION FUNCTION SETTINGS

The protection functions studied in this work were configured according to Table 6.1. These settings were used according to values typically found in the literature and the field (SCHWEIT-ZER ENGINEERING LABORATORIES, INC., 2022). They were optimized based on batch simulations with the scenarios presented in the paper to find the best cost-benefit ratio for the protections. In other words, the parameters where the functions would be as sensitive as possible to internal faults and yet would not operate incorrectly even for the most severe external faults, such as a three-phase fault on the AC bus to which the transformers are connected.

### 6.2 EXTERNAL FAULTS TO CONVERTER TRANSFORMERS

To analyze the operation of the converter transformer protections for external faults, short circuit assessments were performed on the 500 kV Araraquara 2/Taubaté transmission line and the 500 kV busbar at Substation Araraquara 2. Such analyses are justified by the improper operations of these protections that can occur due to voltage variations in the AC system after the extinction of a short circuit and the high level of harmonics caused by a short circuit near the bipoles and even by a possible commutation failure caused by the fault. It is worth noting that the estimation of phasors by the Modified Cosine filter already filters the existing harmonics, keeping only the fundamental; however, the filter does not filter interharmonics that may arise and can impact the calculations of differential functions and leads to erroneous operations.

Table 6.1: Protection function settings

Function	Variable	Settings
87T	SLP	0.3
	$I_{pickumin}$	1.0 p.u.
	$k_2$	15 %
	$k_5$	15 %
87Q	SLP	0.4
	$I_{pickupminq}$	0.1 p.u.
	Delay	0.5 cycles
REF	$k_R$	2.0
	$I_{pickupminr}$	0.2 p.u.
Blocking	$k_{2b}$	25 %
	$k_{5b}$	25~%

**Source:** Own authorship.

# 6.2.1 500 kV Araraquara 2/Taubaté transmission line

Some short circuit scenarios were simulated on the line in two locations, at the beginning (7 km from SUB Araraquara 2) and in the middle (167 km from any terminal). Single-phase-to-ground, phase-to-phase, phase-to-phase-to-ground, and three-phase faults were simulated for each location. All of them occurred within 0.5 seconds of the simulation. Furthermore, considering that one of the problems may arise when the faults are cleared and to simulate an

actual situation, the line was disconnected 100 ms after the onset of each fault.

As a result, there was no improper operation of the transformer protection functions in the simulations performed.

## 6.2.2 500 kV busbar at Substation Araraguara 2

The short-circuit simulations on the 500 kV bus at Substation Araraquara 2 were the same as those simulated on the line: Single-phase-to-ground, phase-to-phase, phase-to-phase-to-ground, and three-phase faults. However, the simulations occurred in only one location on the bus since changing the location would not affect the result. All faults occurred in 0.5 seconds of simulation and were also extinguished after 100 ms. However, the faults were extinguished during the simulations only by removing the fault, without disconnecting equipment, because the system used for simulation considers the substation as a single bus, so disconnecting the bus would disconnect the entire substation.

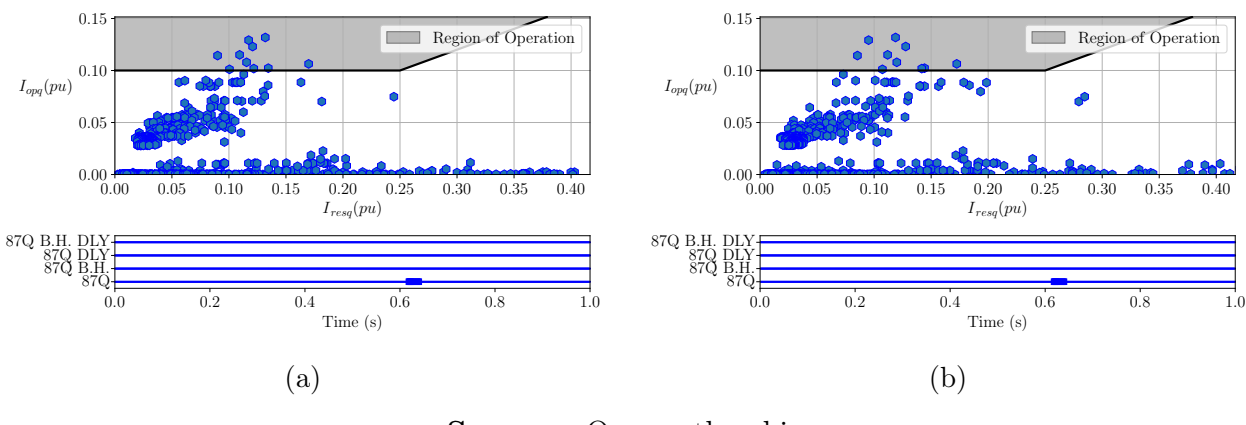
However, in an actual situation in normal operation, since the substation configuration is a one-and-a-half circuit breaker, only the bus in fault would be disconnected, preserving the connected equipment, which was done in simulation.

As a result, as well as for faults in the line, the operation of the transformer protection functions in the simulations was performed correctly. However, as observed in Section 3.5, the 87Q function is very sensitive to phase unbalance and may act improperly for unbalanced external faults. This statement is confirmed in the evaluations of the function for faults on the busbar considering the maximum power transmission in the bipoles, as shown in Figures 6.1b and 6.2a. In the figures, it is possible to verify the logical operation and the operational plan of the 87Q function with and without harmonic blocking and with and without delay. They represent, respectively, the operation of the function in the TFYD for the phase-to-phase-to-ground short circuit on the busbar and the operation in the TFYY for the phase-to-phase short circuit on the busbar.

In the phase-to-phase-to-ground case, there was improper operation of the 87Q function without harmonic blocking and delay, as also perceived in the operational plan of the function  $(I_{opq} \times I_{resq})$ , but with the addition of the safety measures, the function operated correctly.

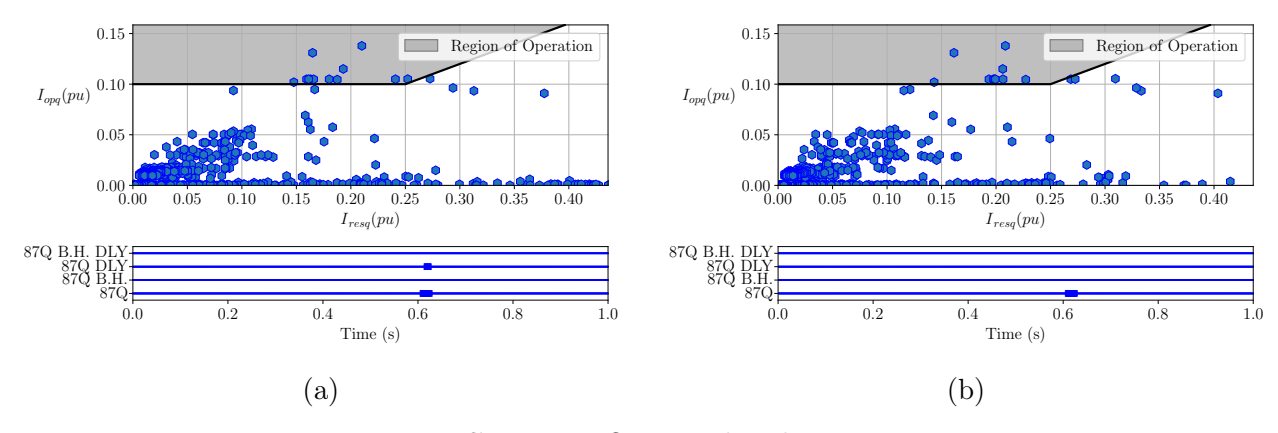
Even without the delay, the harmonic blocking already prevented the operation. The improper operation occurred after 0.6 seconds of the simulation, during the system recovery after the fault (Figure 6.3), when the AC voltage normalizes and allows the control of bipoles to increase the current of converter transformers to operational values (Figure 6.4).

Figure 6.1: 87Q function operation in (a) TFYY and (b) TFYD for a phase-to-phase-to-ground short circuit on the 500 kV busbar at Substation Araraquara 2.



**Source:** Own authorship.

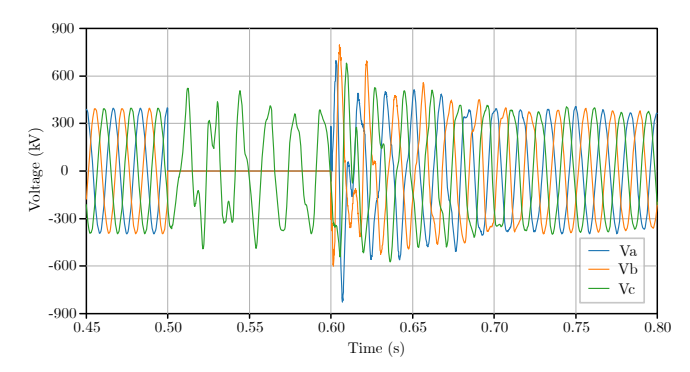
Figure 6.2: 87Q function operation in (a) TFYY and (b) TFYD for a phase-to-phase short circuit on the 500 kV busbar at Substation Araraquara 2.



**Source:** Own authorship.

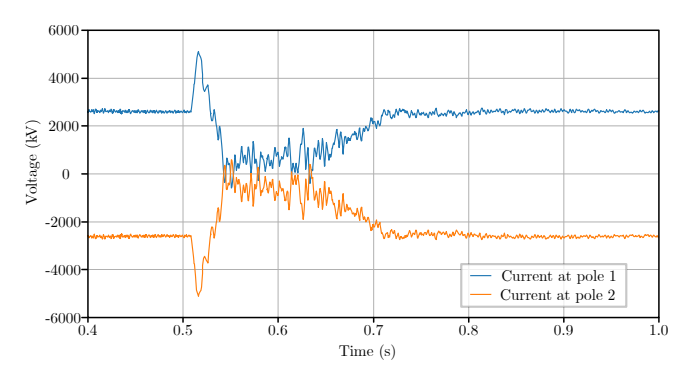
Additionally, in the case of the phase-to-phase fault, there was no incorrect operation; however, the function without blocking or delay nearly operated improperly, as shown in the function's operating plan (Figure 6.2a). The same scenario occurred for the three-phase short circuit on the bus, which, despite not being an unbalanced fault, generally has a more significant impact on the system and the bipole controls. Figure 6.5b demonstrates the operation of the 87Q function in the TFYD for the three-phase fault on the bus.

Figure 6.3: 500 kV busbar voltage of Substation Araraquara 2 for a phase-to-phase-to-ground short circuit on the busbar.



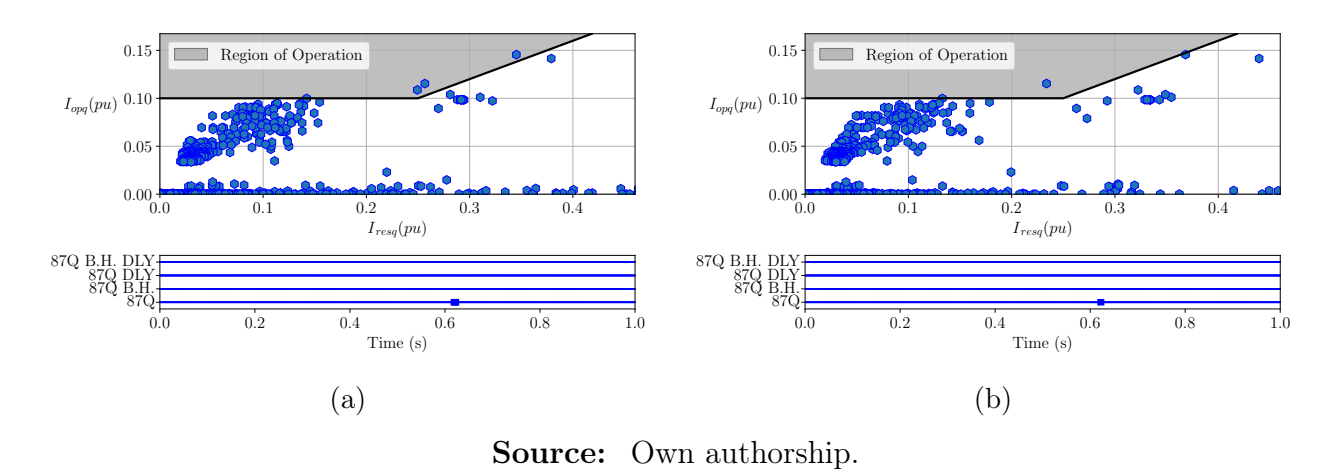
**Source:** Own authorship.

Figure 6.4: Bipole 1 current for a three-phase short circuit on the 500 kV busbar at Substation Araraquara 2.



**Source:** Own authorship.

Figure 6.5: 87Q function operation in (a) TFYY and (b) TFYD for a three-phase short circuit on the 500 kV busbar at Substation Araraquara 2.



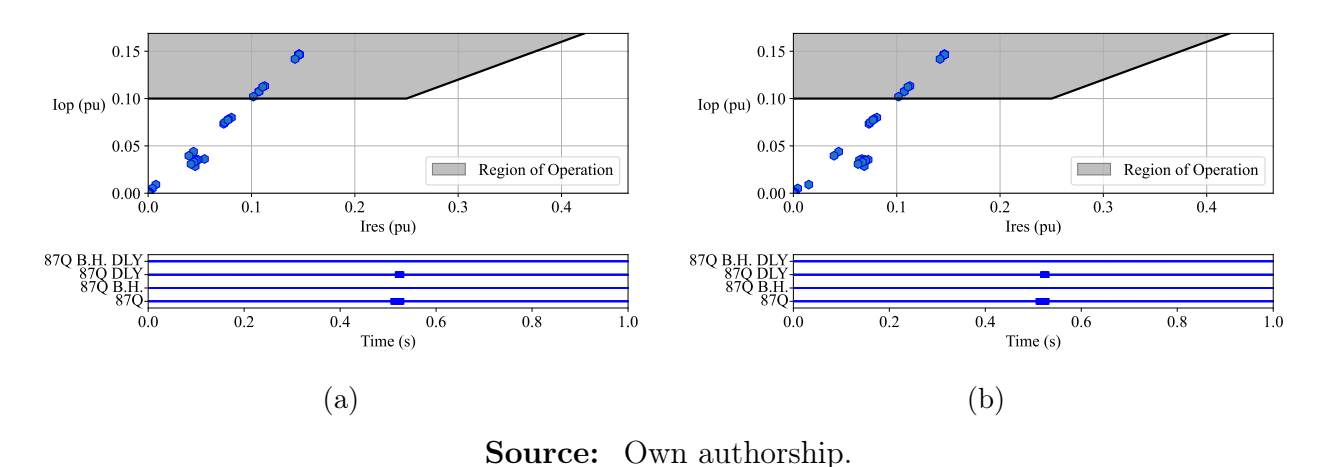
Therefore, despite the non-occurrence of improper operation due to faults on the line, they may still occur in different scenarios of the AC network, repeating what was observed at the

busbar. However, it is essential to emphasize that the improper operation analyzed above occurred in small samples, so their operation for external faults is neither reliable nor recurrent. Furthermore, the safety measures have already prevented incorrect operation, concluding that the function is safe for converter transformers.

#### 6.3 ENERGIZATION OF CONVERTER TRANSFORMERS

For the energization of the converter transformers, there was no trip of the 87T function with restriction and blocking by harmonics or trip of the 87Q with blocking by harmonics, as expected. However, since there is a risk of improper operation for a very sensitive 87Q function, the settings evaluated in Subsection 6.2.2 for the function were evaluated for the energization of the transformers. Therefore, again the settings were sufficient to prevent improper operation of the function due to blocking by harmonics, as verified in Figures 6.6a and 6.6b.

Figure 6.6: 87Q function operation in (a) TFYY and (b) TFYD for the energization of the transformers.



#### 6.4 INTERNAL FAULTS IN CONVERTER TRANSFORMERS

The performance of differential functions in converter transformers differs significantly between faults occurring on the primary and secondary sides, except for turn-to-turn faults. This distinction arises from the transformer's dual connection: to the AC system on the primary side and to the HVDC converters on the secondary side. Accordingly, the analysis of internal faults

was first organized by transformer terminal (primary or secondary) and then further categorized by fault type.

### 6.4.1 Primary side

#### 6.4.1.1 Short circuit turn-to-ground

First considering the transmission of the bipoles at 100% and a SLP of 0.5 according to Table 6.1, the 87T function with and without harmonic restriction and blocking only acted for turn-to-ground short-circuits in the primary of the converter transformers from 8% of turns involved in the fault. This was the case for both the TFYY and the TFYD, as shown in Figures 6.7 and 6.8. Naturally, as detailed in Chapter 3, the 87T function only starts to operate effectively from a specific value of turns involved, making it necessary to use the 87Q and REF functions. However, in some cases, the function identifies the fault starting from 2% of turns involved in the fault for conventional transformers (TAVARES, 2014), a significantly lower value than that observed for converter transformers in this study.

The first point to highlight regarding the low sensitivity of the 87T function is that it is not linked to harmonic restrictions or blocking. Figures 6.7 (87T R.B.H. function operation) and 6.8 (87T function operation) show that using 2<sup>nd</sup> and 5<sup>th</sup>-order harmonics did not reduce the protection sensitivity. Therefore, the probable cause is the systemic conditions in which these transformers are found. In the case of these converter transformers, in the scenario evaluated, the power of the pole to which they are connected at 100% is 1575 MW, with 787.5 MW divided between each transformer. Therefore, with the current in the phases high, for the 87T function to operate, a short-circuit in the turns must involve more turns to cause a sufficient difference in the phase currents, or the protection must have greater sensitivity.

Furthermore, for this scenario, below 8% of turns, the only way for the function to be sensitized is by reducing  $I_{pickupmin}$  below 1 pu, which is unwise and can cause the function to operate improperly due to measurement errors and normal system variations. Therefore, any SLP value below 0.3 makes the protection unnecessarily sensitive, while any SLP value above 0.3 does not reach the minimum of 8% of turns.

Figures 6.9 and 6.10 demonstrate the operation of the 87T function with and without

restraint and blocking by harmonics for a turn-to-ground fault taking 7% of turns in the transformer's primary side, while Figures 6.11 and 6.12 demonstrate a fault taking 8% of turns. The above statements become evident, considering the borderline but consistent performance for 8% of turns and the maximum operating current of less than 1 pu for 7% of turns.

Figure 6.7: 87T R.B.H. function operation in (a) TFYY and (b) TFYD for turn-to-ground short circuits on the primary side, with 100% power transmission in the bipoles.

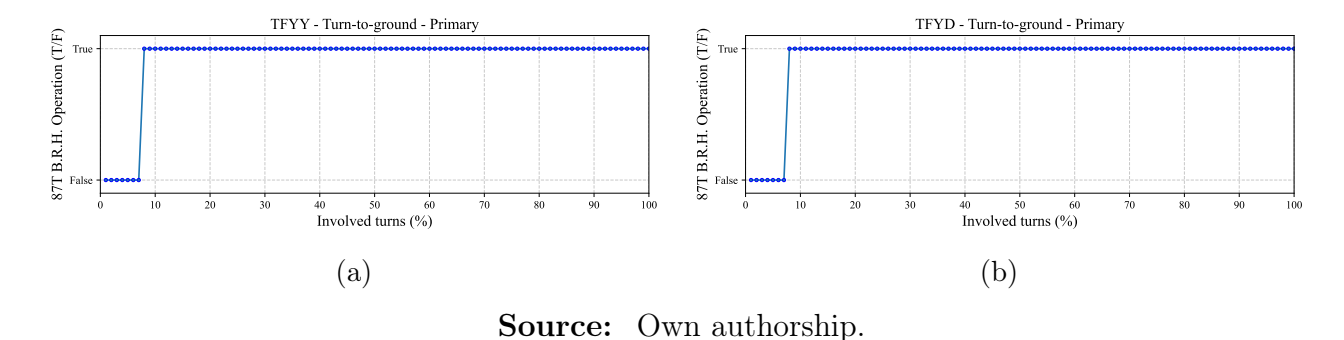


Figure 6.8: 87T function operation in (a) TFYY and (b) TFYD for turn-to-ground short circuits on the primary side, with 100% power transmission in the bipoles.

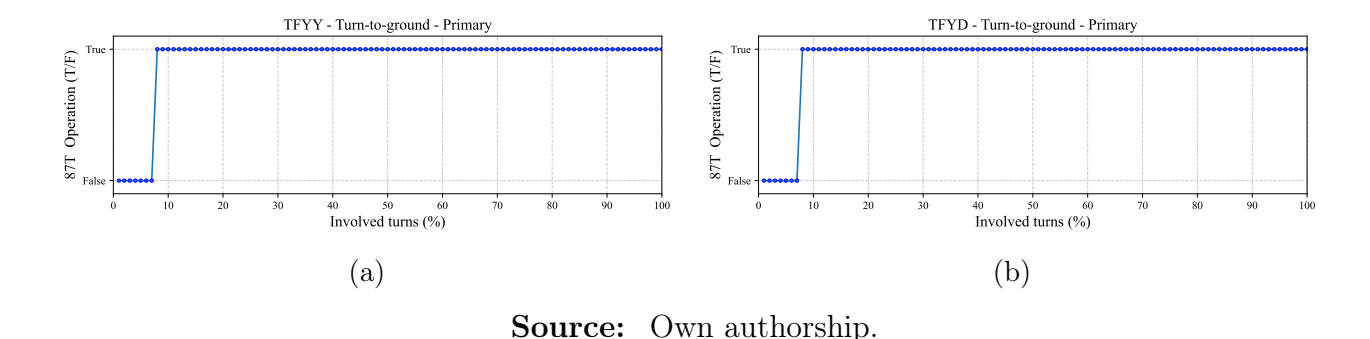


Figure 6.9: 87T R.B.H. function operation in (a) TFYY and (b) TFYD for a turn-to-ground short circuit at 7% of the primary side, with 100% power transmission in the bipoles.

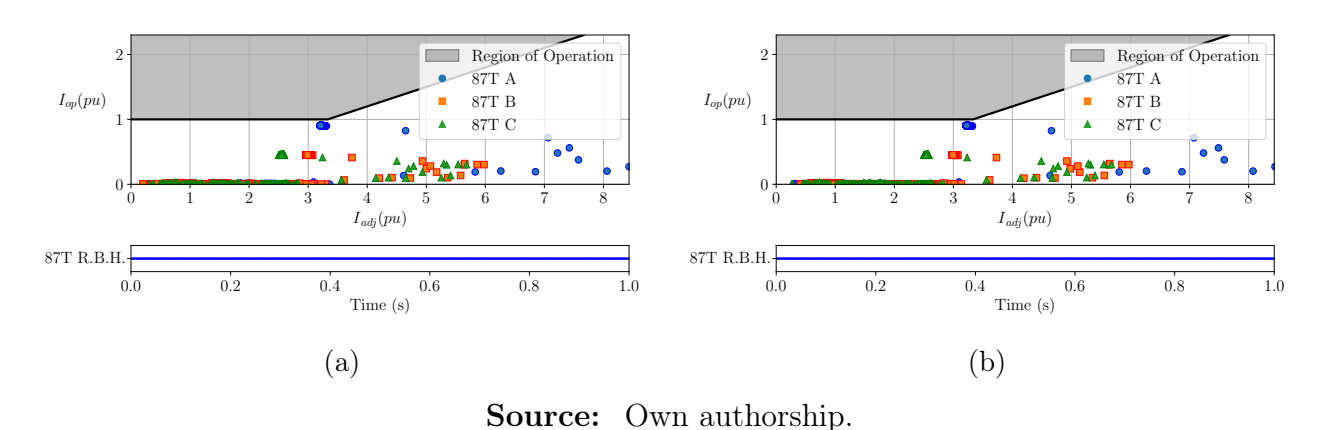
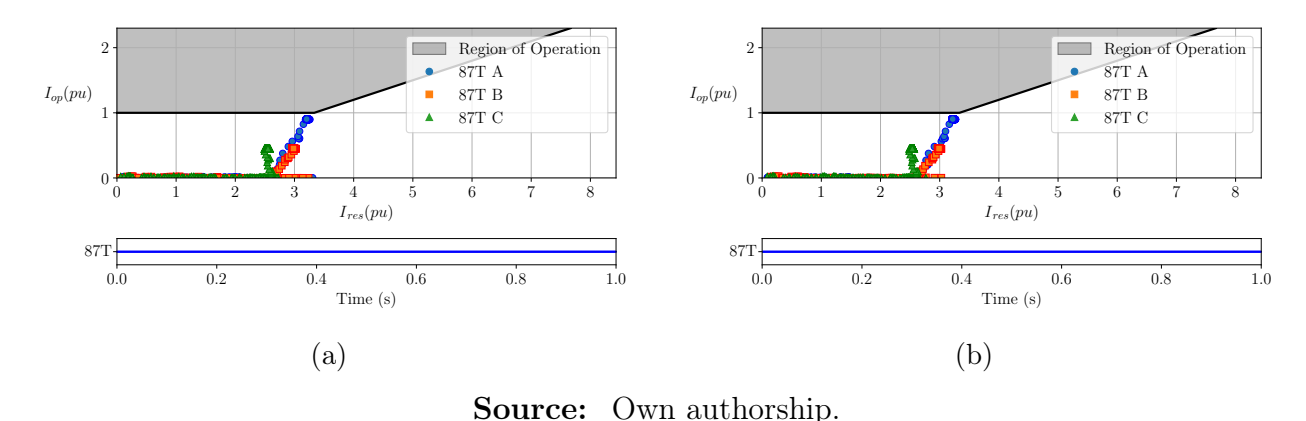


Figure 6.10: 87T function operation in (a) TFYY and (b) TFYD for a turn-to-ground short circuit at 7% of the primary side, with 100% power transmission in the bipoles.



For the same scenario with 100% power transmission in the bipoles and the settings in Table 6.1, the 87Q function operates correctly for almost all percentages of turns (Figure 6.13). This performance is as expected for the function, considering that in its concept, it was designed as a backup for the 87T function, being very sensitive to unbalanced faults. Therefore, since turn-to-ground faults are essentially single-phase-to-ground short circuits, the 87Q function effectively detects and protects the converter transformers in these cases. The only exception to the good performance of the function is the non-action for 1% of turns involved, with this short circuit case being detected by the REF function.

Figure 6.14 shows the operational plan of the 87Q function and its operation considering the blocking for a turn-to-ground fault taking 1% of the turns in TFYY and TFYD transformers. In this case, the operating current is minimal, so it would be necessary to reduce the  $I_{pickupminq}$  current to 0.06 pu to cover 100% of the turns. However, for the 87Q function, such a low  $I_{pickupminq}$  would result in many improper trips for normal conditions and external faults due to the natural sensitivity of the function. Figures 6.1, 6.2, and 6.5 for external faults on the bus confirm this statement.

Nevertheless, the function operation becomes consistent with 2% of the turns involved (Figure 6.15).

When evaluating the performance of the 87T function with the bipoles transmitting 10% of their power, the impact of the link transmission on the performance of the functions is confirmed. With this power value, the 87T function already operates from 7% of turns involved, even

with a SLP of 0.5 (Figure 6.16). This condition is maintained when the SLP is adjusted to 0.3 (6.16). The 87Q function again operates from 2% of turns involved, as expected (Figure 6.18).

Finally, the REF function with blocking by harmonics worked correctly for all turns percentages, considering 100% power in the bipoles and 10%, as shown in Figures 6.19 and 6.20, respectively.

Figure 6.11: 87T R.B.H. function operation in (a) TFYY and (b) TFYD for a turn-to-ground short circuit at 8% of the primary side, with 100% power transmission in the bipoles.

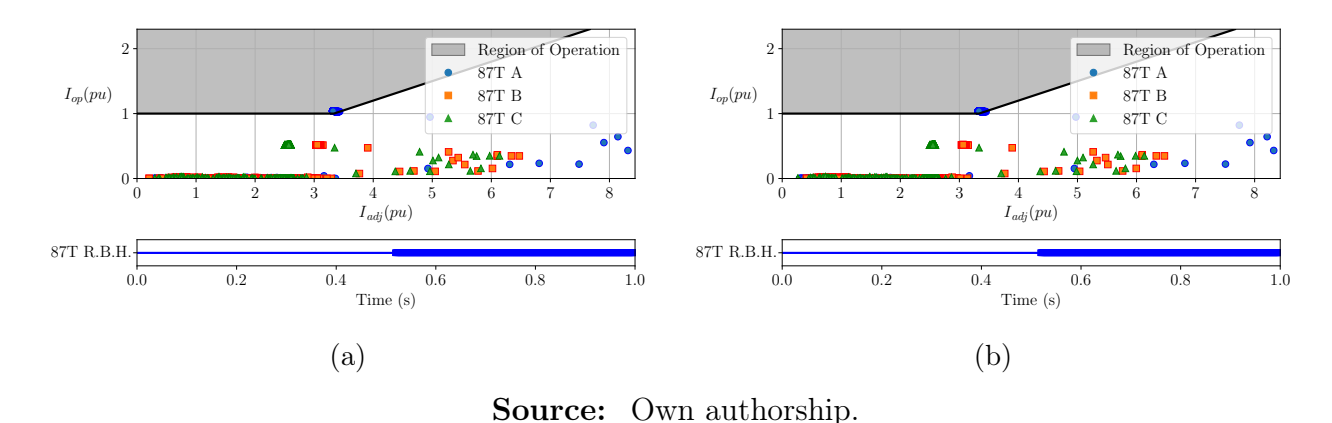


Figure 6.12: 87T function operation in (a) TFYY and (b) TFYD for a turn-to-ground short circuit at 8% of the primary side, with 100% power transmission in the bipoles.

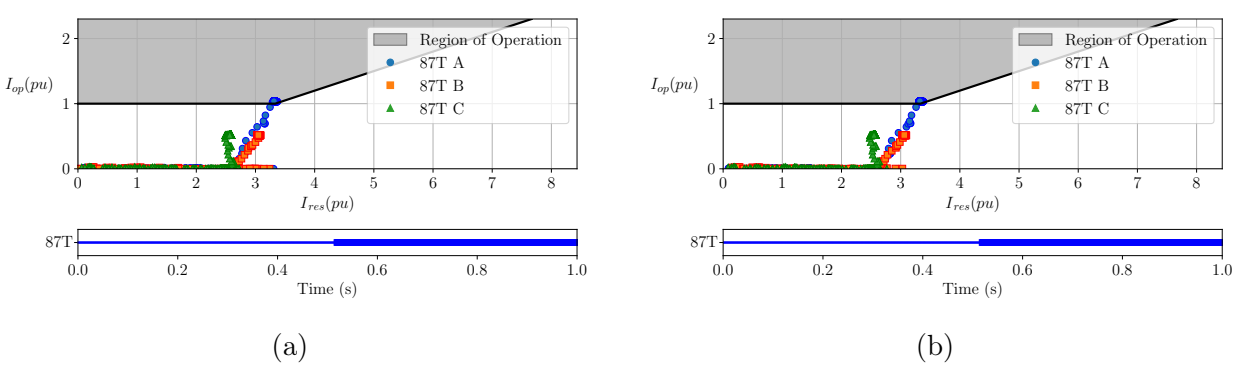


Figure 6.13: 87Q B.H. DLY function operation in (a) TFYY and (b) TFYD for turn-to-ground short circuits on the primary side, with 100% power transmission in the bipoles.

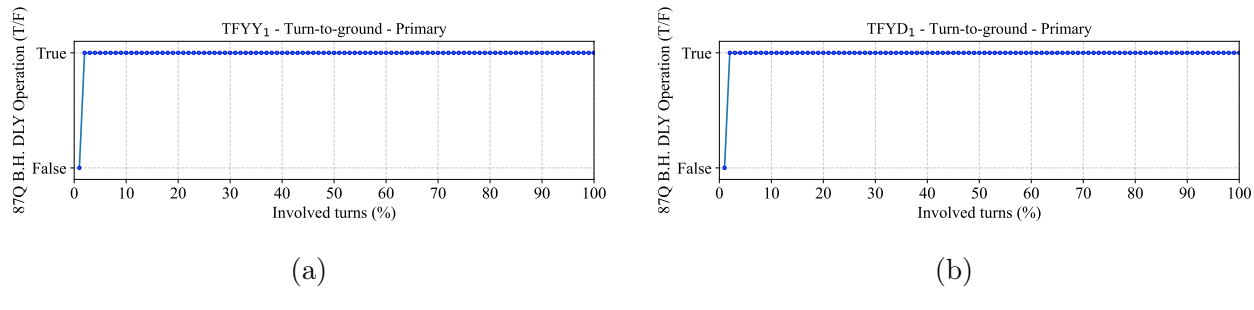
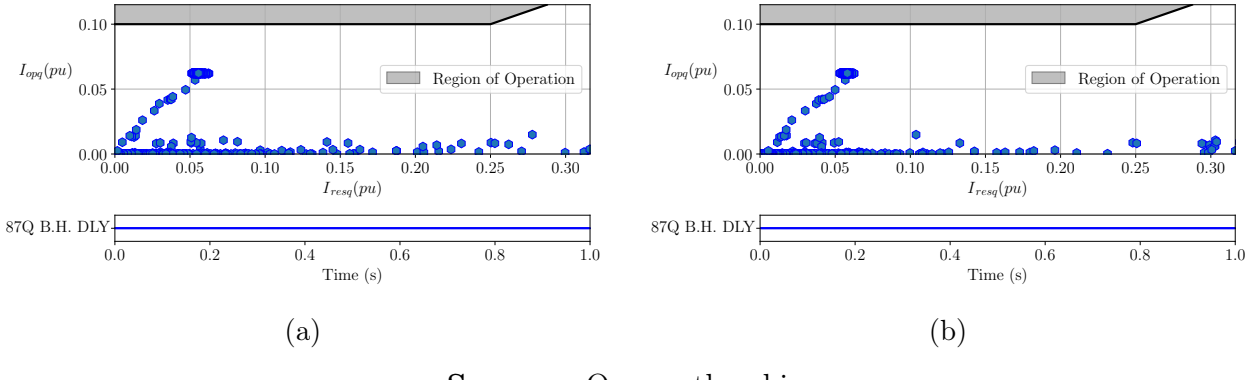


Figure 6.14: 87Q B.H. DLY function operation in (a) TFYY and (b) TFYD for a turn-to-ground short circuit at 1% of the primary side, with 100% power transmission in the bipoles.



**Source:** Own authorship.

Figure 6.15: 87Q B.H. DLY function operation in (a) TFYY and (b) TFYD for a turn-to-ground short circuit at 2% of the primary side, with 100% power transmission in the bipoles.

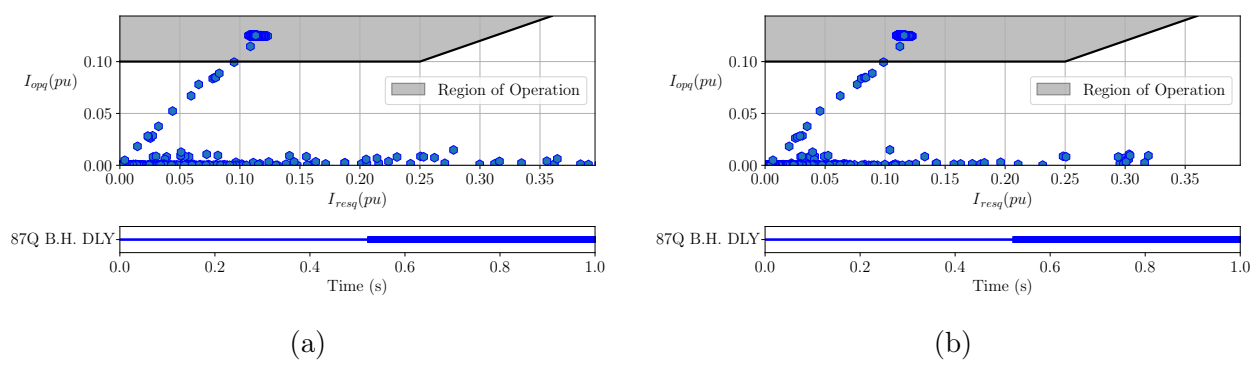


Figure 6.16: 87T R.B.H. function operation with a SLP of 0.5 in (a) TFYY and (b) TFYD for turn-to-ground short circuits on the primary side, with 10% power transmission in the bipoles.

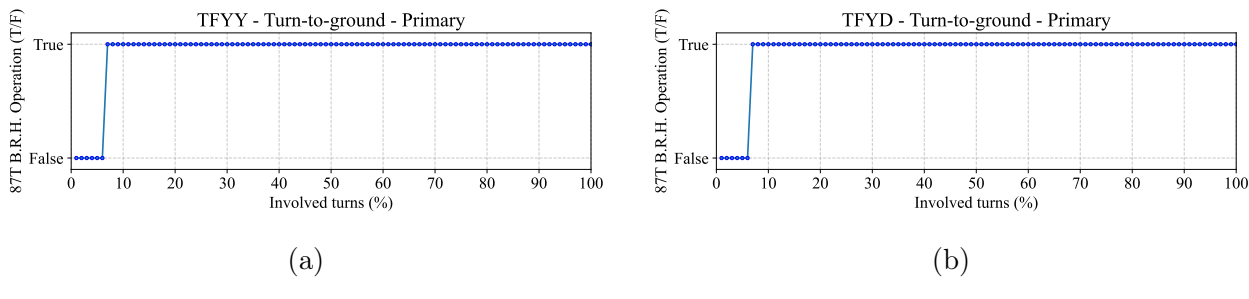
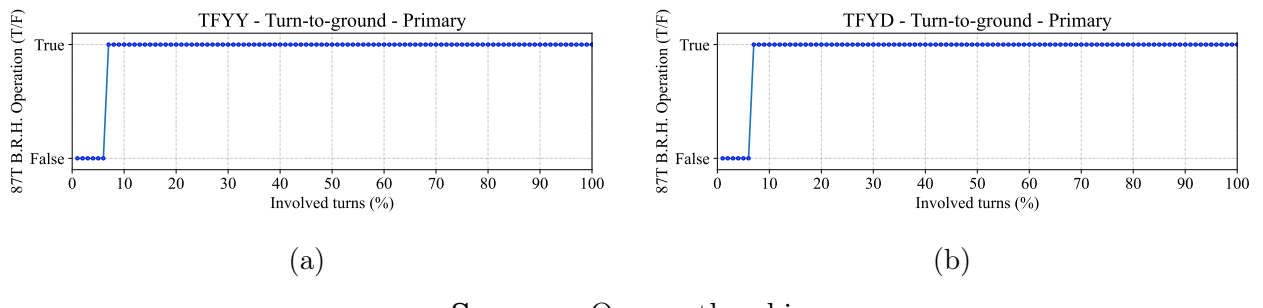


Figure 6.17: 87T R.B.H. function operation with a SLP of 0.3 in (a) TFYY and (b) TFYD for turn-to-ground short circuits on the primary side, with 10% power transmission in the bipoles.



Source: Own authorship.

Figure 6.18: 87Q B.H. DLY function operation in (a) TFYY and (b) TFYD for turn-to-ground short circuits on the primary side, with 10% power transmission in the bipoles.

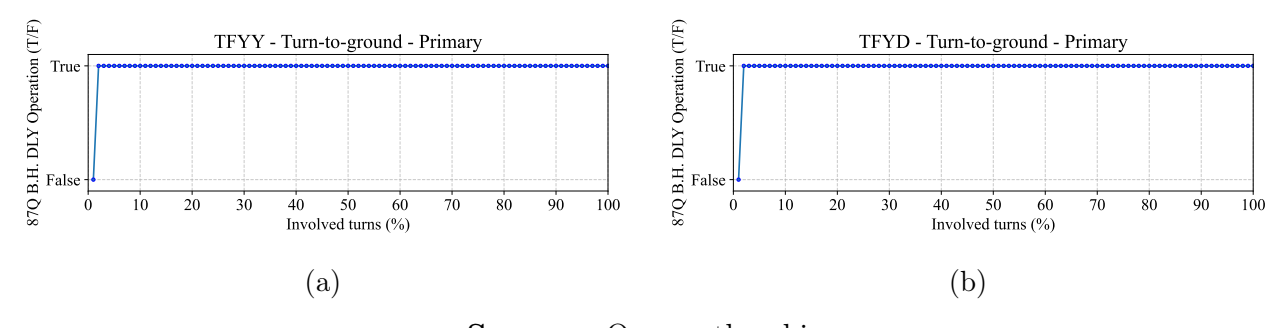


Figure 6.19: REF B.H. function operation in (a) TFYY and (b) TFYD for turn-to-ground short circuits on the primary side, with 100% power transmission in the bipoles.

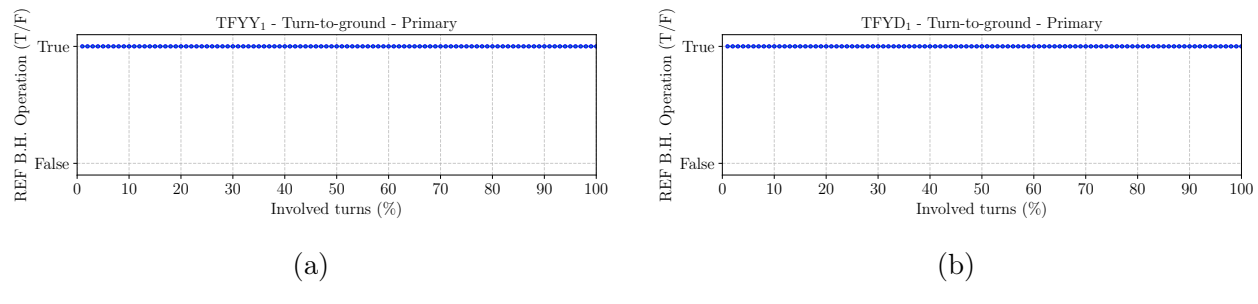
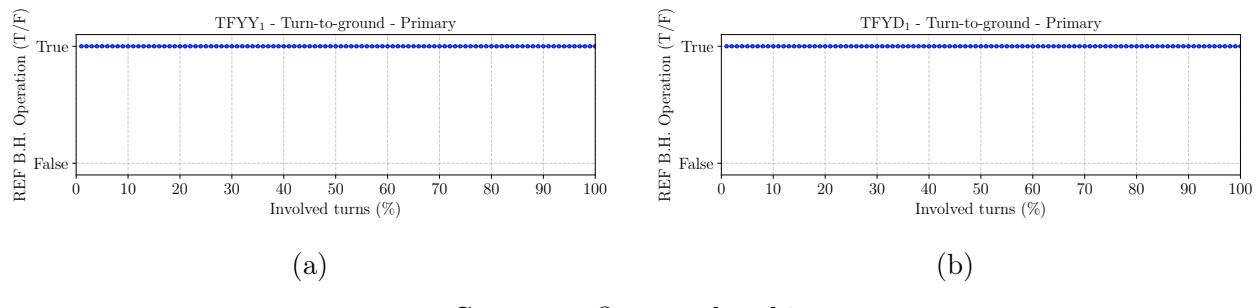


Figure 6.20: REF B.H. function operation in (a) TFYY and (b) TFYD for turn-to-ground short circuits on the primary side, with 10% power transmission in the bipoles.



Source: Own authorship.

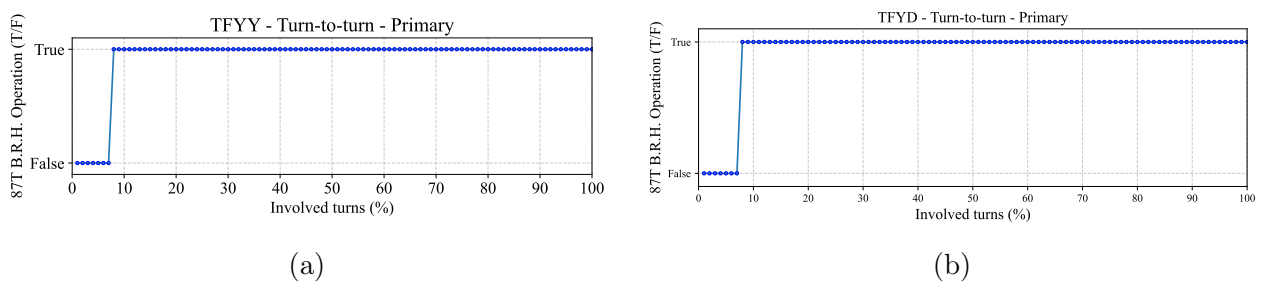
#### 6.4.1.2 Short circuit turn-to-turn

The performance of the 87T and 87Q functions for turn-to-turn short-circuits in the primary of the converter transformers has precisely the same result as that evaluated for turn-to-ground short-circuits in the primary, considering that the primary of the transformers is star-star and the faults cause the same decrease in turns in the windings according to the percentage of turns involved.

Figure 6.21 demonstrates the operation of the 87T function for turn-to-turn faults in the primary side of the converter transformers for bipoles at 100% of power transmission. In contrast, Figure 6.22 demonstrates the operation of the same function for bipoles at 10% of power transmission. Comparing them with Figures 6.7 and 6.17, the equality of the results with the turn-to-ground faults in the primary is confirmed.

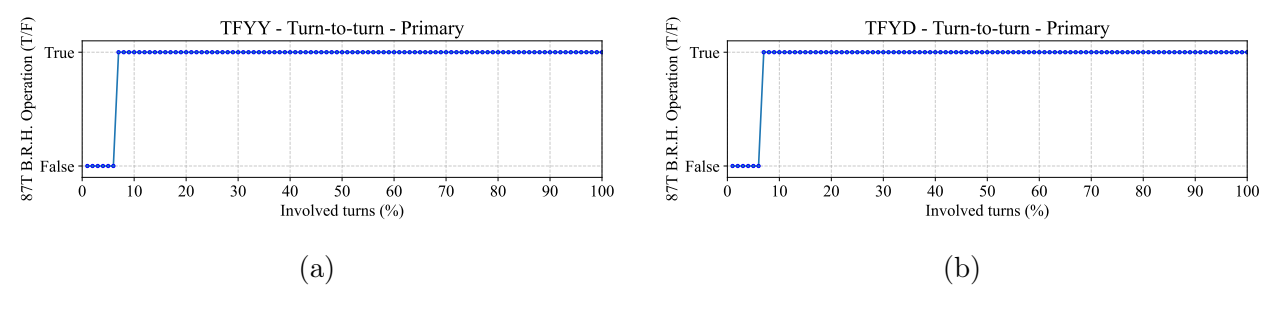
For the 87Q function, Figure 6.23 shows the function operation, and the same result occurs

Figure 6.21: 87T R.B.H. function operation in (a) TFYY and (b) TFYD for turn-to-turn short circuits on the primary side, with 100% power transmission in the bipoles.



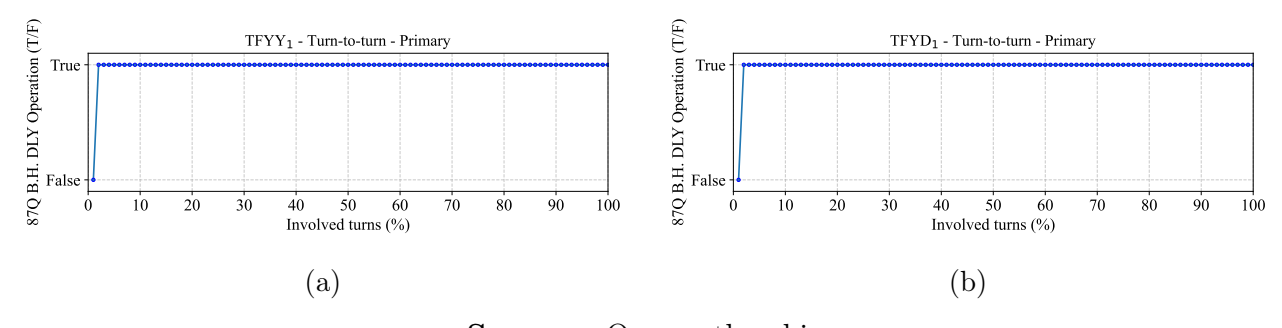
for the bipoles with 10% power transmission.

Figure 6.22: 87T R.B.H. function operation in (a) TFYY and (b) TFYD for turn-to-turn short circuits on the primary side, with 10% power transmission in the bipoles.



Source: Own authorship.

Figure 6.23: 87Q B.H. DLY function operation in (a) TFYY and (b) TFYD for turn-to-turn short circuits on the primary side, with 100% power transmission in the bipoles.



### 6.4.1.3 Single-phase-to-ground short circuit

The results for single-phase-to-ground short-circuits are equivalent to turn-to-ground short-circuits taking 100% of turns. Consequently, the differential functions do not present any error, as previously evaluated. Therefore, as expected, Figures 6.24, 6.25, and 6.26 confirm the results, where Figure 6.24 shows the performance of the 87T function with harmonic restraint and blocking. At the same time, Figure 6.25 demonstrates the performance of the 87Q function, and Figure 6.26 illustrates the operation of the REF function with the original settings. All figures show the results for the TFYY and TFYD transformers.

Considering the bipoles at 10% power transmission the functions had the same performance, as illustrated in Figures 6.27, 6.28, and 6.29.

Figure 6.24: 87T R.B.H. function operation in (a) TFYY and (b) TFYD for a single-phase-to-ground short circuit on the primary side, with 100% power transmission in the bipoles.

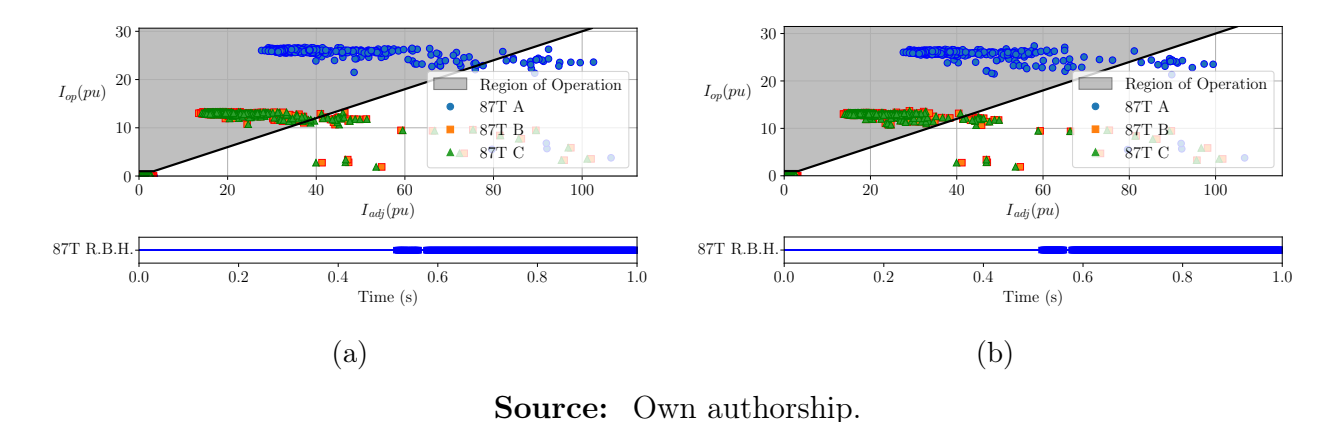


Figure 6.25: 87Q B.H. function operation in (a) TFYY and (b) TFYD for a single-phase-to-ground short circuit on the primary side, with 100% power transmission in the bipoles.

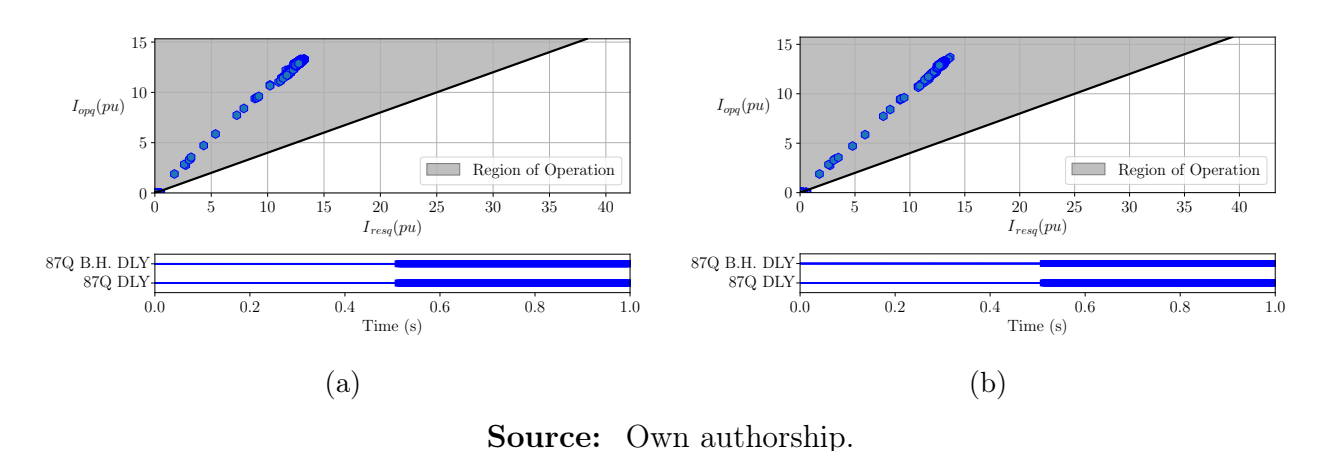


Figure 6.26: REF B.H. function operation in (a) TFYY and (b) TFYD for a single-phase-to-ground short circuit on the primary side, with 100% power transmission in the bipoles.

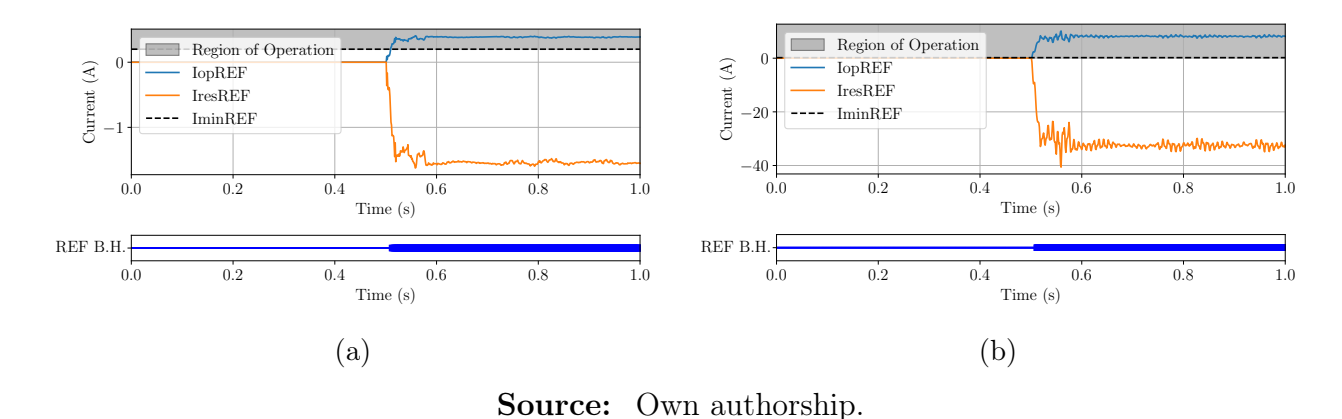


Figure 6.27: 87T R.B.H. function operation in (a) TFYY and (b) TFYD for a single-phase-to-ground short circuit on the primary side, with 10% power transmission in the bipoles.

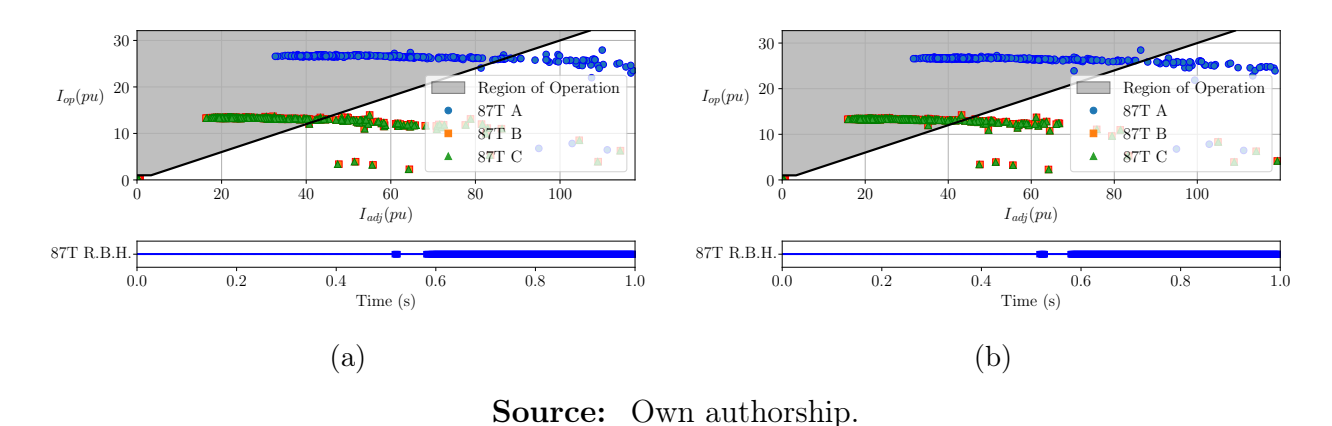


Figure 6.28: 87Q B.H. function operation in (a) TFYY and (b) TFYD for a single-phase-to-ground short circuit on the primary side, with 10% power transmission in the bipoles.

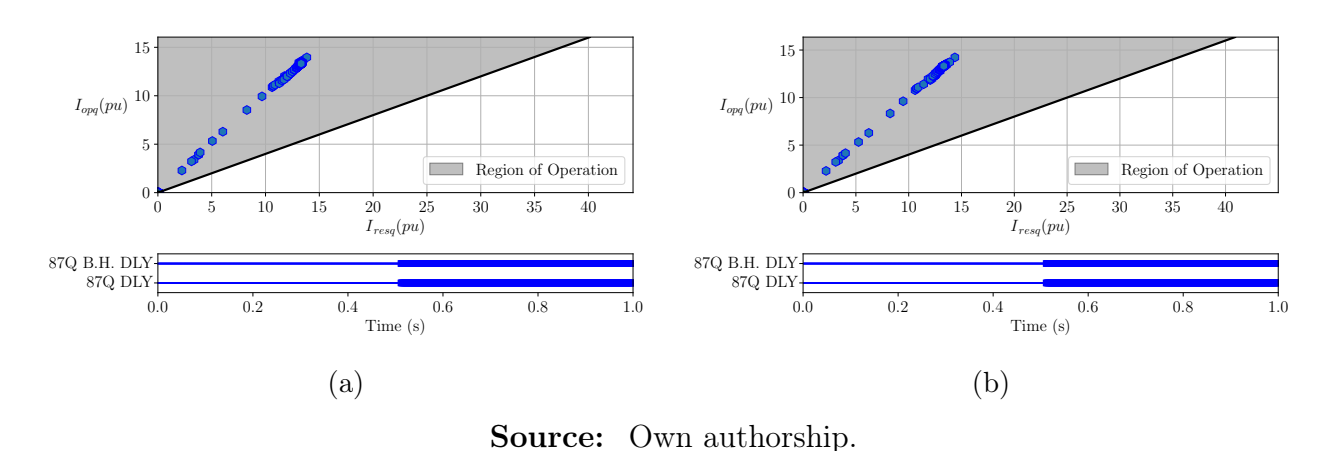
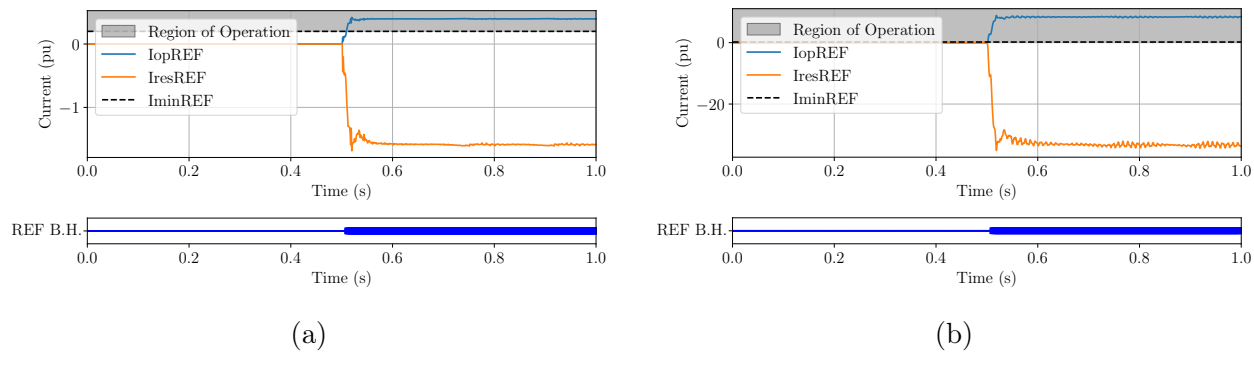


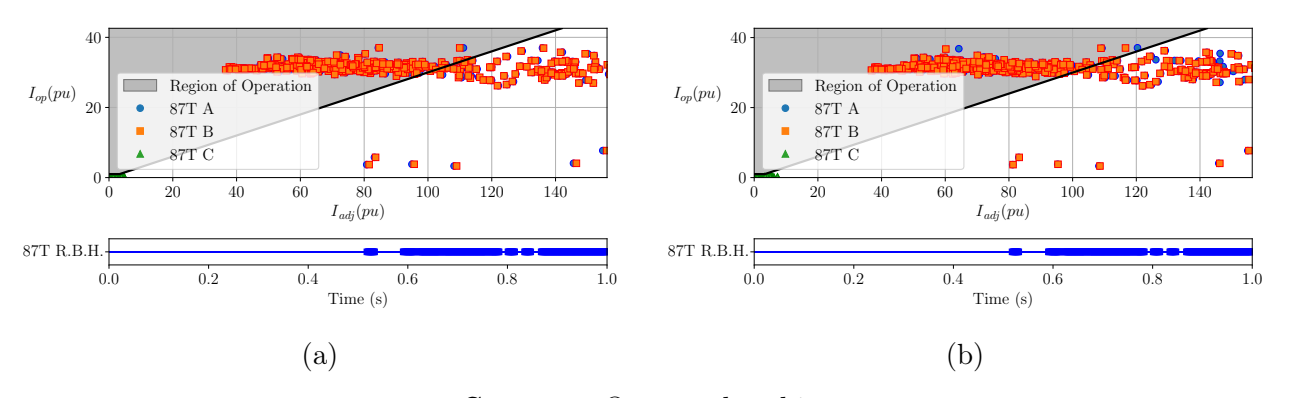
Figure 6.29: REF B.H. function operation in (a) TFYY and (b) TFYD for a single-phase-to-ground short circuit on the primary side, with 10% power transmission in the bipoles.



### 6.4.1.4 Phase-to-phase short circuit

Figures 6.30 and 6.31 show the performance of the differential functions for a phase-to-phase short-circuit in the primary side of transformers TFYY and TFYD with the bipoles at 100% power transmission. As expected, the functions performed correctly. The same result was found with the bipoles at 10% power transmission, as shown in Figures 6.32 and 6.33.

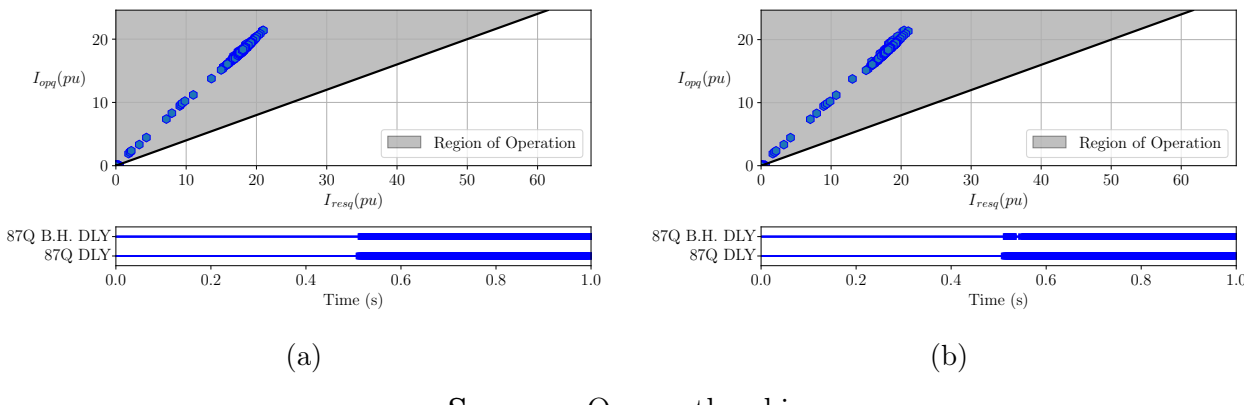
Figure 6.30: 87T R.B.H. function operation in (a) TFYY and (b) TFYD for a phase-to-phase short circuit on the primary side, with 100% power transmission in the bipoles.



# 6.4.1.5 Phase-to-phase-to-ground short circuit

As for the previously evaluated faults in the transformer's primary side, the differential functions also worked correctly for a phase-to-phase-to-ground short circuit in the primary of the TFYY and TFYD transformers, both at 100% power (Figures 6.34, 6.35, and 6.36) and at 10% power (Figures 6.37, 6.38, and 6.39).

Figure 6.31: 87Q B.H. function operation in (a) TFYY and (b) TFYD for a phase-to-phase short circuit on the primary side, with 100% power transmission in the bipoles.



Source: Own authorship.

Figure 6.32: 87T R.B.H. function operation in (a) TFYY and (b) TFYD for a phase-to-phase short circuit on the primary side, with 10% power transmission in the bipoles.

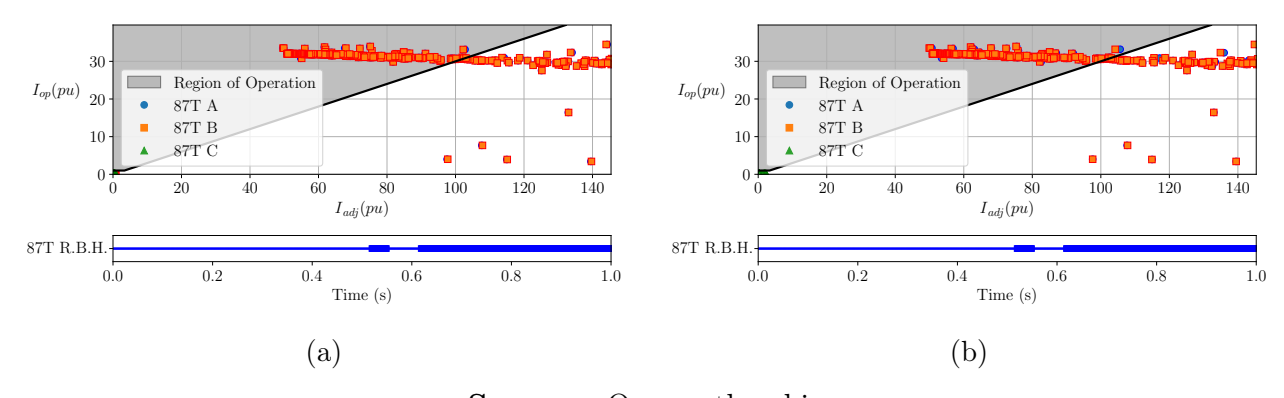


Figure 6.33: 87Q B.H. function operation in (a) TFYY and (b) TFYD for a phase-to-phase short circuit on the primary side, with 10% power transmission in the bipoles.

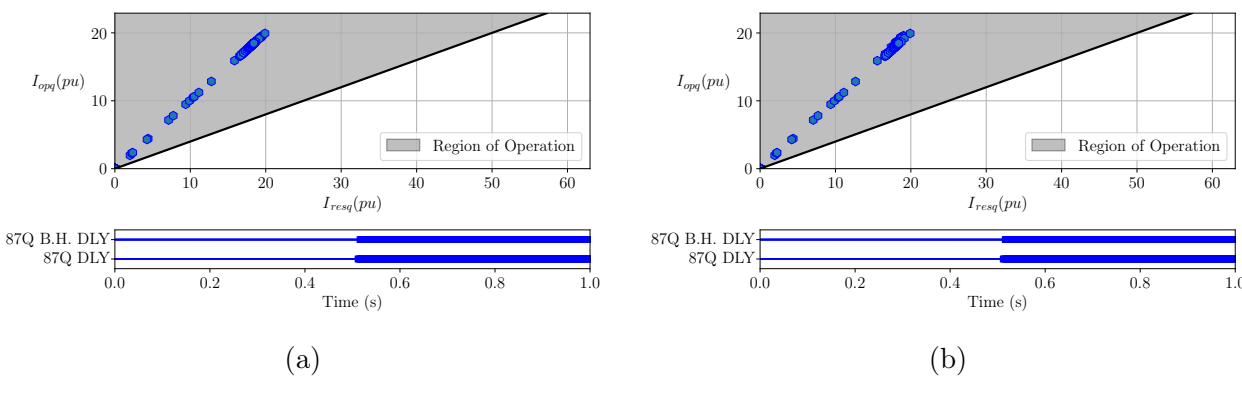
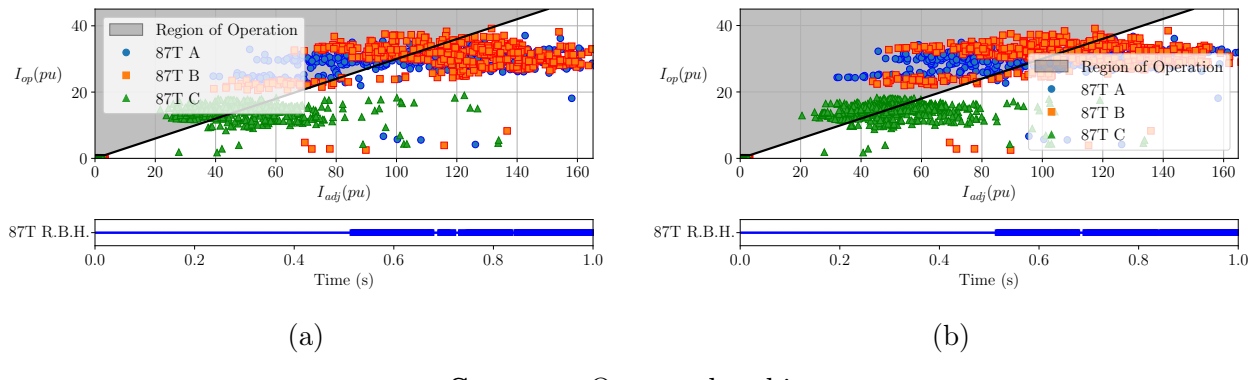


Figure 6.34: 87T R.B.H. function operation in (a) TFYY and (b) TFYD for a phase-to-phase-to-ground short circuit on the primary side, with 100% power transmission in the bipoles.



Source: Own authorship.

Figure 6.35: 87Q B.H. DLY function operation in (a) TFYY and (b) TFYD for a phase-to-phase-to-ground short circuit on the primary side, with 100% power transmission in the bipoles.

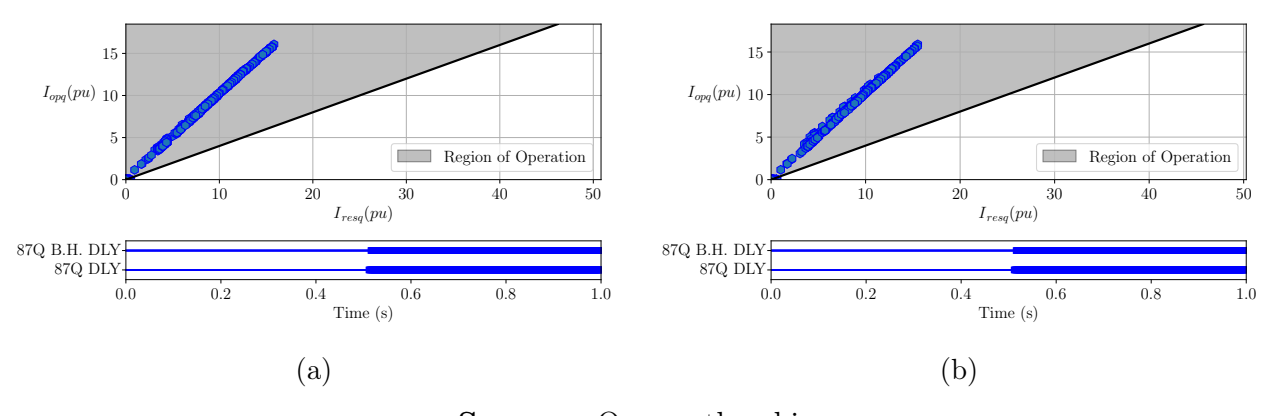


Figure 6.36: REF B.H. function operation in (a) TFYY and (b) TFYD for a phase-to-phase-to-ground short circuit on the primary side, with 100% power transmission in the bipoles.

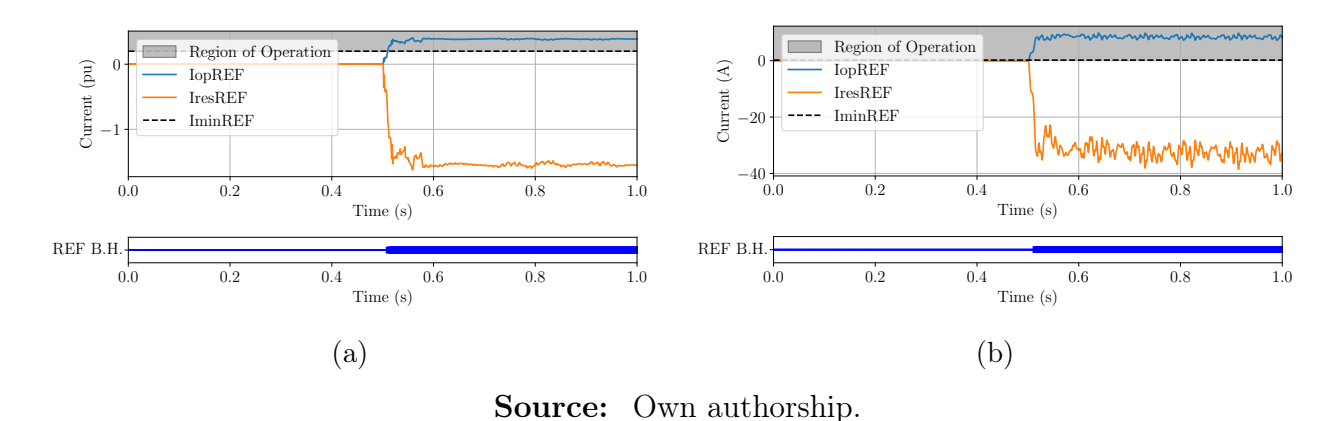


Figure 6.37: 87T R.B.H. function operation in (a) TFYY and (b) TFYD for a phase-to-phase-to-ground short circuit on the primary side, with 10% power transmission in the bipoles.

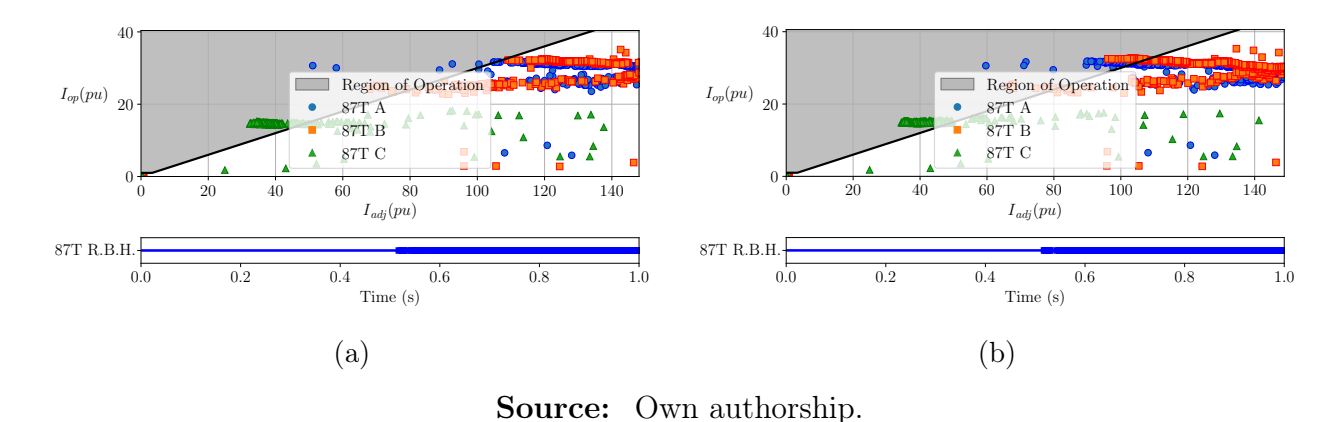


Figure 6.38: 87Q B.H. function operation in (a) TFYY and (b) TFYD for a phase-to-phase-to-ground short circuit on the primary side, with 10% power transmission in the bipoles.

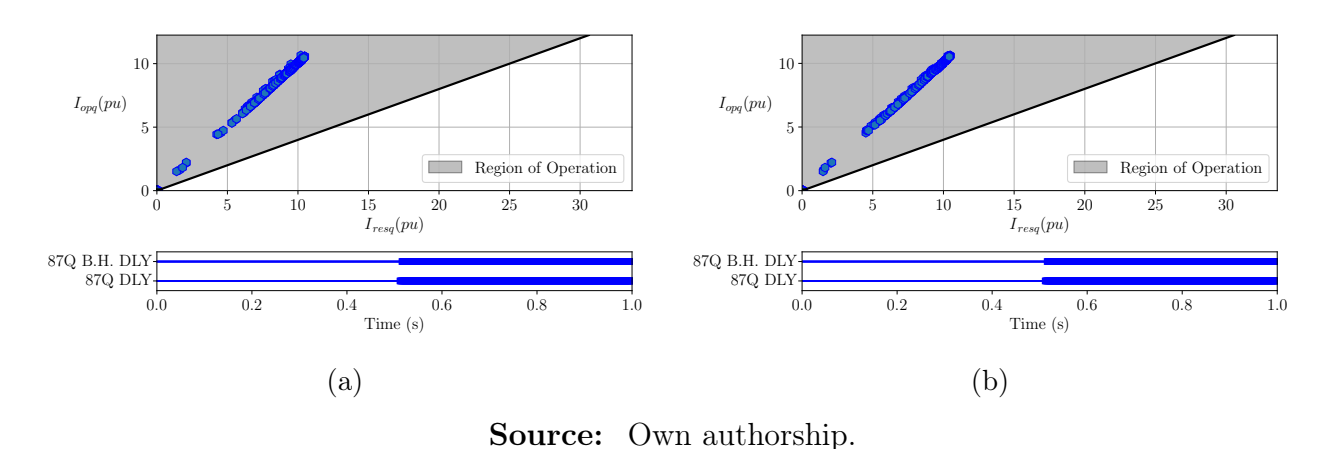
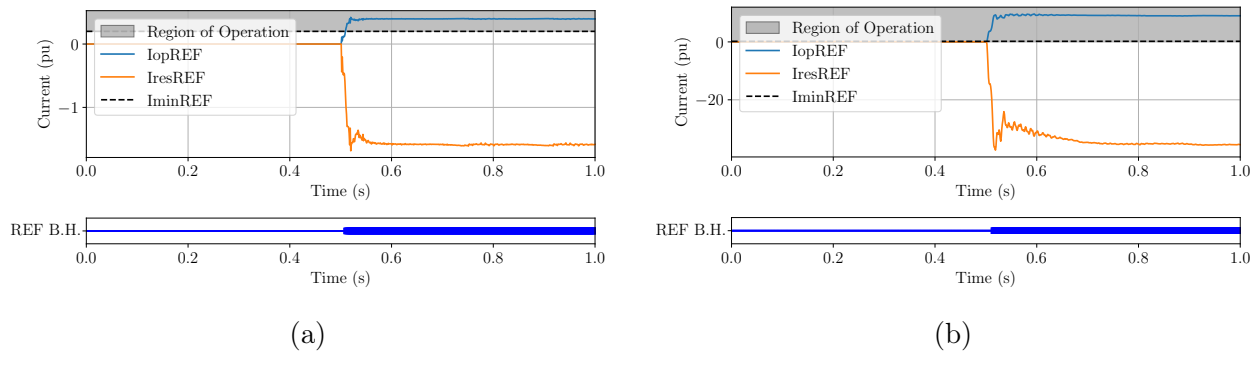


Figure 6.39: REF B.H. function operation in (a) TFYY and (b) TFYD for a phase-to-phase-to-ground short circuit on the primary side, with 10% power transmission in the bipoles.



#### 6.4.2 Secondary side

## 6.4.2.1 Short circuit turn-to-ground

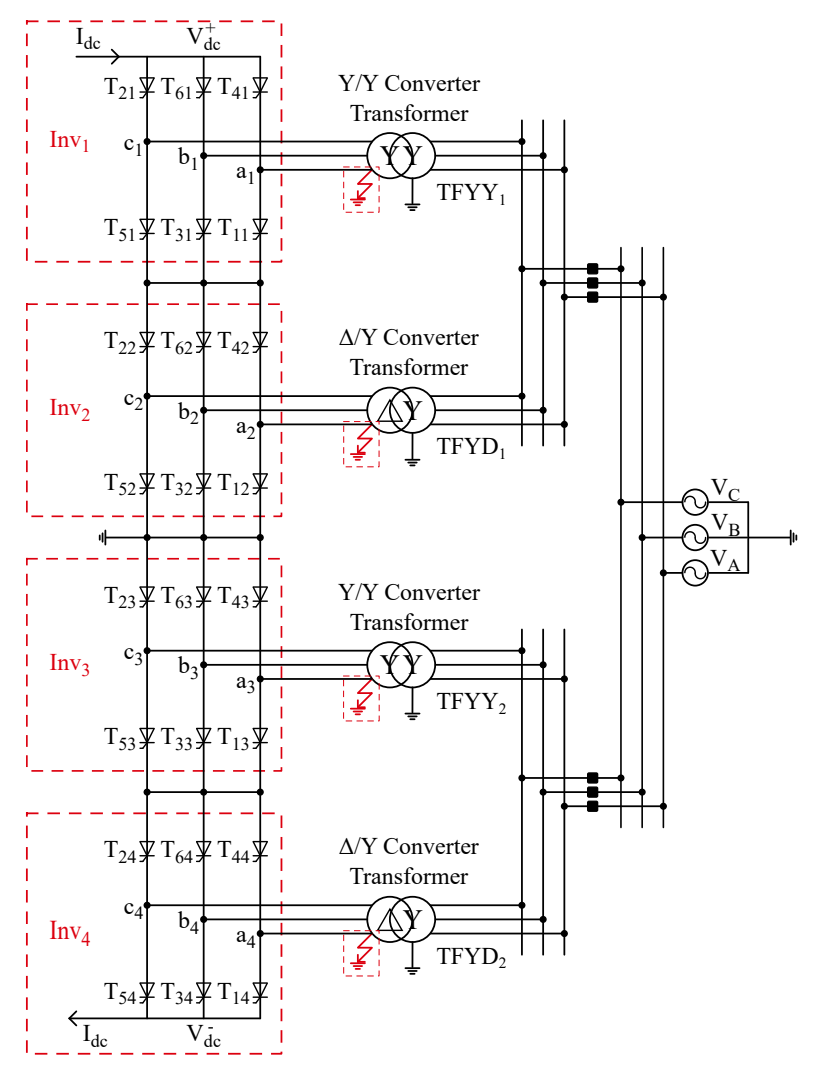
Turn-to-ground faults in the secondary of the converter transformers represent the most significant challenge encountered in this work concerning differential protection functions. Under 100% power transmission in the bipoles, operational failure was observed in the 87T and 87Q functions. This issue is exacerbated by the inability to employ the REF function in the secondary of these transformers, leaving the 87Q function as the sole backup.

To fully understand the observed results and challenges, it is crucial to understand the configuration of the LCC-HVDC inverter being assessed, as illustrated in Figure 6.40 and previously discussed in earlier chapters. In Figure 6.40, for didactic purposes, the six-pulse bridges are highlighted as inverters  $Inv_1$ ,  $Inv_2$ ,  $Inv_3$ , and  $Inv_4$ , with transformers labeled as  $TFYY_1$ ,  $TFYD_1$ ,  $TFYY_2$ , and  $TFYD_2$ . Such distinctions are necessary because, unlike other fault types, the outcomes of turn-to-ground faults in the secondary depend on the transformers' position within the pole. Another key point is that the connection between  $Inv_2$  and  $Inv_3$  is grounded, enabling bipole operation with positive voltage at 600 kV in  $V^+_{dc}$  and negative voltage at -600 kV in  $V^-_{dc}$ .

Starting the discussion with the TFYY<sub>1</sub> and function 87T, it was found that the 87T function, without harmonic restraint or blocking, only operated for turn-to-ground faults in

the secondary taking over 56% of turns (Figure 6.41). In contrast, with harmonic restraint and blocking, the function did not operate for any percentage of turns involved (Figure 6.42).

Figure 6.40: Diagram of the converter inverter evaluated to short circuits in the secondary of its converter transformers.



**Source:** Own authorship.

Lower slopes were evaluated to enhance function sensitivity and to assess the impact of harmonic restraint and blocking individually to help understand the situation and devise a solution. These analyses revealed that even with an  $I_{pickupmin}$  equal to 0.6 pu and a SLP of 0.1, the 87T function is only sensitized at 56% of turns. Additionally, it was noted that from this same 56% threshold, the 2<sup>nd</sup> harmonic block is triggered immediately after the fault inception and remains continuously active while the fault persists (Figure 6.43). Consequently, under these conditions, the differential protection functions do not operate; thus, when harmonic blocking is enabled, the 87T function fails to trip at any turn percentage.

Figure 6.41: 87T function operation in  $TFYY_1$  for turn-to-ground short circuits on the secondary side, with 100% power transmission in the bipoles.

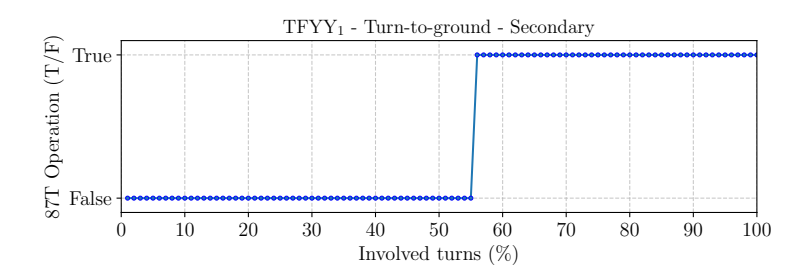
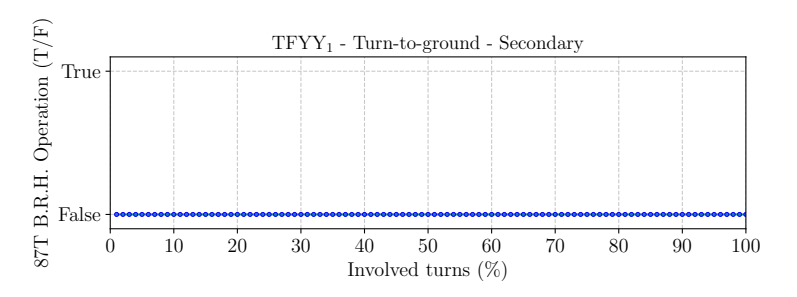


Figure 6.42: 87T R.B.H. function operation in TFYY<sub>1</sub> for turn-to-ground short circuits on the secondary side, with 100% power transmission in the bipoles.



Source: Own authorship.

There is already a 2<sup>nd</sup> harmonic block that continues while the fault persists, beginning at 34% of turns. Nonetheless, there are moments when this block disengages, allowing differential functions to operate if sensitized.

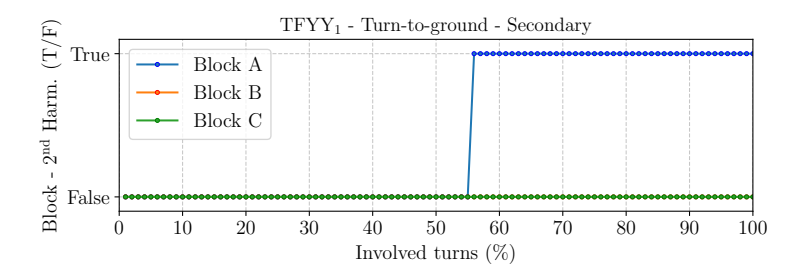
It is important to mention that the 2<sup>nd</sup> harmonic blocking mechanism is already activated and remains engaged throughout the fault for turn-to-ground faults involving as few as 34% of the secondary winding turns. However, in these cases, there are instances when this blocking is temporarily deactivated, allowing the differential protection functions to operate if they are sufficiently sensitized. Hence, in Figure 6.43, full and sustained blocking of the protection functions is considered to occur only from 56% of the winding turns involved in the fault.

Considering only harmonic restraint, the function again did not operate for any percentage of turns, confirming the high levels of harmonics (Figure 6.44).

Overall, the function's performance is unsatisfactory, covering only 44% of turns in the transformer's secondary side under its most sensitive configuration and covering nothing when restriction or blocking by harmonics is active. This performance can largely be attributed

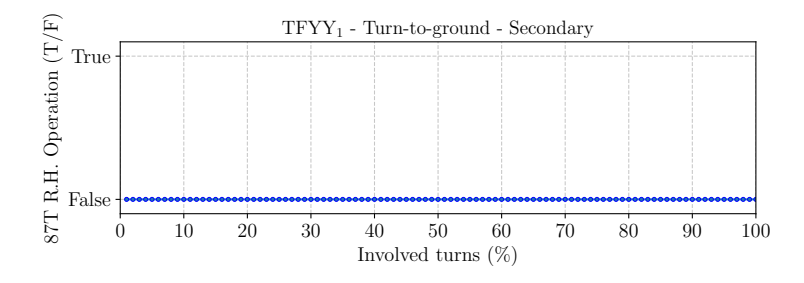
to the DC current circulating within the transformer due to the ground fault. Several authors referenced in Literature Review (Chapter 4) identified this phenomenon arising from connecting transformers to LCC-HVDC converters and their unidirectional thyristors.

Figure 6.43: Blocking by  $2^{nd}$  harmonic for turn-to-ground short circuits in the secondary of the converter transformer TFYY<sub>1</sub>.



**Source:** Own authorship.

Figure 6.44: 87T R.H. function operation in TFYY<sub>1</sub> for turn-to-ground short circuits on the secondary side, with 100% power transmission in the bipoles.



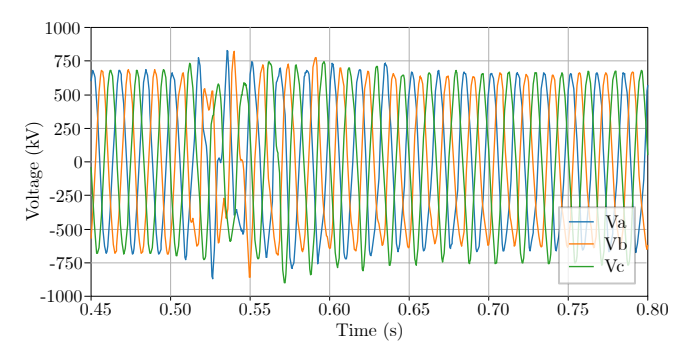
**Source:** Own authorship.

Understanding the inverter condition during the fault is essential to understand the source of the high level of 2<sup>nd</sup> harmonics. First, turn-to-ground faults induce no significant changes in the AC voltage of the system (Figure 6.45). Although commutation failures might occur due to increased phase currents (ZHENG et al., 2021b), the reference needed for thyristor commutation in the converter remains intact, maintaining current within the transformer until the fault is cleared (ZHENG et al., 2021a). Consequently, the pole control can adjust to maintain non-ideal operation. At the same time, the secondary short circuit causes DC current to circulate in the transformer, as illustrated in Figures 6.46 and 6.47.

Figure 6.46 demonstrates the operation of Inv<sub>1</sub> during a turn-to-ground short circuit taking 90% of the secondary winding turns of transformer TFYY<sub>1</sub>, while Figure 6.47 shows the current

in the transformer's secondary side during this same fault, where positive currents correspond to currents from common anode thyristors ( $T_{21}$ ,  $T_{61}$ , and  $T_{41}$ ) and negative currents correspond to common cathode thyristors ( $T_{51}$ ,  $T_{31}$ , and  $T_{11}$ ). Through Figure 6.47, it is possible to verify that there is only one commutation failure in  $Inv_1$  immediately after the fault initiation (between 0.5 and 0.52 seconds), which is confirmed by Figure 6.48, which is an output value from the ATP model used that indicates when there is a commutation failure in the inverter during the simulation.

Figure 6.45: 500 kV busbar voltage of the busbar at the substation Araraquara 2 for a turn-to-ground short circuit at 90% of the secondary of the converter transformer TFYY<sub>1</sub>.



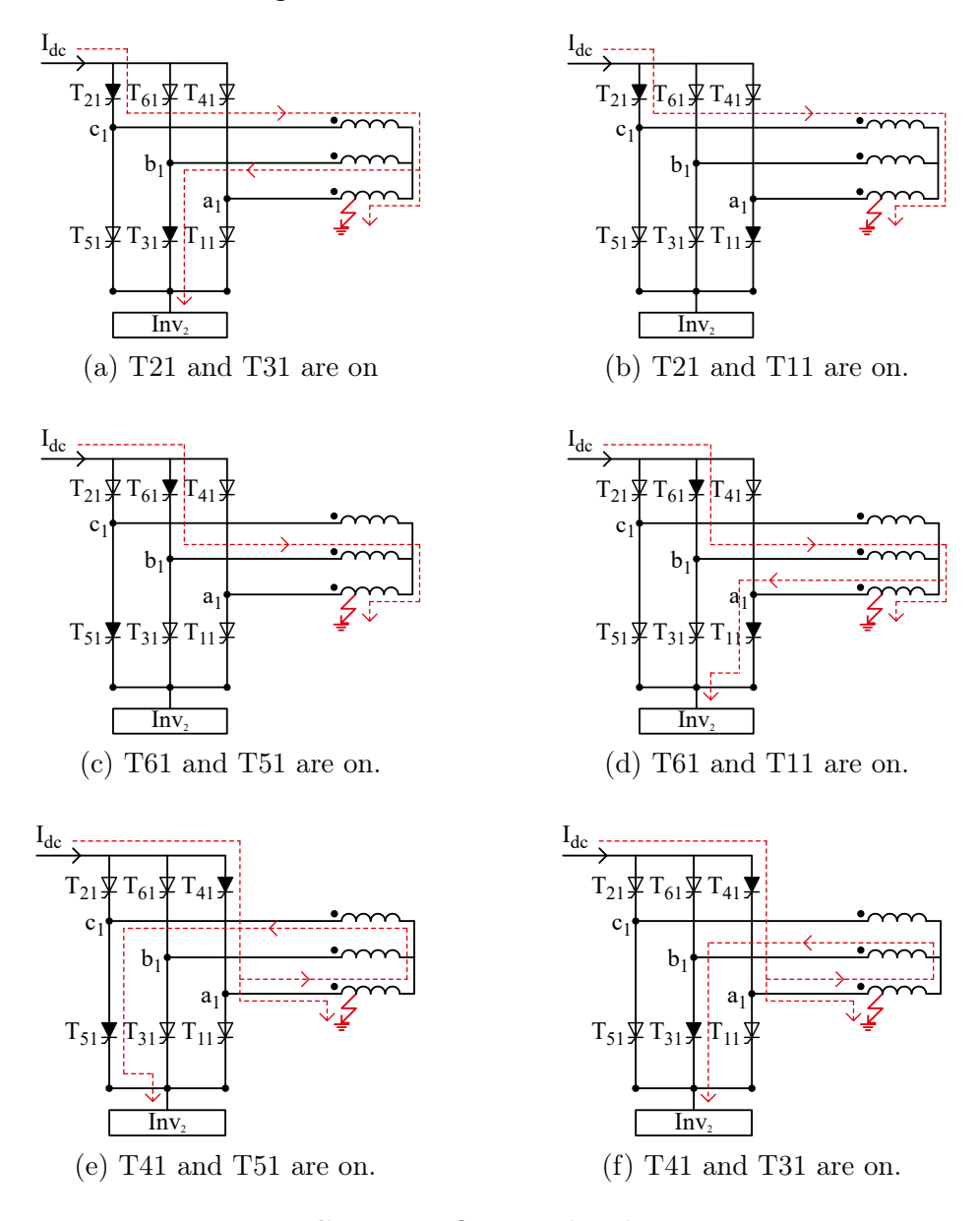
**Source:** Own authorship.

From here, it is apparent that the inverter continues thyristor commutation similarly to the regular operation but with three critical differences: increased current due to the short circuit, non-conduction in some common-cathode thyristors, even though they were connected, and, more notably, the characteristic shape of an inrush current in the phase currents, which is evident when comparing the Figure 6.47 and the Figure 3.4.

As explained in Section 2.1, thyristors of HVDC converters always operate in pairs, so the resulting DC voltage at each inverter terminal corresponds to the phase voltage difference across the secondary of its converter transformer, maintaining either positive or negative DC voltage differences. Consequently, the voltages at each phase of the transformer's secondary side result from the AC system voltage plus the DC voltage from the inverter, depending on which thyristor is conducting in each phase. Figure 6.49 displays pre-fault line and phase voltages on TFYY<sub>1</sub>'s secondary, exemplifying this concept. Due to the grounding from a 90% turn-to-ground fault, the V<sub>a</sub> voltage in the secondary drops to nearly zero, though not entirely, due to the remaining 10% of turns between the phase and fault. This configuration creates a

sinusoidal behavior of  $V_a$ , referenced to phase A's voltage in the AC system. In contrast,  $V_b$  and  $V_c$  secondary phase voltages align with the AC system's line voltages, approximating  $V_{ba}$  and  $V_{ca}$ , respectively, due to the fault's location.

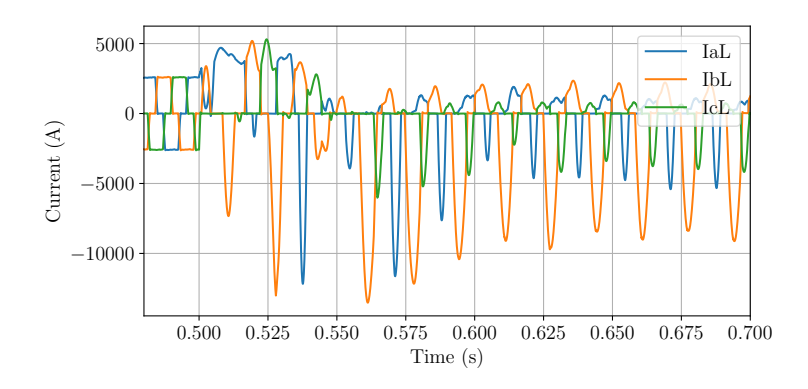
Figure 6.46: Fault current loops in  $Inv_1$  for a turn-to-ground short circuit at 90% of the secondary of the transformer  $TFYY_1$ .



Source: Own authorship.

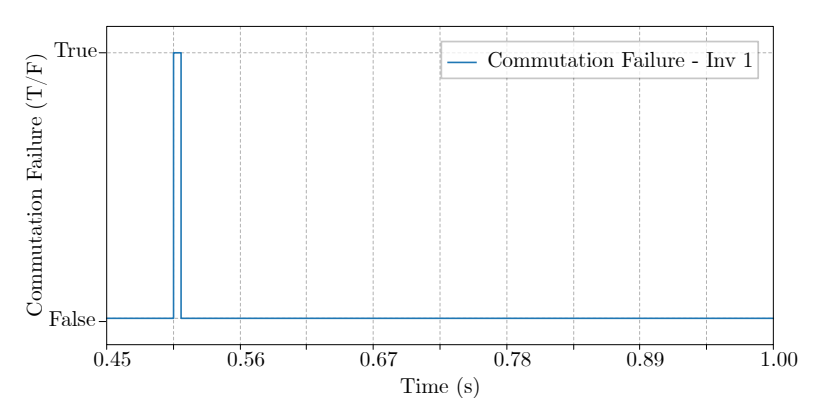
Figure 6.50 depicts the secondary line and phase voltages of transformer  $TFYY_1$  during the fault, illustrating the abovementioned effects. Furthermore, as thyristor commutation continues, voltage "cuts" are observed at  $V_a$ ,  $V_b$ , and  $V_c$  when common-cathode thyristors are turned on, bringing the phase voltage (AC + DC voltage) close to zero, similar to regular operation.

Figure 6.47: Currents on the secondary side of  $TFYY_1$  during a turn-to-ground short circuit at 90% of the secondary side, with 100% power transmission in the bipoles.



Thus, common-cathode thyristors cease conducting when thyristor pairs  $T_{21}$  and  $T_{11}$ , and  $T_{61}$  and  $T_{51}$ , are active (Figures 6.46b and 6.46c), as  $V_a$  and  $V_c$  enter their negative half-cycles, halting current flow. However, no commutation failure occurred, as phase voltage was positive at the commutation.

Figure 6.48: Commutation failures of  $Inv_1$  for a turn-to-ground short circuit at 90% of the secondary of the converter transformer  $TFYY_1$ .

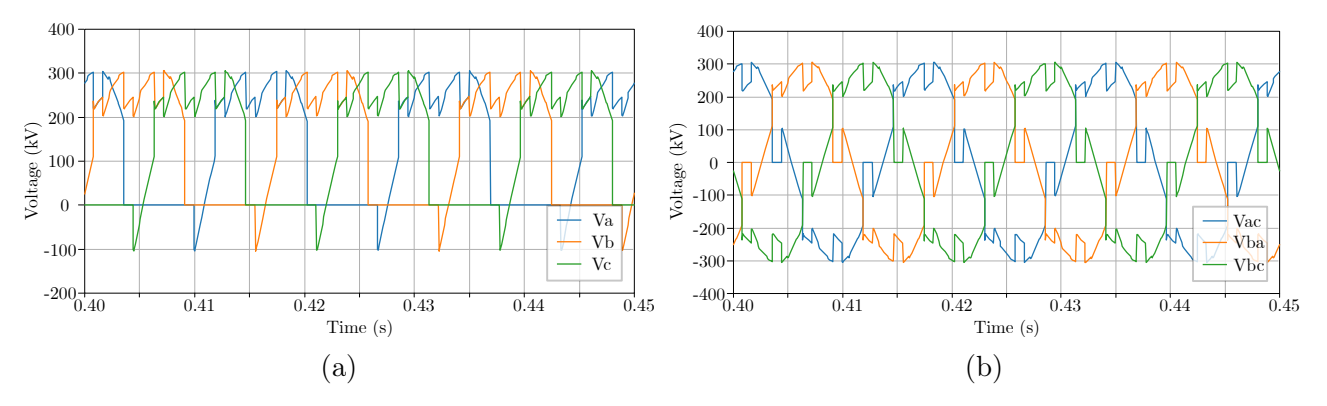


**Source:** Own authorship.

The fault current on the secondary (Figure 6.47) reflects directly on the primary side, as seen in Figure 6.51, which shows the primary current during the fault. The currents of phase B and C mirror those in the transformer's secondary side, yet phase A currents display substantial differences. It is verified that the current of phase A on the primary side is never equal to zero, even when there is no current in the phase A on the secondary side. This difference is due to the phase connection to ground in 90% of the secondary winding and demonstrates that the fault is continuously fed by the common anode thyristors (Figure 6.40), as well as demonstrates how

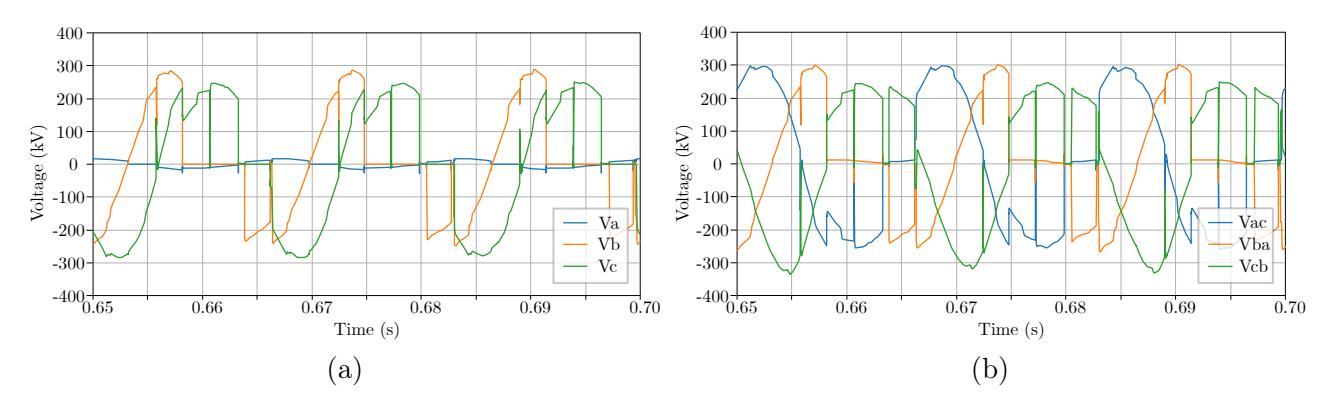
the fault causes a continuous flow of DC current in the transformer, causing the core saturation and, as a consequence, the FIIC (ZHENG et al., 2018; ZHENG et al., 2021a; ZHENG et al., 2021b).

Figure 6.49: Pre-fault phase (a) and line (b) voltages for a turn-to-ground short circuit at 90% of the secondary of the converter transformer TFYY<sub>1</sub>.



**Source:** Own authorship.

Figure 6.50: Faulted-state phase (a) and line (b) voltages for a turn-to-ground short circuit at 90% of the secondary of the converter transformer TFYY<sub>1</sub>.



Source: Own authorship.

This phase A primary-secondary current differences are detected by the 87T function, as shown in Figures 6.41 and 6.52. However, the current offset in the transformer leads to non-operation of the 87T function due to inappropriate restriction or 2<sup>nd</sup> harmonic blocking caused by the FIIC.

Figure 6.52 shows the 87T function's operation without harmonic blocking, while Figure 6.53 displays the function with harmonic restriction and blocking. These figures confirm that both restriction and blocking hindered the protection function, which is especially evident in the 2<sup>nd</sup> and 5<sup>th</sup> harmonic levels and blocking (Figures 6.54 and 6.55).

Figure 6.51: Currents on the primary side of  $TFYY_1$  during a turn-to-ground short circuit at 90% of the secondary side, with 100% power transmission in the bipoles.

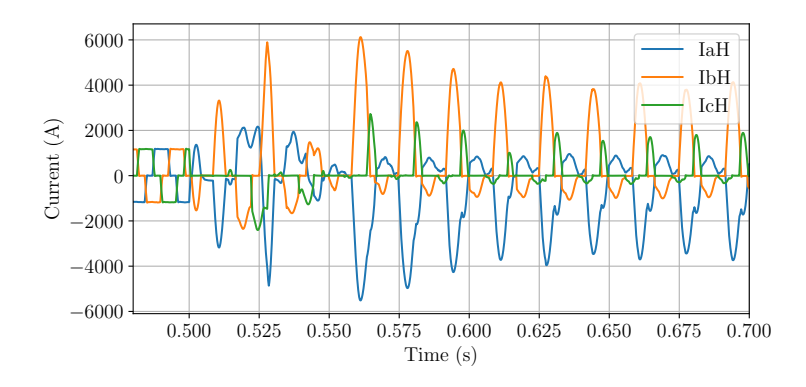
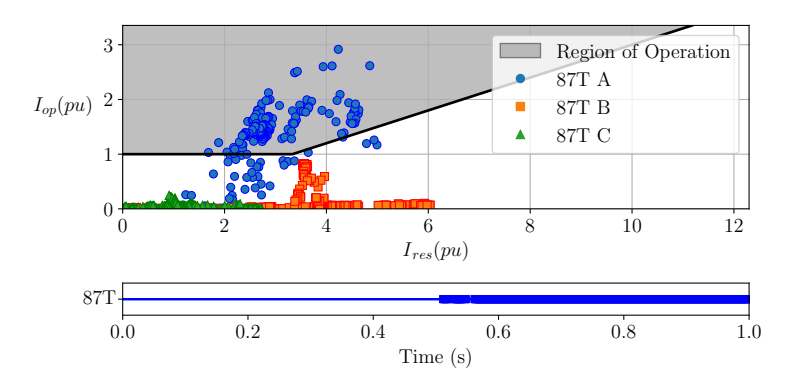
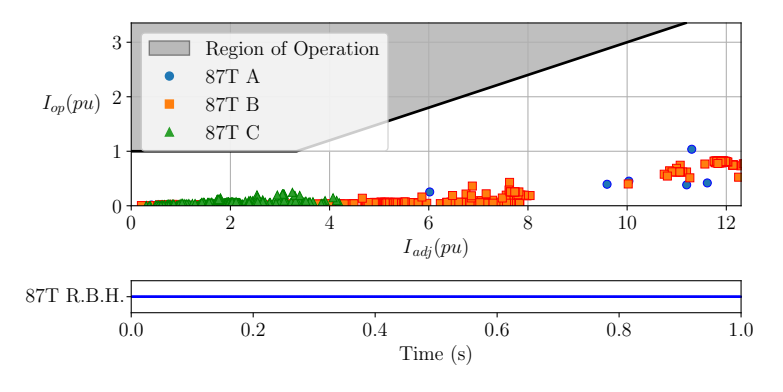


Figure 6.52: 87T function operation in  $TFYY_1$  for a turn-to-ground short circuit at 90% of the secondary side, with 100% power transmission in the bipoles.



**Source:** Own authorship.

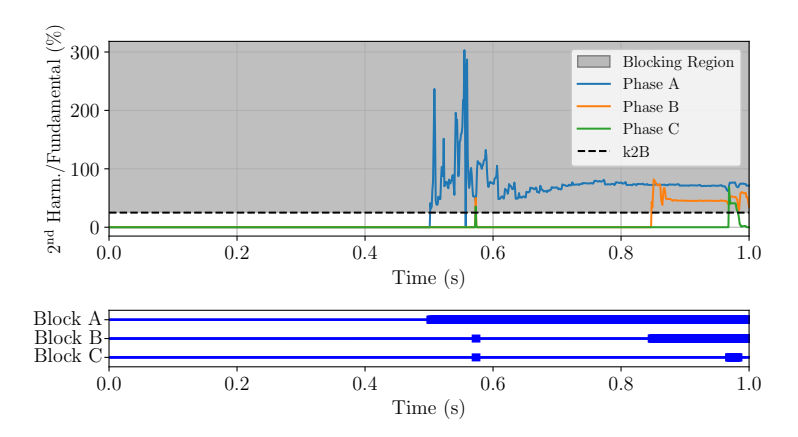
Figure 6.53: 87T R.B.H. function operation in TFYY<sub>1</sub> for a turn-to-ground short circuit at 90% of the secondary side, with 100% power transmission in the bipoles.



The same results are observed for faults involving up to 56% of the winding turns, which is precisely the threshold at which the 87T function—without blocking or harmonic restraint—begins to operate (Figure 6.41). However, the result changes when 55% or fewer turns are involved, and a fault taking 55% of turns provides an accurate example of faults with even fewer turns, so that it will be analyzed in detail.

As expected, for faults involving 55% of turns, neither blocking nor harmonic restraint is responsible for the failure of the function to operate. In this case, the unrestricted and unblocked 87T function no longer detects the fault, as illustrated in Figure 6.56.

Figure 6.54:  $2^{\text{nd}}$  harmonic by fundamental for a turn-to-ground short circuit at 90% of the secondary of the converter transformer TFYY<sub>1</sub>.



**Source:** Own authorship.

Figure 6.55: 5<sup>th</sup> harmonic by fundamental for a turn-to-ground short circuit at 90% of the secondary of the converter transformer TFYY<sub>1</sub>.

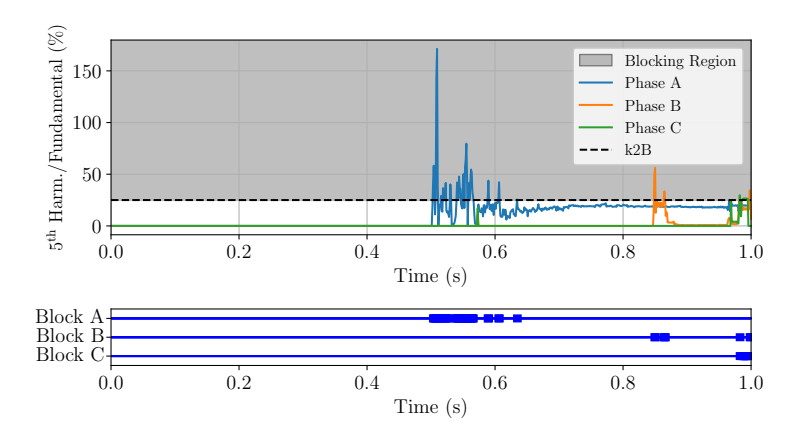


Figure 6.56: 87T function operation in  $TFYY_1$  for a turn-to-ground short circuit at 55% of the secondary side, with 100% power transmission in the bipoles.

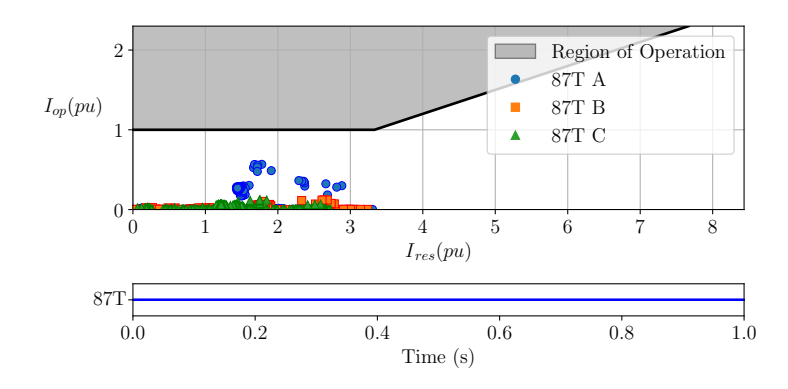


Figure 6.57 shows the current in the transformer's secondary side for a fault taking 55% of turns. Here, the difference is evident compared to the currents resulting from the previously analyzed fault (Figure 6.47). Primarily due to the lack of current conduction in the common-cathode thyristors, except when thyristors  $T_{21}$  and  $T_{31}$  are activated, conducting current on phase B, as illustrated in Figure 6.58. These differences occur because, at this level of turns, the fault currents are smaller, no commutation failure occurs, and the thyristor commutation proceeds as in regular operation (unlike faults taking over 56% of turns, where pole control shifts the commutation, causing the cited effects). Consequently, along with the sinusoidal voltages during the fault (Figure 6.59), the common-cathode thyristors switch moments before the negative half-cycle of  $V_a$  and  $V_b$ , so there is no commutation failure, but these thyristors also do not conduct. This results in a complete offset, confining phase A and C secondary currents to the positive half-cycle only and without the characteristic shape of an inrush current.

Figure 6.57: Currents on the secondary side of  $TFYY_1$  during a turn-to-ground short circuit at 55% of the secondary side, with 100% power transmission in the bipoles.

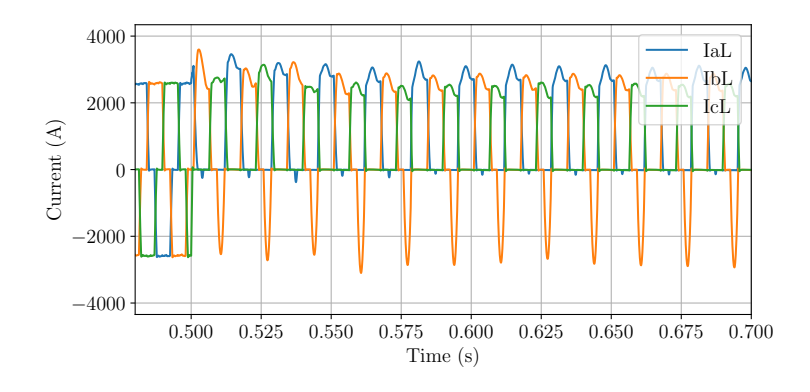
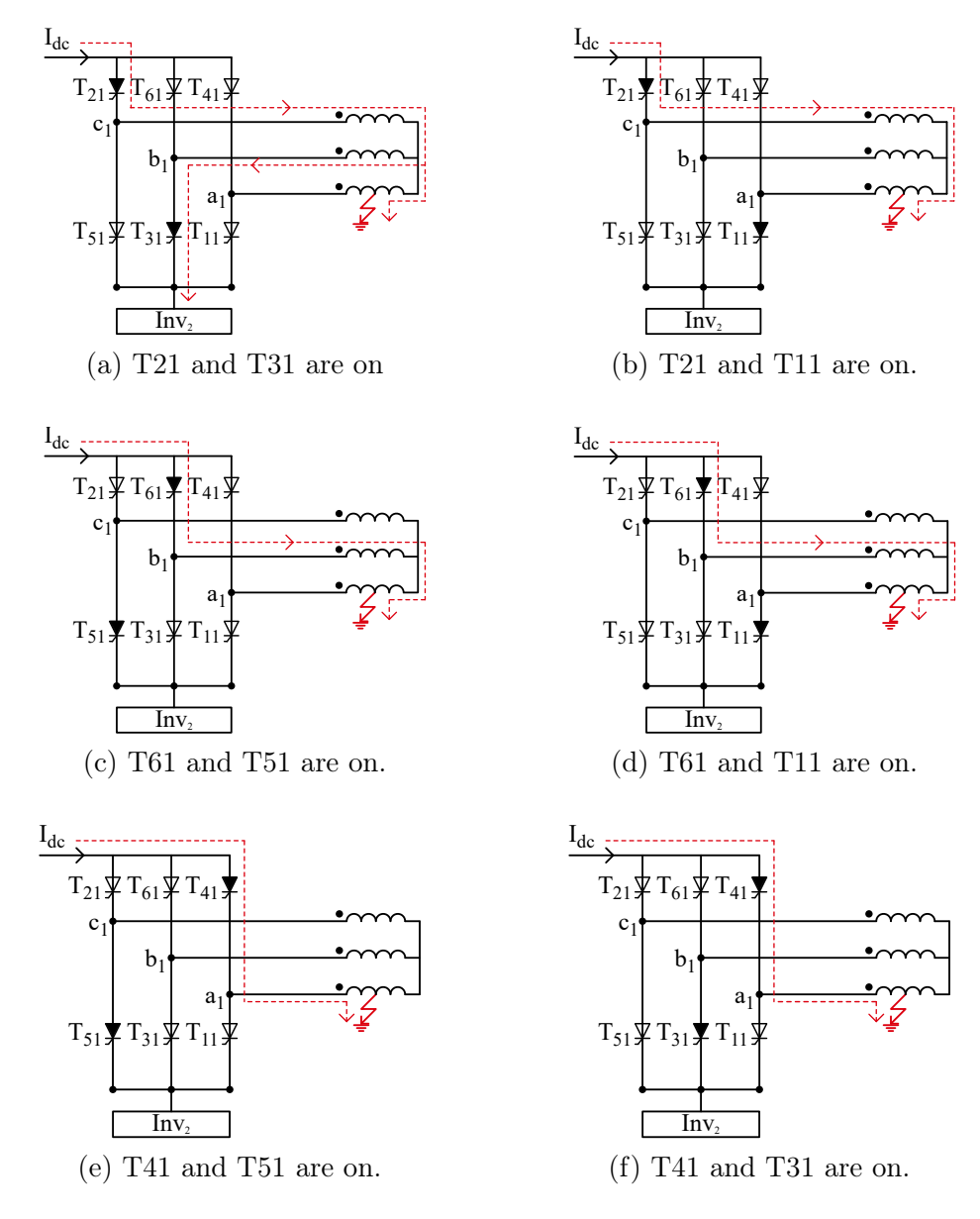


Figure 6.58: Fault current loops in  $Inv_1$  to a short circuit turn-to-ground at 55% of the secondary of the transformer  $TFYY_1$ .



This outcome logically reflects in the transformer's primary side, as seen in Figure 6.60. Here, it is even more evident how the primary currents remain the secondary current pattern, defined by the unidirectional inverter currents. The current disparity in phase A is also maintained, as observed in the 90% turn fault (Figure 6.51). However, with reduced current, there is greater current standardization and less difference in phase A current. Furthermore, when current phasors are estimated for the 87T function, a process that filters out DC components (Figure 6.61), the result is a minimal operating current, as shown in Figure 6.56.

Figure 6.59: Faulted-state phase (a) and line (b) voltages for a turn-to-ground short circuit at 55% of the secondary of the converter transformer TFYY<sub>1</sub>.

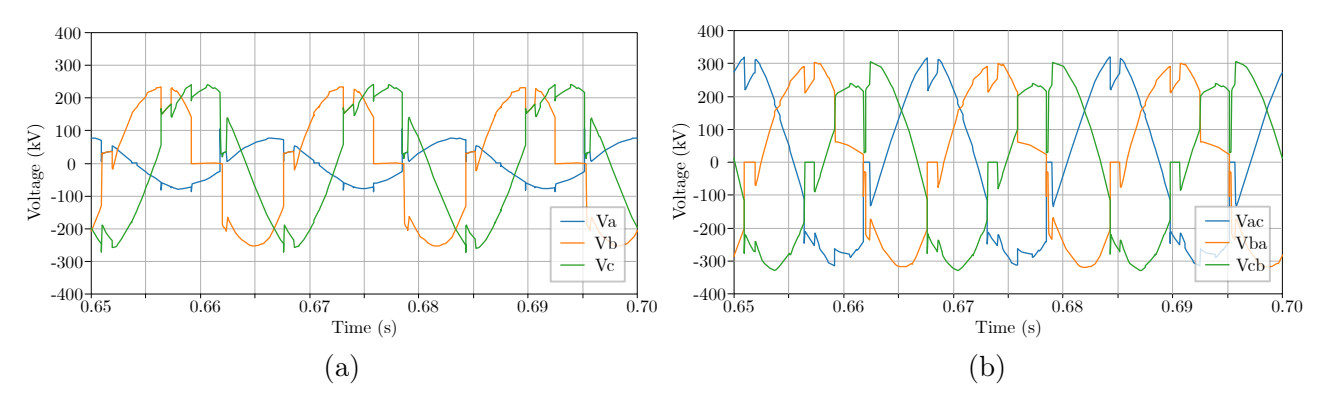
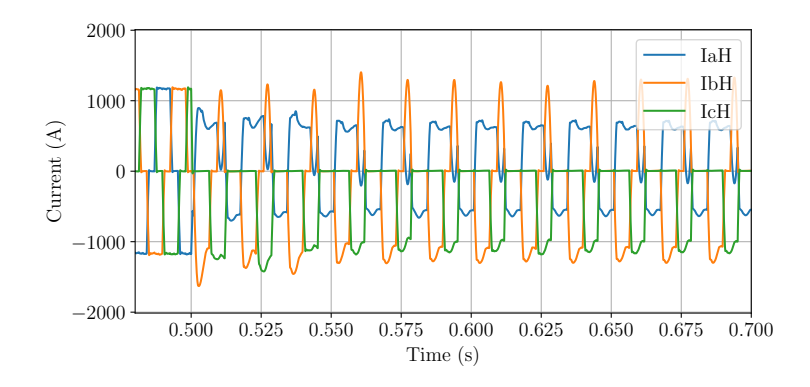
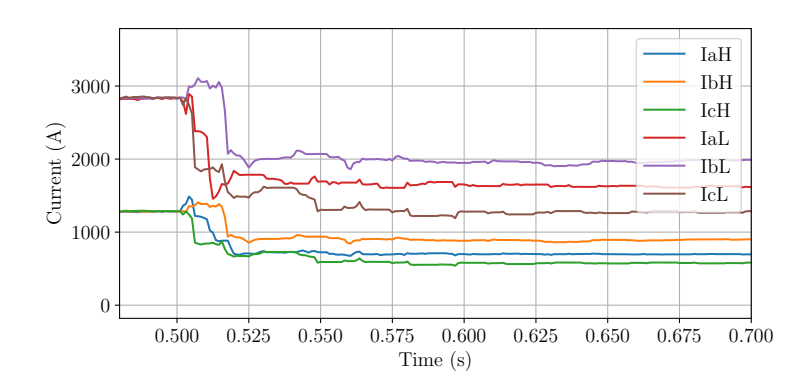


Figure 6.60: Currents on the primary side of  $TFYY_1$  during a turn-to-ground short circuit at 55% of the secondary side, with 100% power transmission in the bipoles.



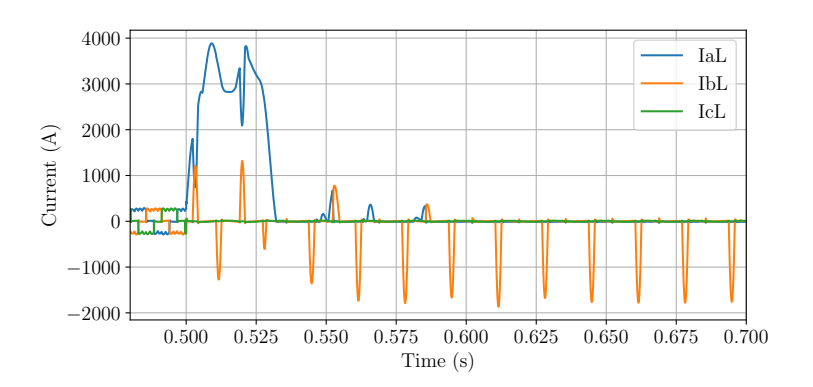
Source: Own authorship.

Figure 6.61: Currents phasor module on TFYY<sub>1</sub> during a turn-to-ground short circuit at 55% of the secondary side, with 100% power transmission in the bipoles.



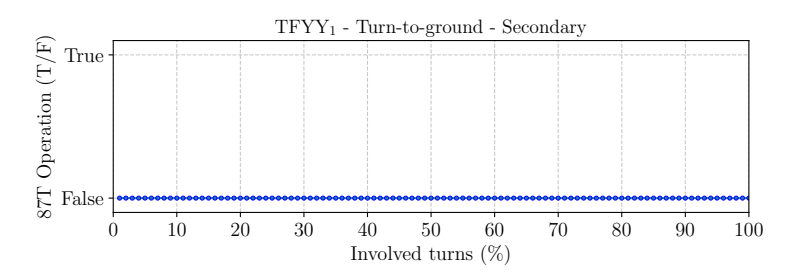
With bipoles transmitting 10% of their power, similar results are observed for TFYY<sub>1</sub>. Immediately after the fault onset, the transient currents approximate the values for faults with bipoles transmitting 100% of power, as they are defined by the difference between the voltage at the rectifier and the voltage at the inverter, and are high due to the DC voltage reduction at the inverter caused by the fault. Thus, for a 90% turn fault, with secondary current results shown in Figure 6.62, the phase A current reaches approximately 4000 A on the secondary, whereas, for the same fault with bipole power at 100%, the current reaches around 5000 A (Figure 6.47). Regardless, the pole control response reduces currents significantly lower after the transient period due to the power setpoint. Thus, the resulting operating current in the phases does not reach the 87T function's minimum operating current threshold (*Ipickumin*), so the function does not operate at any percentage of turns involved (Figure 6.63).

Figure 6.62: Currents on the secondary side of TFYY<sub>1</sub> during a turn-to-ground short circuit at 90% of the secondary side, with 10% power transmission in the bipoles.



**Source:** Own authorship.

Figure 6.63: 87T function operation in  $TFYY_1$  for turn-to-ground short circuits on the secondary side, with 10% power transmission in the bipoles.

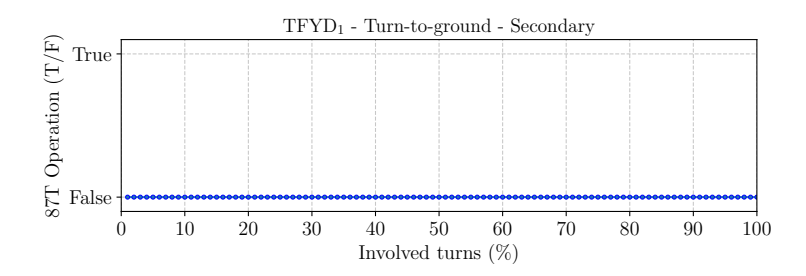


Source: Own authorship.

Even more critical results are found analyzing the 87T function for converter transformer

TFYD<sub>1</sub>: the function does not operate at any percentage of turns, even without harmonic blocking or restraint and a SLP of 0.1, as illustrated in Figures 6.64 and 6.65. This finding shows that the primary issue for this converter transformer is not harmonic blocking or restraint, which is different from TFYY<sub>1</sub>. This contrast is confirmed by assessing the blocking for the  $2^{\text{nd}}$  and  $5^{\text{th}}$  harmonics per percentage of turns in Figures 6.66 and 6.67. There is no function blocking due to harmonic levels. Note that function-blocking in Figures 6.66 and 6.67 was considered for each percentage of turns where blocking was sustained and prevented differential function operation, excluding faults with transient levels of the  $2^{\text{nd}}$  and  $5^{\text{th}}$  harmonics beyond the limit.

Figure 6.64: 87T function operation in  $TFYD_1$  for turn-to-ground short circuits on the secondary side, with 100% power transmission in the bipoles.



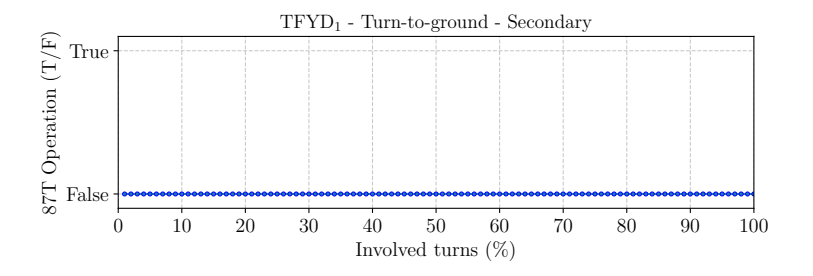
**Source:** Own authorship.

It is essential to examine the configuration of inverter Inv<sub>2</sub> and converter transformer TFYD<sub>1</sub> during the fault to understand this outcome and the difference compared to TFYY<sub>1</sub> transformer results. It is known that differential functions have difficulty detecting turn-to-ground faults involving approximately 50% of the winding, whereas more severe faults occurring near the winding extremities are typically easier to identify (ANDERSON et al., 2022; TAVARES, 2014). However, as shown in Figures 6.64 and 6.65, the 87T function does not operate even under the most critical conditions at the winding ends, so the analyses will focus on a turn-to-ground fault taking 90% of TFYD<sub>1</sub> secondary turns, which exemplifies faults with other percentages of turns.

Inv<sub>2</sub>'s configuration during the fault is illustrated in Figure 6.68 and confirmed by Figure 6.69, showing TFYD<sub>1</sub> converter transformer's secondary side currents during the fault. Configuration and secondary currents during the fault are relatively similar to those observed for the turn-to-ground fault on TFYY<sub>1</sub> taking 55% of turns. This similarity helps explain why the

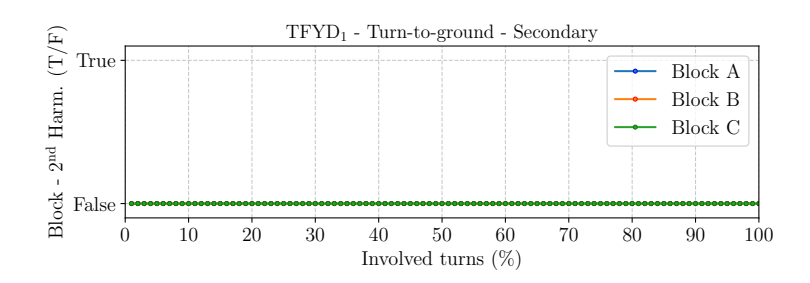
87T function does not operate; however, while turn-to-ground faults on TFYY<sub>1</sub> cause few or no commutation failures, TFYD<sub>1</sub> faults exhibit a consistent commutation failure pattern throughout the fault. This difference is critical, as after commutation failures happen just in the Inv<sub>2</sub>, the pole can be tripped by Commutation Failure Protection (ANDERSON *et al.*, 2022; PADIYAR, 2011), whereas TFYY<sub>1</sub> faults rely on other protections to identify or not the fault.

Figure 6.65: 87T function operation with a SLP of 0.1 in TFYD<sub>1</sub> for turn-to-ground short circuits on the secondary side, with 100% power transmission in the bipoles.



Source: Own authorship.

Figure 6.66: Blocking by  $2^{nd}$  harmonic for turn-to-ground short circuits in the secondary of the converter transformer TFYD<sub>1</sub>.



**Source:** Own authorship.

Figure 6.67: Blocking by  $5^{th}$  harmonic for turn-to-ground short circuits in the secondary of the converter transformer TFYD<sub>1</sub>.

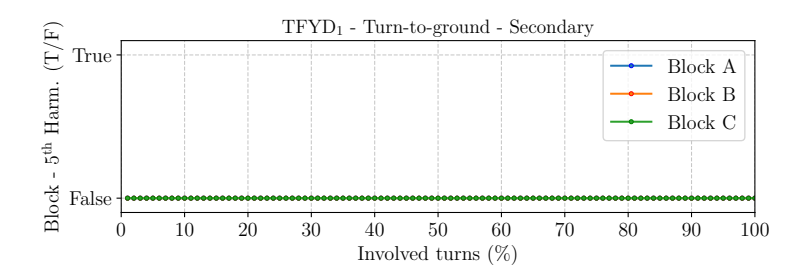
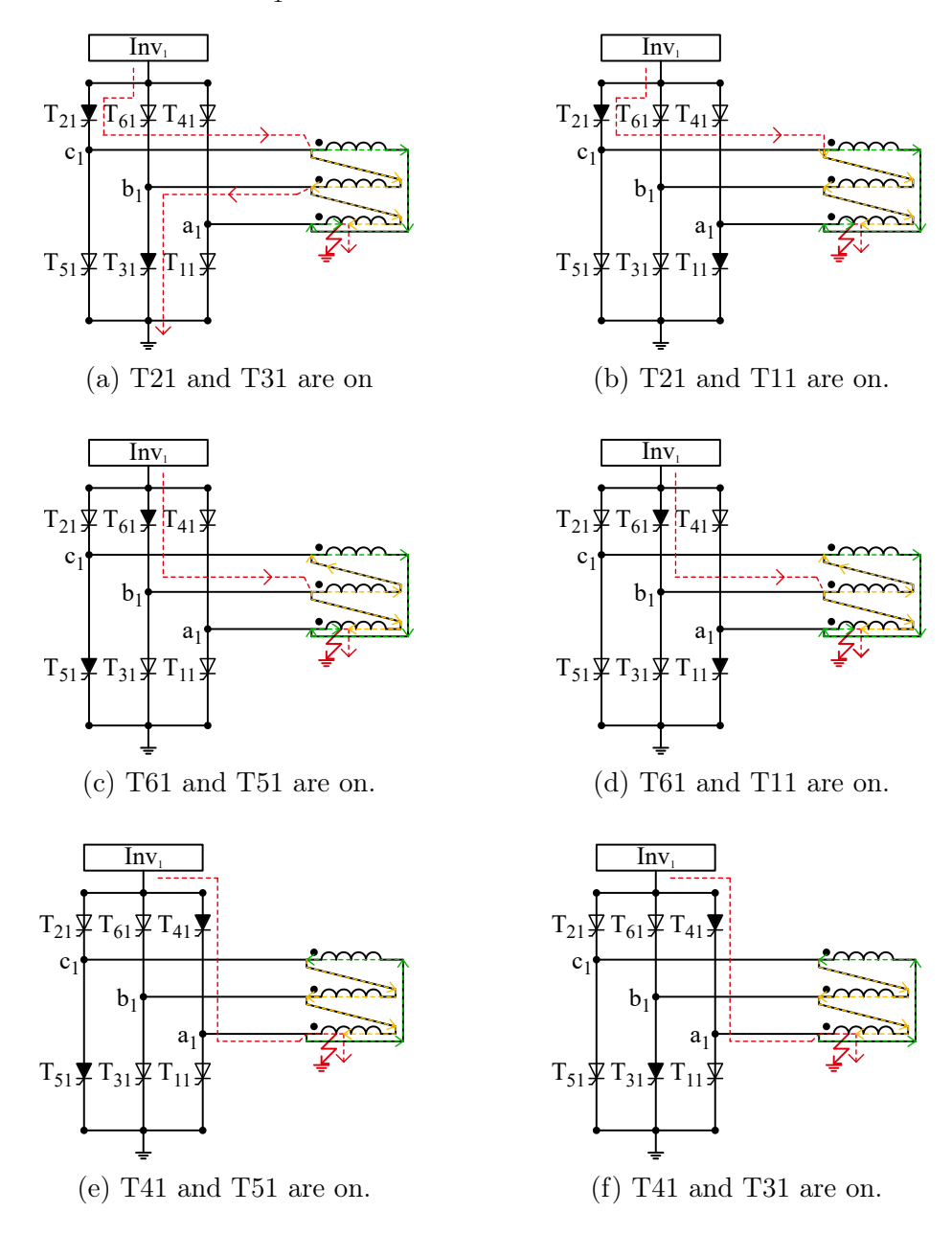


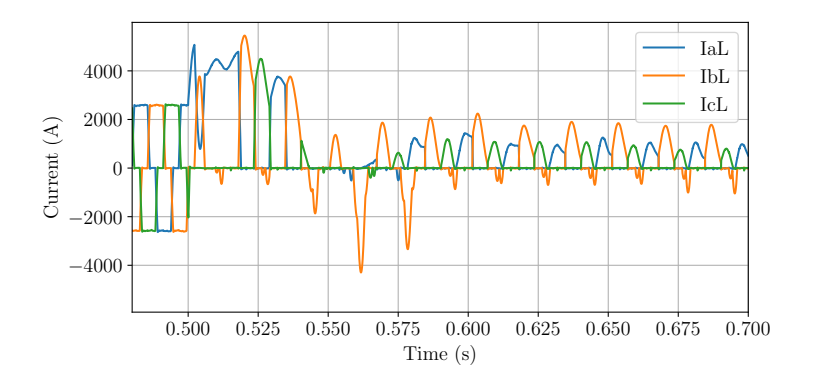
Figure 6.68: Fault current loops in  $Inv_2$  for a turn-to-ground short circuit at 90% of the secondary of the transformer  $TFYD_1$ .



The commutation failures of  $Inv_2$  are illustrated in Figure 6.70. They occur during the commutation from  $T_{41}$  to  $T_{61}$  and from  $T_{51}$  to  $T_{11}$ . Once the fault begins, voltages  $V_a$ ,  $V_b$ , and  $V_c$  also exhibit a sinusoidal behavior, as shown in Figures 6.71 and 6.72, which display the phase and line voltages at the transformer's secondary side before and during the fault. This fault also resulted in a commutation shift among the thyristors, to the point that the commutation attempt from  $T_{41}$  (phase A) to  $T_{61}$  (phase B) and from  $T_{51}$  (phase C) to  $T_{11}$ 

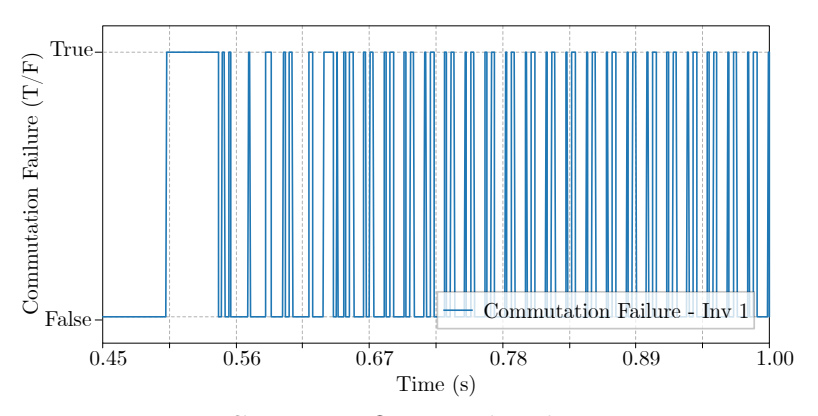
(phase A), occurs when  $V_b$  is lower than  $V_a$  and  $V_c$  is lower than  $V_a$ , respectively, causing the commutation failures. Additionally, non-conduction in the common cathode thyristors occurs for the same reason observed in previous cases. Even when commutation does occur, the phase voltages remain negative.

Figure 6.69: Currents on the secondary side of  $TFYD_1$  during a turn-to-ground short circuit at 90% of the secondary side, with 100% power transmission in the bipoles.



**Source:** Own authorship.

Figure 6.70: Commutation failures of  $Inv_2$  for a turn-to-ground short circuit at 90% of the secondary of the converter transformer  $TFYD_1$ .



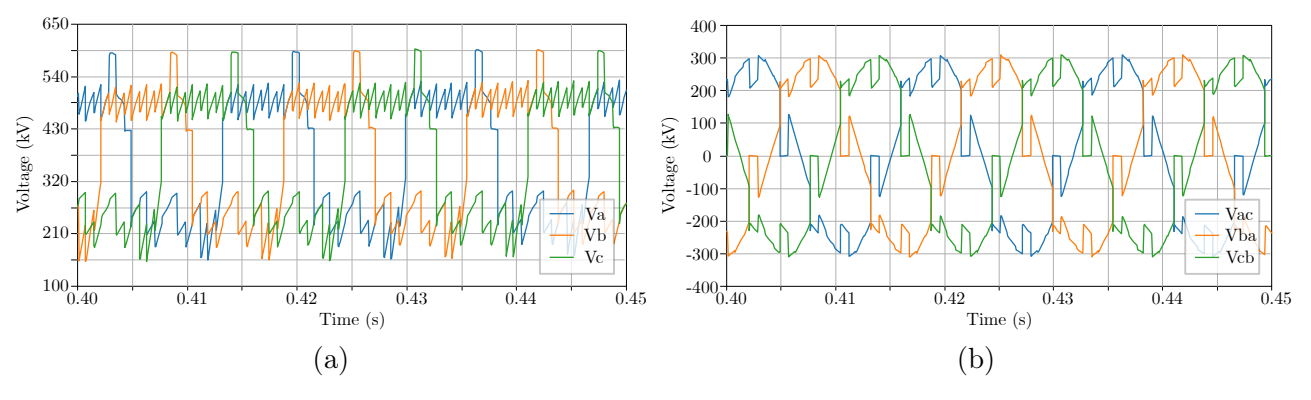
**Source:** Own authorship.

Consequently, the currents are reflected coherently on the primary, except for the phase-A current (Figure 6.73). However, given the reduced current values and the filtering of the DC component during phasor estimation (Figure 6.74), the phase-A operating current is insufficient to sensitize the 87T function, as demonstrated in Figure 6.75.

Figures 6.76 and 6.77 show this fault's  $2^{nd}$  and  $5^{th}$  harmonic blocking. It is evident that DC current effects in the transformer still lead to increased harmonics, particularly in the  $2^{nd}$ 

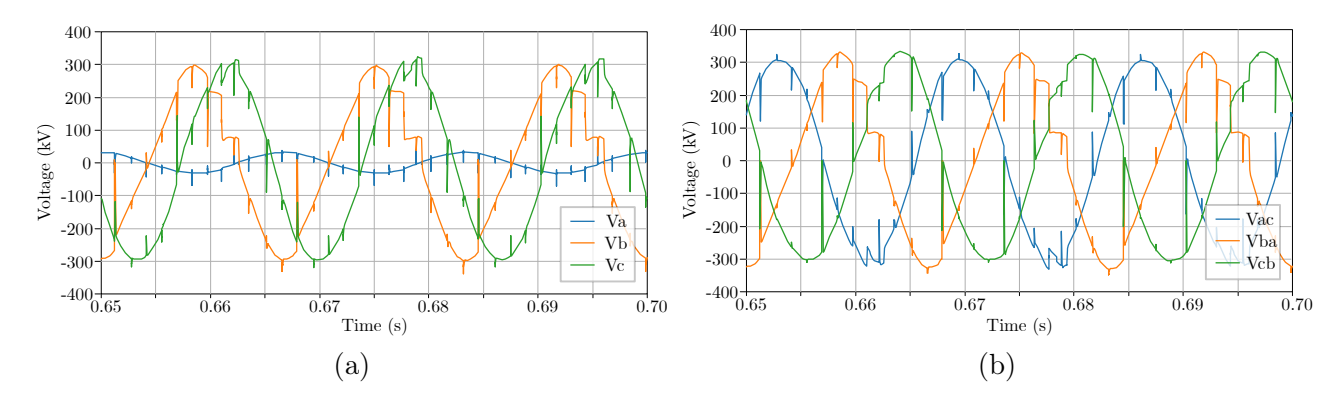
harmonic component because of FIIC, which is notable when comparing Figures 6.69 and 3.4. However, there is no sustained blocking due to harmonic levels, and the function does not operate strictly due to a lack of sensitivity.

Figure 6.71: Pre-fault phase (a) and line (b) voltages for a turn-to-ground short circuit at 90% of the secondary of the converter transformer TFYD<sub>1</sub>.



**Source:** Own authorship.

Figure 6.72: Faulted-state phase (a) and line (b) voltages for a turn-to-ground short circuit at 90% of the secondary of the converter transformer TFYD<sub>1</sub>.



**Source:** Own authorship.

At 10% power transmission in the bipoles, the results in TFYD<sub>1</sub> are similar to those at 100% power, with transient current values close but reduced currents after pole control response. This similarity is confirmed by comparing transformer's secondary side currents for a fault taking 90% of turns with the bipoles at 10% transmitted power (Figure 6.78) and 100% transmitted power (Figure 6.69). Thus, the 87T function does not operate for any turn percentage, as seen in Figure 6.79.

Figure 6.73: Currents on the primary side of  $TFYD_1$  during a turn-to-ground short circuit at 90% of the secondary side, with 100% power transmission in the bipoles.

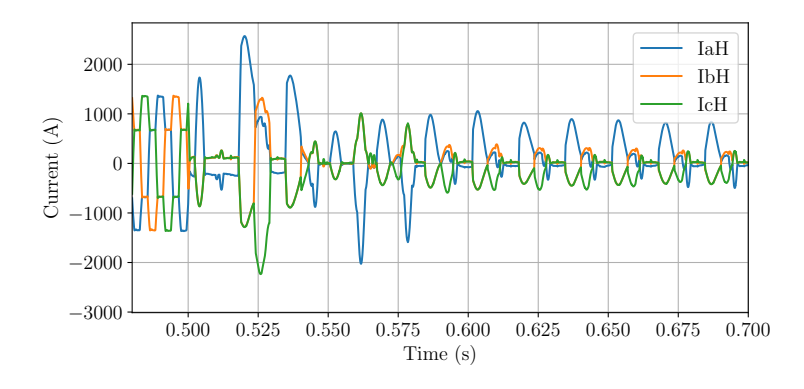
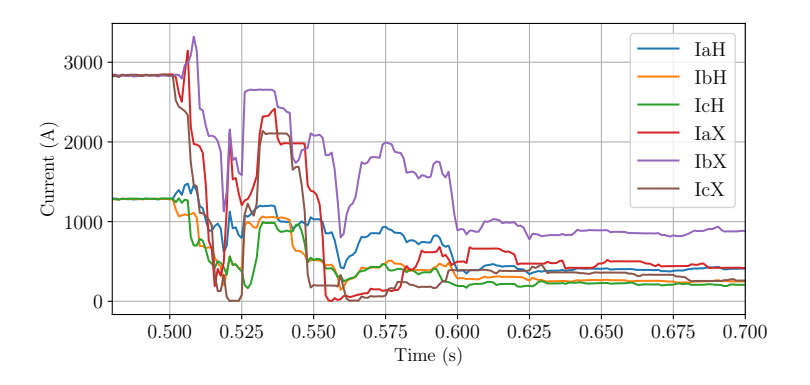


Figure 6.74: Currents phasor module on TFYD<sub>1</sub> during a turn-to-ground short circuit at 90% of the secondary side, with 100% power transmission in the bipoles.



**Source:** Own authorship.

Figure 6.75: 87T function operation in  $TFYY_1$  for a turn-to-ground short circuit at 90% on the secondary side, with 100% power transmission in the bipoles.

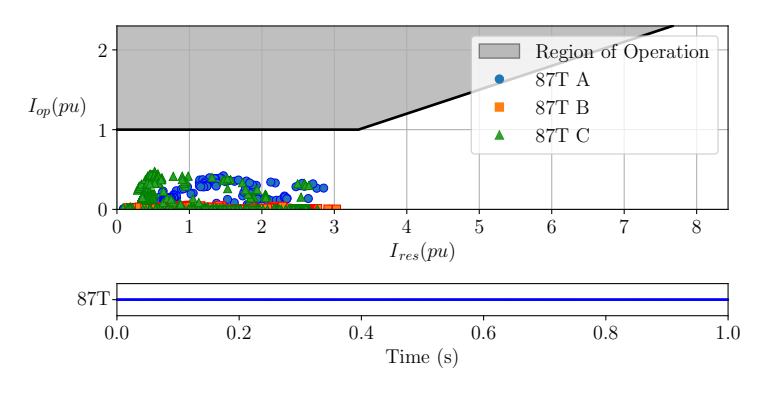


Figure 6.76:  $2^{nd}$  harmonic by fundamental for a turn-to-ground short circuit at 90% of the secondary of the converter transformer TFYD<sub>1</sub>.

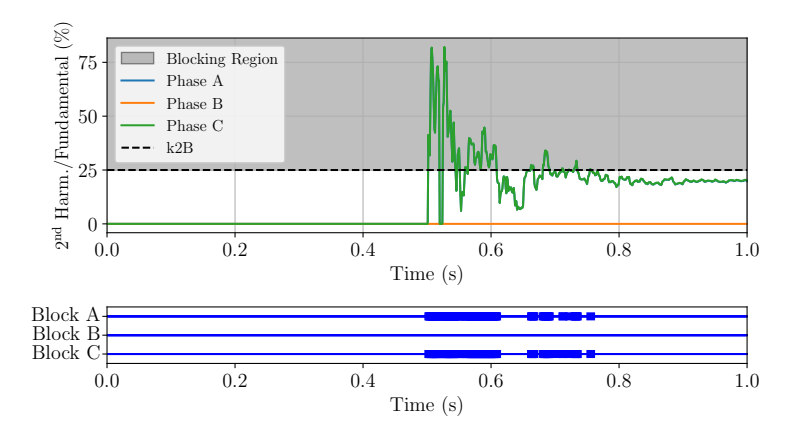
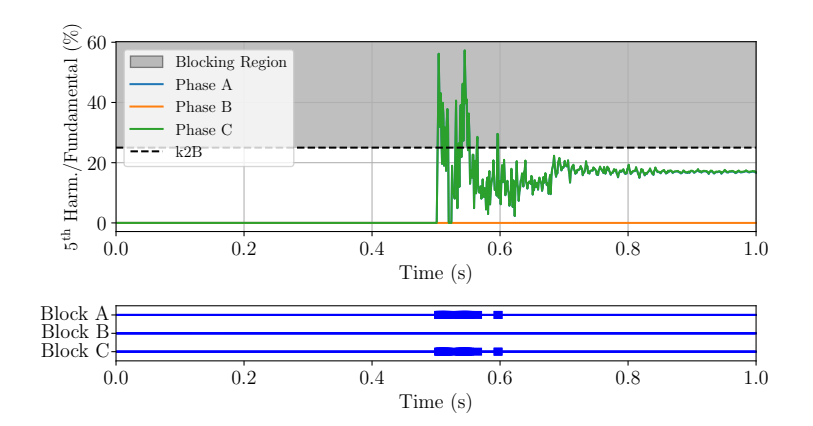


Figure 6.77:  $5^{th}$  harmonic by fundamental for a turn-to-ground short circuit at 90% of the secondary of the converter transformer TFYD<sub>1</sub>.



Source: Own authorship.

Figure 6.78: Currents on the secondary side of  $TFYD_1$  during a turn-to-ground short circuit at 90% of the secondary side, with 10% power transmission in the bipoles.

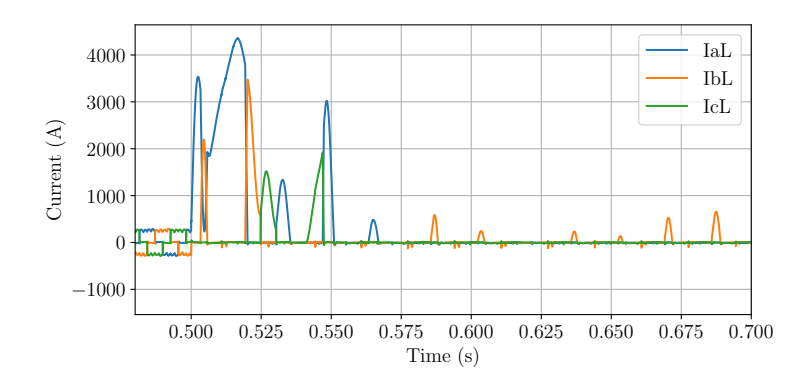
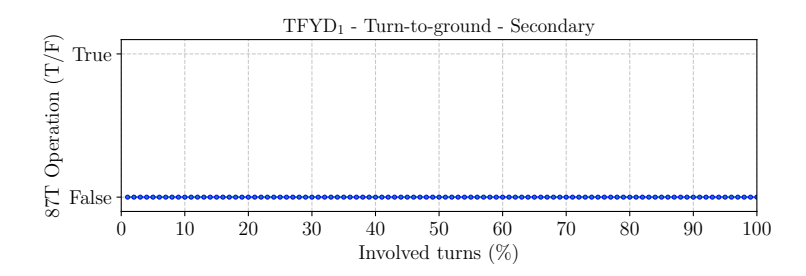


Figure 6.79: 87T function operation in  $TFYD_1$  for turn-to-ground short circuits on the secondary side, with 10% power transmission in the bipoles.



Finally, it is essential to clarify that the differences in results between TFYY<sub>1</sub> and TFYD<sub>1</sub> are not due to the configuration differences between the converter transformers, that is, star-star and star-delta. Besides the reasons already stated, the lower currents and differences in TFYD<sub>1</sub> result from its position in the pole. Turn-to-ground short circuits in TFYD<sub>1</sub> significantly impact TFYY<sub>1</sub> and, consequently, the pole as a whole, considering that the phase voltages in TFYY<sub>1</sub> are the sum of the AC voltage plus the DC voltage resulting from Inv<sub>2</sub>. This impact can be seen in Figure 6.80, which shows secondary currents in TFYY<sub>1</sub> for a turn-to-ground fault taking 90% of turns in TFYD<sub>1</sub>. The figure shows that currents in TFYY<sub>1</sub> are reduced to peak values of 450 and 600 A at brief moments. In the opposite case shown in Figure 6.81, TFYD<sub>1</sub> currents maintain the pattern according to thyristor commutation, with values between 1000 and 2000 A, while in regular operation, the currents maintained a value of 2625 A for 100% of power transmission.

Figure 6.80: Currents on the secondary side of  $TFYY_1$  during a turn-to-ground short circuit at 90% of the secondary side of  $TFYD_1$ .

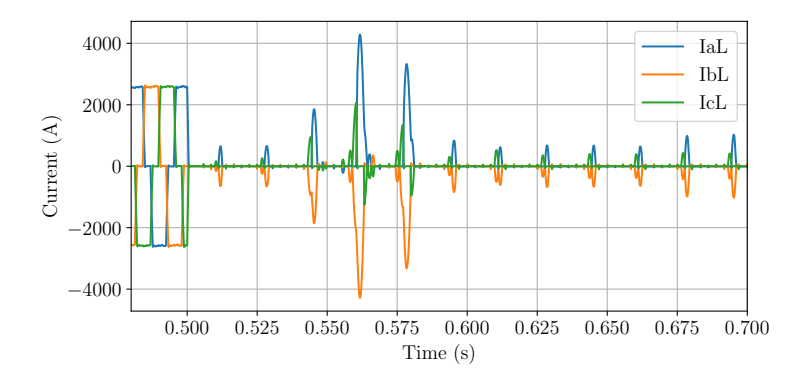
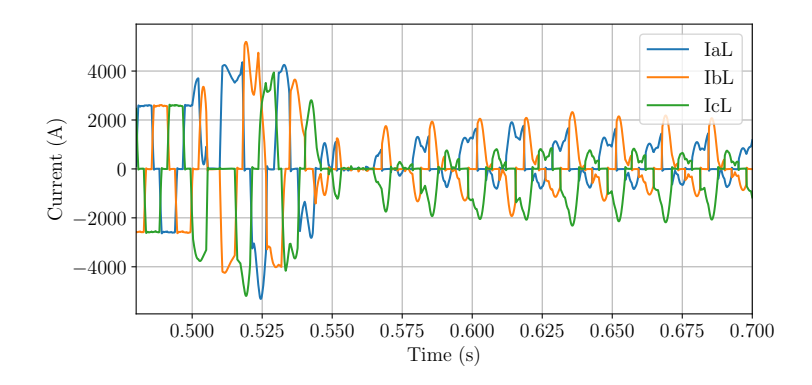


Figure 6.81: Currents on the secondary side of  $TFYD_1$  during a turn-to-ground short circuit at 90% of the secondary side of  $TFYY_1$ .



To confirm the results, a turn-to-ground short circuit taking 90% of turns in the secondary of the converter transformers TFYY<sub>2</sub> and TFYD<sub>2</sub> was also evaluated—the results aligned with expectations relating to pole position and not transformer connection. Figures 6.82 and 6.83 show the secondary currents of transformers TFYY<sub>2</sub> and TFYD<sub>2</sub> for short circuits at 90% of their turns. When compared with the results of transformers TFYY<sub>1</sub> (Figure 6.47) and TFYD<sub>1</sub> (Figure 6.69), it becomes evident how the result depends on the transformer location in the pole. However, corroborating the results of Zheng *et al.* (2021a), in TFYD<sub>2</sub>, the FIIC occurs only in two phases, while in TFYY<sub>1</sub>, it occurs in all three.

Figure 6.82: Currents on the secondary side of  $TFYY_2$  during a turn-to-ground short circuit at 90% of the secondary side, with 100% power transmission in the bipoles.

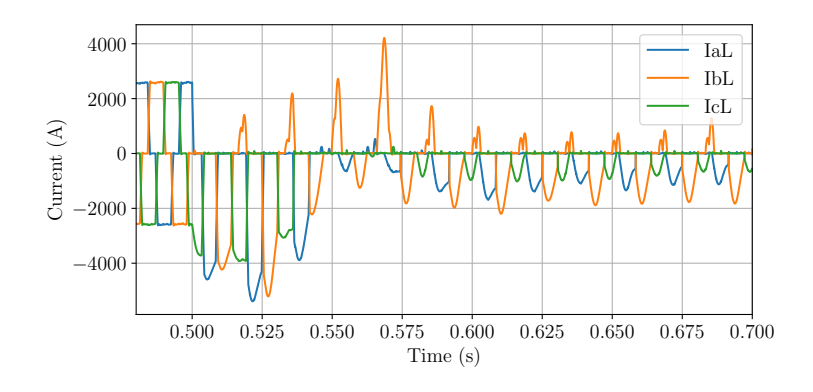
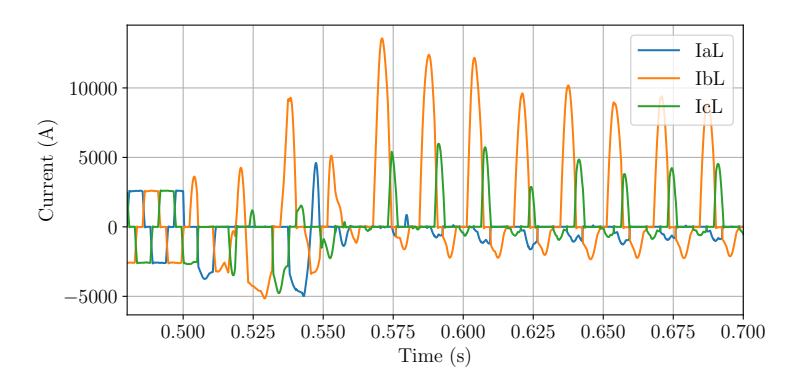


Figure 6.83: Currents on the secondary side of  $TFYD_2$  during a turn-to-ground short circuit at 90% of the secondary side, with 100% power transmission in the bipoles.



In addition to the factors analyzed above, two other details partially discussed above impact fault identification by the differential functions. The first is how the AC system perceives the DC system as a high impedance, as the poles directly control the currents in the transformers, preventing the fault from being fed by the AC system. Thus, the fault result follows as detailed above, where the current of the transformer depends on the inverters. Along the same lines, the second detail concerns the converter control response to the fault, which aims to maintain bipole stability and operation so that the fault current is limited and sometimes reduced after the initial fault current transient. In some cases, as in Figure 6.57, the lower fault impact allows the bipole adjustment to be nearly immediate.

All these points also affect the 87Q function so that, using the settings indicated in Table 6.1, the results match Figures 6.84 and 6.85. Since the delay is necessary, based on the results obtained, the 87Q function does not prove helpful for TFYY<sub>1</sub> beyond the 87T function. This occurs due to the behavior during the fault in the transformer, previously analyzed, where for a fault of 55% of turns or less, the currents of the transformer maintain a pattern controlled by the pole, as observed in Figure 6.57. Therefore, even with the offset, the phase imbalance occurs only momentarily and transiently at the fault moment, and the 87Q function is prevented from operating by the delay (Figure 6.86). For faults above this percentage of turns, the 87T function already identifies the fault, and the harmonic level blocks both equally.

As for the converter transformer TFYD<sub>1</sub>, even with the delay, the function proves useful and serves as a backup for the 87T function. As verified in Figure 6.69 and previously detailed,

a turn-to-ground short circuit in the secondary of TFYD<sub>1</sub> causes such an impact on the inverter that it leads to phase imbalance. However, as expected for a star-delta transformer, the function performs more consistently at the ends of the windings. To better visualize the result, Figures 6.87 and 6.88 show the operation of the 87Q function for a fault taking 10% of the turns and another taking 50% of the turns, respectively.

Figure 6.84: 87Q function operation in (a) TFYY<sub>1</sub> and (b) TFYD<sub>1</sub> for turn-to-ground short circuits on the secondary side, with 100% power transmission in the bipoles.

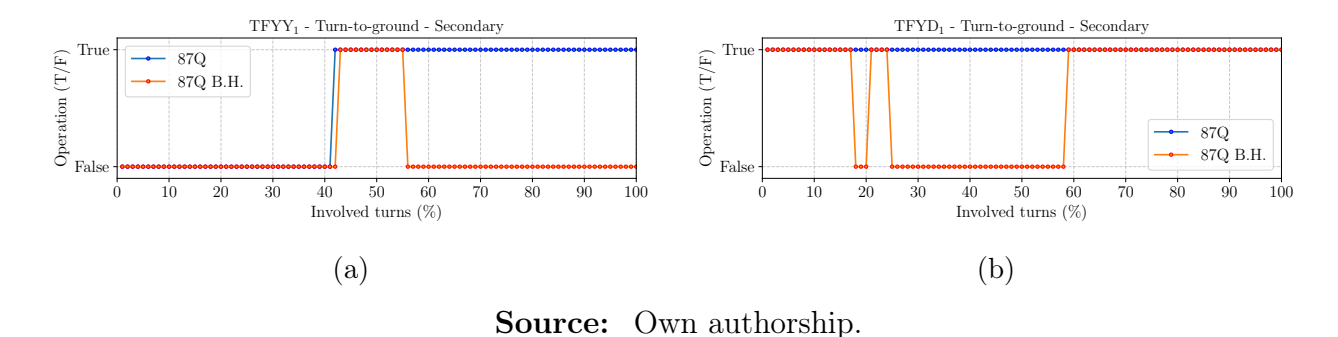


Figure 6.85: 87Q DLY function operation in (a) TFYY<sub>1</sub> and (b) TFYD<sub>1</sub> for turn-to-ground short circuits on the secondary side, with 100% power transmission in the bipoles.

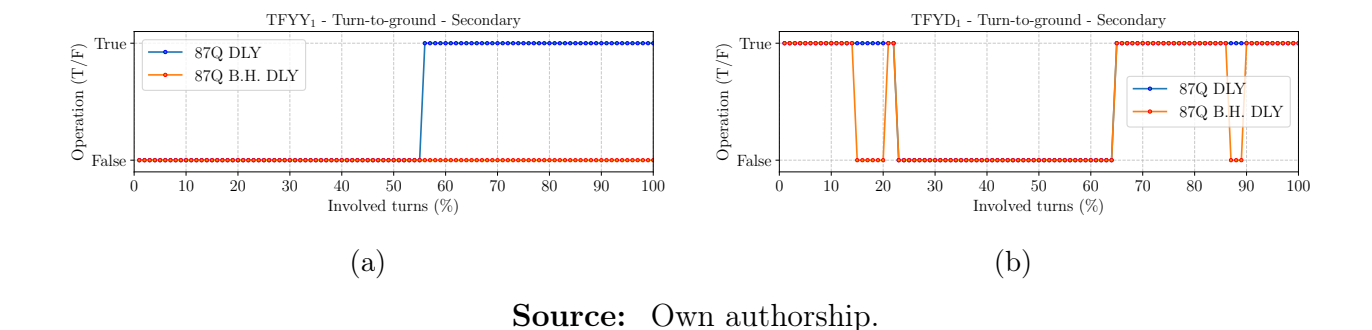


Figure 6.86: 87Q function operation in TFYY<sub>1</sub> for a turn-to-ground short circuit at 55% the secondary side, with 100% power transmission in the bipoles.

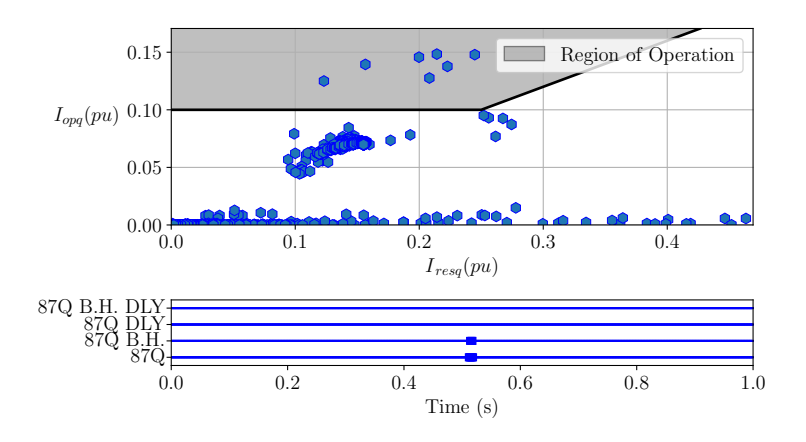


Figure 6.87: 87Q function operation in TFYD<sub>1</sub> for a turn-to-ground short circuit at 10% the secondary side, with 100% power transmission in the bipoles.

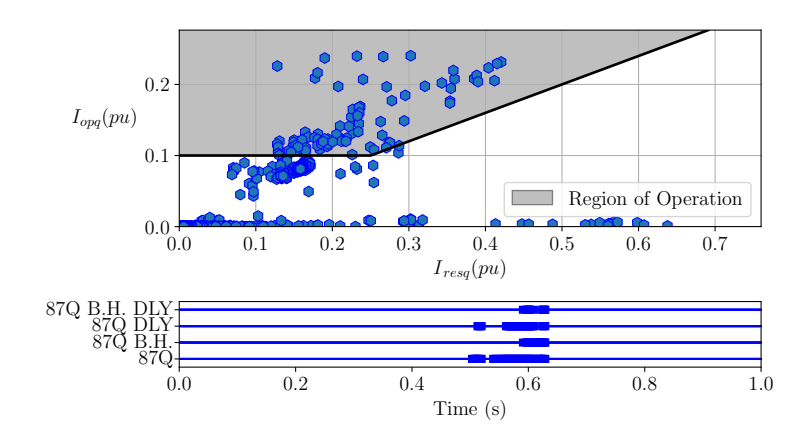
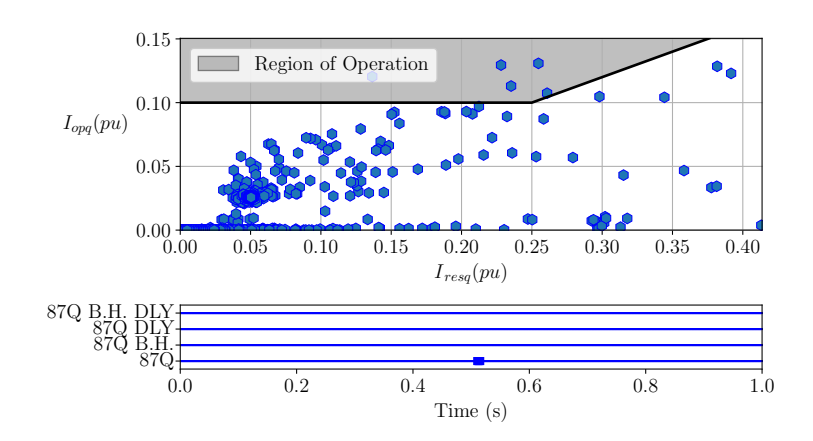


Figure 6.88: 87Q function operation in TFYD<sub>1</sub> for a turn-to-ground short circuit at 50% the secondary side, with 100% power transmission in the bipoles.



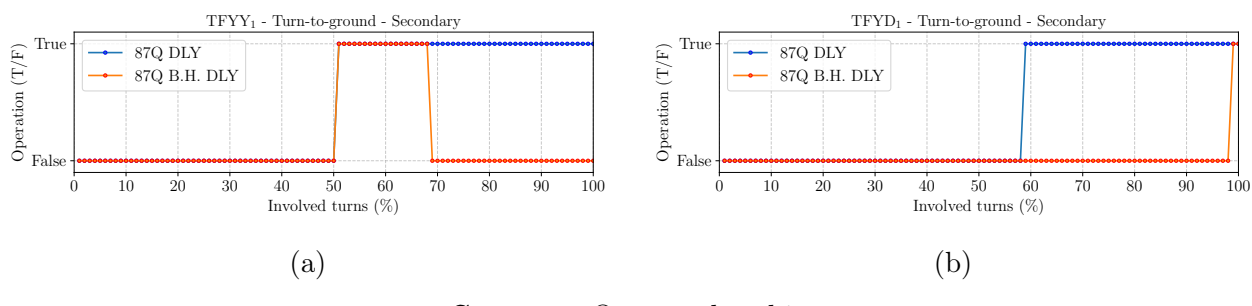
**Source:** Own authorship.

Ultimately, examining the operation of the 87Q function with the bipoles at 10% power transmission reveals interesting results. With a lower power setpoint on the pole, the currents in the transformers during the fault are small, as previously seen in Figures 6.62 and 6.78. This current reduction does not directly prevent the operation of the 87Q function, as it is sensitive to phase imbalances. However, it reduces the level of 2<sup>nd</sup> harmonic current in turn-to-ground faults, allowing the function to operate for faults taking between 51% and 68% of the TFYY<sub>1</sub> windings, as shown in Figure 6.89a.

For TFYD<sub>1</sub>, the currents are reduced to nearly zero, and because of this and the applied

delay, the function is triggered by only a few samples. Consequently, the brief interval in which there is 2<sup>nd</sup> harmonic blocking immediately after the fault onset is sufficient to prevent the function from operating, as shown in Figure 6.89b.

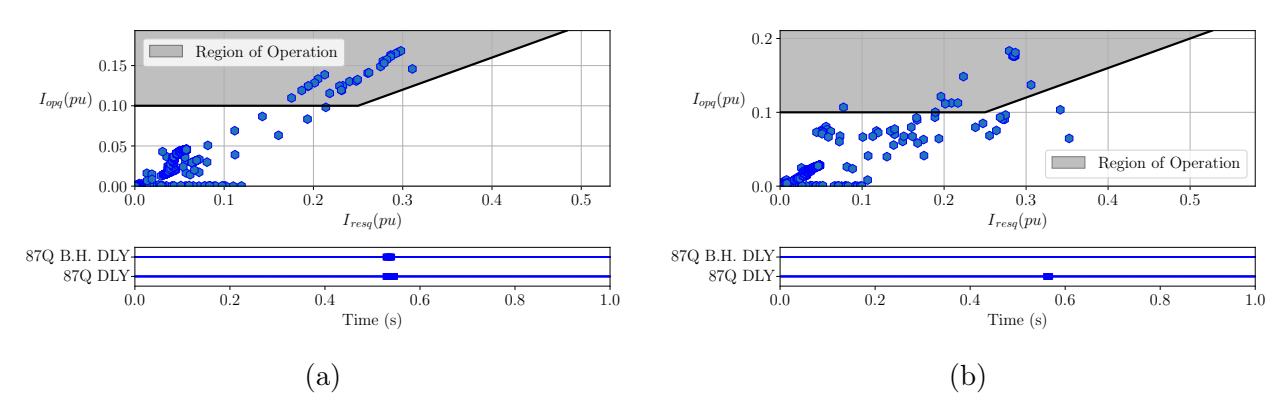
Figure 6.89: 87Q DLY function operation in (a) TFYY<sub>1</sub> and (b) TFYD<sub>1</sub> for turn-to-ground short circuits on the secondary side, with 10% power transmission in the bipoles.



**Source:** Own authorship.

Figure 6.90 demonstrates the operation of the 87Q function for a turn-to-ground fault in the secondary side of transformers TFYY<sub>1</sub> and TFYD<sub>1</sub>, taking 68% of turns with the bipoles at 10% power transmission. These figures are a pertinent example of the results illustrated in Figure 6.89.

Figure 6.90: 87Q DLY function operation in (a) TFYY<sub>1</sub> and (b) TFYD<sub>1</sub> for a turn-to-ground short circuit at 68% the secondary side, with 10% power transmission in the bipoles.



Source: Own authorship.

#### 6.4.2.2 Short circuit turn-to-turn

The performance of the 87T and 87Q functions for turn-to-turn short-circuits in the secondary of the converter transformers has similar results as that evaluated for turn-to-turn

short-circuits in the primary (Subsection 6.4.1.2).

Despite the challenges and issues identified for turn-to-ground faults on the secondary side, these issues do not recur for turn-to-turn faults. This disparity is because the challenges are specifically caused by the fault's contact with the ground. For turn-to-turn faults on the secondary side, the consequence remains an increase in current in the transformer due to the smaller number of turns remaining after the fault initiation. However, this increase is diminished compared to turn-to-turn faults on the primary side because of the control response and the characteristics of the inverter, which prevent a direct fault contribution from the DC system. Consequently, the currents resulting from a turn-to-turn short circuit taking 90% of the secondary windings are shown in Figure 6.91 and can be compared with the resulting currents for the same short circuit on the primary side, presented in Figure 6.92.

Figure 6.91: Currents of (a) TFYY and (b) TFYD during a turn-to-turn short circuit at 90% of the secondary side, with 100% power transmission in the bipoles.

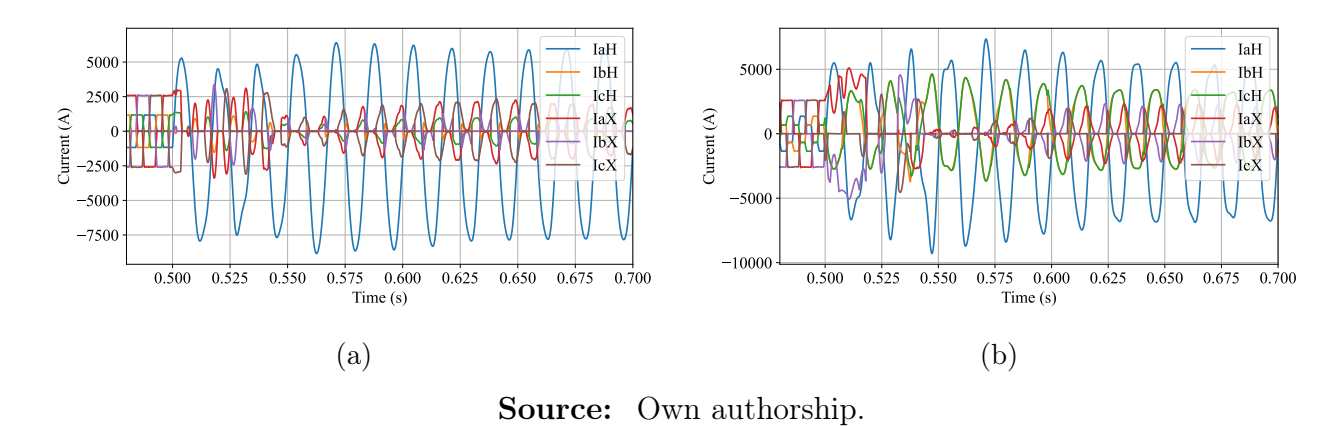
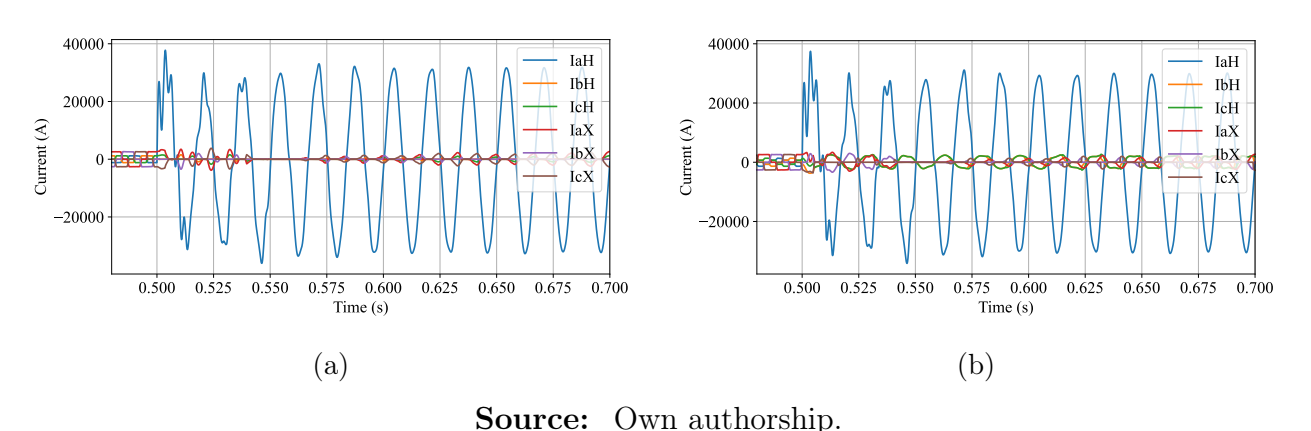


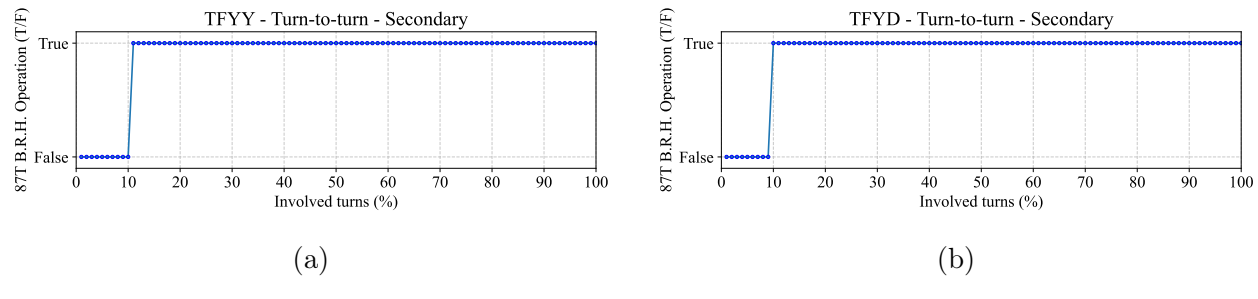
Figure 6.92: Currents of (a) TFYY and (b) TFYD during a turn-to-turn short circuit at 90% of the primary side, with 100% power transmission in the bipoles.



As a result, while primary turn-to-turn faults have the same result as primary turn-to-ground faults, secondary turn-to-turn faults have a slightly smaller coverage by the 87T function due to the lower current values. However, the 87Q function operates from 2% of turns for both cases.

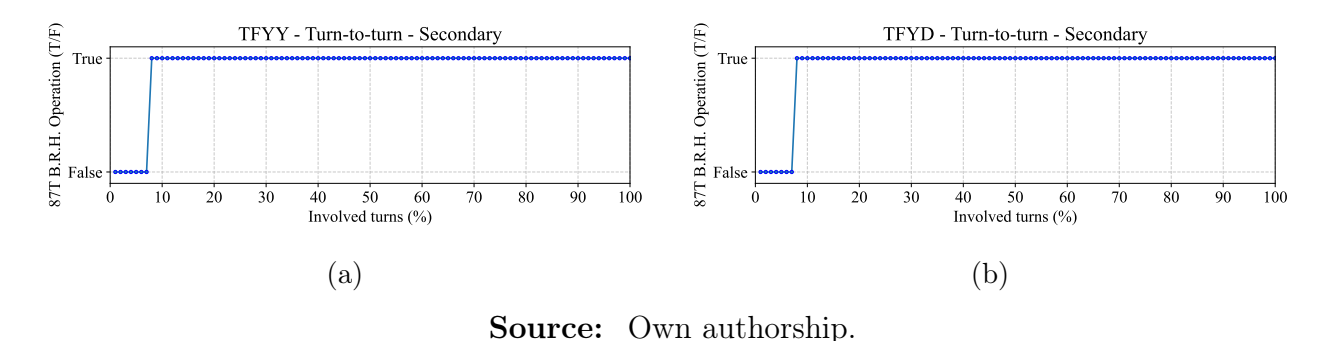
Confirming the slight difference, Figure 6.93 demonstrates the operation of the 87T function for bipoles at 100% power transmission in cases of turn-to-turn faults on the secondary side of the converter transformers. Due to the lower currents, the function operates from 10% of turns for the TFYD and 11% for the TFYY. For 10% power in the bipoles (Figure 6.94), the operation threshold decreases to 8% of turns.

Figure 6.93: 87T R.B.H. function operation in (a) TFYY and (b) TFYD for a turn-to-turn short circuit on the secondary side, with 100% power transmission in the bipoles.



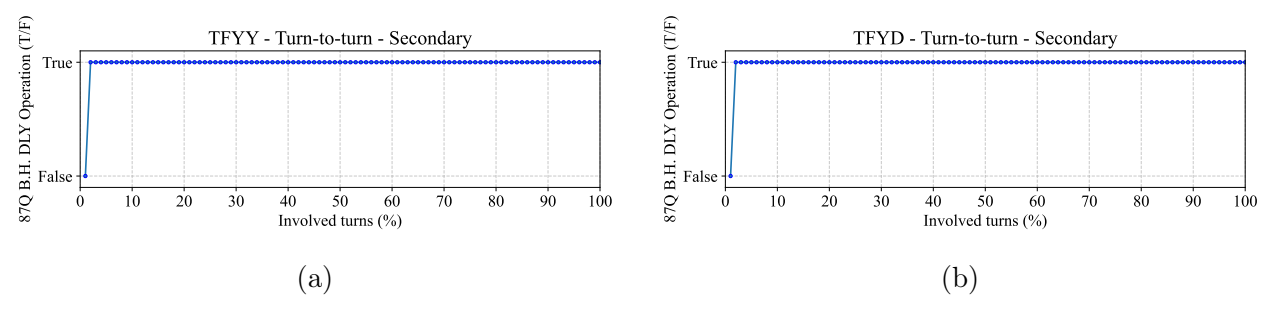
**Source:** Own authorship.

Figure 6.94: 87T R.B.H. function operation in (a) TFYY and (b) TFYD for a turn-to-turn short circuit on the secondary side, with 10% power transmission in the bipoles.



For the 87Q function, Figure 6.95 compared with Figure 6.23 show how the function operates the same for both terminals. The same result occurs for the bipoles with 10% power transmission.

Figure 6.95: 87Q B.H. DLY function operation in (a) TFYY and (b) TFYD for turn-to-turn short circuits on the secondary side, with 100% power transmission in the bipoles.

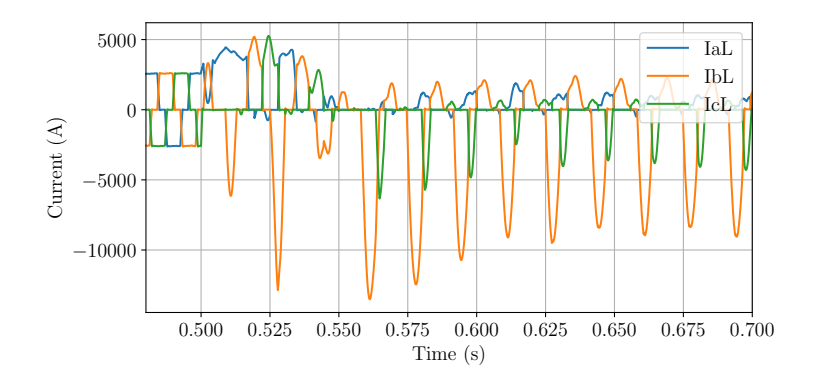


#### 6.4.2.3 Single-phase-to-ground short circuit

As a single-phase-to-ground fault essentially represents a single-phase-to-ground fault taking a certain number of turns, the results for single-phase-to-ground faults in the secondary resemble those for ground faults taking 90% of the turns, which were previously presented and analyzed in detail in Subsection 6.4.2.1. Thus, the fault is equivalent to faults to ground taking 100% of the turns. Given this similarity, using the nomenclature from Figure 6.40 is again appropriate to better interpret the results.

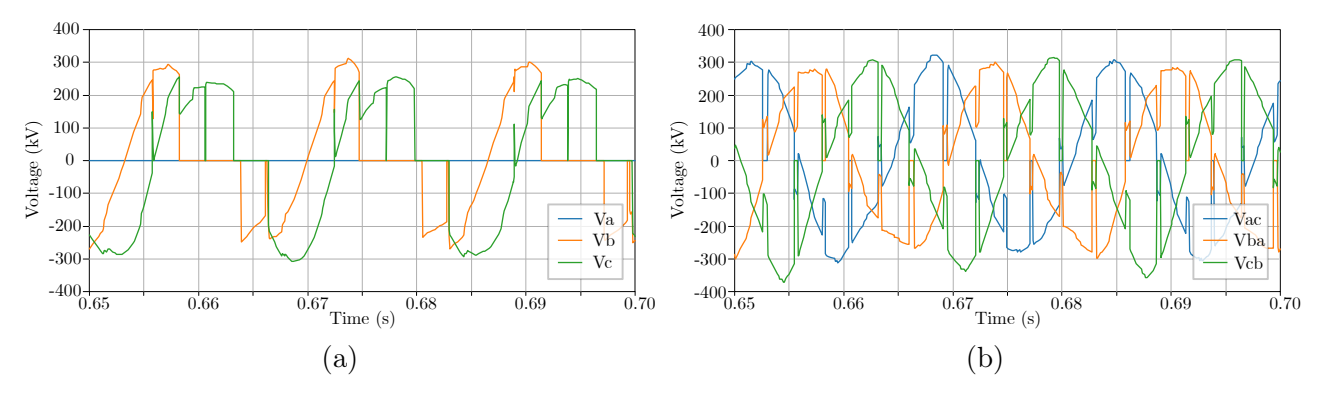
Starting the analysis with TFYY<sub>1</sub>, Figure 6.96 shows the fault currents in its secondary. Higher fault currents are observed here compared to the turn-to-ground fault with 90% (Figure 6.81). However, the same current pattern is maintained, demonstrating that the operation of Inv<sub>1</sub> during the fault follows the diagram shown in Figure 6.46.

Figure 6.96: Currents on the secondary side of  $TFYY_1$  during a single-phase-to-ground short circuit on the secondary side, with 100% power transmission in the bipoles.



The reasoning behind this behavior remains the same, as shown in Figure 6.97a, which represents the phase voltages  $V_a$ ,  $V_b$ , and  $V_c$  in the transformer's secondary side and follows the same pattern as the turn-to-ground fault (Figure 6.50a). The only expected difference is that, in a single-phase-to-ground fault, the  $V_a$  voltage is effectively reduced to zero. This similarity logically extends to the line voltages  $V_{ac}$ ,  $V_{ba}$ , and  $V_{cb}$ , as observed in Figure 6.97b compared to Figure 6.50b.

Figure 6.97: Faulted-state phase (a) and line (b) voltages for a single-phase-to-ground short circuit on the secondary side of  $TFYY_1$ .



**Source:** Own authorship.

Consequently, the primary-side currents of the transformer follow the pattern shown in Figure 6.98, and the 87T function without harmonic restraint or blocking is triggered by the fault (Figure 6.99). Meanwhile, the 87T function with harmonic restraint and blocking is not triggered due to both 2<sup>nd</sup> harmonic blocking (Figure 6.54) and 2<sup>nd</sup> harmonic restraint (Figure 6.100).

Figure 6.98: Currents on the primary side of  $TFYY_1$  during a single-phase-to-ground short circuit on the secondary side, with 100% power transmission in the bipoles.

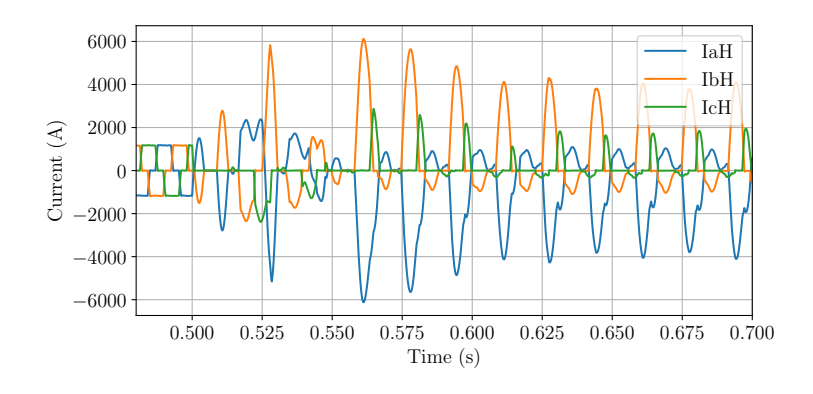
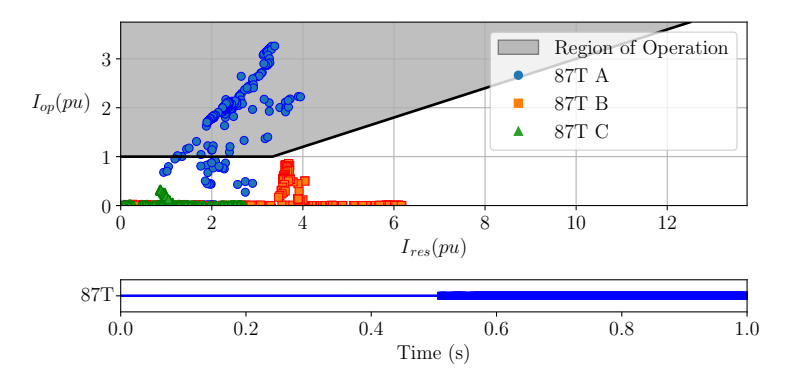


Figure 6.99: 87T function operation in  $TFYY_1$  for a single-phase-to-ground short circuit on the secondary side, with 100% power transmission in the bipoles.



With the bipoles at 10% power transmission, the results remain almost identical to turn-to-ground faults taking nearly 100% of the turns. The fault current pattern remains consistent (Figure 6.102), but the pole control keeps these currents lower, so the operating current is too small to reach  $I_{pickupmin}$  (Figure 6.103).

The exact same relationship applies to TFYD<sub>1</sub>. Fault currents follow the diagram in Figure 6.68 so that both secondary and primary currents of the transformer follow the pattern of turn-to-ground faults, as observed by comparing Figures 6.104 and 6.105 with Figures 6.69 and 6.73 for faults with the bipoles at 100% power transmission. Thus, again, there is no operation of the 87T function without harmonic restraint or blocking, 6.106, and with bipoles at 10% power transmission, the function remains not sensitized (Figures 6.107 and 6.108).

Figure 6.100:  $2^{nd}$  harmonic by fundamental for a single-phase-to-ground short circuit on the secondary side of TFYY<sub>1</sub>.

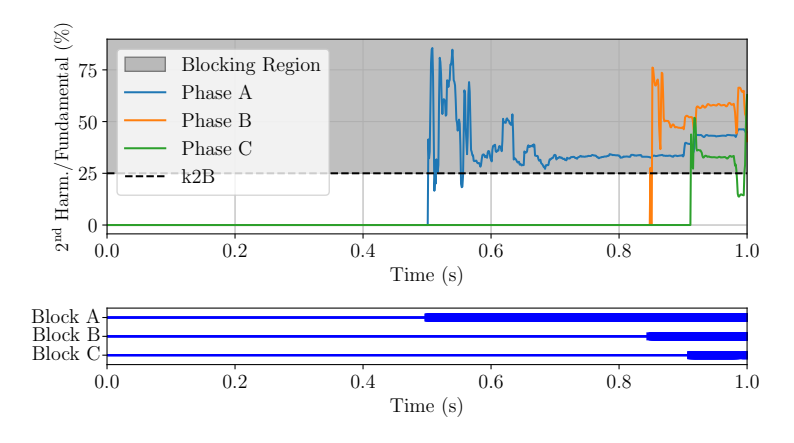


Figure 6.101: 87T R.B.H. function operation in TFYY<sub>1</sub> for a single-phase-to-ground short circuit on the secondary side, with 100% power transmission in the bipoles.

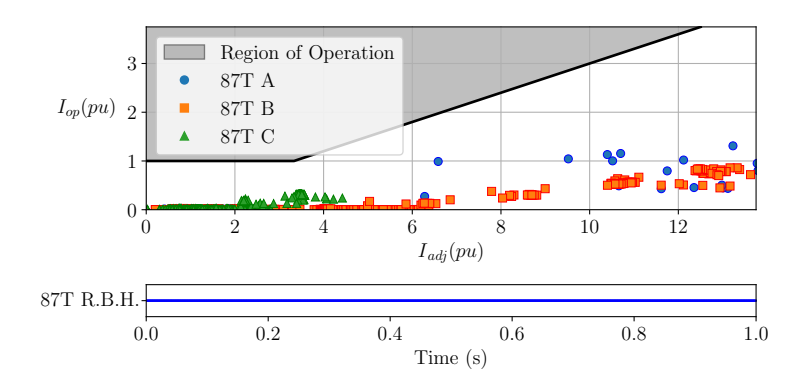
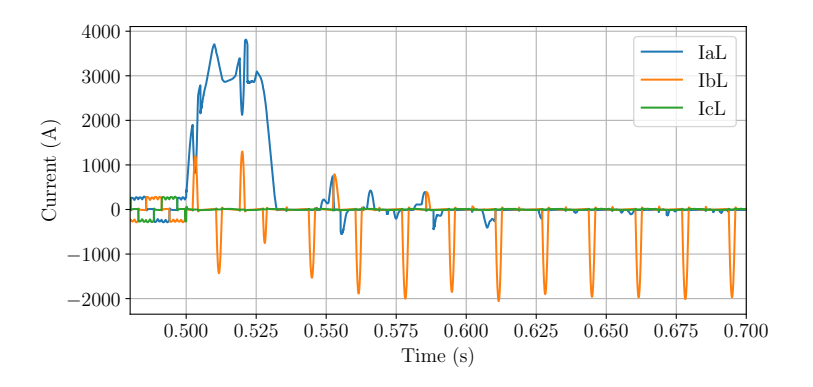


Figure 6.102: Currents on the secondary side of  $TFYY_1$  during a single-phase-to-ground short circuit on the secondary side, with 10% power transmission in the bipoles.



**Source:** Own authorship.

Figure 6.103: 87T function operation in  $TFYY_1$  for a single-phase-to-ground short circuit on the secondary side, with 10% power transmission in the bipoles.

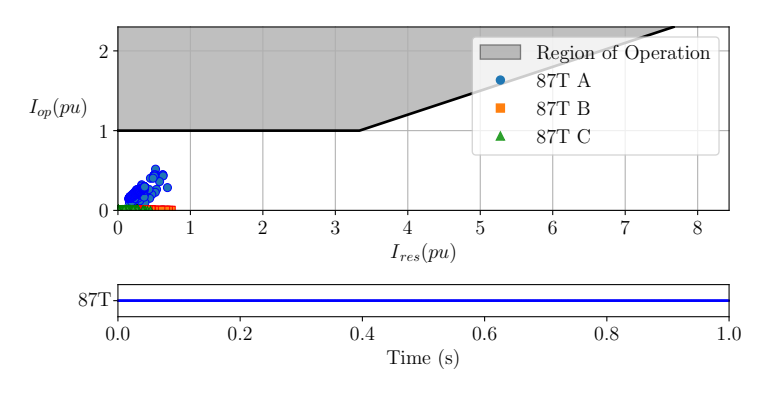


Figure 6.104: Currents on the secondary side of  $TFYD_1$  during a single-phase-to-ground short circuit on the secondary side, with 100% power transmission in the bipoles.

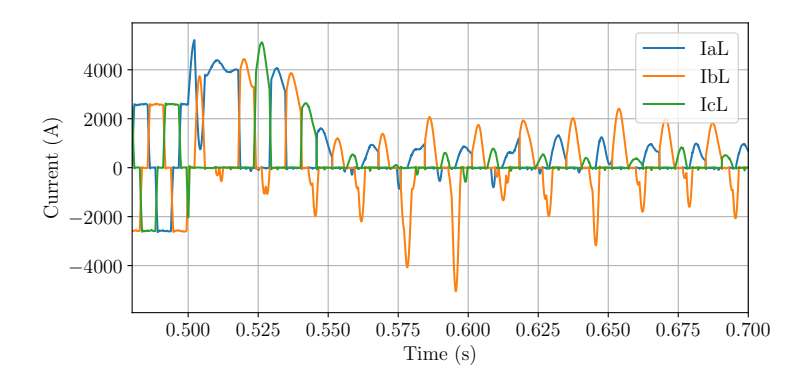
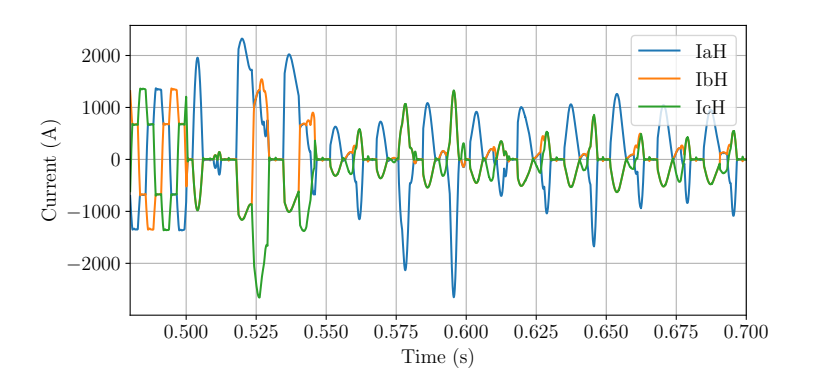


Figure 6.105: Currents on the primary side of  $TFYD_1$  during a single-phase-to-ground short circuit on the secondary side, with 100% power transmission in the bipoles.



**Source:** Own authorship.

Figure 6.106: 87T function operation in  $TFYD_1$  for a single-phase-to-ground short circuit on the secondary side, with 100% power transmission in the bipoles.

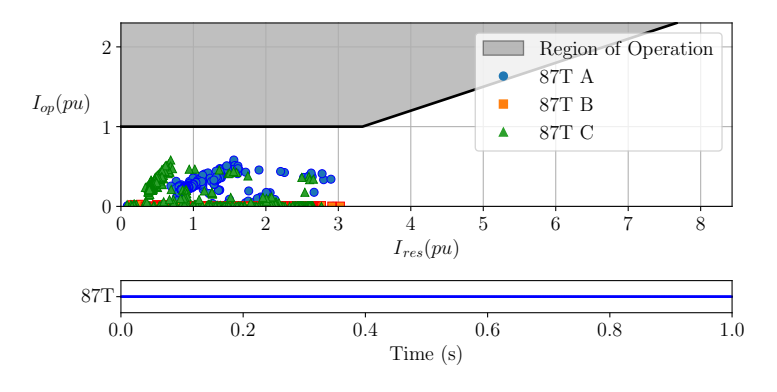


Figure 6.107: Currents on the secondary side of  $TFYD_1$  during a single-phase-to-ground short circuit on the secondary side, with 10% power transmission in the bipoles.

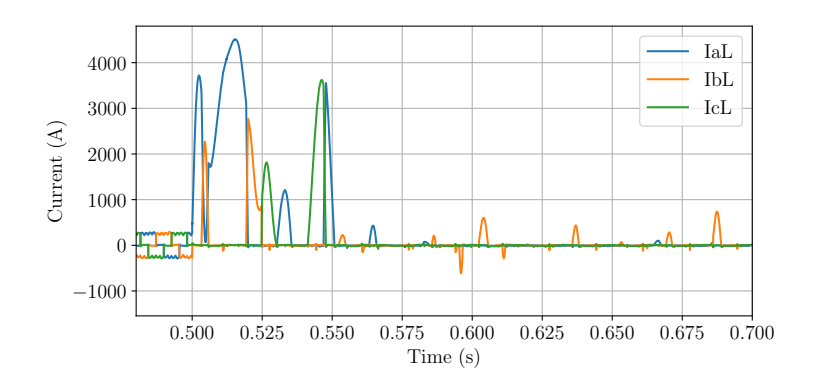
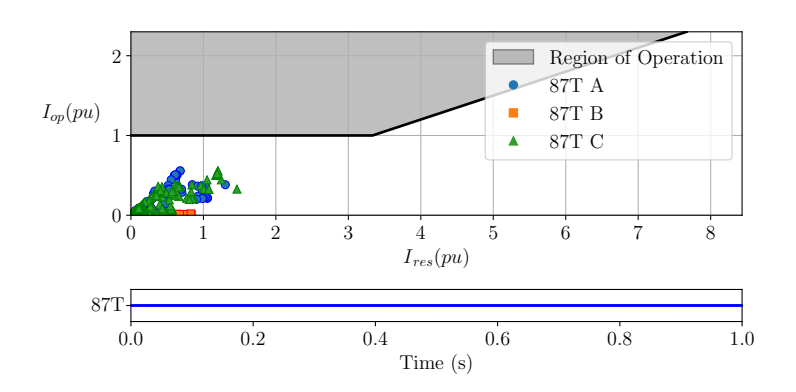


Figure 6.108: 87T function operation in  $TFYD_1$  for a single-phase-to-ground short circuit on the secondary side, with 10% power transmission in the bipoles.



Source: Own authorship.

Additionally, the phase and line voltages for the fault shown in Figure 6.109 confirm the same causes for the observed results, as commutation failures also persist following the same pattern (Figure 6.110).

Finally, confirming the relationship between results and the converter transformer position in the pole, Figures 6.111 and 6.112 respectively show the secondary currents for transformers TFYY<sub>2</sub> and TFYD<sub>2</sub>, which follow the same pattern as the secondary currents for TFYY<sub>1</sub> and TFYD<sub>1</sub> according to their position in the pole rather than their star-star or star-delta connections.

Figure 6.109: Faulted-state phase (a) and line (b) voltages for a single-phase-to-ground short circuit on the secondary of TFYD<sub>1</sub>.

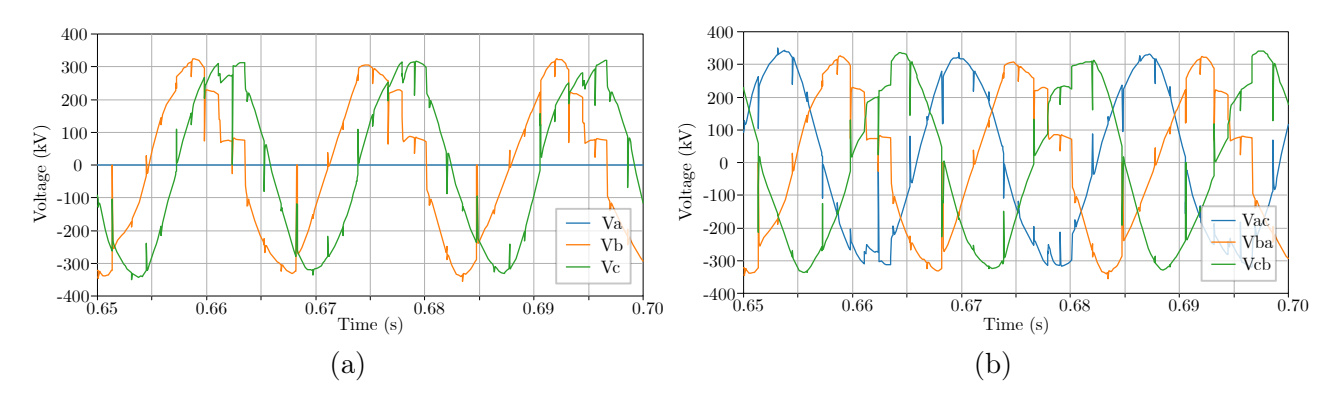
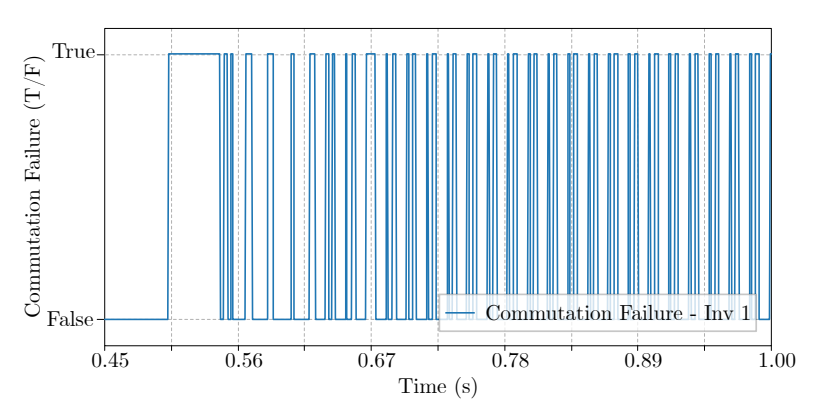


Figure 6.110: Commutation failures of  $Inv_2$  for a single-phase-to-ground short circuit on the secondary of the converter transformer  $TFYD_1$ .



Source: Own authorship.

Figure 6.111: Currents on the secondary side of  $TFYY_2$  during a single-phase-to-ground short circuit on the secondary side, with 100% power transmission in the bipoles.

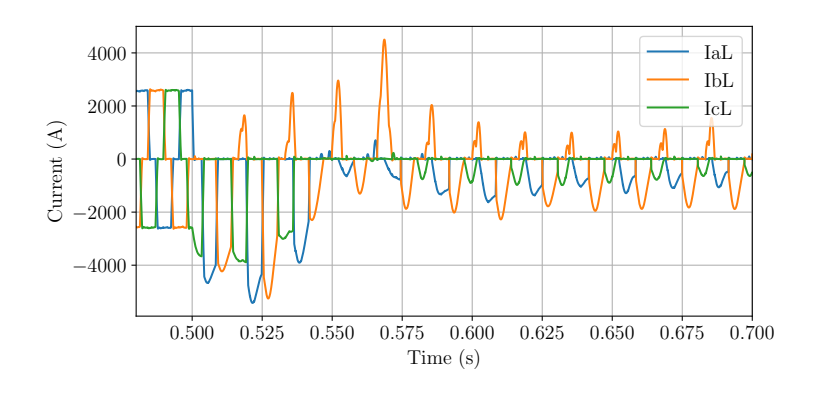
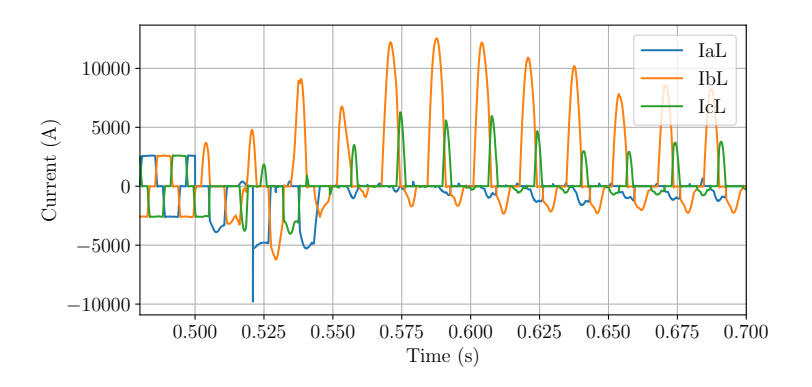


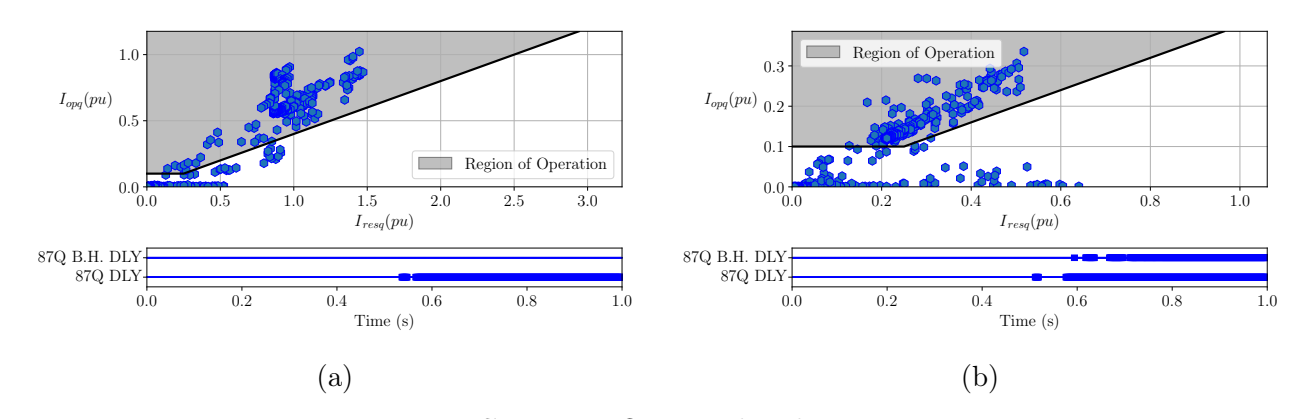
Figure 6.112: Currents on the secondary side of  $TFYD_2$  during a single-phase-to-ground short circuit on the secondary side, with 100% power transmission in the bipoles.



The equivalence is again observed regarding the 87Q function with bipoles at 100%. The function operation for a single-phase-to-ground fault in the secondary of transformers  $TFYY_1$  and  $TFYD_1$  is shown in Figures 6.113a and 6.113b, respectively. Its results are consistent with those verified in Figure 6.85.

The same happens with bipoles at 10% power transmission, as seen in Figures 6.114a and 6.114b.

Figure 6.113: 87Q DLY function operation in (a) TFYY<sub>1</sub> and (b) TFYD<sub>1</sub> for a single-phase-to-ground short circuit on the secondary side, with 100% power transmission in the bipoles.



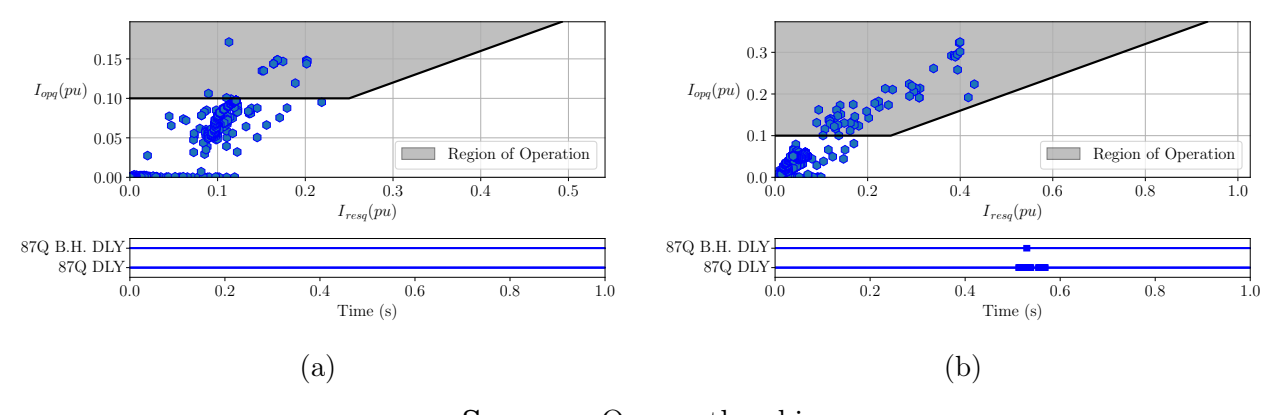
**Source:** Own authorship.

#### 6.4.2.4 Phase-to-phase short circuit

When a phase-to-phase short circuit occurs in  $TFYY_1$ , the variations in the transformer's secondary side voltages cause a reduction in  $V_{dc}$ , similar to that observed in turn-to-ground

and single-phase-to-ground faults. Consequently, there is an increase in current and commutation failures in the inverter. With the response of the pole control, the currents in INV<sub>1</sub> behave as shown in Figure 6.115. During the periods when thyristors in phases A and B are conducting, there is a short circuit between the two phases, as illustrated in Figures 6.121d and 6.115f. Meanwhile, the phase voltages  $V_a$  and  $V_b$  become equal, so only there is current in phase C when paired with phase A (Figures 6.115b and 6.115e), and inverter currents are interrupted when pairs  $T_{21}$  and  $T_{31}$ , and  $T_{61}$  and  $T_{51}$ , are on (Figures 6.115a and 6.115c). As a result, the secondary currents of transformer TFYY<sub>1</sub> follow the pattern shown in Figure 6.116, corresponding to the phase-to-phase fault with bipoles at 100% power transmission.

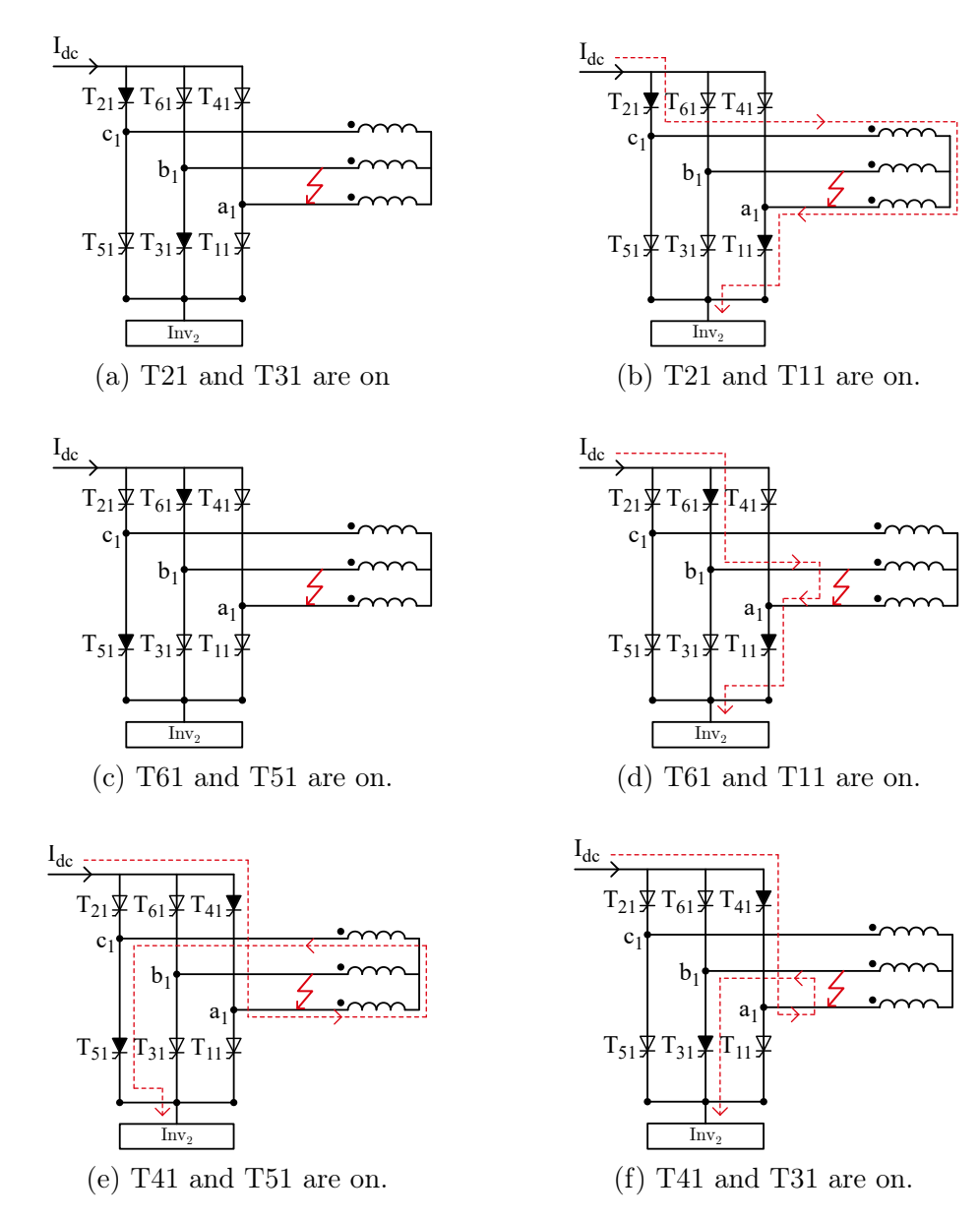
Figure 6.114: 87Q DLY function operation in (a) TFYY<sub>1</sub> and (b) TFYD<sub>1</sub> for a single-phase-to-ground short circuit on the secondary side, with 10% power transmission in the bipoles.



**Source:** Own authorship.

With this result in the current of the transformer, it is expected that the differential functions are triggered, and, unlike single-phase-to-ground and turn-to-ground faults, since there is no ground contact, no DC offset appears in the currents of the transformer, as previously observed in Figure 6.116. Thus, there is neither half-cycle saturation nor inrush current induced by the fault, meaning that the level of the 2<sup>nd</sup> harmonic component is not elevated, and it does not block or restrain the differential functions (6.117). Consequently, the 87T functions with harmonic restraint and blocking, as well as the 87Q function with harmonic blocking, operate normally, as demonstrated in Figures 6.118 and 6.119.

Figure 6.115: Fault current loops in  $Inv_1$  for a phase-to-phase short circuit on the secondary of  $TFYY_1$ .



Without ground contact, the fault effects on TFYD<sub>1</sub> remain unchanged compared to TFYY<sub>1</sub>. Figure 6.120 shows the transformer's secondary side currents, while Figure 6.121 shows the currents during the fault in Inv<sub>2</sub>. From these figures, it is evident that the result is equivalent to Figures 6.116 and 6.115. Thus, the 87T and 87Q functions operate precisely once again, even with harmonic blocking and restraint, as seen in Figures 6.122 and 6.123.

With the bipoles at 10% power transmission, the results remain equivalent, allowing the differential functions to operate correctly, as shown in Figures 6.124 and 6.125.

Figure 6.116: Currents on the secondary side of  $TFYY_1$  during a phase-to-phase short circuit on the secondary side, with 100% power transmission in the bipoles.

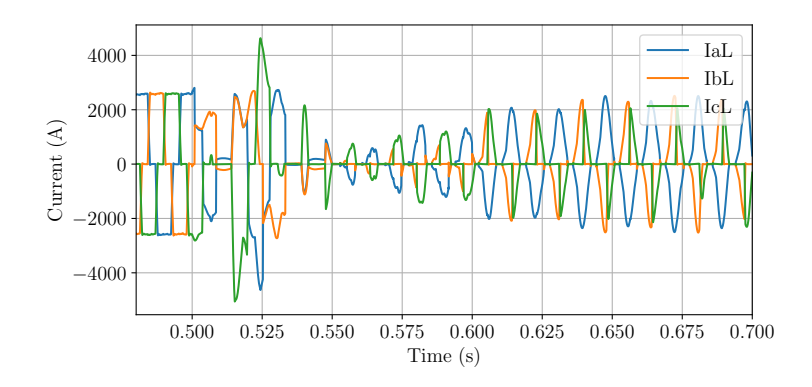
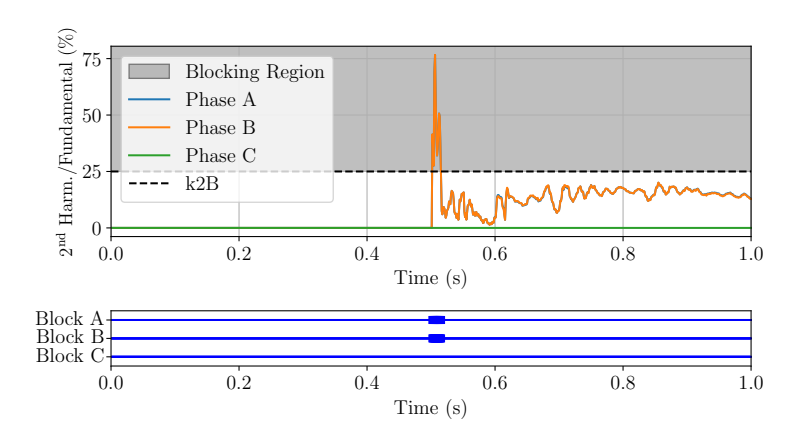


Figure 6.117:  $2^{nd}$  harmonic by fundamental for a phase-to-phase short circuit on the secondary side of TFYY<sub>1</sub>.



Source: Own authorship.

Figure 6.118: 87T R.B.H. function operation in  $TFYY_1$  for a phase-to-phase short circuit on the secondary side, with 100% power transmission in the bipoles.

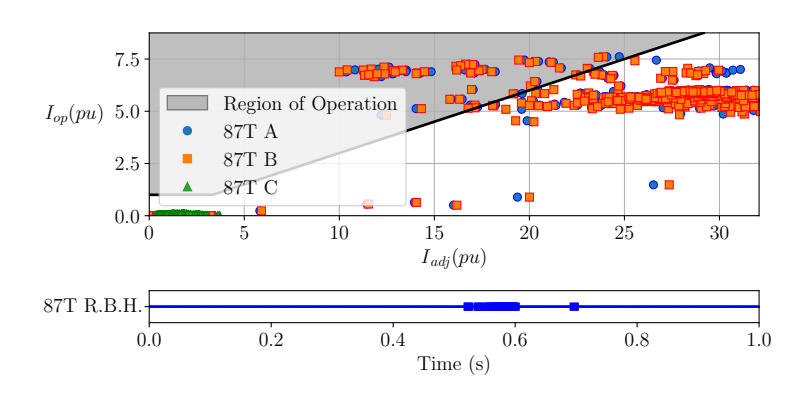


Figure 6.119: 87Q DLY function operation in  $TFYY_1$  for a phase-to-phase short circuit on the secondary side, with 100% power transmission in the bipoles.

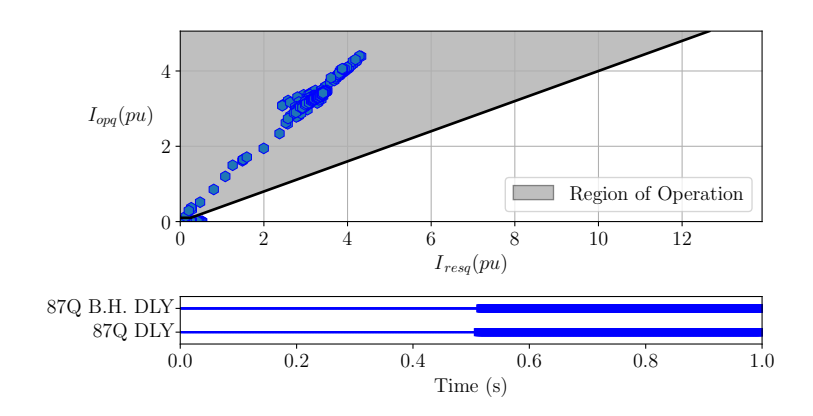
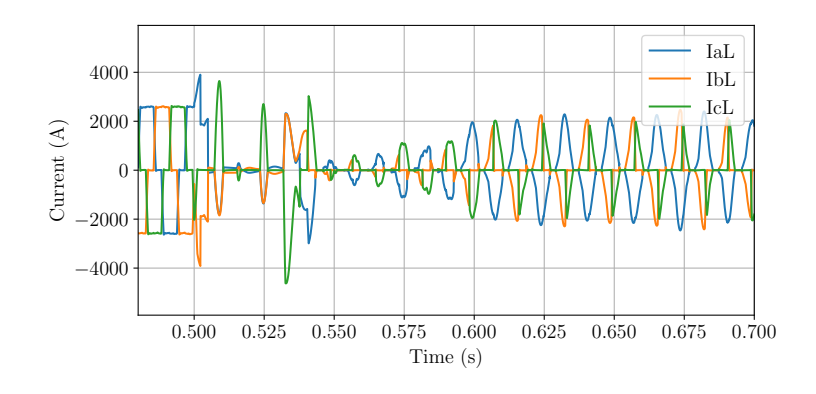


Figure 6.120: Currents on the secondary side of TFYD<sub>1</sub> during a phase-to-phase short circuit on the secondary side, with 100% power transmission in the bipoles.

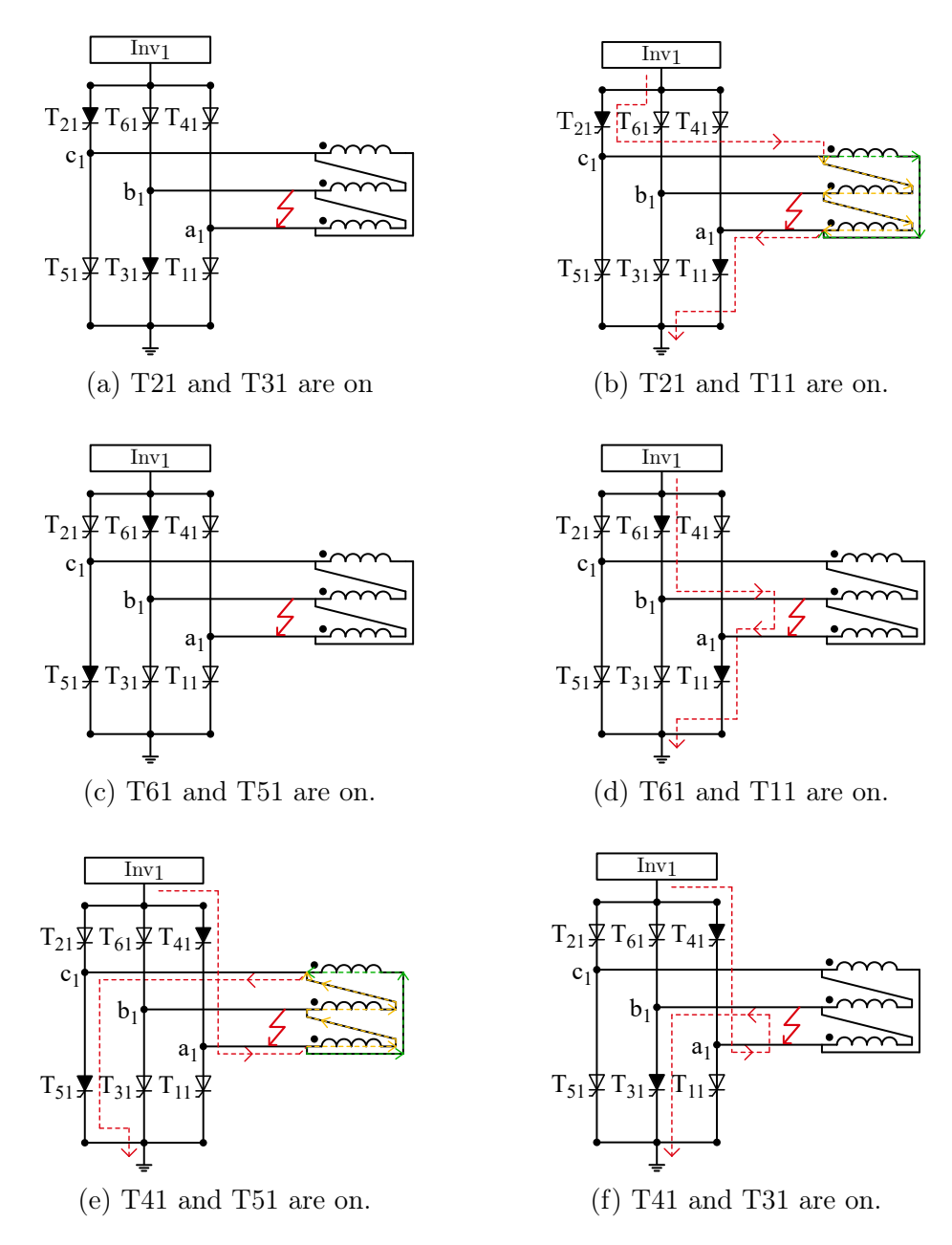


**Source:** Own authorship.

#### 6.4.2.5 Phase-to-phase-to-ground short circuit

The results obtained for phase-to-phase-to-ground short circuits are, logically, a combination of the outcomes for single-phase-to-ground and phase-to-phase faults. To verify this, considering the results for bipoles at 100% power transmission, it suffices to compare the secondary currents of transformers TFYY<sub>1</sub> and TFYD<sub>1</sub> shown in Figure 6.126 with the currents for single-phase-to-ground faults (Figures 6.96 and 6.104) and phase-to-phase faults (Figures 6.116 and 6.120).

Figure 6.121: Fault current loops in  $Inv_1$  for a phase-to-phase short circuit on the secondary of  $TFYD_1$ .



The ground contact increases the  $2_{nd}$  harmonic component in the current of the transformer, with higher values in transformer TFYY<sub>1</sub> (Figure 6.127). However, this does not block the functions for a k2B of 25%, as the  $2^{nd}$  harmonic currents are divided between the two faulted phases.

Hence, the differential functions operate correctly for the fault, even with some impact of harmonic restraint on  $TFYY_1$ , as shown in Figures 6.128 and 6.129.

Figure 6.122: Operational plan and operation logic of the 87T function and with harmonic and blocking by harmonics for phase-to-phase short circuit in the secondary of the converter transformer  $TFYD_1$ .

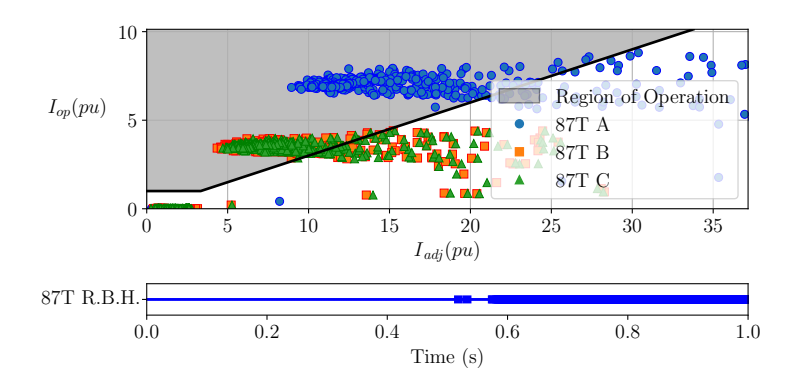
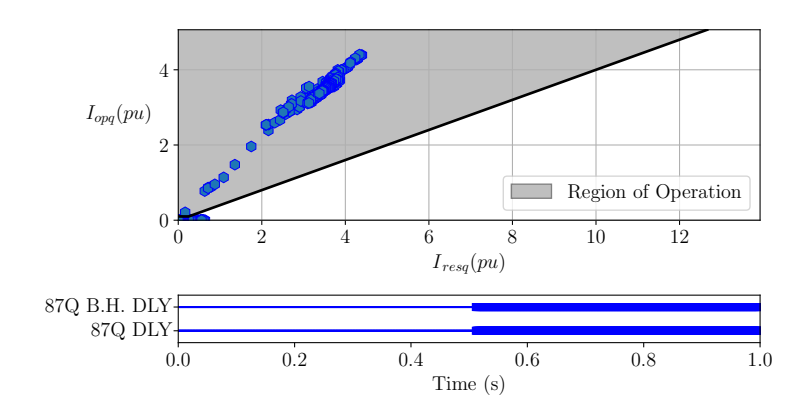


Figure 6.123: 87Q DLY function operation in  $TFYD_1$  for a phase-to-phase short circuit on the secondary side, with 100% power transmission in the bipoles.



Source: Own authorship.

Figure 6.124: 87T R.B.H. function operation in (a) TFYY<sub>1</sub> and (b) TFYD<sub>1</sub> for a phase-to-phase short circuit on the secondary side, with 10% power transmission in the bipoles.

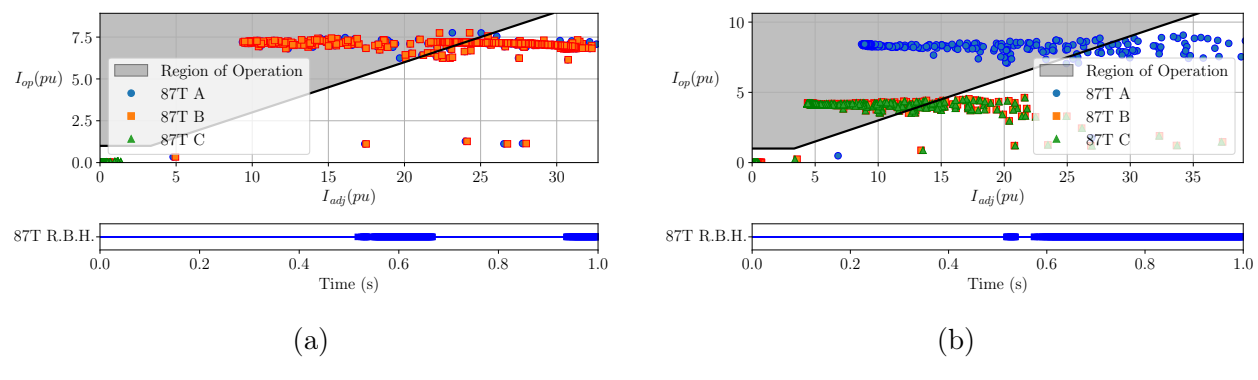


Figure 6.125: 87Q DLY function operation in (a) TFYY<sub>1</sub> and (b) TFYD<sub>1</sub> for a phase-to-phase short circuit on the secondary side, with 10% power transmission in the bipoles.

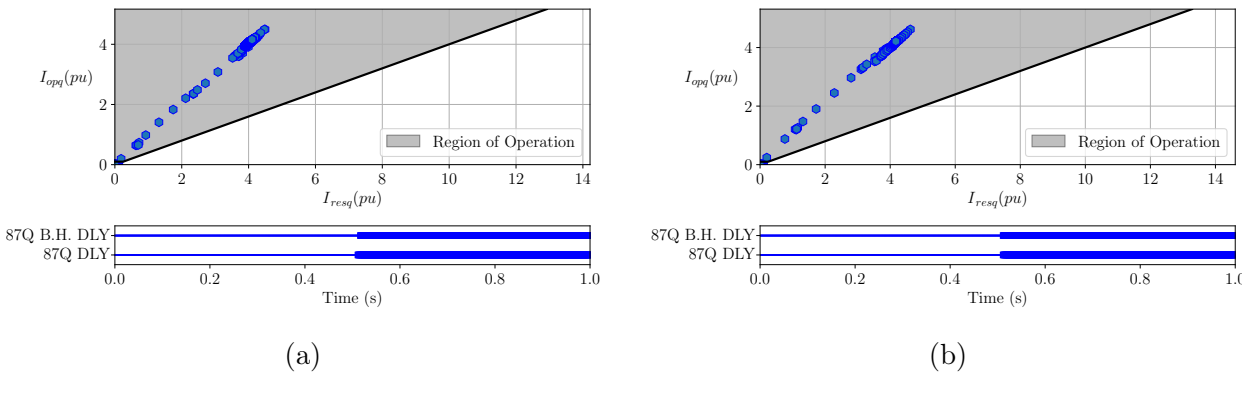


Figure 6.126: Currents on the secondary side of (a) TFYY<sub>1</sub> and (b) TFYD<sub>1</sub> during a phase-to-phase-to-ground short circuit on the secondary side, with 100% power transmission in the bipoles.

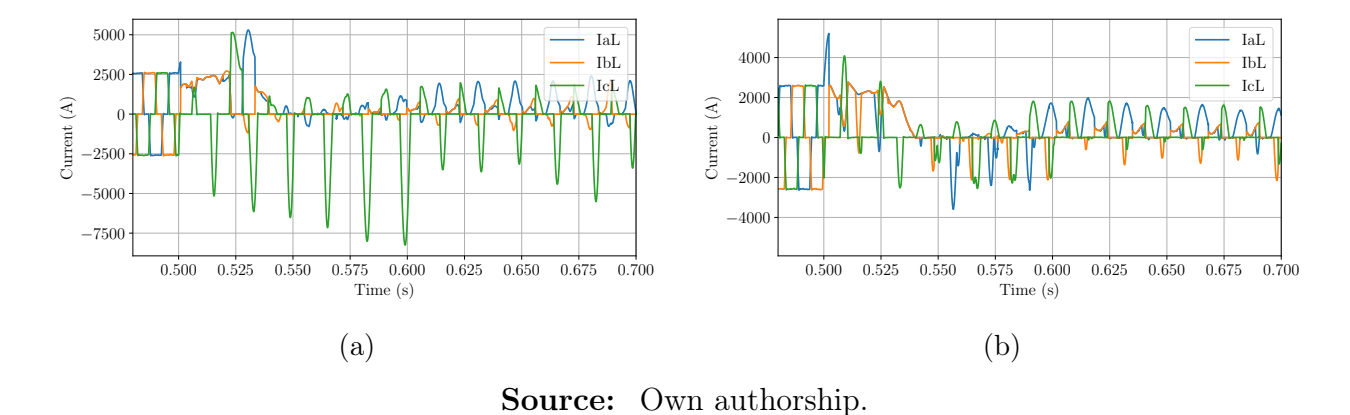


Figure 6.127:  $2^{nd}$  harmonic by fundamental for a phase-to-phase-to-ground short circuit on the secondary of (a) TFYY<sub>1</sub> and (b) TFYD<sub>1</sub>.

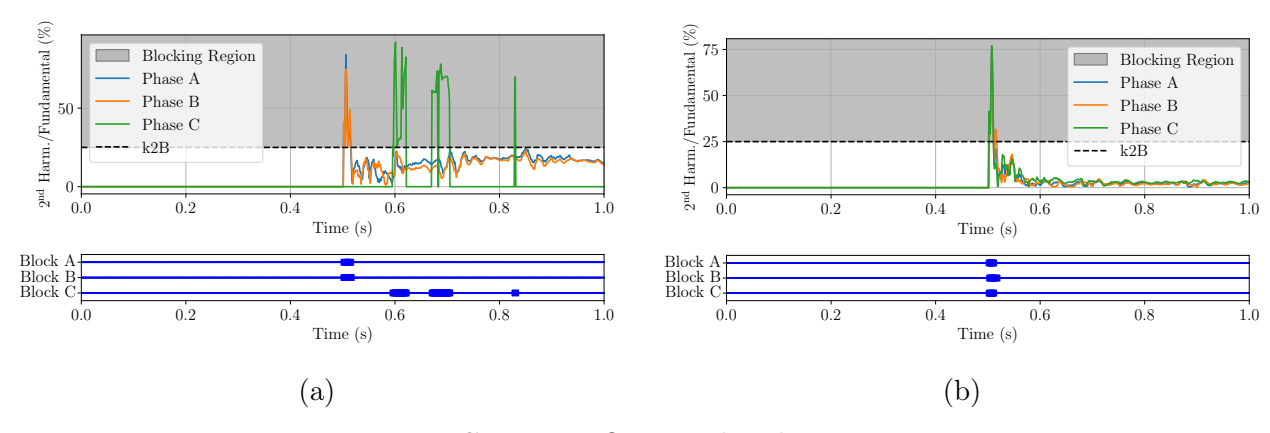


Figure 6.128: 87T R.B.H. function operation in (a) TFYY<sub>1</sub> and (b) TFYD<sub>1</sub> for a phase-to-phase-to-ground short circuit on the secondary side, with 100% power transmission in the bipoles.

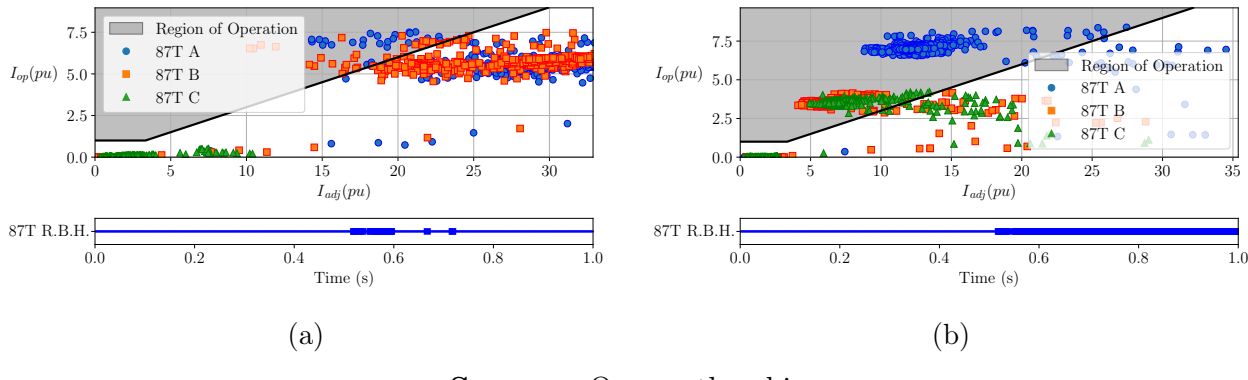
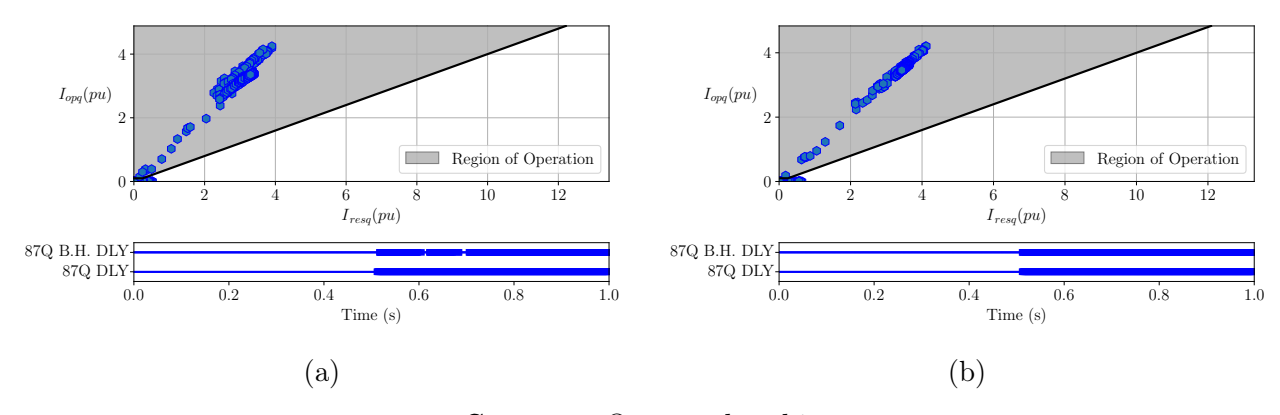
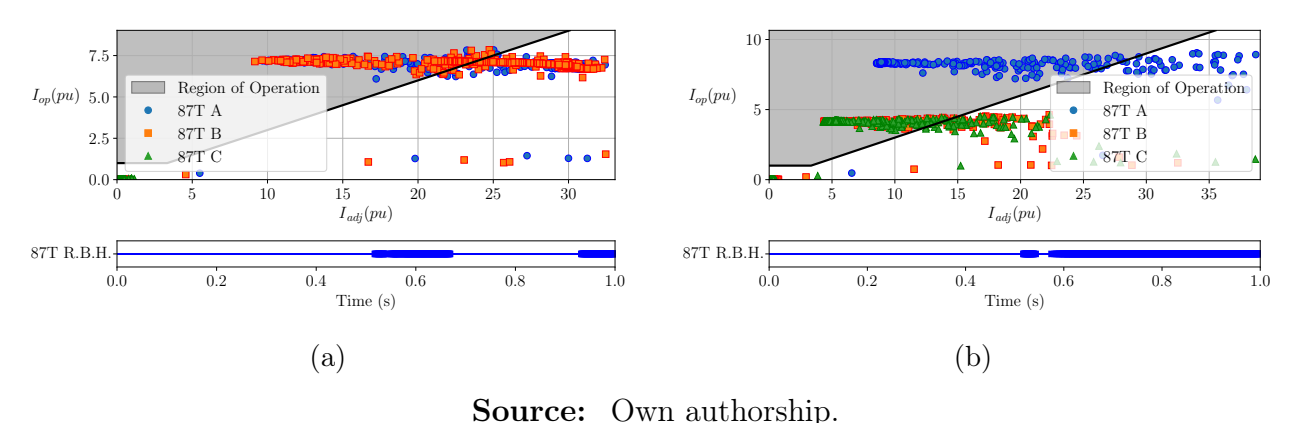


Figure 6.129: 87Q DLY function operation in (a) TFYY<sub>1</sub> and (b) TFYD<sub>1</sub> for a phase-to-phase-to-ground short circuit on the secondary side, with 100% power transmission in the bipoles.



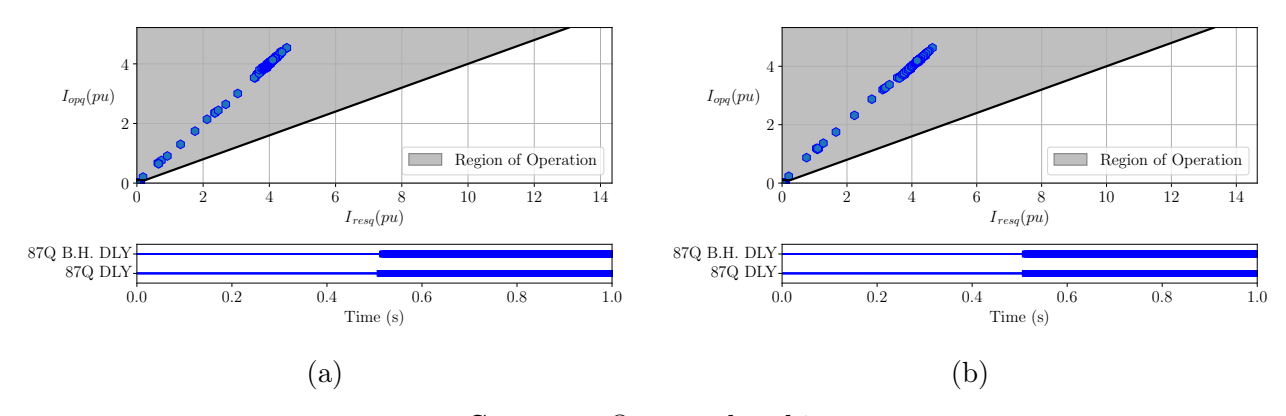
The same result is found with the bipoles at 10% power transmission: Figures 6.130 and 6.131.

Figure 6.130: 87T R.B.H. function operation in (a) TFYY<sub>1</sub> and (b) TFYD<sub>1</sub> for a phase-to-phase-to-ground short circuit on the secondary side, with 10% power transmission in the bipoles.



Source. Own authorship

Figure 6.131: 87Q DLY function operation in (a) TFYY<sub>1</sub> and (b) TFYD<sub>1</sub> for a phase-to-phase-to-ground short circuit on the secondary side, with 10% power transmission in the bipoles.



**Source:** Own authorship.

## 6.5 SUMMARY OF THE RESULTS

### 6.5.1 External Faults and Energization

Table 6.2 presents a summary of the behavior of the differential protection functions 87T, 87Q, and REF under external fault and energization scenarios. These events are not expected to trigger differential function operation. The table confirms that all protection functions maintained security during transmission line and busbar faults. However, during transformer

energization, the basic versions of 87T and 87Q were susceptible to misoperation, which was successfully mitigated by the application of harmonic blocking.

Table 6.2: Summary of external faults and energization scenarios.

${\bf Function\ Operations-External\ Faults\ and\ Energization}$							
Event	87T 87T R.B.H. 87Q DLY 87Q B.H. DLY REF						
Transmission Line Faults	✓	✓	✓	✓	✓		
Busbar Faults	✓	✓	✓	✓	✓		
Energization	×	✓	×	✓	<b>√</b>		

Source: Own authorship.

## 6.5.2 Internal Faults on Primary side

Tables 6.3 and 6.4 summarize the performance of the 87T, 87Q, and REF protection functions during internal faults on the primary side of converter transformers TFYY and TFYD, considering power transmission levels of 100% and 10%, respectively.

All protection functions demonstrated high sensitivity to conventional faults (e.g., single-phase-to-ground, phase-to-phase, and phase-to-phase-to-ground). For turn-to-ground and turn-to-turn faults, the performance is expressed as the number of fault scenarios that led to function operation out of the total simulated scenarios, followed by the maximum percentage of winding turns involved that were detected.

#### 6.5.3 Internal Faults on Secondary side

Tables 6.5 and 6.6 summarize the operation of the 87T and 87Q protection functions for turn-to-ground faults on the secondary side of converter transformers TFYY and TFYD. The results are presented separately for 100% and 10% power transmission scenarios.

For turn-to-ground faults on the secondary side, the 87T function showed limited performance. In TFYY, it was occasionally unduly blocked by 2<sup>nd</sup> harmonic components and failed to detect faults involving less than 56% of the winding. In TFYD, it did not operate in any case.

The 87Q function, with harmonic blocking and delay, proved to be more effective. It ope-

rated in TFYD for specific ranges of the winding at maximum power, covering 48% of the winding, although just 2% at minimum power. In TFYY, it detected faults between 51–68% at minimum power only. Without blocking, 87Q function detected faults from 56% at maximum power and from 51% at minimum power in TFYY, and in TFYD from 1–22% and 65–100% at maximum power, and from 59% onward at minimum power.

Tables 6.7 and 6.8 present the performance of the protection functions for other internal faults on the secondary side of TFYY and TFYD under the same power transmission conditions. The results align with the previously described behavior. It is also noteworthy that during phase-to-phase-to-ground faults, the presence of inrush-like currents (FIIC) was identified, but with magnitudes insufficient to block any of the protection functions.

Table 6.3: Summary of internal faults – Primary side with 100% transmission.

Transmission power in Bipoles: $100\%$							
Function Operations - Primary Side							
Fault	87T	87T R.B.H.	87Q DLY	87Q B.H. DLY	REF		
TFYY							
Single-phase-to-ground	✓	✓	✓	<b>√</b>	✓		
Phase-to-phase	<b>√</b>	✓	<b>√</b>	<b>√</b>	N/A		
Phase-to-phase-to-ground	<b>√</b>	✓	<b>√</b>	<b>√</b>	✓		
TD 4 1	<b>√</b>	✓	<b>√</b>	<b>√</b>	<b>√</b>		
Turn-to-ground		8 - 100%	2-100%		100%		
Turn-to-turn	<b>√</b>	✓	<b>√</b>	<b>√</b>	NI / A		
		8 - 100%	2-100%		N/A		
TFYD							
Single-phase-to-ground	<b>√</b>	✓	<b>√</b>	<b>√</b>	<b>√</b>		
Phase-to-phase	<b>√</b>	✓	<b>√</b>	<b>√</b>	N/A		
Phase-to-phase-to-ground	<b>√</b>	✓	<b>√</b>	<b>√</b>	✓		
Thomas 4 1	<b>√</b>	✓	<b>√</b>	<b>√</b>	<b>√</b>		
Turn-to-ground	8 - 100%		2-100%		100%		
T 4 - 4	<b>√</b>	✓	<b>√</b>	<b>√</b>	NI / A		
Turn-to-turn		8 - 100%	2	N/A			

Table 6.4: Summary of internal faults – Primary side with 10% transmission.

Transmission power in Bipoles: $10\%$								
Function Operations - Primary Side								
Fault	87T	87T R.B.H.	87Q DLY	87Q B.H. DLY	REF			
TFYY								
Single-phase-to-ground	✓	✓	✓	✓	<b>√</b>			
Phase-to-phase	✓	✓	✓	✓	N/A			
Phase-to-phase-to-ground	✓	✓	✓	✓	<b>√</b>			
Turn-to-ground	✓	✓	✓	✓	<b>√</b>			
Turn-to-ground		7-100%	2	100%				
Turn-to-turn	✓	✓	✓	✓	N/A			
Turn-to-turn	7-100% $2-100%$							
TFYD								
Single-phase-to-ground	✓	✓	✓	✓	✓			
Phase-to-phase	✓	✓	<b>√</b>	✓	N/A			
Phase-to-phase-to-ground	✓	✓	✓	✓	<b>√</b>			
m , 1	<b>√</b>	✓	<b>√</b>	<b>√</b>	<b>√</b>			
Turn-to-ground		7 - 100%	2-100%		100%			
Tum to tum	✓	✓	<b>√</b>	<b>√</b>	NI / A			
Turn-to-turn		7 - 100%	2	N/A				

Table 6.5: 87T and 87Q function operation summary for turn-to-ground short circuit in the secondary of  $TFYY_1$  for bipoles at 100% of power transmission.

Transm	ission	power in Bipo	oles: 100%				
Function Operations - Turn-to-ground - Secondary Side							
Percentage of Turns (%)	87T	87T R.B.H.	87Q DLY	87Q B.H. DLY			
	TFYY						
1 to 55%	×	×	×	×			
56 to 100%	✓	×	<b>√</b>	×			
TFYD							
1 to 14%	×	×	<b>√</b>	✓			
15 to 20%	×	×	<b>√</b>	×			
21 to 22%	×	×	<b>√</b>	✓			
23 to 64%	×	×	×	×			
65 to 86%	×	×	<b>√</b>	✓			
87 to 89%	×	×	<b>√</b>	×			
90 to 100%	×	×	<b>√</b>	<b>√</b>			

Table 6.6: 87T and 87Q function operation summary for turn-to-ground short circuit in the secondary of  $TFYY_1$  for bipoles at 10% of power transmission.

Transmission power in Bipoles: 10%							
Function Operations - Turn-to-ground - Secondary Side							
Percentage of Turns (%)	87T	87T R.B.H.	87Q DLY	87Q B.H. DLY			
	TFYY						
1 to 50%	×	×	×	×			
51 to 68%	×	×	<b>√</b>	✓			
59 to 100%	×	×	✓	×			
TFYD							
1 to 58%	×	×	×	×			
69 to 98%	×	×	<b>√</b>	×			
99 to 100%	×	×	<b>√</b>	✓			

Table 6.7: Summary of internal faults – Secondary side with 100% transmission.

Transmission power in Bipoles: $100\%$						
Function Operations - Secondary Side						
Fault	87T	87T R.B.H.	87Q DLY	87Q B.H. DLY		
		TFYY				
Single-phase-to-ground	✓	×	<b>√</b>	×		
Phase-to-phase	<b>√</b>	✓	<b>√</b>	✓		
Phase-to-phase-to-ground	✓	✓	<b>√</b>	✓		
Turn-to-turn	✓	✓	<b>√</b>	✓		
1 4111-00-04111	-	11 - 100%	100%			
TFYD						
Single-phase-to-ground	×	×	<b>√</b>	✓		
Phase-to-phase	<b>√</b>	✓	<b>√</b>	✓		
Phase-to-phase-to-ground	✓	✓	<b>√</b>	✓		
Turn-to-turn	✓	✓	<b>√</b>	✓		
1 1111-10-11111	10 - 100%		100%			
			1.			

Table 6.8: Summary of internal faults – Secondary side with 10% transmission.

Trans	missio	n power in Bij	poles: 10%				
Functi	on Op	erations - Seco	ondary Side				
Fault	87T	87T R.B.H.	87Q DLY	87Q B.H. DLY			
TFYY							
Single-phase-to-ground	×	×	×	×			
Phase-to-phase	<b>√</b>	✓	<b>√</b>	✓			
Phase-to-phase-to-ground	✓	✓	✓	✓			
Turn-to-turn	✓	✓	✓	✓			
1 11111-00-011111		8 - 100%	2 - 100%				
	TFYD						
Single-phase-to-ground	×	×	✓	✓			
Phase-to-phase	✓	✓	✓	✓			
Phase-to-phase-to-ground	✓	✓	✓	✓			
Turn-to-turn	✓	✓	✓	✓			
1 11111-10-11111	8 - 100%		2 - 100%				

# CONCLUSIONS AND PROPOSALS FOR FUTURE WORK

This master's dissertation evaluated the performance of differential functions (87T, 87Q, and REF) in protecting converter transformers connected to the inverter station of HVDC-LCC systems. For this purpose, a model of the bipoles of the HVDC complex of Rio Madeira, developed using the ATP/ATPDraw software, was used. Several internal and external fault scenarios for the converter transformers of one pole were simulated using this model, along with an energization scenario. Among the external faults, single-phase-to-ground, phase-to-phase, phase-to-phase-to-ground, and three-phase faults were simulated at the bus of the substation to which the inverter station is connected, as well as at the beginning and in the middle of a transmission line connected to the same substation. For internal faults, single-phase-to-ground, phase-to-phase, and phase-to-phase-to-ground faults were simulated at the terminals of the converter transformers, as well as turn-to-turn and turn-to-ground short circuits involving 1 to 100% of the winding at their terminals. Then, the responses of the 87T, 87Q, and REF functions (when applicable) were verified and analyzed for each simulated scenario, with the functions being implemented in Python.

The results of the 87T function met expectations for transformer energization and external faults, without any false trips, and for internal faults in the phases of the primary side of the converter transformers (the terminal connected to the AC system), acting correctly in all cases. For turn-to-turn and turn-to-ground faults in the primary, the function did not operate only for faults taking a small percentage of turns, which was already expected. In these cases, the power transmitted in the pole affected the function's performance, with lower sensitivity for higher powers. Nevertheless, with an SLP setting of the function to 0.3 and an Ipickupmin of 1 pu, the function worked correctly from 8% of turns involved with the pole power at maximum and 7% of turns involved with the pole power at minimum.

Regarding the results of the 87T function for internal faults in the secondary terminal of the converter transformers (terminal connected to the inverter), the function also operated correctly for phase-to-phase, phase-to-phase-to-ground, and turn-to-turn faults, with only slightly reduced sensitivity. However, it presented failures for single-phase-to-ground and turn-to-ground faults. The failures were caused by different reasons depending on the position of the converter transformer on the pole. In the TFYY transformer, connected to the six-pulse inverter connected to the DC line in the analyzed system, single-phase-to-ground and turn-to-ground faults were detected by the 87T function. Nevertheless, the function was improperly blocked and restricted by high levels of the 2nd harmonic component in the fault current. This component is caused by the characteristic of inverter operation during the fault, resulting in an offset in the converter transformer currents due to the incidence of the inverter's DC current on the neutral. Such offset leads the transformer to a half-cycle saturation in the core and/or an inrush current induced by the fault. In addition, the 87T function of TFYY was not sensitized for turn-to-ground faults involving less than 56% of the turns, which is a high percentage for this function. In these cases, the presence of 2nd harmonic was insufficient to block the function, but the faults were not even identified. The offset also occurs in these cases, and there is a difference in the currents of the terminals of the faulted phase; however, due to the resulting connection in the secondary of the converter transformer and the inverter control, there is no significant increase in the phase currents. Therefore, when the fault currents are estimated and the DC current is filtered, the resulting operating current value is insufficient for the protection to operate.

For the TFYD converter transformer (connected to the grounded six-pulse inverter in the analyzed system), the 87T function did not activate for single-phase-to-ground faults in the secondary, nor did it identify the turn-to-ground fault for any percentage of turns involved. For these faults in this transformer, due to its position in the pole, the resulting voltages at the transformer's secondary terminal during the fault directly impacted the inverter connected to the HVDC line so that the inverter control response caused a reduction in the transformer current instead of an increase, resulting in a minimum operating current and the non-sensitization of the 87T function. Again, the 2<sup>nd</sup> harmonic component was present in the fault current, but not enough for the blocking to actuate. Furthermore, to confirm the influence of the transformer position on the pole, single-phase-to-ground and turn-to-ground faults were simulated on the

converter transformers of another pole, whose connection order of the converter transformers is reversed, and the results were the same. With the bipoles at minimum, the results were similar in terms of current characteristics; however, the pole control reduced the fault current to the point that the function again failed to identify the fault.

The 87Q function, in turn, was adjusted with an SLP of 0.4 and a delay of two cycles as a minimum setting to avoid undue actuation. With this, the function also acted correctly for external faults and all faults in the primary of the transformers, not being sensitized only to turn-to-ground and turn-to-turn faults involving 1% of the turns. It also operated correctly for turn-to-turn, phase-to-phase, and phase-to-phase-to-ground faults in the secondary. However, its performance was compromised by the particularities of single-phase-to-ground and turn-to-ground faults in the secondary side of converter transformers. For single-phase-to-ground faults, however, the function proved to be an alternative for the TFYD transformer, working effectively with both maximum and minimum pole power. For the TFYY, the function was also blocked due to the presence of the 2nd harmonic, with the pole power at maximum, and it did not identify the fault when the power was at its minimum.

In cases of turn-to-ground faults in the secondary, since negative sequence currents depend on the control of the HVDC system, the function did not operate in some instances with particular percentages of turns involved; however, it proved to be a possible alternative. With the pole at its maximum power, the function had the same result as the 87T function for the TFYY transformer; nonetheless, for the TFYD, the function operated correctly for faults at the ends of the winding, covering at least 48% of the winding. With the bipole at minimum power, the function worked for faults between 51 and 68% of the TFYY winding since, with the current reduction, there was also a reduction in the 2nd harmonic, and it only worked in 99 and 100% of the TFYD winding because the fault current was practically zero in this transformer.

In addition, the REF function worked correctly in all cases to which it was applied: short circuits with a ground connection in the transformer's primary. The function also worked for all turn-to-ground faults in the primary, ensuring complete coverage of the transformer's primary winding for this type of fault.

Therefore, the differential functions proved effective for short-circuits in the AC terminal of converter transformers and for phase-to-phase, phase-to-phase-to-ground, and turn-to-turn

faults in the DC terminal, reinforcing the role of the equipment's primary protections. However, for single-phase-to-ground and turn-to-ground short circuits in the DC terminal, the 87T function presented malfunctions due to improper blocking and inability to detect faults. In contrast, the 87Q function proved to be a possible alternative. Still, more efficiency is needed, necessitating continued investigation of the subject and the proposal and evaluation of solutions for protecting converter transformers.

This work contributes to the state of the art by advancing beyond the analysis of single-phase-to-ground faults and harmonic blocking, which have already been addressed in the literature. It presents a broader evaluation of the challenges faced by differential protection functions in covering the entire winding of converter transformers connected on the inverter station of LCC-HVDC systems, revealing that improper blocking by 2<sup>nd</sup> harmonic components is not the only critical limitation. In this context, the study demonstrates that new philosophies for energization detection may not fully overcome the limitations encountered. Moreover, the assessment of the 87Q function as a complementary or alternative solution offers valuable insights for the selective application of protection functions in LCC-HVDC systems. The findings are relevant to guide the selection and parameterization of protection schemes for converter transformers, contributing to the reliability and safety of HVDC system operations.

Below, we list proposals for future work within the theme addressed in this text:

- Extend the analysis to include converter transformers connected to converters operating in rectifier mode.
- Validate the results found in this work using commercial IEDs and Hardware-in-the-Loop simulations.
- Evaluate new solutions for identifying the energization of converter transformers that do not cause improper blocking and restrictions.
- Evaluate new methods of protecting converter transformers that are effective for internal short circuits, considering the particularities of converter transformers and their connections to the AC and DC networks.

## REFERENCES

- ANDERSON, P. M.; HENVILLE, C. F.; RIFAAT, R.; JOHNSON, B.; MELIOPOULOS, S. *Power system protection*. [S.l.]: John Wiley & Sons, 2022. Cited 5 times in pages 5, 24, 32, 105, and 106.
- ARRILLAGA, J. *High Voltage Direct Current Transmission*. 2. ed. [S.l.]: The Institution of Engineering and Technology, 2008. ISBN 9780852969410. Cited 4 times in pages 17, 21, 23, and 25.
- BLACKBURN, J. L.; DOMIN, T. J. *Protective Relaying: Principles and Applications.* 3. ed. [S.l.]: CRC Press Taylor & Francis Group, LLC, 2007. ISBN 9781574447163. Cited 4 times in pages 5, 32, 33, and 34.
- CIGRÉ, C. international des grands réseaux électriques. Joint working group A.-B. . *HVDC Converter Transformers, Design Review, Test Procedures, Ageing Evaluation and Reliability in Service.* [S.l.]: CIGRÉ, 2010. Cited in page 27.
- CIGRÉ, C. international des grands réseaux électriques. Joint working group B. . *Modern Techniques for Protecting, Controlling and Monitoring Power Tranformers*. [S.l.]: CIGRÉ, 2011. Cited in page 32.
- CIGRÉ, C. international des grands réseaux électriques. Joint working group B.-B. *Impact of HVDC Stations on Protection of AC Systems*. [S.l.]: CIGRÉ, 2011. Cited 2 times in pages 46 and 51.
- DANHUI, W.; YU, C.; JUNCHAO, Z.; MINGHAO, W. A countermeasure for the restraint of the differential protection in converter transformer. In: IEEE. 2018 IEEE International Conference on Automation, Electronics and Electrical Engineering (AUTEEE). [S.l.], 2018. p. 97–101. Cited 3 times in pages 47, 48, and 52.
- DENG, Y.; LIN, S.; FU, L.; LIAO, K.; LIU, L.; HE, Z.; GAO, S.; LIU, Y. New criterion of converter transformer differential protection based on wavelet energy entropy. *IEEE Transactions on Power Delivery*, IEEE, v. 34, n. 3, p. 980–990, 2019. Cited 2 times in pages 51 and 52.
- EMTP Reference Models for Transmission Line Relay Testing. *IEEE Power System Relaying Committee*, 2004. Cited in page 55.
- EPE. *Matriz Energética e Elétrica*. Rio de Janeiro, Brazil, 2021. [Online]. Available: <a href="https://www.epe.gov.br/pt/abcdenergia/matriz-energetica-e-eletrica">https://www.epe.gov.br/pt/abcdenergia/matriz-energetica-e-eletrica</a>. Cited in page 3.
- EPE. Estudo para Escoamento de Geração da Região Nordeste e Ampliação da Capacidade das Interligações Regionais. Rio de Janeiro, Brazil, 2022. [Online]. Available: <a href="https://www.epe.gov.br/sites-pt/areas-de-atuacao/energia-eletrica/ArquivosGrupoEstudosTransmissao/GET-Nordeste-Apresentacao%2030.03.2022%20Estudos%20NE-Interligacao%20GET%20N.pdf">https://www.epe.gov.br/sites-pt/areas-de-atuacao/energia-eletrica/ArquivosGrupoEstudosTransmissao/GET-Nordeste-Apresentacao%2030.03.2022%20Estudos%20NE-Interligacao%20GET%20N.pdf</a>>. Cited in page 4.

References 147

FERNANDES, P. C. Um novo método de localização de faltas baseado em ondas viajantes para aplicações em linhas de transmissão de corrente contínua. Dissertação (Mestrado) — University of Brasília, 2020. Cited in page 16.

- FERRER, H. J. A.; SCHWEITZER, E. O. et al. Modern solutions for protection, control, and monitoring of electric power systems. [S.l.]: Schweitzer Engineering Laboratories Pullman, WA, USA, 2010. Cited 6 times in pages 30, 34, 37, 39, 41, and 43.
- GAJIC, Z. Differential protection methodology for arbitrary three-phase power transformers. [S.l.]: IET, 2008. Cited in page 36.
- GRID, A. Network protection & automation guide. Alstom grid, p. 7, 2011. Cited in page 27.
- GUZMAN, A.; ALTUVE, H.; TZIOUVARAS, D. Power transformer protection improvements with numerical relays. *CIGRE Study Committee B5–Protection and Automation*, v. 11, 2005. Cited 4 times in pages 28, 30, 33, and 34.
- GUZMÁN, A.; FISCHER, N.; LABUSCHAGNE, C. Improvements in transformer protection and control. In: IEEE. 2009 62nd Annual Conference for Protective Relay Engineers. [S.l.], 2009. p. 563–579. Cited 2 times in pages 39 and 42.
- HART, D. G.; NOVOSEL, D.; SMITH, R. A. Modified cosine filters. S. Patent, v. 6154687, 2000. Cited in page 61.
- HUGHES, T. P. Networks of power: electrification in Western society, 1880-1930. [S.l.]: JHU press, 1993. Cited 2 times in pages 1 and 2.
- IEC. Publication 60076-1 Power transformers Part 1: General. 2011. Cited in page 36.
- IEEE. Ieee guide for protecting power transformers. *Proceedings of the IEEE Std C37. 91-2008 (Revision of IEEE Std C37. 91-2000)*, IEEE Piscataway, NJ, p. 1–139, 2008. Cited 5 times in pages 27, 36, 37, 39, and 40.
- Itaipu Binacional. *Integração ao sistema brasileiro*. [S.l.], 2024. Available online at <a href="https://www.itaipu.gov.br/energia/integração-ao-sistema-brasileiro">https://www.itaipu.gov.br/energia/integração-ao-sistema-brasileiro</a>. Cited in page 3.
- JOVCIC, D.; AHMED, K. *High-voltage Direct-current Transmission: Converters, Systems and DC Grid.* 1. ed. [S.l.]: John Wiley & Sons Inc., 2015. ISBN 9781118846667. Cited 19 times in pages 2, 4, 5, 9, 11, 12, 13, 14, 15, 16, 17, 18, 19, 20, 21, 23, 24, 25, and 26.
- JR, D. L. M. Reviewing the history of electric power and electrification. *Endeavour*, Elsevier, v. 26, n. 2, p. 60–63, 2002. Cited in page 1.
- KAMAKSHAIAH, S.; V., K. *HVDC Transmission*. [S.l.]: Tata McGraw-Hill Education, 2011. ISBN 9780071072533. Cited in page 11.
- KASZTENNY, B.; FISCHER, N.; ALTUVE, H. J. Negative-sequence differential protection-principles, sensitivity, and security. In: IEEE. 2015 68th Annual Conference for Protective Relay Engineers. [S.l.], 2015. p. 364–378. Cited 2 times in pages 40 and 41.
- KIM, C.-K.; SOOD, V. K.; JANG, G.-S.; LIM, S.-J.; LEE, S.-J. *HVDC Transmission: Power Conversion Applications in Power Systems.* 1. ed. [S.l.]: John Wiley & Sons (Asia) Pte Ltd., 2009. ISBN 9780470822951. Cited 8 times in pages 1, 2, 10, 15, 17, 23, 24, and 26.

References 148

KIMBARK, E. W. Direct current transmission. [S.l.]: John Wiley & Sons, 1971. Cited 2 times in pages 2 and 15.

- Leuven EMTP Center. ATP-Alternative transient program-rule book. *Herverlee, Belgium*, 1987. Cited in page 55.
- LIN, X.; LU, J.; TIAN, Q.; WENG, H.; LI, Z.; TONG, C.; LI, M.; SUN, J.; YANG, D. Abnormal operation behavior analysis and countermeasures on the differential protection of converter transformer. *International Journal of Electrical Power & Energy Systems*, Elsevier, v. 64, p. 516–525, 2014. Cited 3 times in pages 46, 47, and 51.
- ONS. Recordes de Geração Eólica e Solar. [S.1.], 2023. Available online at <a href="https://www.ons.org.br/Paginas/resultados-da-operacao/historico-da-operacao/recordes.aspx">https://www.ons.org.br/Paginas/resultados-da-operacao/historico-da-operacao/recordes.aspx</a>. Cited in page 4.
- ONS. Energia Agora Carga e Geração. [S.l.], 2024. Available online at <a href="https://www.ons.org.br/paginas/energia-agora/carga-e-geracao">https://www.ons.org.br/paginas/energia-agora/carga-e-geracao</a>. Cited in page 3.
- PADIYAR, K. R. *HVDC Power Transmission Systems*. 2. ed. [S.l.]: New Academic Science Limited, 2011. ISBN 9781906574772. Cited 9 times in pages 1, 2, 17, 19, 20, 21, 23, 26, and 106.
- PDB5627. pyATP: Libraries for interfacing to ATP-EMTP and line impedance calcs. 2016. <a href="https://github.com/pdb5627/pyATP">https://github.com/pdb5627/pyATP</a>. Accessed: 2025-04-21. Cited in page 69.
- PERES, L. M. Proteção diferencial de transformadores de potência baseada na corrente de sequência negativa. Tese (Doutorado) University of Brasília, 2020. Cited 2 times in pages 35 and 43.
- SARCINELLI, G.; CATTAN, F.; CARVALHO, D.; GOMES, S. Hvdc transmission line modeling analysis in pscad and atp programs. In: *XIII SEPOPE*. [S.l.: s.n.], 2014. Cited in page 59.
- SCHWEITZER, E. O.; HOU, D. Filtering for protective relays. In: IEEE. *IEEE WESCANEX 93 Communications, Computers and Power in the Modern Environment-Conference Proceedings.* [S.l.], 1993. p. 15–23. Cited in page 61.
- SCHWEITZER ENGINEERING LABORATORIES, INC. SEL-487E-3,-4 Data Sheet. [S.l.], 2022. Available online at <a href="https://selinc.com/api/download/99384/">https://selinc.com/api/download/99384/</a>. Cited in page 71.
- SILVA, C. C. de S.; OLIVEIRA, G. S.; RIBEIRO, N. S. S.; SILVA, K. M. Hvdc converter transformers protection part 1: Signal processing aspects. 2023 Workshop on Communication Networks and Power Systems (WCNPS), p. 1–7, 2023. Cited in page 58.
- SILVA, K. M.; TAVARES, J. J. C.; RIBEIRO, N. S. S.; LOPES, F. V. Impact of dft-based phasor estimation errors due to commutation failures of lcc-hvdc links on the protection of ac lines in the near vicinity. *Electric Power Systems Research*, v. 196, p. 107287, 2021. ISSN 0378-7796. Cited in page 58.
- STAN, A.; COSTINAS, S.; ION, G. Overview and assessment of hvdc current applications and future trends. *Energies*, MDPI, v. 15, n. 3, p. 1193, 2022. Cited in page 1.

References 149

TAJ, B. N.; MAHMOUDI, A.; KAHOURZADE, S. Comparison of low-impedance restricted earth fault protection in power-transformer numerical relays. *Australian Journal of Basic and Applied Sciences*, v. 5, n. 12, p. 2458–2474, 2011. Cited in page 43.

- TAVARES, J. J. C. Influência de Sistemas HVDC no Desempenho da Proteção de Distância de Linhas de Transmissão CA. 93 p. Dissertação (Dissertação de Mestrado em Engenharia Elétrica) University of Brasília, 2020. Cited 4 times in pages 6, 55, 57, and 59.
- TAVARES, K. A. Modelagem e simulação da proteção diferencial de transformadores de potência no ATP. Dissertação (Mestrado) University of Brasília, 2014. Cited 3 times in pages 35, 77, and 105.
- T&D India. Siemens tests world's first  $1,100kV\ HVDC\ transformer$ . 2017. <a href="https://www.tndindia.com/siemens-tests-worlds-first-1100kv-hvdc-transformer/">https://www.tndindia.com/siemens-tests-worlds-first-1100kv-hvdc-transformer/</a>. Accessed: 2025-04-22. Cited in page 25.
- WATSON, N. R.; WATSON, J. D. An overview of hvdc technology. *Energies*, MDPI, v. 13, n. 17, p. 4342, 2020. Cited in page 1.
- XIAO, Y.-c.; WEN, J.; YUAN, Y.; LIU, W. Protection of converter transformer in hvdc. *Automation of Electric Power Systems*, v. 30, n. 9, p. 91–94, 2006. Cited in page 48.
- ZHAO, Y. Protection of HVDC Converter Transformers and Role of IEC 61850. 229 p. Tese (Doutorado) University of Manchester, 2018. Cited 9 times in pages 4, 5, 23, 24, 27, 46, 47, 52, and 56.
- ZHAO, Y.; CROSSLEY, P. Countermeasure to prevent the incorrect blocking of differential protection applied to converter transformers. *IEEE Transactions on Power Delivery*, IEEE, v. 35, n. 1, p. 95–105, 2019. Cited 3 times in pages 48, 49, and 52.
- ZHENG, T.; HU, X.; WANG, X.; GUO, X. Research on the fault-induced inrush current of the converter transformer and its impacts. In: IEEE. 2018 2nd IEEE Conference on Energy Internet and Energy System Integration (EI2). [S.l.], 2018. p. 1–6. Cited 5 times in pages 48, 49, 50, 52, and 98.
- ZHENG, T.; LIU, X.; GUO, X. Analysis of fault-induced inrush current of converter transformer in lcc hvdc system considering dc control and protection. *International Journal of Electrical Power & Energy Systems*, Elsevier, v. 125, p. 106536, 2021. Cited 6 times in pages 49, 50, 52, 94, 98, and 113.
- ZHENG, T.; LIU, X.; GUO, X.; WANG, X.; DU, Z.; ZHANG, K. Fault-induced inrush current of inverter-side converter transformer and its impact on differential protection. IET, 2021. Cited 5 times in pages 49, 50, 52, 94, and 98.
- ZHENG, T.; LIU, X.; YANG, X.; HE, R. A method to prevent differential protection for converter transformer from inappropriate-blocking under fault-induced inrush current. In: IEEE. 2021 IEEE Power & Energy Society General Meeting (PESGM). [S.l.], 2021. p. 1–5. Cited 2 times in pages 50 and 52.
- ZIEGLER, G. Numerical differential protection: principles and applications. [S.l.]: John Wiley & Sons, 2012. Cited in page 35.